

Faculty of Science and Engineering

Department of Spatial Sciences

**Impact of Land Use Change on Urban Surface Temperature and
Urban Green Space Planning; Case Study of the Island of Bali,
Indonesia**

I Gusti Agung Ayu Rai Asmiwyati

**This thesis is presented for the Degree of
Doctor of Philosophy
of
Curtin University**

July 2016

DECLARATION

To the best of my knowledge and belief this thesis contains no material previously published by any other person except where due acknowledgement has been made.

This thesis contains no material which has been accepted for the award of any other degree or diploma in any university.

Signature:

Date: 22/07/2016

ABSTRACT

This thesis focuses on the monitoring of land use/cover (LULC) changes and urban heat island (UHI) effects with temporal and spatial variation, using Advanced Spaceborne Thermal Emission and Reflection Radiometer (ASTER) and Landsat Thematic Mapper (TM) data, in order to examine the development of urban green space. The study area was located in the central urban area of Bali including southern coastal areas that have been experiencing pressures from various human activities, leading to the rapid LULC changes and UHI effects. This study would be useful for providing a comprehensive foundation for understanding relationships and interactions between human and natural resources to better manage and use the natural resources, in formulating urban green space, as well as in LULC management and planning. For detecting LULC and Land Surface Temperature (LST) changes over three different periods, Landsat TM of 1995 and two ASTER images of 2003 and 2013 were collected. LULC change was determined using an object-based image classification method. Built-up areas, paddy fields and vegetation were the main LULC types, and these have all changed through time. Urban areas, associated with built-up areas, were mainly formed by intensive conversion of vegetation and paddy fields, and the increase of built-up areas was related to the factors of economic growth, population, land value and new roads to urban and suburban centers. To visualize the UHI, LST was retrieved from thermal bands of ASTER (band 10-15) and Landsat TM (band 6). Detection of the UHI effects from 1995 to 2013 show that the UHI effects (defined as LST of over 29 °C) were found to be centralized in downtown Denpasar and spreading to the some surrounding areas. It was particularly caused by built-up areas; areas such as these have high density building, residents, transportation and roads. The areas with lowest LST were found in swamp and mangrove areas, while others included paddy fields, vegetation, mangrove, and water bodies. Some separate samples of regions were selected to represent three different types of urban areas. Mean LSTs used as a comparison among urban areas. The density of urban areas has been proven to have influence on the UHI

effects that create a limitless array of energy balance and microclimate systems. This can be seen from examining the LST of diversity of LULC types in the very dense urban areas, where the temperature was higher than temperatures in other urban areas. The higher mean LST in very dense urban areas was also related to a lower NDVI. The density of urban areas, NDVI, and LST was used to determine priority zones for green spaces. The thesis concludes that Landsat TM and ASTER imagery provide efficient, relatively low-cost techniques for studying LULC changes and locating UHIs for a typical small tropical island. Moreover, satellite RS can facilitate local and micro level UHI detection and implementing low-cost UHI mitigation.

ACKNOWLEDGMENTS

I would like to convey my gratitude to my main supervisor Dr. Robert J. Corner for extending his generous support and patience as well as clarifying what I was thinking and contributing to the development of this research. My appreciation also goes to my co-supervisor Dr. Ashraf M. Dewan for a huge contribution to my learning and success in the PhD process. My endless gratitude is devoted to my beloved father, I Gusti Ketut Gde Darsika who passed away September 20, 2014 when I was doing this PhD journey and my mother I Gusti Ayu Ketut Suryati, for her unconditional warming love and continuous prayers. My sincerest appreciation goes to my beloved husband, Made Kurniawan, for his patience and undying support which provide me with the confidence in my PhD study. This thesis is dedicated to my beloved children: Anandaichi C. Sudarsana and Kireina Maharashtri. My motivation and commitment to my study would not have been possible without their loves, warming hugs and kisses. I wish to thank Prof. Made Sudiana Mahendra who introduced Curtin University to me, Mr. Christopher Brown for proofreading drafts of my writing, Gema Sakti and Abd. Rahman Asyaktur for sharing their knowledge in RS and GIS. I wish to thank my fellow graduate students and staff members at Curtin University for sharing their proficiency and knowledge the intangible sources that actually went into producing this research. I owe my deepest gratitude to Directorate General of Higher Education (DGHE or DIKTI) Ministry of National Education, Indonesia that financed my PhD.

RELATED PUBLICATION

Asmiwyati I G.A.A., R. J. Corner, & A. M. Dewan. “Seasonal Comparison of LANDSAT ETM+ Derived Land Surface Temperature for Southern Bali”. *The 34th Asean Conference on Remote Sensing (ACRS)*, 20-24 October 2013, Bali Indonesia.

TABLE OF CONTENTS

ABSTRACT	iii
ACKNOWLEDGEMENTS	v
RELATED PUBLICATION	vi
TABLE OF CONTENTS.....	vii
LIST OF TABLES.....	xi
LIST OF FIGURES	xii
LIST OF ABBREVIATIONS	xiv
1 INTRODUCTION	1
1.1 Background Information.....	1
1.1.1 Land use and land cover change	1
1.1.2 The effects of LULC change on increasing land surface temperatures	2
1.1.3 Use of spatial data and spatial analysis.....	3
1.2 Research Objectives.....	4
1.3 Significance of the Research.....	4
1.4 Overview of Thesis.....	5
2 REVIEW OF LAND USE, LAND COVER AND URBAN HEAT ISLAND..	8
2.1 Urban land use and land cover dynamics	8
2.2 Urban heat island.....	9
2.2.1 Spatial structure of UHI effects.....	10
2.2.2 UHI assessment	14
2.2.3 Impacts of UHI.....	16
2.3 Influencing factors of UHI formation.....	17
2.3.1 Surface energy balance	18
2.3.2 Vegetative surfaces in UHI formation.....	19
2.3.3 Impervious surfaces and UHI formation	21
2.3.4 Anthropogenic heat and pollutants.....	24
2.4 Green Space Planning for UHI Mitigation	25
2.4.1 Characteristics of green space.....	26
2.4.2 Vegetation cover indices to represent vegetation condition and the impacts on surface temperature	28
2.5 The Impact of Vegetation Change on Surface Temperature.....	28
2.6 Chapter Summary.....	31
3 REVIEW OF RS IMAGERY AND GIS PROCESSING FOR MEASURING LULC AND LST	32
3.1 Choice of RS Imagery for Measuring LULC and LST	32

3.1.1	Characteristics of RS imagery.....	32
3.1.2	Choice of imagery for detecting UHI effects and LULC	37
3.2	Previous UHI Studies	40
3.3	Choice of RS and GIS Pre-processing Method.....	42
3.3.1	Geometric correction	42
3.3.2	Atmospheric Correction.....	44
3.4	Selecting a System of LULC Classification	46
3.5	Image Classification	49
3.5.1	Methods of image classification.....	50
3.5.2	Pixel-based classification versus object-based classification method	53
3.5.3	Training and validation dataset	55
3.5.4	Assessment of image classification accuracy	58
3.5.5	Techniques for change detection.....	60
3.6	Chapter Summary	62
4	STUDY AREA AND DATA	63
4.1	General Description of Study Area	64
4.1.1	Socioeconomic condition.....	64
4.1.2	Climate and traditional growing season	65
4.1.3	Urbanization in Bali.....	68
4.1.4	Balinese traditional concept of conserving nature	69
4.2	Remotely Sensed Data Preparation	70
4.2.1	Landsat TM data.....	71
4.2.2	ASTER data	72
4.2.3	Ancillary data	73
4.2.4	Field survey to obtain ground truth data and LULC types	74
4.3	Research Design Process	75
4.4	Chapter Summary	75
5	ANALYSIS OF LAND USE/COVER CHANGE IN SOUTHERN BALI ..	77
5.1	Classification Process	78
5.1.1	Training data collection	78
5.1.2	LULC classification system.....	78
5.1.3	Pre-processing of satellite images	81
5.1.4	Object-based classification method.....	84
5.1.5	Classification accuracy assessment	87
5.1.6	Post-classification comparison change detection.....	88
5.2	Classification Result	88
5.2.1	Landsat image classification and accuracy assessment	88
5.2.2	ASTER image classification and accuracy assessment	89
5.2.3	General LULC condition and distribution	90
5.2.4	LULC changes.....	89
5.3	Discussion	104
5.3.1	Seasonal difference impact on LULC changes	104
5.3.2	Possible error sources of LULC classification and	

	change detection.....	107
5.3.3	LULC change trend and impacts on environment.....	109
5.3.4	Driving Forces.....	110
5.4	Chapter summary.....	112
6	IMPACT OF LAND USE AND LAND COVER CHANGE ON LAND SURFACE TEMPERATURE	114
6.1	Method of NDVI and Land Surface Temperature Retrieval.....	115
6.1.1	Retrieving NDVI	115
6.1.2	Preparation of the land surface emissivity and the normalized difference vegetation index.....	115
6.1.3	Retrieving LST from Landsat 5 TM.....	117
6.1.4	Retrieving LST from Aster	120
6.1.5	Cloud removal.....	122
6.1.6	Standardization of LST.....	122
6.1.7	The LST pattern using transect analysis	124
6.1.8	Analysis of relationship between LST and LULC and NDVI.....	125
6.2	Results.....	126
6.2.1	Spatial pattern of NDVI.....	126
6.2.2	Standardization of the LST	130
6.2.3	Spatial pattern of LST changes	130
6.2.4	The LST of different LULC types.....	140
6.2.5	The correlation between LST and NDVI by LULC.....	144
6.3	Discussion	145
6.3.1	Impact of LULC change on LST.....	145
6.3.2	The increasing LST and driving factors	146
6.4	Chapter summary.....	152
7	GREEN SPACE PLANNING AND MANAGEMENT TO MITIGATE UHI IN BUILT-UP AREAS	154
7.1	Method of analysis.....	155
7.1.1	Analysis the impact of LULC on LST in urban area types.....	155
7.1.2	Data and analysis of green space zone	155
7.2	Results.....	157
7.2.1	Sample distribution.....	157
7.2.2	The LST fluctuation by diversity of LULC types in built-up area types.....	158
7.2.3	The change of LST by urban area types	159
7.2.4	Analysis of green space planning	162
7.2.5	MUHI detection in urban area types.....	166
7.3	Discussion	171
7.3.1	Factors that influence LST changes among built-up areas	171
7.3.2	Concept of green space planning.....	173
7.3.3	Adaptation of local cultural concepts in green space management	176
7.4	Chapter summary.....	178

8	CONCLUSION AND FUTURE DIRECTION.....	180
8.1	Spatial and temporal LULC rates and patterns	180
8.1.1	Recommendations	182
8.2	Spatial and temporal LST rates and patterns.....	182
8.2.1	Recommendations	183
8.3	The relationship between LULC change on LST and NDVI.....	184
8.3.1	Recommendations	184
8.4	Mitigating the UHI effect through green space planning	185
8.4.1	Recommendations	186
	REFERENCES	187
	APPENDICES	213

LIST OF TABLES

Table 1.1	Summary of research design.....	7
Table 2.1	Characteristics of surface and atmospheric UHI (Voogt and Oke, 1997).....	16
Table 3.1	Characteristics of the most common sources of remotely sensed data (modified from Loveland and Defries, 2013).....	36
Table 3.2	Characteristics of spectral resolution of orbital sensor systems (Stefanov et al., 2004).....	37
Table 3.3	Land classification of USGS in urban area and NLCD 92.....	48
Table 3.4	LULC classes from previous studies in Bali and Indonesian National Standard.....	50
Table 3.5	Population error matrix with p_{ij} representing the proportion of area in the mapped LULC category i and the reference LULC category (Liu et al., 2007).....	59
Table 4.1	Gross Regional Domestic Product of Bali (2010-2013) (Statistics Office of Bali, 2014).....	66
Table 4.2	Satellite data used in this study.....	71
Table 4.3	Characteristic of ASTER and Landsat TM imagery.....	72
Table 5.1	The LULC classification schema (modification from Land Use Map of Bali JICA (2003) and National Standardization Agency of Indonesia (2010) for Bali.....	79
Table 5.2	Accuracy assessment of LULC map of 1995.....	89
Table 5.3	Results of first accuracy assessment for the LULC maps of Aster in 2003 and 2013.....	90
Table 5.4	Area statistics of LULC change of Southern Bali.....	99
Table 5.5	Major LULC conversions from 1995 to 2013.....	103
Table 5.6	The 1995-2003's transformation LULC classes.....	105
Table 5.7	The 2003-2013's transformation LULC classes.....	106
Table 6.1	Unit conversion coefficients and calibration constants of ASTER thermal bands.....	121
Table 6.2	Comparison of the LST image means for pre- and post-standardization in 1995, 2003, and 2013.....	130
Table 6.3	Statistical features of standardized LST by LULC type.....	140
Table 6.4	Pearson's correlation coefficients between LST and NDVI by LULC types (significant at 0.05).....	145
Table 7.1	Criteria of scoring and weighting for each factor.....	156
Table 7.2	Polygon samples of built-up areas types.....	158
Table 7.3	Change of LST by the LULC types in urban area types.....	160
Table 7.4	Statistical result of t-test paired two means of LST (significant at 0.05).....	162
Table 7.6	Priority zone of urban green space based on district areas.....	164

LIST OF FIGURES

Figure 2.1	Spatial vertical structure of the city atmosphere on (a) a whole city (mesoscale), (b) a LULC area (local scale) and c) a street canyon (microscale). The three UHI types linking to each scale is located on red shaded areas (thick line following surface in (b)) (Oke, 1988; Voogt and Oke, 2003; Roth, 2013).	11
Figure 2.2	Fluctuations in intensity of UHIs vary over different LULC areas and at different times of the day (Roth et al., 1989; Voogt & Oke, 2003)....	13
Figure 2.3	Influencing factors created UHI (modified from Oke, 1997; Rizwan et al., 2008; Aguiar, 2012).....	18
Figure 2.4	Energy balance system and physical properties of surfaces that influence the local temperature (modified from Iguski and Jackson, 2008).....	19
Figure 2.5	The impact of roof surface colors and materials on the LST (modified from cooltexasbuildings, 2015).....	23
Figure 2.6	The impacts of impervious surfaces on UHI formation (Voogt and Oke, 2003).....	25
Figure 2.7	Capacity of green space in climate adaptation (Matthews, 2015).	27
Figure 2.8	Reduced green space and impacts of impervious surface on UHI (US EPA, 2009).....	29
Figure 2.9	The impact of afforestation on surface temperature.	30
Figure 3.1	A Landsat timeline (NASA, 2015).	39
Figure 3.2	The transformation in geometric correction processes (Murai, 1998) ...	43
Figure 3.3	Typical classification methods (Murai, 1998).....	52
Figure 3.4	Examples of over segmentation (left) and under segmentation (right) in the bright colour areas when generating land parcel objects (Smith and Morton, 2008).....	55
Figure 3.5	Sampling methods (Congalton, 1991).....	57
Figure 4.1	Location of the study area	65
Figure 4.2	Pattern of monthly average temperature for the period of 2004-2008 and pattern of wet and rainy seasons during three periods in Bali (Setiawan, 2012).....	67
Figure 4.3	Urbanization trend in large Indonesian provinces (Sutriadi and Haryo, 2009).....	69
Figure 4.4	An overview of the research design.....	76
Figure 5.1	LULC types	82
Figure 5.2	LULC types	83
Figure 5.3	Workflow for LULC classification and change analysis	84
Figure 5.4	Sample of segmentation result (scale parameter of 50)	85
Figure 5.5	LULC of 1995	92
Figure 5.6	Urban and non urban area of 1995.....	93

Figure 5.7	LULC of 2003	94
Figure 5.8	Urban and non urban area of 2003.....	95
Figure 5.9	LULC of 2013	96
Figure 5.10	Urban and non urban area of 2013.....	97
Figure 5.11	LULC distributions in South Bali	98
Figure 5.12	LULC changes of Southern Bali.....	98
Figure 5.13	Major LULC conversions in Bali of 1995–2003	100
Figure 5.14	Major LULC conversions in Bali of 2003-2013.....	101
Figure 5.15	Areal increase and decrease of three main LULC types	102
Figure 6.1	LST and NDVI retrieval.....	116
Figure 6.2	Scaled NDVI of 1995	127
Figure 6.3	Scaled NDVI of 2003.....	128
Figure 6.4	Scaled NDVI of 2013	129
Figure 6.5	Spatial distribution of normalized LST in 1995	132
Figure 6.6	Spatial distribution of normalized LST in 2003	133
Figure 6.7	Spatial distribution of normalized LST in 2013	134
Figure 6.8	Statistics of LST area (ha) in 1995, 2003, and 2002.....	135
Figure 6.9	The changes in the number of LST areas (ha) from 1995 to 2013	136
Figure 6.10	Transect graphs transect graphs of the LSTs (West-to-East)	138
Figure 6.11	Transect graphs transect graphs of the LSTs (South-to-North).....	139
Figure 6.12	The LST by LULC type	141
Figure 6.13	Box plots of the standardized LST of each LULC type	143
Figure 6.14	The different change of UHI pattern at Kuta and Sanur in 1995, 2003 and 2013	148
Figure 6.15	Spatial distributions of the increasing LST from 1995 to 2003.....	149
Figure 6.16	Spatial distributions of the increasing LST from 2003 to 2013.....	150
Figure 6.17	Spatial distributions of the increasing LST from 1995 to 2013.....	151
Figure 7.1	Reclassification of raster map of built-up area type, NDVI and LST	157
Figure 7.2	LST changes of urban area types	161
Figure 7.3	Block plan of green space in urban areas	165
Figure 7.4	Suggested locations for new urban parks in high-priority zone	166
Figure 7.5	Cooling thermal spots provided by features of parks, lawns, vacant land, paddy fields, and cemeteries, illustrated by white and green shaded areas in very dense urban areas	167
Figure 7.6	Typical thermal sample in densely urban areas (Niti Mandala Park	169
Figure 7.7	Typical thermal sample in semi-dense urban areas.....	170
Figure 7.8	A cooling pavement in a very dense urban area	175
Figure 7.9	The applied THK concept of green space	177
Figure 7.10	The relationship between applied THK concept and Indonesia green space structure (Adapted from Space Plan Bureau of Indonesia, 2006; Paturusi and Diartika, 2010)	178

LIST OF ABBREVIATIONS

LULC	Land Use and Land Cover
UHI	Urban Heat Island
SUHI	Surface Urban Heat Island
LST	Land Surface Temperature
UCL	Urban Canopy Layer
UBL	Urban Boundary Layer
MUHI	Micro Urban Heat Island
ET	Evapotranspiration
NDVI	Normalized Difference
RS	Remote Sensing
GIS	Geographical Information System
GPS	Global Position System
ASTER	Advanced Space-borne Thermal Emission and Reflection Radiometer
VNIR	Visible and Near-Infrared
SWIR	Shortwave Infrared
THK	<i>Tri Hita Karana</i>
<i>Subak</i>	Water irrigation system in Bali
GDRP	Gross Regional Domestic Product
DN	Digital numbers
OBIA	Object Based-Image Analysis
FLAASH	Fast line-of-sight atmospheric analysis of hyper-cubes

1 INTRODUCTION

1.1 Background Information

1.1.1 Land use and land cover change

The earth's surface has changed significantly around the world over recent decades. Urbanization is one of the most important global changes and has led to profound changes in land use and land cover (LULC). These considerable LULC changes have involved a decrease in rural areas and an expansion of urban areas through development. Urbanization is usually triggered by the increase in land demand for diverse urban activities, which is caused by the rise in urban population levels. The migration of people from rural areas to the cities triggers the high population growth.

Much urbanization has occurred recently in East-Southeast Asia, including Indonesia, which has become one of the world's fastest growing urbanizing areas. In addition, large-scale human development and movement have taken place not only in inland areas but also in coastal areas, which are typically more sensitive and fragile to deleterious changes than inland areas. This is because they are located between land and sea, and are likely to receive more diverse disturbances from both land and sea. About 14 of the 17 largest cities in the world are on the coastline of the Asia Pacific (Mimura, 2008). Despite occupying less than 15% of the earth's land surface, this area accommodates more than 60% of the population of the world (Tibbetts, 2002). Moreover, peri-urbanization and a chaotic mixture of rural and urban LULC have become a major feature of Asian urbanizing areas (McGee, 1991; Murakami et.al., 2005). Peri-urbanization refers to the urban growth process in an area located between rural and urban areas that has mixed urban and rural characteristics in physical, economic, and social terms.

The patterns and rates of change of the massive LULC transition currently occurring need to be monitored. They are critical factors of global changes that impact human life in terms of hydrological balance, landslide risks, air and water pollution levels, habitat disturbance, as well as the livelihoods and vulnerability of populations in the region. Therefore, the quantification of spatial and temporal change in LULC is important not only to reflect the underlying human processes in the environment but also to understand interactions between human activities and the environment in urban and sub-urban landscapes. Furthermore, information about the rate and pattern of LULC change can also be used to manage the pressures of human activity and development on urban areas, and thus, this information acts as a baseline plan that can determine the future direction of urban land utilization.

1.1.2 The effects of LULC change on increasing land surface temperatures

Due to rapid population growth and the growth of urbanizing areas worldwide, more attention is being paid of late to urban climate change at both local and regional scales. This is because growing urbanizing areas have caused tremendous replacements of soil and vegetation by impervious surface materials that have profound impacts on the local surface energy balance. These materials lead to increased land surface temperatures (LST) (Yuen and Kong, 2009), which is an important index for examining the behavior of the urban thermal regime. LST is determined by energy fluxes between the surface and the atmosphere (Voogt & Oke, 2003). Therefore, the measurement of LST driven by LULC changes can provide indications about the extension of thermal distribution related to LULC patterns and human-related changes.

Increasing LST in urban areas leads to the formation of Urban Heat Islands (UHIs), where urban areas show higher LST than the surrounding rural areas (Buyantuyev and Wu, 2009). UHIs are a direct outcome of a degraded urban environment. Moreover, UHIs are also associated with a deterioration of air

quality, negative effects on public health and welfare, and secondary effects on local meteorology, including transforming micro-wind patterns, developing cloud and fog, and increasing humidity and the rate of precipitation (Arizona Board of Regents, 2007; Kim, 2007).

The increased human activity that potentially escalates UHIs' effects indicates an important need to measure the impact of LULC change on UHI effects. Information on the impact of LULC change on LST is of interest, as the amount of human pressure and the impact on LST is unique in each area. This is due to the fact that UHI phenomena are determined by the characteristics of local conditions and human activities. In addition, understanding both past and ongoing phenomena by monitoring the urbanizing area processes enables an early response to address the anticipated increase in UHI effects and to reduce other deleterious UHI impacts on the environment caused by LULC changes.

1.1.3 Use of spatial data and spatial analysis

Remote sensing (RS) has proven useful for characterizing LULC changes. Integration with Geographic Information Systems (GIS) is a cost effective and increasingly used technique for updating urban LULC at high spatial and temporal frequency (Selcuk et al., 2003). Satellite RS collects multi-spectral and multi-temporal spatial data and changes them into valuable information for monitoring and understanding urban LULC while GIS, a computer-based system, enables collecting, maintaining, storing, analyzing, and displaying spatially organized information (Weng, 2001).

Application of RS and GIS is an appropriate solution for this study of the thermal effect of LULC change, as these technologies can provide consistent and detailed spatial information about LULC, LST and changes in suburban and urban areas. This subsequently improves representation and understanding of heterogeneous urban areas and the urban development's impact on the surrounding environment.

Although a large amount of research has been conducted using satellite-derived LULC data, only a few efforts have been made to explore LULC change and its effect on LST in tropical areas. In addition, research that is conducted using RS in tropical urban areas often faces challenges since detailed monitoring of urban LULC change remains expensive, problems exist due to the highly heterogeneous city land use leading to spectral similarity among LULC types, and a lack of cloud-free data. The basic premise of this study is to quantify LST change driven by LULC change through the use of RS and GIS. This study is enabled by the availability of LST data from remotely sensed thermal imagery and the distinctive differences in the temperature of LULC characters.

1.2 Research Objectives

The primary aim of this research is to explore the spatio-temporal dynamics and changes in LULC in the southern part of the island of Bali and to analyze the impact of these changes on LST as an aid to developing strategies for urban green space planning and management. This study is conducted through time series analysis of medium spatial-resolution satellite imagery for the period between 1995 and 2013. Its aims are reached through the following sub-objectives:

- a) To determine the trend, rate, location and magnitude of LULC and LST that represents typically tropical climatic conditions.
- b) To analyse and verify the relationship between changes in LULC and LST.
- c) To investigate the driving factors of UHI effects in order to generate a theoretical basis for mitigating the effect of UHI through urban green space.

1.3 Significance of the Research

Analyzing the spatio-temporal characteristics of LULC and the interrelationships between biophysical factors and LST is necessary to provide the required information on the change of the rate, pattern, and growth process of urban expansion. Information about UHI formation is useful to improve understanding

not only of the urban climate and its dynamics, but also the effects of LULC decisions on the microclimates of urban areas. Moreover, an understanding of the spatiotemporal pattern of LST has important implications for further planning in many other tropical coastal cities, as Bali is one of fastest urbanizing areas in Indonesia. It is also useful to understand the fluctuations of UHIs' effects and LST distribution for a typical small tropical island.

As has been stated above, although the spatial patterns of urban thermal condition may have been extensively studied, a comprehensive understanding of the LULC heterogeneity that affects LST distributions in temporal change on a typical small island in a humid tropical area is still limited. Moreover, there is still little information about LST that would eventually be applied to help determine comprehensive green space management to effectively mitigate UHIs. Therefore, the outcome of this study can be used as a considered reference for professionals such as landscape architects, environmental engineers, and urban planners for urban green space management that mitigates the effects of UHIs and works towards sustainable development.

1.4 Overview of Thesis

This thesis consists of eight chapters with the general research design is summarized in Table 1.1. Chapter 1 introduces the expansion of urban areas that leads to UHI effects. The research objectives are defined, as are the expected outcomes and the benefits of the study. Both of chapter 2 and chapter 3 review relevant literature and methodologies required to reach the study objectives. The chapter 2 focuses in discussing the LULC dynamics, the system of UHI effects and the mitigation strategy using green spaces. The chapter 3 begins with the role of remote sensing for mapping LULC and LST. The background information for selecting the appropriate source of RS data, the correct interpretation and mapping of spatially complex urban LULC and LST, and the principles of spatial methods for measurement are discussed. This chapter also extensively discusses existing

RS and GIS approaches and techniques employed in LULC and LST quantification. Chapter 4 describes the remotely sensed datasets used and the study site's characteristics. Chapter 5 analyses LULC change rates and patterns in 1995, 2003 and 2013 over the 240 km² study site using a temporal series of multispectral RS images. This chapter also demonstrates the usefulness of object-based image analysis in deriving LULC classification. This type of information is important for updating spatial data for urban management and determining the past and current levels of LULC and change rate for LULC monitoring. Chapter 6 analyses the LST over the capital city of Bali and the surrounding area and compares the trend and average value of LST as it varies from year to year. This chapter also describes how LULC classes and urban development are related to LST changes and quantifies the relationship between LST and biophysical parameters (LULC and NDVI). The analysis of the relationship between temperature, LULC, and NDVI and driving factors would provide the basis for mitigation of UHI effects and improving city living conditions. Chapter 7 examines the application of resulted dataset (LST, NDVI, urban area types) to determine block plan or priority areas for green space planning. The local scale of LST mapping was fragmented into samples of the smaller thermal pattern of "hot and cool spots" at the micro-scale of the heat island that was taken from three types of urban areas to assess their LST difference. This chapter also describes detection of the micro level heat islands in three types of urban areas. Chapter 8 is a summary of these studies described with recommendations for planning, management, and future study.

Table 1.1 Summary of research design

Main research objectives	To explore the spatio-temporal dynamics and evolution of LULC in a rapidly expanding tropical urban area and its impact on LST in developing strategies of urban green space management		
Specific objectives	To measure temporal change in LULC and identify LST distribution To analyse the relationship between changes in LULC and LST To investigate the driving factors of UHIs in order to generate optimal allocation of urban green space		
Sub-objectives	Respective research question	Techniques of analysis	Data and software
To analyse the proportion of LULC and the change over the period 1995-2013	<ul style="list-style-type: none"> • What are the composition, proposition, and distribution of LULC types in southern Bali? • What are the LULC changes? • Can RS and GIS assess the LULC changes? 	RS and GIS analysis	Literatures, Landsat and Aster imagery, ArcMap, ENVI, SPSS, Microsoft Excel
To analyse the spatial distribution of LST and the change over the period 1995-2013	<ul style="list-style-type: none"> • What is the spatial pattern of LST in southern Bali? • What are the LST changes? • Can RS and GIS provide an efficient method in analyzing spatial thermal patterns? 	RS and GIS analysis	Literature review, SPSS, Microsoft Excel
To analyse the relationship between LULC and LST and its change	<ul style="list-style-type: none"> • Is there a correlation between the spatial temporal characteristics of the LST pattern and LULC? • Which LULC types have obvious impacts on MUHI? • Do anthropogenic activities on LULC types influence UHI effects? • What is the influence of the various types of LULC and the change in urban LST? 	Statistical analysis	
To analyse the relationship between LST and biophysical factors (NDVI)	<ul style="list-style-type: none"> • Are there any correlations between characteristics of LST and NDVI? 	Statistical analysis	
To determine the possible future location of green space	<ul style="list-style-type: none"> • What is the Balinese local cultural concept of green space? • Where areas should be most planted with vegetation/trees? • What implications do the outcomes have for green space plans? 	Micro urban heat island (MUHI) analysis	Green space planning and management data

2 REVIEW OF LAND USE, LAND COVER AND URBAN HEAT ISLAND

Many theories and methodologies have been proposed to examine and explain the dynamics of land use and land cover (LULC) and how they relate to urban heat islands (UHIs). Since this thesis may be read by people without a remote sensing background (e.g. planner, landscape architects), some initial introductory reviews relating to those two topics were required. This review will focus on nine major themes, although the literature covers a broad range of such theories. The themes to be covered are, urban LULC dynamics, UHI, green space planning for UHI mitigation, the impact of vegetation change on surface temperature, choice of RS imagery for measuring LULC and LST, previous UHI studies, choice of RS and GIS pre-processing, selecting a system of LULC classification and image classification. Those themes are discussed throughout the following two chapters.

2.1 Urban land use and land cover dynamics

Changes to the land surface are a result of both natural and human forces. Generally, the description of land surfaces is divided into two categories; land cover and land use. Land cover relates the physical state of the land surface (i.e. forest, vegetation, building and wet land) (Cheng et al., 2008). Land use denotes the human employment of land such as farm land, parks, settlements and cultivation. Given the close relationship of LU and LC, they are often used interchangeably (Verburg et al., 2009). A change of LULC is defined as the transformation of one LULC type on Earth's surface to another (Petit & Lambin, 2002).

Urbanized areas consist of mixed, complex interactions of social and economic development and regional resource exploitation that continuously support productivity levels and regional standards of living. Increasing human activity within the urban area brings massive changes in LULC patterns and has an

obvious effect on changes to urban ecosystems that make urban areas fragile (Weng, 2001; Yu, 2016). It has the effect of significant degradation in urban environmental conditions (Herold et al., 2003). These detrimental disturbances of environment are linked to global environmental and climate change due to their interactions with global carbon cycles, ecosystem processes, biogeochemical cycles, bio-diversity and human activities (Xiao et al. 2006; Yin et al., 2011).

As urban areas are strongly affected by population pressures and human activities, their size has constantly increased and turned them into highly dynamic regions. It has been projected that most of the world's mega cities are going to be in developing countries by the year 2017 (United Nations, 2007). Understanding the impact of surface processes requires long-term historical reconstructions at local and global levels and investigation of urban LULC can provide a viewpoint of the change trajectory from the past to the present. This information is useful for developing plans to reduce the deleterious effects on the environment linked to urban growth and to keep ecosystems functioning optimally (Serra et al., 2008). Spatiotemporal LULC information is important to develop rational economic, environmental and social policies (Long et al., 2007) and for understanding the impacts of various human activities on the overall urban environment.

2.2 Urban heat island

The term UHI commonly refers to the appearance of several micro and meso-scale climates that are warmer than the original climate at that scale, and that of surrounding areas (Zhou & Wang, 2011). Voogt (2004) refers to UHI as closed isotherms indicating areas at the surface or near the ground (canopy layer) that have relatively warmer air temperatures and are commonly associated with areas of human disturbance such as cities and towns. The UHI effect often decreases as city size decreases (Roth, 2013) and the precise size and form of this UHI effects varies in space and time as a result of meteorological, regional and city

characteristics. This means UHI formation is strongly influenced by the characteristics of LULC of each city.

2.2.1 Spatial structure of UHI effects

The size of a UHI is more related to the amount and type of city development than to the actual size of the city or the population (Xian & Crane, 2006). This means that fast growing, smaller megacities in developing countries may have more UHI than bigger and older cities situated in developed countries (Weng, 2009). Urban locations with ongoing urbanization trends experience dramatic increases in temperature due to the decrease in surface moisture and fractional vegetation cover (Owen et al., 1998; Srivanit et al., 2012). UHI occurs at various levels of the atmosphere and surface of the urban environment and have slightly different underlying mechanisms (Mitchell, 2011). Generally, there are two basic UHI types; atmospheric UHI that exists at urban canopy layer (UCL) and urban boundary layer (UBL), as well as surface UHI (SUHI) (Voogt & Oke, 2003). Those UHI types are different in the process of their formation, the techniques applied to measure them, their impacts and, the methods available to mitigate them (Oke, 1988). Figure 2.1 shows the spatial structures of the various UHI effects.

2.2.1.1 Boundary layer of UHI

An increase in urban air temperature at the urban boundary layer (UBL) (Fig. 2.1(a)) generates a dome of air that extends downwind of the city, with the warmer air dome often changed to a plume shape by wind (Voogt, 2004). As air flows from rural to urban areas, the boundary layer of UHI is largest under light winds when strong rural surface inversions exist. Conversely, the boundary layer of UHI is smallest under strong winds when the vertical air temperature distribution is more uniform. Moreover, the boundary-layer heat island is a local-to-meso scale phenomenon (Roth, 2013).

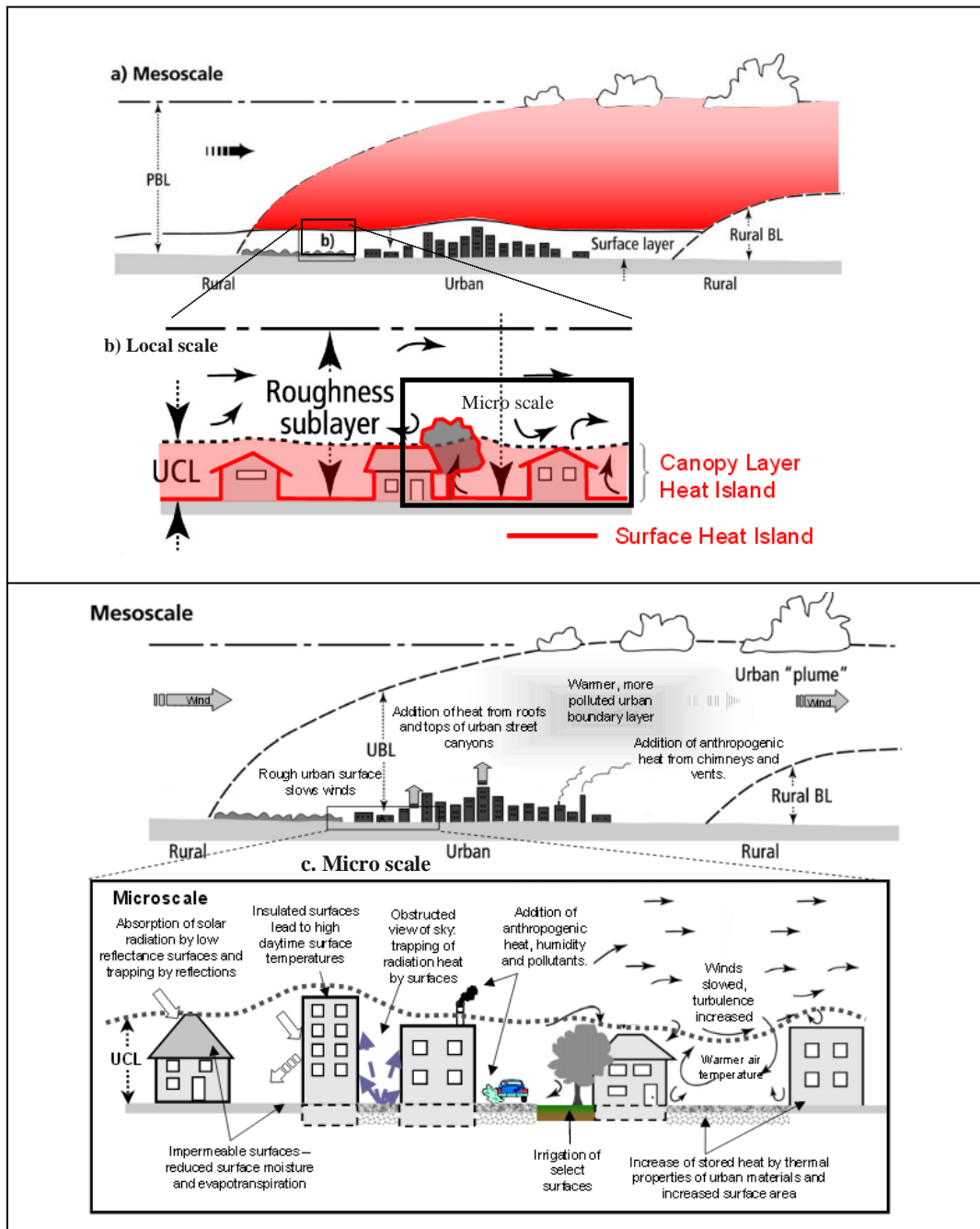


Figure 2.1 Spatial vertical structure of the city atmosphere on (a) a whole city (mesoscale), (b) a LULC area (local scale) and (c) a street canyon (microscale). The three UHI types linking to each scale is located on red shaded areas (thick line following surface in (b)) (Oke, 1988; Voogt & Oke, 2003; Roth, 2013).

2.2.1.2 Canopy-layer heat island

The urban canopy-layer (UCL) heat island is a local-scale phenomenon that is located in the area that starts from the ground, or just above the land surface, and extends to about the height of the trees and buildings or the roof-top level (Voogt & Oke, 2003). In addition, the canopy-layer heat island expresses the surface energy balance and it influences air volume inside the urban street canyon (Roth, 2013). The urban street canyon can be understood as the space between two parallel rows of buildings that are separated by a street and is the primary unit in new cities (Syrios & Hunt, 2008). Changes in street canyon temperature occur mainly through sensible heat transfer from the surface (Roth, 2013). The airflow processes known as ducting and trapping, as well as multiple reflections of radiation, occur within the UCL of UHI (Collier, 2006). Above the UCL, there is a turbulent wake layer called a roughness sub-layer (Figure 2.1 (b)) within which occur the wakes and urban boundary layers from individual buildings, groups of buildings, plumes of heat, pollutants and humidity (Collier, 2006).

Differences of rural-urban air temperature that are measured in the canopy-layer show remarkable temporal and spatial variation within a city and vary from one city to another. In addition, the diurnal variability of the canopy-layer heat island is highly pronounced (Roth, 2013). The most intense UHI often occurs on summer nights because impermeable construction surfaces absorb high amounts of solar radiation during the day and have a higher thermal conductivity and capacity for releasing heat stored at night (Xian & Crane, 2006), while most rural surfaces have cooled down. During the day, the sun's energy is absorbed by both rural and urban surfaces, heating rural vegetated surfaces more slowly, thus causing a difference in surface temperature between the two areas.

In the vertical dimension at meso and local scales of urban atmosphere, the atmospheric UHI presents significant variations between UCL (urban canopy-layer) and UBL (urban boundary-layer). The atmospheric UHI that is recorded at

canopy-layer may exhibit higher spatiotemporal variations because of the thermal properties of built-up surfaces that modify neighboring air temperatures. In contrast, UHI variations at the UBL may remain more stable as they are less influenced by the city structure (Voogt, 2004). Figure 2.2 shows the fluctuations in intensity that UHIs have over different LULC areas.

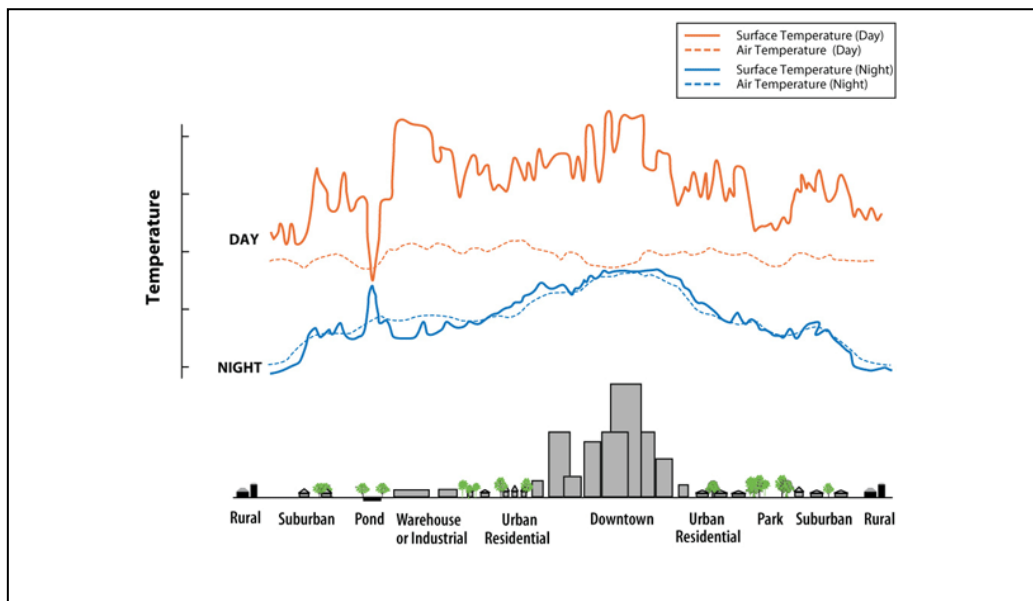


Figure 2.2 Fluctuations in intensity of UHIs vary over different LULC areas and at different times of the day (Roth et al., 1989; Voogt & Oke, 2003).

2.2.1.3 Surface UHI

Even though surface temperature is not equal to air temperature, it is the primary causal factor of ground temperature and is a critical factor that controls the urban thermal environment (Sun & Pinker, 2003; Mitchell, 2011). SUHI describes the heat island which can be detected from land surface temperature (LST) (Voogt and Oke, 2003). The SUHI exists over the entire three dimension (3-D) envelope of the surface and is recognized as a surface energy balance phenomenon that involves all city features (i.e., roads, roofs, walls, trees) (Roth, 2013). The surface temperatures in a micro-scale phenomenon commonly known as Micro Urban Heat Island (MUHI) are characterized by small SUHIs associated with the temperature of individual structures or groups of structures (Mitchell, 2011). The

spatial micro scale often occurs from sub-metre to 1 km scale and the spatial local scale occurs from 100 m up to 50 km (Oke, 1988; Roth, 2013). Thus, an overlap between the two scales is created. Consequently, to study SUHI at the micro scale, the lowest resolution of available thermal imagery from 90 m up to 1 km can be used. The same SUHI study at the micro scale was employed on the local scale extending from 1 km up to 20 km (Mitchell, 2011).

The patterns of MUHI are strongly governed by the orientation of the surface features to the sky and the sun and their thermal characteristics, such as heat capacity and reflective properties (albedo) (Voogt, 2004; Roth, 2013). Due to those conditions, and the strong heterogeneity of surface structures (i.e., vegetation, buildings, open soil), LST becomes a non-constant phenomenon and often displays rapid variations that fluctuate in intensity and spatial distribution over time. Moreover, the temporal fluctuations are diurnal, weekly and seasonal with the seasonal variability depending on latitude, daily warming pattern and cloud cover in the area (Oke, 1988).

LST in a given location is influenced by surface radiation and energy interchange and is often strongest during the daytime due to large differences in the response of solar heating between vegetated surfaces and roof or pavement surfaces (Roth, 2013). The amount of solar radiation absorbed and reflected back to the atmosphere is greatly affected by the surface material. Some materials absorb more energy while other materials reflect more energy. For example, vegetation absorbs more energy than open soil; the forest is normally cooler than an open field. At night, some of the processes are reduced, and therefore, urban-rural differences of LST are smaller than during the day (Roth et al., 1989) (Figure 2.2).

2.2.2 UHI assessment

Traditionally, atmospheric temperature data for UHI study are directly measured from climatology stations or collected along mobile traverses by thermometers. It

is inconvenient to obtain detailed spatial distribution of temperature because of limited locations for atmospheric temperature quantification (Zhang & Wang, 2008). However, a direct assessment of atmospheric UHI through RS is still possible. RS sensors can only assess surface temperature at coarse scale (Colombi et al., 2007) and higher altitudes or at the boundary-layer (Voogt and Oke, 2003). Besides being used to measure air temperature, RS sensors with the thermal remotely sensed data are also used to acquire UHI temperature distribution at the surface because RS sensors usually observe thermal radiation on the surface. This is a type of indirect measurement of UHI as UHI is actually a phenomenon of atmospheric air temperature.

The air temperature tends to be lower than surface temperature and the daytime correlation between LST and LULC is much stronger than that for air temperature (Roth, 2013). Relating LST and air temperatures is complicated and their variability is difficult to predict and depends on such factors as albedo, emissivity, thermal capacity of the surface, wind speed and moisture level of the atmosphere (Roth, 2013). Moreover, there is no simple general relationship available (Mitchell, 2011). As a result, it is easy to misinterpret canopy-layer heat islands using assessments of LST without examining the differing source areas for the two assessments and atmospheric effects that affect air temperatures (Roth, 2013). To deal with these problems and considering the nature of LULC, extracted LST of remotely sensed data using Planck's function requires adjustment for spectral emissivity (Artis & Carnahan, 1982). The emissivity corrected LSTs can be applied by estimating land surface emissivity that can be obtained using NDVI threshold (Sobrino et al., 2004; Oltra- Carrio et al., 2012). Moreover, in order to correct the different year and seasonal factors of multi-temporal datasets, standardization of LST is also needed. It is necessary to accommodate the temporal consistency and spatial comprehensiveness of the dataset comparison (Salama et al., 2012). Table 2.1 shows the summary of characteristics of surface and atmospheric UHI.

Table 2.1 Characteristics of surface and atmospheric UHI (Voogt & Oke, 1997)

Feature	Atmospheric UHI	Surface UHI
Typical identification method	Direct measurement <ul style="list-style-type: none"> • Fixed climatology stations • Mobile traverses 	Indirect measurement: RS analysis
Typical representation	<ul style="list-style-type: none"> • Isotherm map • Temperature graph 	Thermal map
Peak intensity	Less variation: Day : (-1 -3°C) Night: (7-12°C)	More spatial and temporal variation: Day: (10-15°C) Night: (5-10°C)
Temporal development	<ul style="list-style-type: none"> • Small/non-existent during the day • Most intense at night/predawn/winter 	<ul style="list-style-type: none"> • Appear at all times of the day and night • Most intense in the summer and during the day

2.2.3 Impacts of UHI

The global average LST increased by about 0.6 °C in the 20th century (IPCC, 2007). It is predicted that by 2050 it will be 1-2°C warmer than in 1980-99 (Meehl, 2007). There has been rising concern about the impact of the increase of temperatures on urban environments and the interaction with UHIs (Coutts et al., 2010) that can have serious detrimental effects on human health, economic activity and environmental well-being.

a) Health

UHI intensity peaks often can cause fatalities due to thermal stress on cardiovascular and respiratory systems. The elderly and people with medical problems are most at risk (US EPA, 2009). Extreme heat can lead to heat related stresses such as heat stroke, sun burn, heat cramps, dehydration and heat-related mortality. India experienced a severe heat wave in the summer of 2015 resulting in more than 2,000 deaths (United Nations, 2015) and heat stroke can continue to affect inhabitants up to two years after the event as identified by Argaud et al. (2007).

b) Economic

Increasing heat islands leads to an increase of energy consumption as air conditioners work against a large heat gradient to maintain optimal temperature of buildings. Uncomfortably hot conditions increase electricity

costs per year. The increase of energy demand and costs may induce significant economic impacts.

c) Environmental

UHIs can cause a host of environmental problems. The overall energy consumption for cooling impacts CO₂ levels and thermal pollution. Stormwater that falls in the city often runs across impermeable surfaces (i.e.; pavement and rooftop) that transfer excess heat to the runoff. This heated storm water also picks up additional dust and chemical loads before it drains into sewers. Higher water temperatures affect the life cycles of organisms living in the waterways (Krause et al., 2004). In terms of meteorological impacts, UHIs are associated with smog formation, induction of precipitation and thunderstorms, reduction of snowfall frequency and intensity and modification of the diurnal and seasonal range of freezing temperatures (Bornstein & Lin, 2000). UHIs also affect surrounding wildlife and ecosystems. Changing precipitation patterns and increased UHIs can mean that species move outside their thermal tolerance range and that vegetation is more prone to fire (Valle-Díaz et al., 2009). With all of these negative impacts of UHIs, learning and controlling factors that influence them is required.

2.3 Influencing factors of UHI formation

Many factors contribute to the spatial characteristics of UHI formation that also can be linked to UHI mitigation efforts. Figure 2.3 shows these factors with solar energy as the key driving energy of UHIs. These factors can be generally divided into controllable factors that are influenced by features of urban areas and uncontrollable factors (Harman & Belcher, 2006; Rizwan et al., 2008; Aguiar, 2012). The detailed processes of these influencing factors in creating UHI effects should be explained together with the physical properties of the controllable factors. This is because mitigation efforts focused on altering controllable factors, mainly through increasing green spaces, are the most feasible in developing

countries where most green space around the existing infrastructure is still open and the structural elements of the city is still able to be changed.

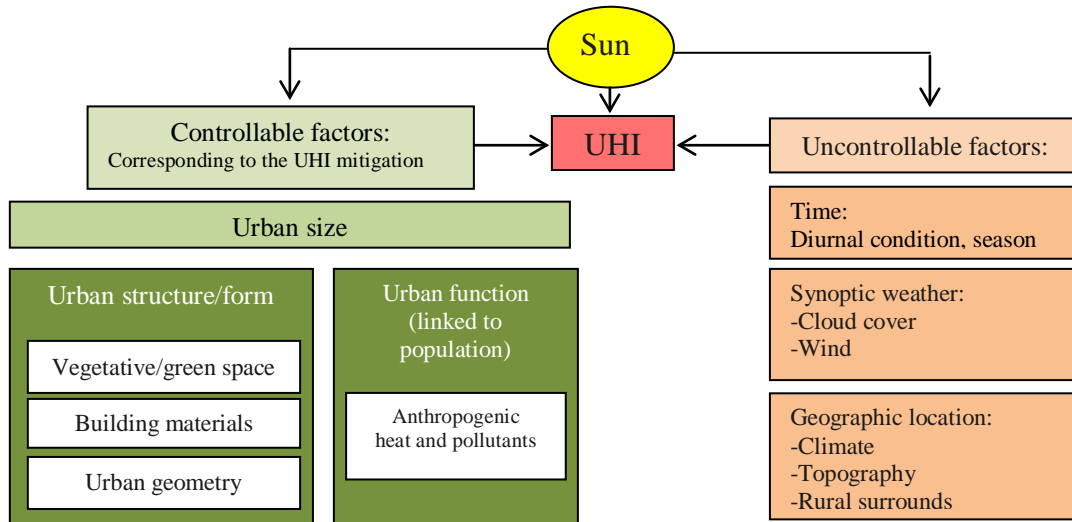


Figure 2.3 Influencing factors created UHI (modified from Oke, 1997; Rizwan et al., 2008; Aguiar, 2012).

2.3.1 Surface energy balance

UHI formation is strongly sensitive to the flows of energy and water in order to balance the surface energy budget. An equation that measures the balance of outgoing and incoming energy flows is given by a surface energy budget. The surface energy budgets between urban and rural areas are different because of differences in LULC, level of human activity and surface characteristics (USA EPA, 2009). These differences influence the production and flow of heat that leads to different air temperature and LST in cities versus rural areas.

Figure 2.4 illustrates the surface energy balance system that is influenced by physical properties of surfaces particularly vegetative and soil surfaces and creates an impact on local temperature. The short wave radiation refers to radiant energy within the wavelengths of 0.1 μm and 5.0 μm in the visible (VIS), near-ultraviolet (UV), and near-infrared (NIR) spectra and the long-wave radiation is the energy radiating from the Earth as infrared radiation at low energy to Space (Sundstrom,

2014). Both the incoming short-wave energy and the emitted long-wave energy have to be balanced through the process of radiating energy, conduction of heat and evaporation. Particular surfaces' properties, including albedo, emissivity and soil moisture, determine the amount of energy that is available for latent heat, emitted or reflected (USA EPA, 2009). When surfaces hold more energy than their surroundings, they give off sensible heat (Iguski and Jackson, 2008) and the hotter the surface, the more energy it radiates (USA EPA, 2009).

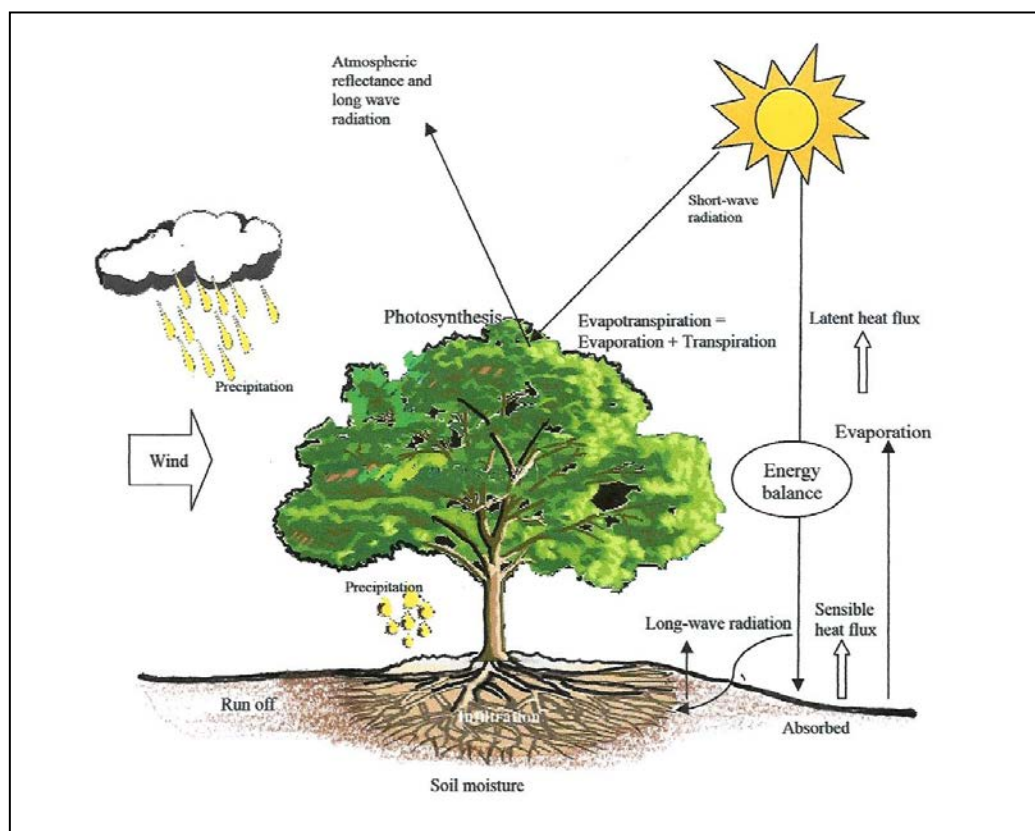


Figure 2.4 Energy balance system and physical properties of surfaces that influence the local temperature (modified from Iguski and Jackson, 2008).

2.3.2 Vegetative surfaces in UHI formation

Vegetation can influence the amount and type of energy exchanged between the land and the atmosphere because vegetation takes in carbon dioxide for photosynthesis and gives off water in a process called evapotranspiration and thus,

can reduce local surface and air temperature and alleviate UHI effects. In order to balance the energy budget, a change in the incoming energy and/or evaporation leads to a change of surface temperature. In vegetative surfaces, evaporation occurs during the conversion of water from a liquid to a gas in the surrounding soil of vegetation. Vegetation regulates its temperature using absorbed energy with stomatal conductance and transpiration (Igusky & Jackson, 2008), meanwhile, moisture on the soil's surface affects the availability of latent heat to control evaporation (Kessler & Jaeger, 1999; Godfrey et al., 2007). Water vapor that is given off through evaporation stores latent heat that, when released, condenses in the atmosphere and gives off water, reducing the air temperature (Kessler & Jaeger, 1999). Latent heat is usually detached to the atmosphere when water is evaporated and the latent heat transforms to sensible heat when water alters phase from water vapour to liquid water (FAO, 2005). Flux refers to the rate of flow at which energy is moved and the net energy flux of each surface is affected by physical properties of the land surface (Snyder et al., 2005) that vary between different LULC types.

In addition to evapotranspiration (ET), the ability of vegetative surfaces to influence temperature is mostly influenced by surface albedo and roughness (Kim, 2007; Igusky & Jackson, 2008; Chen et al., 2013). The surface's solar reflectance or albedo determines the amount of short-wave radiation that is reflected or absorbed. Since the color of vegetation influences its capability to absorb different amounts of energy it also influences albedo. Light-colored surfaces that have high albedo reflect shortwave radiation and dark-colored surfaces that have low albedo absorb shortwave radiation (Portier et al, 2010) For example, compared to grasses, trees are darker and commonly have a lower albedo. Thus, trees absorb more solar radiation than grasses and crops at the surface. The roughness of vegetative surface also can affect near-surface wind leading to varying impacts on fluxes of water and energy from the land surface. The rougher the surface, the more it slows the winds down (Igusky & Jackson, 2008). All these tree

capabilities give more benefits in tropical areas, such as the study area, since they only have a dry and rainy season and are mostly covered by evergreen trees.

The surface's emissivity determines the amount of long-wave radiation that is emitted and exiting to clouds that absorb or re-emit this radiation (Kessler and Jaeger, 1999). In the tropics that commonly consists of persistent clouds. The process of evaporation also leads to cloud formation. Clouds absorb both short-wave radiation and long-wave radiation although absorption by clouds is very small that are reflected from the surface of the Earth. Some energy is emitted as atmospheric long-wave radiation and the remaining energy is re-emitted to the Earth's surface where it is absorbed and becomes heat energy (US EPA, 2009).

2.3.3 Impervious surfaces and UHI formation

Compared to vegetation that mostly cover rural areas, impervious surfaces in urban areas, such as rooftops, buildings, and parking lots emit less long-wave radiation back to the atmosphere. More solar radiation that contributes to higher air temperature is absorbed by impervious surfaces. As a result, thermal storage increases in cities. Thermal storage is governed by the thermal properties of urban geometry and building material properties as shown below:

a) Building material properties

The materials of buildings' surfaces are important in determining the interaction between the surface and incoming solar radiation. The physical properties of building material (i.e. albedo, solar reflectance, emissivity, heat capacity, thermal conductivity) influence UHI formation. These properties are responsible for heating surfaces (Golden & Kaloush, 2006) and determine the amount of solar radiation that is reflected, emitted and absorbed (US EPA, 2009).

Building surfaces with high solar reflectance can emit most of the incoming heat energy. Therefore, less heat is absorbed and stored in the object and vice

versa. With more impervious surfaces, absorbed heat increases surface temperatures and contributes to the formation of surface and atmospheric UHIs. Solar reflectance is strongly correlated with a material's color because most solar energy comes in visible wavelengths. Darker buildings tend to have lower solar reflectance and albedo than lighter buildings. Hence, light-colored materials reflect more of the incoming energy of the sun than dark objects that absorb most of the incoming energy (Chudnovsky et al., 2004). Therefore, roofs may be designed to reduce the amount of heat that is transferred directly to the building by employing the use of materials and colors that have a high albedo (Aguilar, 2012). A dark roof, which absorbs most of the incoming solar radiation, heats the house and surrounding area and increases energy consumption required for cooling.

Parker and Barkaszi (1997) found that applying high albedo coatings to a building's roof results in reduction of air conditioning energy use by 2% - 43% in the homes. However, some materials have a high solar absorption even when light-colored, such as asphalt (Bretz et al. 1998; US EPA, 2009). Cool roads reduce the absorption of asphalt by using highly reflective aggregate in the asphalt (Aguilar, 2012). Some dark colored materials also have the ability to reflect short-wave radiation due to the use of special materials that have a solar reflectance close to that of white or light-colored materials (US EPA, 2009). Figure 2.5 shows the impact of the difference of colored materials and roughness of material surfaces on LST. Surface temperatures are measured on different roof colors in an ambient temperature of 35°C.

Besides solar reflectance, emissivity, heat capacity and albedo also play important roles in the determination of a material's LST. Thermal emissivity is a descriptor of surface capability to store heat or emit infrared radiation. High emissivity can keep a surface cool because the heat will be released immediately. Most construction materials have high thermal emittance values with the exception of metal. A material's heat capacity refers to its capability

to store heat. For example, a surface that is constructed of steel and stone in cities typically absorbs and stores more of the sun’s energy as heat than does a surface composed of soil (US EPA, 2009).

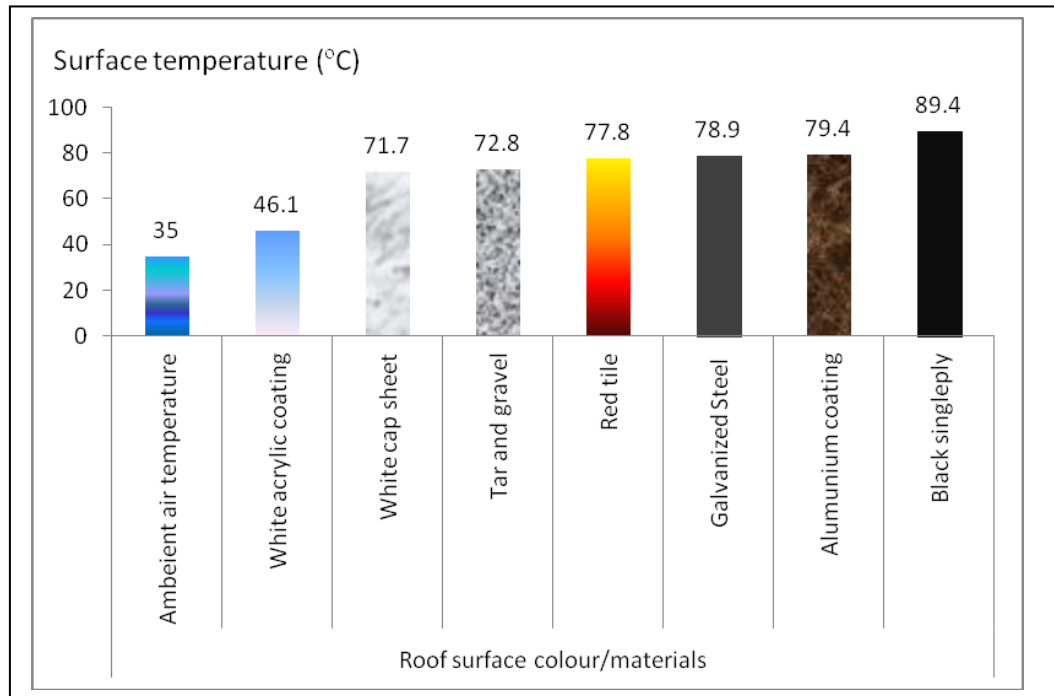


Figure 2.5 The impact of roof surface colors and materials on the LST (modified from cooltexasbuildings, 2015).

b) Urban geometry

Urban geometry describes the dimensions and spacing of buildings within a city and influences UHI formation mainly at night. It determines wind flows and influences the solar radiation that can be received and absorbed as well as emitted back to atmosphere as long-wave radiation (US EPA, 2009).

The urban canyon, as explained above, is one aspect of urban geometry (Sundara Kumar et. al., 2012). Urban geometry can lead to incoming short-wave radiation being reflected on close surfaces, such as vertical walls within the urban canyon. The reflected short-wave radiation then is absorbed or stored rather than emitted to the atmosphere as long-wave radiation or heat.

As a result, buildings tend to have high daytime surface temperatures. In this process, the wind that reaches the inner city tends to flow slower and leads to turbulence within the street canyon.

At night, because of the dense buildings in developed cities with low sky view factor (SVF) (see Figure 2.6), the stored long-wave radiation cannot easily be released to the atmosphere. This trapped heat then contributes to the UHI. The air temperature above downtown areas particularly at night is warmer than air temperature over rural areas (US EPA, 2009). Furthermore, the incoming short-wave radiation absorbed by ground surfaces such as roads and pavement is not easily released out of the urban region because there is only a small “sky view” from the ground. Therefore, physical objects absorb most of the emitted heat from the ground, keeping the heat within the city (Sailor & Fan, 2002). In a well-planned city, to reduce the formation of UHI, urban street canyons are constructed in such a way as to allow good airflow between buildings, thus enabling surfaces to release radiation more readily into the atmosphere.

2.3.4 Anthropogenic heat and pollutants

Anthropogenic heat and pollutants are considered as secondary contributors (Li & Zhao, 2012) that affect atmospheric UHI (Ferreira et al. 2010). Anthropogenic heat refer to the heat produced from human activity such as from industrial facilities, motor vehicles, air conditioners, and various other human sources which contribute to the energy budget. Athropogenic heat varies by urban activity and infrastructure and it typically contributes to UHI formation in dense urban areas. Reduction of waste heat through reducing the use of electrical sources is a possible effort to mitigate UHI effects. For example, Kikegawa et al. (2003) found that a reduction in the waste heat of air conditioners could result in a temperature decrease of 1°C and an efficiency increase of 6%.

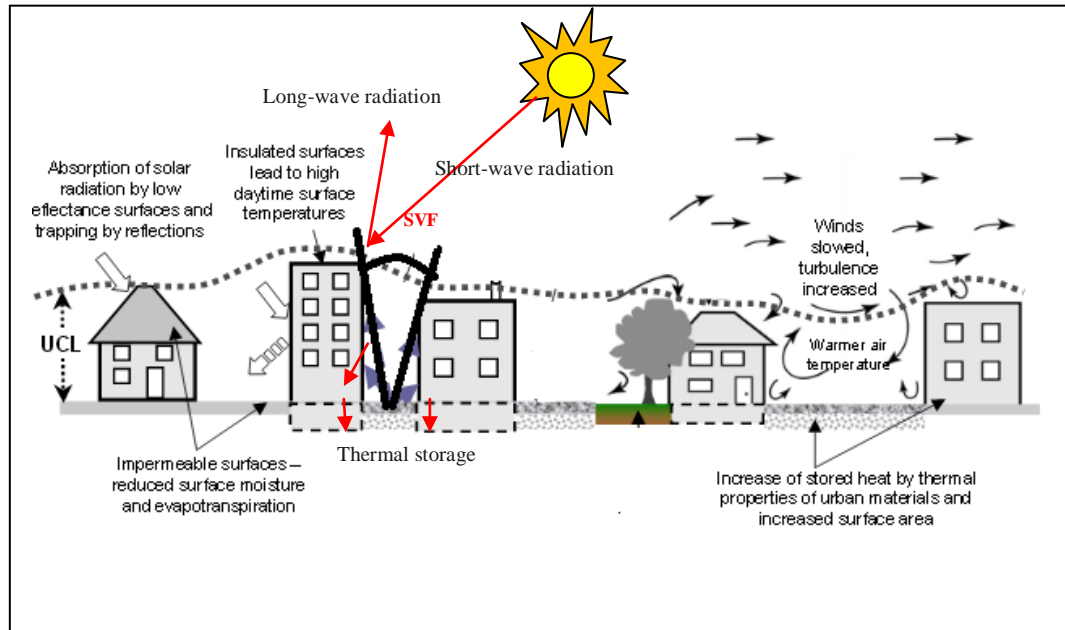


Figure 2.6 The impacts of impervious surfaces on UHI formation (Voogt and Oke, 2003).

2.4 Green Space Planning for UHI Mitigation

Green space plays an important role in controlling temperatures, particularly in urban areas. Green spaces can be understood as areas that are covered by planted and natural vegetation in built-up and planned areas and consist of permeable surfaces (i.e grass, open soil, bush, and tree). Urban green spaces exist as semi-natural areas, such as managed gardens and parks provided by separated vegetative pockets linked to roads and subsidiary places (Jim and Chen, 2003; M'Ikiugu et al., 2012).

In Indonesia, law 26 on spatial planning of the year 2007 defines green space as an open area for plants, both naturally and intentionally planted, to grow. Types of urban green spaces include recreational areas, green belts at a riverbank or along a beach, agricultural land, urban forests, botanical gardens, nurseries and residential parks. This law also rules that, in order to control human activity and urban development, at least 30% of the urban area should be established as open green space (Indonesia Ministry of Public Works, 2010). Because green spaces

have been proven to reduce UHI directly (Feizizadeh et al., 2013) a causal link between LST and green space changes is required in order to plan and manage green space. It is also in accordance with the study purpose to reduce UHI effects using the potential information from spatiotemporal distribution of LSTs and spatial variability of LULC elements which consists of vegetation.

2.4.1 Characteristics of green space

Numerous studies have shown that an increase in the proportion of vegetation cover can significantly decrease LST because the increasing size of green space affects enhanced ET of vegetation that can cool daytime surface temperature (Hamada and Ohta, 2010). Moreover, it is necessary to carefully consider the location of tree planting to achieve potential climatic benefits. Information about vegetation characteristics is required to understand a surface's energy budget and the effect on the local and regional climate. The minimum area (size) and structure (i.e. population, size, and type of selected plant) of green space are essential characteristics in optimizing green space planning for local climate amelioration (Indonesia Ministry of Public Work, 2010).

According to Matthews (2015), the planning, design and management of green space infrastructure for adapting climate change should recognize multiple rationales linked to green infrastructure. They include the scale of the area available for greening (i.e. rooftop, building wall, and a city block), history of site, soil compaction, drainage problems, structural engineering, geological concerns and the climatic zone (i.e. temperature, precipitation, wind effects). The choice of vegetation used is also important, including its structure, growth form and tolerance limits. For instance, groundcovers require different water, light, nutrient, temperature and root-mass compared to broad-leaf trees. Each vegetation type has different rates of growth, levels of disease resistance, and capacities to provide biogenic services (e.g. sequestering carbon, filtering water, lowering ambient temperatures). Thus, in order to have a maximum greening result, those

biophysical factors of vegetation to be used for urban greening should be considered. Despite biophysical factors, the successful green space infrastructure for mitigating climate change was determined by agency and institutional capacities that are often ignored while they have essential roles for decision-making and cross-departmental coordination in making effective green space infrastructure interventions (Matthews, 2015). Figure 2.7 shows the measurement concept of green infrastructure for adapting cities to climate change that should have to be taken into account (Matthews, 2015).

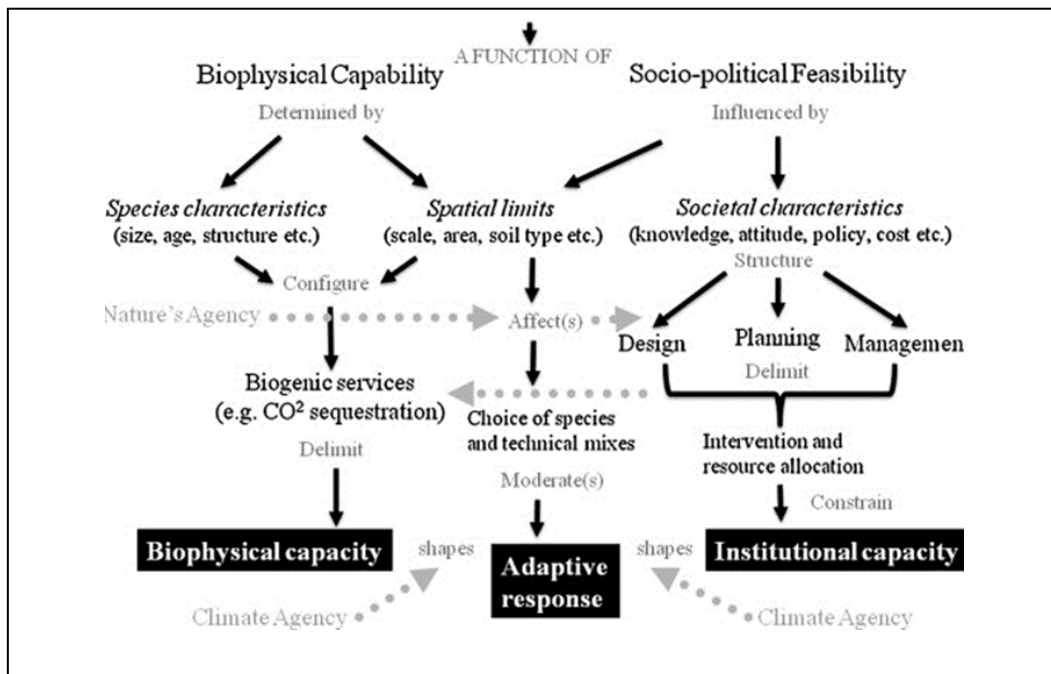


Figure 2.7 Capacity of green space in climate adaptation (Matthews, 2015).

The effects of green space in order to reduce UHI effects can also be achieved by suitable composition and configuration of green space (Li et al., 2012; Li et al., 2013, Maimaitiyiming et al., 2014). Composition of green space refers to the form and structure of vegetation that determine the capability of the vegetation to lower the air temperature (Igusky and Jackson, 2008; Chen et al., 2013), while configuration of green space places emphasis on the green space distributions. Irwan (2008) reported that a spreading form of stratified urban forest can reduce air temperature by 2.28%, while a clustered form of stratified urban forest can

reduce air temperature by 3.04%. In addition, compared to evergreen forests, deciduous or mixed forests appear to have lower LST over the evergreen forest canopy as they have higher albedo (Igusky and Jackson, 2008). This is due to the relative amounts of transpiration from each forest and the energy budget of the vegetative surfaces (Igusky and Jackson, 2008). Therefore, for tropical areas that only have dry and rainy seasons, selection of evergreen structure for the vegetated areas would give greater long-term benefits in reducing LST.

2.4.2 Vegetation cover indices to represent vegetation condition and the impacts on surface temperature

More vegetated areas have a higher level of latent heat exchange, while sensible heat exchange is more favored by sparsely vegetated areas (Oke, 1982). This finding encourages study of the relationship between vegetation abundance and LST (Weng et al., 2003; Salah 2011). It is known that vegetation indices such as NDVI obtained from RS images are able to be used for assessing vegetation cover and are ideal to represent the condition of vegetation (Tian and Xiangjun, 1998; Chen et al., 2006). Soil background and shadow, plant species, and leaf area contribute to the NDVI variability (Jasinski, 1990). It is also possible to use NDVI to characterizing the LULC types thus establishing the relationships between NDVI and LST. NDVI measurement is a function of the near-infrared and visible reflectance from plant with Eq. (2.1) and is generally used to express the density of vegetation (Rouse et al., 1974).

$$NDVI = (NIR - R)/(NIR + R) \quad (2.1)$$

2.5 The Impact of Vegetation Change on Surface Temperature

Vegetative surfaces utilize solar radiation for transpiration and release water vapour that contributes to a reduction in air temperature. However, urban impervious surfaces typically replace vegetation throughout the city. As vegetative surfaces have different properties, any alteration to them not only

changes the physical properties of the surface, but also changes local climatic conditions such as wind speed, humidity, and air temperature (Rost and Mayer, 2006), potentially increasing the chance of surface heat. Figure 2.8 shows the different impact between green space and impervious surfaces on ET, infiltration and run off processes.

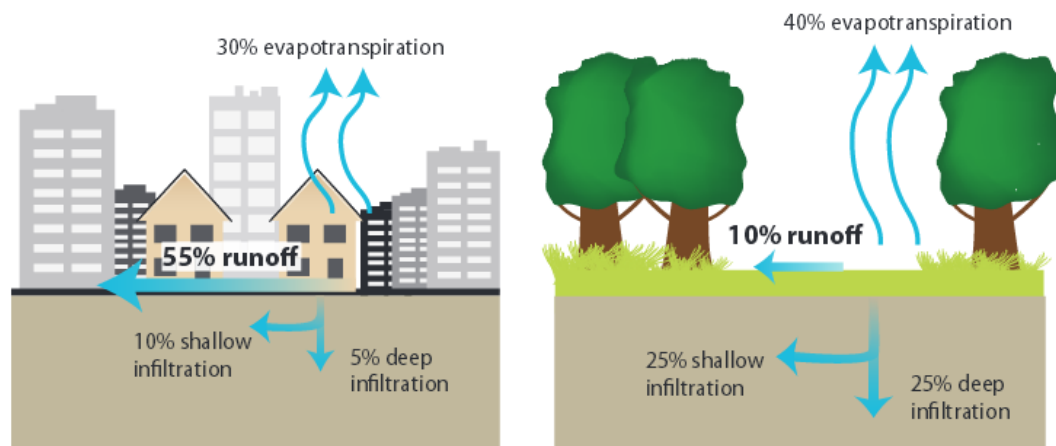


Figure 2.8 Reduced green space and impacts of impervious surface on UHI (US EPA, 2009).

Afforestation should provide a cooling effect. The increase of vegetation cover affects the surface energy budget, LST and air temperature by redistributing surface energy (Ma et al. 2013). Ma et al., (2013) state that the effect of a change of vegetation cover on short term climate showed that annual mean LST significantly decreased by 0.93 °C in response to afforestation. Another study shows afforestation can decrease LST by about 1.1 ± 0.5 °C (mean \pm 1 SD), on average (Peng et al., 2014). On the other hand, the loss of trees replaced by impervious surfaces can significantly increase LST in neighborhoods (Rogan, 2013). A decreased or fragmented vegetative area causes a decrease in surface evaporation that leads to an increase in LST (Deo, 2011).

A study by Tursilowati et al. (2012) combining modelling of LULC and air temperature data concluded that significant reduction of UHI area can be achieved by the addition of widespread grassland. However, another comparison study by

Swann et al., (2010) shows that compared to grassland, forest (linked to woody trees), can provide a greater advantage in terms of direct surface cooling effects. Forest that was converted to grassland and crop land also shows a surface temperature increase of 3-5 °C (Hollinger et al., 2010). The color of woody trees is darker than grassland (lower albedo) causing them to absorb more solar energy to be used for transpiration and creation of more water vapor (Swann et al., 2010). Thus, it has also been noted that the cooling effect of vegetation is mainly driven by enhanced ET produced by increased vegetation cover. Figure 2.9 shows the impact of afforestation on surface temperature properties.

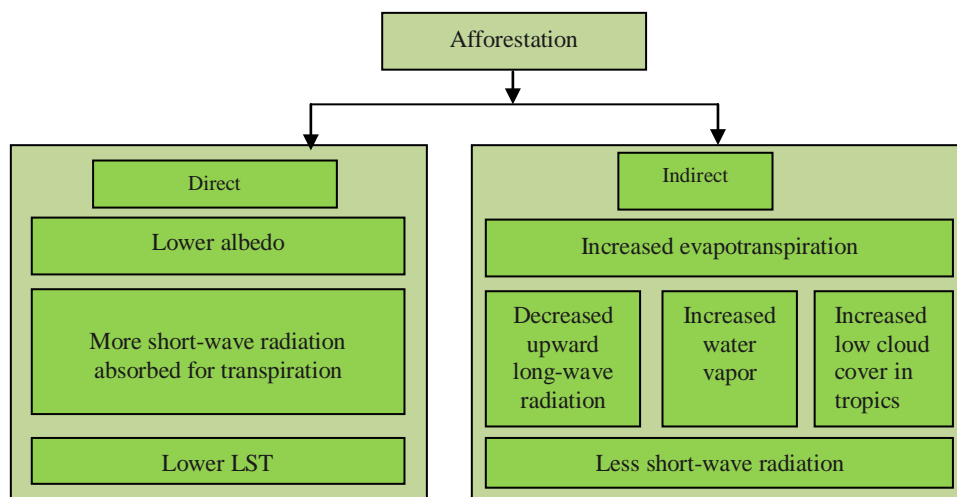


Figure 2.9 The impact of afforestation on surface temperature.

The ability of trees to provide more indirect cooling also comes through their shadows, an effect that cannot be provided by grassland. The shade of a tree can reduce the LST of grass by 4 °C and the LST of concrete surfaces by 12 °C (Armson et al., 2012). The lower LST of forest as compared to grasslands is also due to forest being rougher and thus, able to exchange sensible heat more effectively and transpire more across a smaller temperature gradient (Balddochi & Ma, 2013). As a result, forests provide less run-off for stream flow (Marc & Robinson, 2007) and recharge less groundwater (Kim & Jackson, 2012).

2.6 Chapter Summary

The purpose of this review was to examine some aspects of LULC dynamics and spatial characteristics of UHI effects, and planning urban green space infrastructure. It is important to evaluate the relationship between these themes given UHI's effects on environment quality, human health and energy use. UHI formation is sensitive to different flows of energy and water between urban and rural areas that are caused by differences in LULC, level of human activity and surface characteristics. Those differences influence the production and flow of heat that leads to different air temperature and LST in cities versus rural areas. Controllable factors (vegetation, building material, urban geometry, anthropogenic heat and pollutants) and uncontrollable factors (time, synoptic weather and geographical location) contribute to the spatial characteristics of UHI formation. There is no doubt that the main impact of UHI phenomena are from the very considerable replacement of vegetation cover. However, as the precise size and form of UHI's effects varies in space and time and depends on controllable urban surface characteristics and surface properties, the linkage between local-micro LULC change and the level of UHI effects, particularly in developing tropical areas, still requires deeper study.

3 REVIEW OF RS IMAGERY AND GIS PROCESSING FOR MEASURING LULC AND LST

3.1 Choice of RS Imagery for Measuring LULC and LST

Studies of UHI effects have shown that the partitioning of latent heat and sensible fluxes, and the resulting surface temperature response, is a function of varying water content, soil surface, and vegetation cover (Weng et al., 2006). The latest multi complex ability of RS and spatial analysis technology has made information on spatial pattern and condition available. “The development of RS and GIS technology has not only led to greater understanding of the spatial relationship between different uses of the land, but also facilitates the recording of emitted energy from throughout the electromagnetic spectrum and provides historical evidence at particular times”(Loveland & Defries, 2013). Moreover, RS imagery is also valuable in assessing both LULC and enabling detailed mapping of LST at the same time. The thermal data made available by RS sensors offer the ability to produce accurate models of urban climatic phenomena, such as UHI effects, correlating and modeling LST with LULC types and vegetation, in addition to being a useful tool for monitoring the increasing urbanization and environmental effects of regional climate change (Quattrochi et al., 2000, Taubenbock et al., 2011, Aduah et al., 2012; Tursilowati, 2012). The availability of LST data from remotely sensed thermal imagery over a whole city makes it possible to see distinct differences in the temperature of multiple LULC characteristics at once (Voogt & Oke, 2003; Yuan & Bauer, 2007;).

3.1.1 Characteristics of RS imagery

The increased availability of satellite imagery offers repetitive data coverage at a range of spatial, radiometric, spectral, and temporal resolutions (Stoney, 2006). The exact resolution to be used is decided by the type of mission and sensor characteristics. Choosing the appropriate RS sensor for any study requires

consideration of the study objectives, image costs and the technical processes that are involved in image analysis and interpretation.

a) Spatial resolution

The spatial resolution of an RS sensor describes the minimum area or size of detail of a feature and pattern that can be identified on an image and it is generally divided into three categories: coarse, moderate and fine resolution (Loveland & Defries, 2013). Fine spatial resolution of RS data reduces the size of the gap between field and remotely sensed data perceived with coarse resolution satellites (Rocchini, 2007). Sensors with spatial resolutions of 5 m/pixel or less are considered to be very fine resolution. Spatial resolutions greater than 5 m/pixel and up to 30 m/pixel are considered moderate and sensors with greater than 30m/pixel ground resolution are considered coarse resolution (Stefanov et al., 2004). A lot of effort has been put into delineating LULC from a local scale to global scale by applying different multi-temporal and multi-source remotely sensed data. Moderate-fine resolution data is useful to detect the changes in classes and is most accurate when distinguishing LULC types in a heterogeneous, complex urban area (Loveland & Defries, 2013).

Moderate resolution satellite imagery such as Landsat is the most common data type for monitoring and mapping LULC changes. It has been successfully utilized for assessing LULC changes, especially in land areas that have been affected by human activities to varying degrees. For example, Pan et al., (2013) used Landsat Multi-Spectral Sensor (MSS), Landsat Thematic mapper (TM) and Enhanced Thematic Mapper (ETM+) for detecting LULC changes in the Eastern Gulf coastal between 1985 and 2005. Reis (2008) used Landsat MSS and Landsat ETM+ images for detecting LULC in Turkey. However, the relatively coarse-medium spatial resolution image often is not able to meet specific project requirements of a complex LULC classification, especially in a complex urban rural landscape (Lu & Weng, 2005). Even though the utility of coarse-medium spatial resolution images may not be good for working at

urban and local scale, it is useful while working at regional, metropolitan and higher scales.

The use of high spatial resolution sensor data, such as SPOT, IKONOS and Quickbird, enables highly detailed detection of LULC of urban and rural areas and impervious surface mapping in urban areas (Wang et al., 2004; Lu and Weng, 2005). The highest available resolution of satellite imagery is desirable when used for land applications, urban vegetative information, detecting open spaces, streets and individual buildings in the urban environment (Yüksel et al., 2008). A major advantage of these high spatial resolution images is that such data greatly reduce the mixed-pixel problem (Lu & Weng, 2005), providing a greater potential to extract much more detailed information on LULC structures than medium or coarse spatial resolution data. However, when using high spatial resolution images some new problems emerge, notably the shadows caused by topography, tall buildings, and trees (Zhou et al., 2008), and high spectral variation within the same LULC class. These disadvantages may lower classification accuracy if the classification method cannot effectively deal with those problems (Moran, 2010). A high spatial resolution image is also much more expensive compared to the coarse-medium resolution images that are often freely available. Moreover, the utility of higher spatial resolution images at the regional level is complicated by the cost of how long they take to analyze. It can also prove to be impractical as it provides too much detail for the level of generalization appropriate to decision making.

RS techniques in LULC mapping principally uses passive (optical) RS sensors which work during daylight hours as their optical sensors record reflected radiation in the electromagnetic spectrum. Passive RS can be ineffective in a humid tropical area with persistent cloud cover, as is often the case in Indonesia. Therefore, radar as an active RS would be a good alternative source because it can penetrate the persistent clouds. Synthetic aperture radar (SAR)

has an advantage over optical data (high, medium and low-resolution images) and is able to acquire data both day and night (IPCC, 2003). The increasing availability of SAR data from satellites has also contributed to urban studies in the areas of urban feature mapping and LULC classification (Dell'Acqua et al., 2003). However, SAR data is from commercial systems that tend to be more expensive relative to government built and operated programs. Thus, the use of SAR in a large study area has an impact on the study costs which is a significant issue in developing countries. Moreover, it also has less spectral information and a problem with speckle noise that makes detection of heterogeneous LULC challenging (Chen, 2008). The characteristics of the most common sources of remotely sensed data are shown in Table 3.1 .

b) Spectral resolution

Spectral resolution refers to the number and width of spectral bands of a particular sensor. The spectral resolution achievable is categorized into three types; multispectral, panchromatic, and hyper spectral sensors. Multispectral imagery is a powerful tool for discriminating LULC by utilizing several bands. However, as the bandwidths of these sensors are generally quite large, subtle differences between LULC types are hard to recognize. A panchromatic channel is available in some satellites such as SPOT and Landsat ETM+. Both multispectral and panchromatic sensors are sensitive to radiation across several wavelengths from the visible to near infrared portions of the spectrum. Hyper spectral sensors have many more bands of imagery than multispectral sensors at narrower bandwidths but hyper spectral sensors have a much higher cost. Precise information may enable the distinguishing of more subtle differences in LULC. To reliably identify a particular object, the spectral resolution of the sensor must match to the spectral reflectance curve of the particular object in question. Spectral coverage of high spatial resolution images data is often limited to the near infrared and visible wavelengths (Jensen, 2000; Stefanov, 2004). Moreover, the lack of thermal bands and relatively short-period archives limits their effective use for the multiple applications of the spatial temporal study of LULC and LST information.

Characteristics of the spectral resolution of orbital sensor systems can be seen in Table 3.2.

Table 3.1 Characteristics of the most common sources of remotely sensed data (modified from Loveland and Defries, 2013)*

Type	Sensor/product	Spatial resolution	Date of observation	Temporal resolution	Cost
Coarse resolution satellite sensor (100 to >1 km)	NOAA-TIROS	1.1 km	1978-present	1 day	Free
	SPOT VEGETATION	1.15 km	1998-present	26 days	Free
	ADEOS II	7 km x 6 km, 250 m -250 km	2002-2003	10 days	
	EOS AM and PM (MODIS)	250-1000 m, 275 m	1999-present	2 day ⁻¹	Free
	Envisat	350-1200 m, 150-1000 m	2002-present	35 days	Not free and free
Moderate Resolution Satellite sensor (10-100 m)	SPOT	20 m; 10 m	1986-present	26 days	Not free
	ERS	30 m	1995-present	30 days	Not free and free
	Radarsat	10-100 m	1995-present	24 days	Not free
	Landsat	30 m	1984-present	16 days	Free
	Landsat	15-100 m	2013	16 days	Free
	EOS	15-90 m	1999-present	16 days	Not free and free
	JERS	18 m, 18 m x 24	1992-1998	41 days	Not free
High resolution satellite sensor (<10 m)	IKONOS	1 m panchromatic 4 m multispectral	2000-present	3-5 days	Not free
	QuickBird	0.61 m panchromatic; 2.44 m multispectral	2001-present	3-7 days	Not free
	Geo eye*	34 cm panchromatic; 1.36 m multispectral	2008	< 3 days	Not free
	RADAR (ALOS PALSAR)*	10 m	2006	2 days	Not free

*The availability of data at the start of the project work in 2011

c) Radiometric resolution

Radiometric resolution means the number of digital quantification levels used to store the data. The greater the number of digital quantification levels the greater the detail of the information collected by the sensor.

d) Temporal resolution

Temporal resolution denotes to the revisit rate of the sensor. To see the specific change of LULC and LST, accurate mapping depends upon acquiring imagery at a specific time of year. Landsat data is the most common data used due to its long history of space-based data collection at a global scale (Morran; 2010).

Table 3.2 Characteristics of spectral resolution of orbital sensor systems (Stefanov et al., 2004; Powell, 2007)

Sensor	Spatial resolution	Wavelength (bands)	Temporal coverage
TM	30/120	VSWIR (6) TIR (1)	1984-
ETM+	15/30/60	PanVNIR (1) VSWIR (6) TIR (1)	1999-
ASTER	15/30/90	VNIR (3) SWIR (6) TIR (5)	1999-now
SPOT HRV (Visible high-resolution)	10/20	Pan VNIR (1)	1986-1996
SPOT HRVIR (Visible and infrared high-resolution)	10/20	VNIR (3) or VSWIR (4)	1998-2013
IKONOS	1/4	Pan VNIR (1) VNIR (4)	1999-2015
Quickbird	0.6/70 2.4/2.8	Pan VNIR (1) VNIR (4)	2001-
RADARSAT	10-100	5.7 cm (C-band)	1995-

3.1.2 Choice of imagery for detecting UHI effects and LULC

Traditionally, LST data for UHI study are collected from fixed climatology stations. Acquisition of detailed spatial distribution information of the temperature is difficult because of limited locations for temperature measurement (Zhang &

Wang, 2008). Another way to comparatively assess simultaneously across a wide area is by using a RS satellite platform. It offers a way to capture data regarding detailed quantitative LST across the LULC categories recorded by sensors in the thermal infrared (TIR) spectral range. TIR sensors capture the radiance of the top of the atmosphere (TOA) (Zhang & Wang, 2008).

Previous comparisons have shown that the results of TIR observations are in close agreement with direct measurements (Mallick & Rahman, 2012). However, radiation recorded by the sensor is often influenced by atmospheric constituents. In order to obtain realistic values, this original data needs to be corrected for emissivity and atmospheric effects. Radiometric corrected temperature can be used to calculate LST in Kelvin or Celsius degrees (Voogt et al., 2003; Weng, 2009).

Early studies of UHI effects using satellite-derived LST measurements were conducted primarily using NOAA's Advanced Very High Resolution Radiometer (AVHRR) data for mapping of regional-scale LST (Streutker, 2003; Roth, 2013). Recently, other satellite data such as Landsat and MODIS have also been used to examine both LULC and LST simultaneously. Among all these satellites, Landsat is the best-known for its frequent and high quality data.

Landsat spectral bands have been identified as effective tools not only for identifying LULC and the extent of urbanization (Koutsias and Karteris, 2003), but also for measuring changes in LST, vegetation cover and for global hotspot analysis (Loveland & Defries, 2013). Landsat TM and ETM+ thermal infrared data (band 6) with 120 m and 60 m spatial resolutions, respectively, provide a spatial resolution that is adequate for UHI effect studies and a reasonably accurate method for measuring LST. Those have been utilized for local-scale studies of UHI effects and for analysis of SUHI at a local (city-wide) and micro (large structure) levels (Yuan & Bauer, 2007).

Landsat's main limitations are centered around providing moderate-resolution images and the fixed acquisition schedule sometimes needed in a particular place at a specific time. Nevertheless, the huge archive of Landsat data from Landsat 1 which starts from 1972 to Landsat 8 which starts from 2013, is ideal for use in long-term monitoring. On 1 March 1984, Landsat 5 was launched that carried multispectral Scanner System (MSS) and Thematic Mapper (TM) instruments. However, from 1995 only Landsat 5 TM was functioning well. Landsat 6 was then launched on 5 October 1993 but failed to achieve orbit. On 15 April 1999 Landsat 7 ETM+ was then successfully launched. However, from 2003 Landsat 7 ETM+ shows linear gaps due to the failure of the scan-line corrector. As a result, from 2003 only Landsat TM was still available to provide better images, but it stopped functioning in 2011 due to a rapidly degrading electronic component. The linear gaps of Landsat 7 ETM+ were then replaced with the launch of Landsat 8 on 11 February 2013 (NASA, 2015). Figure 3.1 shows a Landsat timeline.

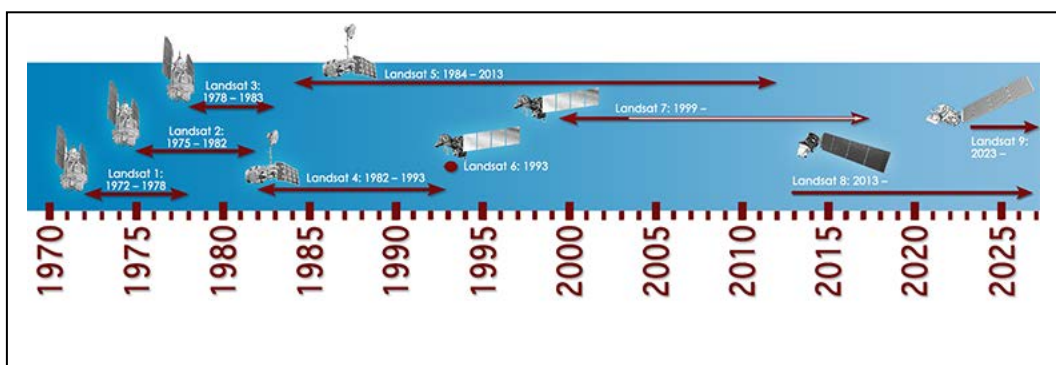


Figure 3.1 A Landsat timeline (NASA, 2015).

A combination of data from other satellite sources for the specific times is needed to overcome the unavailability of good RS image from the same sensor. Several researchers have worked to combine different sensor data for temporal monitoring of LULC and LST changes. Wen (2011) used a combination of Landsat MSS and Quick Bird data. Zoran and Anderson (2006) used multi-spectral and multi-temporal satellite data from ASTER, MODIS, SAR ERS, Landsat MSS, TM, and ETM. The use of NOAA's AVHRR and MODIS satellites was found suitable

only for meso-scale mapping of LST as their coarse spatial resolutions with 1 and 1.1 km/pixel, respectively limit their use for examining relationships between LULC and LST at both local and micro scale level. Another satellite instrument, ASTER, provides higher spatial resolution data that can be combined with Landsat, as was done in a study conducted by Liu and Zhang (2011). ASTER operates over a wider spectral region with 14 bands ranging from a thermal band at 90 m per pixel and multispectral bands at 15 m and 30 m per pixel with coverage from the year 2000 until the present (Abrams, 2000; NASA, 2015). Both Landsat and ASTER have 16 day ground coverage cycles that can ensure consistent period histories. The moderate resolution satellite imagery of both Landsat and ASTER are ideal when monitoring LULC changes (Franklin and Wulder, 2002; Powell et al., 2007).

ASTER imagery is valuable to assess not only LULC maps, but also for relating detailed, simultaneous mapping of LST. ASTER's spatial resolution allows us to distinguish more and various surface materials mainly for sub-urban and urban areas which have a typically complex surface structure. The principal disadvantage of ASTER is that the SWIR bands of 4, 5, and 6 have not been useable since April 2008 due to saturation of values and severe striping (ASTER Science Office, 2009).

3.2 Previous UHI Studies

Incorporating RS and GIS analysis using thermal RS technology enables the study of UHI and LST distribution over urban areas. Analysis of UHI using GIS to obtain more detailed information of SUHI has been used widely. Lo et al. (1997) utilized data from a thermal infrared sensor to study UHI and found that it was helpful to clarify the distribution of the location of the UHI through additions to the GIS data layers such as paths, roads, streams and distribution of buildings. Liu and Zhang (2011) studied LST changes using GIS tools in Hongkong. Weng

(2003) conducted a fractal analysis of SUHI in the city of Guangzhou for the years of 1989, 1996 and 1997 by using Landsat TM data.

Other studies have examined the impact of SUHI and found many related factors that affected SUHI, such as the roughness properties of the land surface and soil moisture (Ahmad and Hashim, 2007; Liu and Zhang, 2011) and population density (Malick and Rahman, 2012). In some research, much attention has been paid to the relationship between vegetation abundance and LST (Weng 2003; Amiri et al., 2009; Dewan and Corner 2014; Weng et al., 2007) studied the relationship between LST and urban fragmentation in Indianapolis, Weng (2001) and Solecki et al. (2005) showed the impact of urban expansion on LST resulting in constructive suggestions concerning management in New Jersey. It is clear that UHI effects vary at different times of day and seasons. Kazimierz and Krzysztof (1999) and Liu and Weng (2008) found that the greatest differences of UHI effects occurred when the sky was clear during summer nights.

Researchers have also investigated the relationship between spatiotemporal UHI and LULC in various places. Notably resources have been devoted to the study of UHI effects mostly in the U.S and the mid-latitude regions of Europe (Poland) (Kazimierz and Krzysztof, 1999; Walawender et al., 2014), and in Mexico (García-Cueto *et al.* 2007). Studies in developing tropical countries often received less attention due to lack of financial, scientific and technical resources. Recently, study and measurement of tropical UHI is receiving more emphasis due to the large population increases expected in the developing regions of the world. Dewan and Corner (2014) have looked at this issue in Bangladesh. In Indonesia, assessment of LST changes in major cities such as Bandung, Bogor, and Semarang have been conducted (Tursilowati, 2005; Tursilowati, 2007). Effendy (2007) focused on the effects of green open spaces on UHI phenomenon in the greater Jakarta area. However, the study area of tropical regions still remains insufficiently covered (Mitchell, 2011).

3.3 Choice of RS and GIS Pre-processing Method

Successfully identifying LULC change from RS imagery is not only determined by the choice of appropriate imaging systems but also by the methodology used and by the understanding of landscape features. Before the main data analysis and extraction, two major corrections are required: geometric correction and atmospheric correction.

3.3.1 Geometric correction

Raw RS imagery is not directly useable for LULC identification because it still contains geometric errors. There are two main errors; systematic and unsystematic. Most errors are predictable and systematic errors that come from external distortion caused by external parameters other than the sensor (i.e. topographic relief, position of platform, variation of attitude, and Earth curvature). This type of error can be accounted for by accurate modeling of the sensor and platform motion, as well as the geometric relationship of the platform to the Earth. Unsystematic or random errors are caused by the sensor (variation of sampling rate, lens distortion, improper arrangement of detectors,) which cannot be modeled and corrected (Murai, 1998; Hermann, 2007). Compensating these distortions is geometric correction's purpose so that the geometric representation of the imagery is as close as possible to the real world (Lillesand et al., 2008). Landsat TM level 1 from U.S. Geological Survey has been geometrically corrected, however topography and/or cloud cover situations that are dominant in the study area may result in some pixel-to-pixel mismatches and/or have a degree of accuracy that is relatively low. Thus, as the purpose of this research to make a time series of LULC changes using different remote sensing data, geometric correction of Landsat TM is required.

Geometric registration can be carried out by using image-to-image registration or image-to-map. In image-to-image registration, instead of to geographic

coordinates, images are registered to another image (Figure 3.2). The process of image-to-map or image registration is made according to the following steps:

- a) Step 1: Identify the image coordinates (column and row) of some clear points in the distorted image or ground control point (GCP).
- b) Step 2: Match them to their true positions in ground coordinates (latitude, longitude) of the map.
- c) Step 3: When GCP pairs have been identified and the coordinate information is processed, the proper transformation equations are determined and then applied to transform the original map/image coordinates into their new ground coordinates.

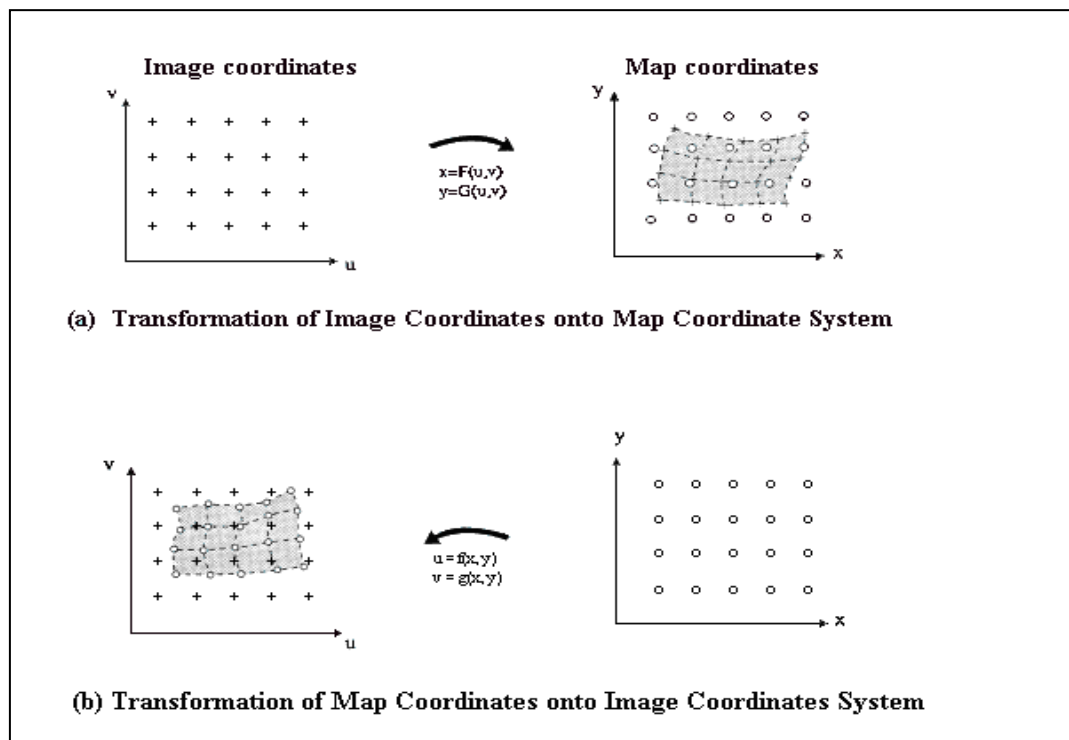


Figure 3.2 The transformation in geometric correction processes (Murai, 1998).

In order to geometrically correct the original distorted image, a re-sampling procedure is applied to calculate pixel values for the rectified grid from the original data grid. There are three common methods for re-sampling; nearest

neighbor, bilinear interpolation and cubic convolution (Canada Centre for Mapping and Earth Observation, 2015):

- a) Nearest neighbor re-sampling takes the digital number (DN) from the pixel in the original image nearest to the new pixel location in the corrected image. Nearest neighbor re-sampling does not alter the original values and is the simplest method and does not alter the original values. However, this process can result in a blocky or disjointed image appearance, some duplication and loss of pixel values.
- b) Bilinear interpolation re-sampling uses a weighted average of four pixels in the original image nearest the new pixel location. As a result, an entirely new DN in the output image is created as the original DN is altered. This may be undesirable for further LULC classification analysis that is based on spectral response. Thus, re-sampling should be applied after the classification process if this method is used for LULC classification.
- c) Cubic convolution re-sampling measures a distance-weighted average of a block of 16 pixels from the original image that surround the new output pixel location. This method also creates totally new pixel values. However, the appearance of the created image using both bilinear interpolation and cubic convolution methods is much sharper and less blocky in appearance than from using the nearest neighbor method and becomes the advantage of these methods.

3.3.2 Atmospheric Correction

Remote sensors require solar radiation to pass through the atmosphere to record electromagnetic radiation from Earth's surface. During travel from Earth's surface to the RS sensors, electromagnetic radiation signals are modified by gases and aerosols. As a result, the value recorded at any pixel location on RS images also includes information about the atmosphere and does not represent the true ground level radiance at that point (Hadjimitsis and Clayton, 2008). Thus, removing the influence of the atmosphere is critical in many applications of RS

analysis that involves classification and change detection over time to put multi-temporal data on the same radiometric scale. The purpose of atmospheric correction is to produce more accurate surface reflectance values and to potentially improve the extraction of surface parameters from satellite images (Chrysoulakis, 2010). Since May 2013, a new Landsat TM 5 and ETM surface reflectance products (level 2A) have been freely available through the Climate Data Record (CDR) (U.S. Geological Survey, 2016). Since atmospherically corrected Landsat was not available at the start of this project in 2011, atmospheric correction for Landsat TM used in this study is required. Moreover, although the list of existing reflectance products is continuously updated, CDR product distribution from the USGS archive is currently not complete because the scenes from the National Landsat Archive Processing System (NLAPS) are not fully processed yet (Pons et al., 2014).

Two main approaches for atmospheric correction are the relative approach (Image-based method) and the absolute approach (Radiative Transfer Modeling) (Kayadibi, 2011). The relative approach uses atmospheric modeling (e.g. Empirical Line, Flat Field, Log Residual and IAR Reflectance) while the absolute approach often retrieves target reflectance with a relatively high accuracy using ground data during satellite overpass (e.g. FLAASH, ATCOR, and ACORN) (Kayadibi, 2011). However, these models need the atmosphere information at the time of satellite overflight, for example the spectral optical thickness of several atmospheric elements (Hadjimitsis and Clayton, 2008) that are sometimes difficult to obtain (Kayadibi, 2011). Researchers have made atmospheric correction studies on different RS images by using many methods of atmospheric correction. Kayadibi (2011) applied and compared four atmospheric correction methods for Landsat 7 ETM + and ASTER images. The comparison showed that the models fast line-of-sight atmospheric analysis of hyper-cubes (FLAASH) and Atmospheric correction (ATCOR) achieved ideal results and were better than the relative methods of atmospheric corrections.

The FLAASH method is designed to correct wavelengths in the visible, near-infrared and short-wave infrared spectral areas (ENVI, 2009). The principle of FLAASH in performing its atmospheric correction model is based on an atmospheric radiative transfer mode that incorporates MODTRAN (moderate spectral resolution atmospheric transmittance) calculations. In addition, FLAASH can remove most of the influence which the air, light and other factors have on reflectance to gain accurate parameters of reflectivity, emissivity, surface temperature and other real physical models of surface features (ENVI, 2009). Therefore, FLAASH's approach can be used in local level applications related to LULC. Manakos et al., (2011) investigated the effects of atmospheric correction on LULC classification and found that FLAASH outperformed the atmospheric and topographic correction (ATCOR) module.

3.4 Selecting a System of LULC Classification

The selection of an LULC classification scheme plays an essential role as it influences results and interpretations. According to Jensen (2000) a good classification system should be informative, exhaustive and separable. In proposing the USGS classification system, Anderson et.al (1976) stated that an effective LULC classification system should meet the following criteria:

- a) The lowest level of interpretation accuracy in LULC categories is at least 85%. However, Monserud and Leemans (1992) state that an overall kappa statistic of 0.55 for the sample error matrix suggests a good overall classification.
- b) The class accuracies should be about equal.
- c) Obtain repeatable results from different interpreters and RS imaging time.
- d) Applicable classification system across an extensive area.
- e) The categorization system should permit LULC types to be used as substitutes for activity.
- f) Suitable to be used for different times of the year.

- g) Effective use of subcategories that is able to be obtained from ground surveys.
- h) Possibility to use larger scale or enhanced RS data and to aggregate categories.
- i) Possibility to compare with future LULC and to recognize multiple uses of land.

In the LULC classification system used by USGS for urban/built up areas, the standard categories are characterized by buildings, concrete, parks and streets. The urban/built-up category can be broken into classification such as residential, commercial, industrial, transportation, mixed built-up and recreational land (USGS, 2012). This classification system has the flexibility for breaking down into more detailed LULC classification to meet a specific purpose at the third and fourth levels. The classification levels of USGS' system are decided by the spatial resolution of the image. Maximum resolution for classification at level 3 is 0.9 m, level 2 is 2.5 m, and level 1 is 80 m. In the LULC classification system of NLCD 92, Anderson's LULC classification is modified and has 21 LULC classes (USGS, 2012).

Table 3.3 shows the USGS' and NLCD's LULC classification system. Since this research studies non-homogeneous areas of relative spectral complexity, a more detailed, imagery-based LULC classification might give better clarity of dynamic spatial patterns and distribution of LST. In addition, a greater understanding of the influence of anthropogenic activities on UHI dynamics may be achieved. Some prior research has generated LULC maps that were applied for monitoring UHI in big cities across the world and the LULC types of classification used in these were varied. Zhou et al. (2014) classified the main urban LULC types into water, barren land, developed low, developed medium, developed high, developed open space, cropland, forest, shrub, grassland, pasture, and wetland.

Table 3.3 Land classification of USGS in urban area and NLCD 92

LULC classification system	Level 1	Level 2	Level 3		
USGS	Urban/built up development	Residential	High density residential		
			Low density residential		
			Commercial and services		
			Industrial		
			Transportation, communications and services		
			Industrial and commercial complexes		
			Mixed urban/build-up land		
			Other urban/built-up land		
		NLCD 92	Water	Open water	
				Snow	
Developed areas	low intensity residential				
	high intensity residential				
	commercial/industry/transportation				
Barren	bare rock/sandy/clay				
	gravel pits				
	transitional				
Forested upland	deciduous forest				
	evergreen forest				
	mixed forest				
Shrub land	shrub land				
Non-natural woody	orchard/vineyard/other				
Herbaceous upland	grassland/herbaceous				
Planted/cultivated	pasture/hay				
	row crops				
	small grain				
	fallow				
	urban/recreational grasses				
wetland	woody wetlands				
	emergent herbaceous wetland				

Looking at the LULC mapping in South East Asian countries like Malaysia and Singapore reveals they use six similar LULC types. These are urban, forest, permanent crop, grass, and bare soil (Bin Md Hashim et al., 2007). Other LULC and LST studies in Malaysia used the following classes; infrastructure and utilities, residential, commercial, transportation, industry, open space and recreation, forest, agriculture, institution and public utilities, as well as water bodies (Bin Jamaludin, 2010).

In Indonesia, the LULC classification system used has been standardized based on the Indonesian National Standard (National Standardization Agency of Indonesia, 2010). However, most prior studies of urban mapping in Indonesia used a variety of LULC types. For example LULC mapping in Semarang City, to detect LST distribution, classified urban LULC into forest, plantation, paddy field, settlement, industry, open space, water bodies and clouds. Baja et al. (2011) classified a city in South Sulawesi into forest, mixed agriculture, grassland, water bodies, plantation, settlement, paddy field, seasonal agriculture and open land. In Jakarta, the capital city of Indonesia, Prasasti et al. (2014) defined the LULC classes as being forest, bush land, grass land, mining area, paddy field, industry, and dry land, plantation, mixed garden, water bodies, settlement and open land. Previous LULC mapping in Bali showed that there were 15 major of LULC types in the study site which were bare land (open land), building, bushes, dry land, fishpond, fresh water, grass, irrigated paddy field, mangrove, plantation, residential, sand, sand beach, swamp and unirrigated paddy field (JICA, 2005; As-syakur, 2011). In accordance with the purpose of this study and the available image data, the classification system used will adapt both the previous study in Bali and the SNI. Table 3.4 shows LULC types of a previous study in Bali and SNI.

3.5 Image Classification

Obtaining thematic LULC maps from the satellite images requires classification of the images. Image classification techniques group pixels to represent LULC classes. Image classification methods can be applied either to the varying spectral data of a series of multi-date images or to the spectral data of a single date image.

Table 3.4 LULC classes from previous studies in Bali and Indonesian National Standard

JICA (2005)	Indonesian National Standard (National Standardization Agency of Indonesia, 2010)	As-syakur (2011)
Bare land	Irrigated paddy field	Water bodies
Building	Unirrigated paddy field	Built-up area
Bushes	Polder	Forest
Dry land	Dry farm land	Dry farm land
Fishpond	Plantation	Mangrove
Freshwater	Mixed plantation	Beach sand
Grass	Mixed garden	Sandy land
Irrigated paddy field	Dry forest	Settlement
Mangrove	Wet forest	Salty land
Unirrigated paddy field	Bush land	Grass land
Plantation/yard	Grass land	Irrigated paddy field
Residential	Savannah	Unirrigated paddy field
Sand	Swam area	Fishpond
Sand beach	Open space	Open space
Swamp	Beach sand	Plantation
	River sediment	Bush land
	Sandy land	
	Built-up area	
	Unbuilt-up area	
	Lake	
	Fishpond	
	Freshwater	
	Salty pond	
	River	
	Irrigation network	

3.5.1 Methods of image classification

There are three common image classification techniques; supervised classification, unsupervised classification and object based analysis. The supervised classification method needs the collection of both validation and training data to retrieve thematic maps of features of interest (e.g. wetland, agriculture) ground truth data in the form of sample sets (Sudhakar & Kameshwara, 2010). Well representative training samples for each LULC category are necessary to identify the LULC classes across the image. The classification is run based on the spectral signature defined in the training set then each class is determined based on what it resembles most in the training set. In the unsupervised classification method, only spectral features without the use of ground truth data are required. Pixels are grouped in clusters, based on their reflectance properties. In the object-based classification method, objects of

different shape and scale are generated via segmentation, and homogenous image objects are then created by the grouping of pixels. The classification algorithms that are used to classify depend on the spectral characteristics and availability of ground truth data (Murai, 1998) as shown in Figure 3.3.

- a) Ratioing: a classification for non-vegetation and vegetation classes.
- b) Box classifier: a simple method using level slicing where accuracy levels tend to be low.
- c) Discriminant function: the method is good to be applied for classification with few LULC classes.
- d) Clustering: an unsupervised classification method where the spectral value regroups into a few clusters with spectral similarity.
- e) Minimum distance method: determines the classes required by some statistical distance measures.
- f) Maximum likelihood classifier: one of the typical supervised classification methods and the most popular method for LULC mapping with multi spectral images due to its robustness, simplicity and relatively good accuracy level. However, some errors occur if the number of training/sample data points is not sufficient. In this case, the distribution does not follow normal distribution or the categories have lots of overlap in their distribution (Perumal & Bhaskaran, 2010). The training data are known areas that are demarcated on the digital image (Richards, 2012).

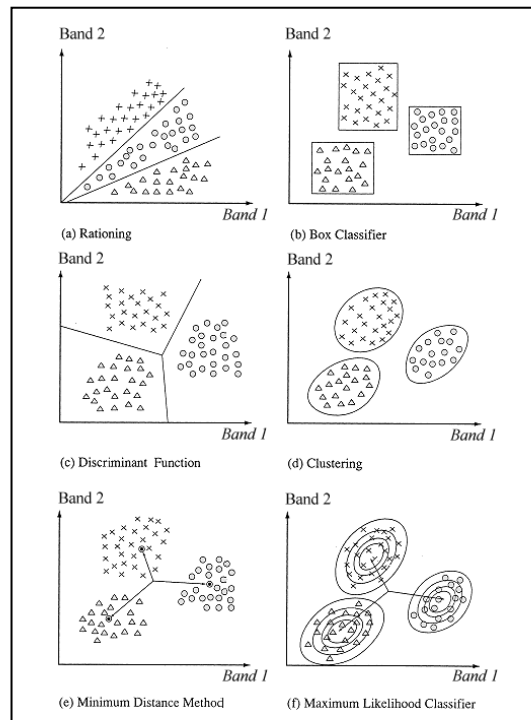


Figure 3.3 Typical classification methods (Murai, 1998).

A number of known training pixels are required for the maximum likelihood classifier to allow representative signatures to be developed for each information category (Richards, 2012). The training data sets should meet the general requirements including homogeneity, having a sufficient number of pixels representing a normal distribution and should be dispersed widely over the whole image. The training data also should be collected preferably for all categories in the segment of the image to be classified and at least for all categories of interest (Richards, 2012). The training data that is not fully representative can be solved by applying thresholds on the discriminant functions that is imposed in maximum likelihood classification (Richards, 2012). Another way is by limiting a classification. Therefore, poor quality pixels in the image, as characterized by the training data, will not be classified to identify the weakness in the selection of training data that can be rectified. Unrepresentative pixels in the training data can be excluded in a trial classification (Richards, 2012).

3.5.2 Pixel-based classification versus object-based classification method

In the past, pixel-based classification played a role of great importance mainly in classifying low-resolution images (Yüksel et al., 2008). However, it is often difficult to obtain satisfactory results using a finer spatial and spectral resolution in mapping heterogeneous urban LULC as high spectral variations within the same LULC category often occur (Rozenstein and Karnieli, 2011). When per-pixel spectral-based classification is applied for LULC classification, each pixel is grouped into a certain category. However, due to high spatial frequency, the results will be noisy and resulting in inaccuracies in LULC classification (Riggan and Weih, 2009). In addition, spectral heterogeneity of the LULC reduces the separability between classes (Nichols, 2012) and can thus lead to a ‘salt and pepper’ effect or rogue pixels appearing within classes (Shan and Hussain, 2010).

In order to alleviate the confusion of these heterogeneity problems, different human pattern-recognition capabilities, absent in automated classifiers, have been examined by many researchers. Two examples of such capabilities are the use of textures in classification and object-based classifiers. Object-based image analysis (OBIA) was suggested as an effective solution to the high spectral variation problem within the same LULC types (Benz et al., 2004; Zhou et al., 2008; Galletti and Myint, 2014). ENVI 5.3, available from Exelis Visual Information Solution is one example of a recent software product for performing OBIA (Exelis, 2015).

OBIA can provide finer LULC classification results than per-pixel spectral-based classification methods, especially from medium to high spatial resolution RS data (Mallinis et al., 2008). It offers an improvement in separability between most of the spectrally similar classes and thus, improves the accuracy of the final LULC classification. The thematic map produced is also qualitatively clearer, more homogenous and visually appealing (Shan and Hussain, 2010). The advantage of OBIA is that it does not only offer a meaningful statistical calculation, but also

topological features. In addition, the close relationship between real world objects and images is one of OBIA's benefits that are not addressed by pixel-based approaches (Benz et al., 2004). The correlation among those benefits indicates that OBIA is able to delineate and classify LULC more efficiently.

Although OBIA offers good outcomes, fast, consistent and less subjective monitoring, some disadvantages, particularly in the stage of segmentation, persist (Omran, 2012). However, the OBIA approach has been used successfully to delineate urban areas throughout the world and produce large scale maps and fine quantitative information. It also has successfully been used to map urban and agriculture areas using ASTER (Galletti and Myint, 2014). While this review provides significant potential for OBIA of classification in change detection, this concept has not yet been used in the Bali area. Image segmentation and classification are two main stages that are involved in an object-oriented classification (Baatz et al., 2008). In the image segmentation processes, pixels are combined into objects and instead of using individual pixels, a classification is then carried out based on those objects. The classification is considered as a supervised classifier because it often requires training data in the analysis process.

Segmentation is the process of partitioning an image into segments by grouping neighboring pixels with similar feature values (brightness, texture, and color). According to Smith and Morton (2008), when segmenting and creating correct object shapes, there are two aspects required; the appropriateness of an object's delineation and the precision of boundary delineation. Wrongly delineated image objects can occur as segmentation is difficult to apply in areas where different appearance does not imply different meaning and in low contrast areas (Kanjir et al, 2008). Moreover, the absence and occurrence of an object class is determined by scale level as a classification result is affected by the size of an object (Jensen, 2004). An edge-based segmentation algorithm that is very fast and only requires one input parameter (scale level) is often employed. By suppressing weak edges to different levels, the algorithm can yield multi-scale segmentation results from

finer to coarser segmentation (ENVI, 2008). Values range from 0.0 (finest segmentation) to 100 (coarsest segmentation; all pixels are assigned to one segment) (ENVI, 2008). Increasing the scale level causes fewer segments to be defined, and reducing the scale level causes more segments to be defined.

When over-segmentation is a problem, merging can be an optional step used to combine small segments with similar spectral information within larger areas (ENVI, 2008). For example, if the image shows thick vegetation, the results may be over-segmented if a small scale level value is set or under-segmented if a large scale level value is set. Therefore, merging can be a useful option for improving the delineation of tree boundaries. The merge level in ENVI has ranges from 0.0 to 100.0 (ENVI, 2008). Figure 3.4 shows examples of over and under segmentation when generating land parcel objects.

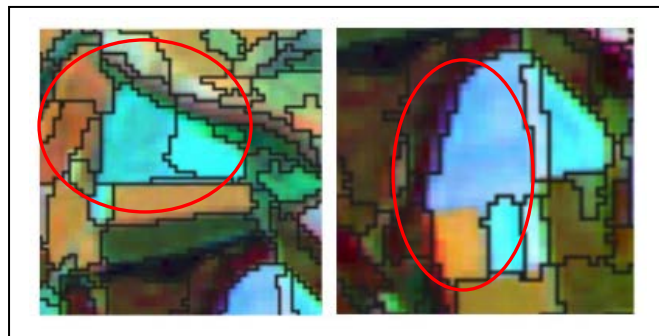


Figure 3.4 Examples of over segmentation (left) and under segmentation (right) in the bright colour areas when generating land parcel objects (Smith and Morton, 2008).

3.5.3 Training and validation dataset

When LULC maps are created, training and validation datasets from the region of interest are required to obtain a truly accurate LULC map (Sai, 2010). A training data set is used to assign class labels to image pixels, while a validation dataset is used to test the performance of the produced map through estimating the accuracy of the individual classes (Sai, 2010; McInerney and Kempeneers, 2014).

The dataset can be digitized from the existing reference map or collected in the field. If the dataset is to be taken from a map, the scales of the map and the image need to be comparable (McInerney and Kempeneers, 2014). Ideally, to characterize the classes on the image accurately, data should be collected at or near the time of the satellite over pass. Data collected from field visits also need to be georeferenced, so that the point where the data were collected can be located on the RS imagery. GPS receivers are commonly required to record this location information (Sudhakar & Kameshwara, 2010). However, the acquisition of verification data can be expensive, mainly if access is difficult and/or a statistical design is rigorously followed. Within these obstacles, Kalkhan et al. (1997), combined the use of a sample of ground truth data and air photo interpretation to assess the accuracy of Landsat analysis with 200 point samples for the training dataset at the first stage and only 25 point samples in the field for the validation dataset. Ground truth may not necessarily be correct either; its errors can be because of inconsistencies in labeling, small LULC patches used, incorrectly specified locations, the inability to see a larger area of the surface (Liu et al, 2007). Therefore, accuracy assessment is a matter of compromise between the affordable and the ideal, or "a balance between what is statistically sound and what is practically attainable must be found" (Congalton, 2007).

The training and validation datasets should be representative of the image and landscape, independent (not clustered) and should have sufficient training data in all classes. There is a range of sampling methods including (Figure 3.5):

- a) Simple random sampling (observations are randomly placed).
- b) Stratified random sampling (observations randomly placed in each class).
- c) Systematic sampling (observations are placed at same interval)
- d) Systematic non-aligned sampling (a grid provides even distribution of random distributions).
- e) Cluster sampling (random centroids used as a base of observations).

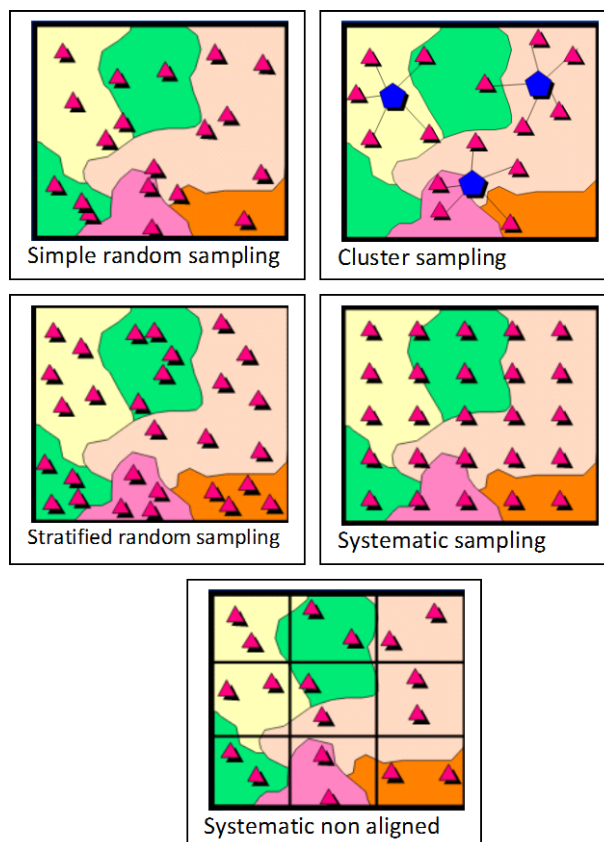


Figure 3.5 Sampling methods (Congalton, 1991).

To attain the assumption of independence, a random sampling strategy should be applied. The disadvantage of this method is that it is difficult to implement when field validation is needed for each point and time consuming. Yet, if validation and training data are not randomly distributed this can lead to a biased and inaccurate classification. To judge the quality of the training dataset, there are three options of preliminary statistical studies that can be conducted as follows (Gupta, 2003):

- a) A normally distributed curve represents good quality training samples for that category.
- b) A matrix showing statistical separability for each spectral band to check two categories are distinguishable in any one or more spectral bands. Therefore, categories with poor statistical separability should be merged.

- c) To depict the mutual relations of responses in different spectral bands for all categories, cross plots between various spectral bands are plotted.

3.5.4 Assessment of image classification accuracy

Accuracy assessment is useful since mapping errors are inevitable. It is important to estimate the accuracy level of a map by calculating the number of ground truth pixels that were classified correctly. The accuracy of a classification is usually assessed by comparing the thematic maps produced with the validation dataset that is believed to accurately reflect the true LULC. Several methods of accuracy assessment have been developed (Liu et al., 2007), such as a category-level measure developed by Hellden in 1980 called the mean accuracy index, the classification success index (CSI) as introduced by Koukoulas and Blackburn in 2001 and Cohen's (1960) introduction of the kappa statistic to RS in the early 1980s.

None of the measures can be used as a standard measure for chance-corrected accuracy. However, Liu et al. (2007), comparing twenty accuracy measurement methods, said that the primary measure of overall accuracy should be at map level showing that accuracy measures are highly consistent with each other. An error matrix is often created to investigate thematic map accuracy. Such a matrix consists of numbers set out in rows and columns which express the number of sampling units assigned to a particular class relative to the actual category as verified in the field. A population error matrix (Table 3.5) can also be constructed if both the reference and produced map classifications for all areas on the map are available (Stehman, 1997; Smits et al., 1999; Liu et al., 2007).

Table 3.5 Population error matrix with p_{ij} representing the proportion of area in the mapped LULC category i and the reference LULC category (Liu et al., 2007)

Classified	Reference				
	1	2	...	m	Total
1	ρ_{11}	ρ_{12}	...	ρ_{1m}	ρ_{1+}
2	ρ_{21}	ρ_{22}	...	ρ_{2m}	ρ_{2+}
.		
.		
m	ρ_{m1}	ρ_{m2}	...	ρ_{m2}	ρ_{m+}
total	ρ_{+1}	ρ_{+2}	...	ρ_{+m}	

In the error matrix, a tabulated view of map accuracy, overall accuracy, user's and producer's accuracies are presented (Congalton, 2007):

- a) Overall accuracy is the simplest and one of the most popular accuracy measures. It is computed by dividing the total number of correctly classified pixels (the sum of the element along the major diagonal) by the total number of pixels in the reference pixels (Congalton, 2007). Accuracies of individual categories to describe the success of the classification can also be calculated in a similar way by dividing the number of correctly classified pixels in each category by either the total number of pixels in the corresponding row or column pixels in the corresponding row or column (Sundara Kumar, 2006).
- b) Producer's accuracy results from dividing the number of correctly classified pixels in each category (on the major diagonal) by the number of training set pixels used for that category (the column total) (Liu et al., 2007). It is to indicate the probability of a reference pixel being correctly classified (Congalton, 2007) with the formula below:

$$\rho_{ai} = \rho_{ii} / \rho_{+i} \quad 3.1$$

- c) User's accuracy is to indicate the probability that a pixel classified on the map represents that category on the ground (Congalton, 2007). It is calculated by dividing the number of correctly classified pixels in each

category by the total number of pixels that were classified in that category (the total of row) with the eq 3.2 as below (Liu et al., 2007):

$$u_{ai} = \rho_{ii}/\rho_{i+} \quad 3.2$$

This figure is a measure of commission error and indicates the probability that a pixel classified into a given category actually represents that category on the ground (Sundara Kumar, 2006).

- d) The Kappa coefficient is not as sensitive to differences in sample sizes between classes. It is therefore; considered a more reliable measure of accuracy acquisition, Kappa should always be reported (Liu et al., 2007). Eq 3.3 shows the kappa formula. A kappa result of 0.8 or above is considered good, between 0.6 and 0.8 is substantial and below 0.4 is considered poor (Ear-Slater, 2002).

$$\hat{K} = \frac{M \sum_{i=j=1}^r n_{ij} - \sum_{i=j=1}^r n_i n_j}{M^2 - \sum_{i=j=1}^r n_i n_j} \quad 3.3$$

Where:

- r = number of rows in error matrix
- n_{ij} = number of observations in row i , column j
- n_i = total number of observations in row i
- n_j = total number of observations in column j
- M = total number of observations in matrix

3.5.5 Techniques for change detection

According to Bhatt (2012), factors that need to be considered when choosing a change detection method are the objectives of the change detection (i.e., change monitoring, increased efficiency or quality mapping), the extracted change type (i.e., spectral, long term LULC, shape) and the thematic change type (i.e., LULC, vegetation, wetland, or urban change). Various change detection techniques have been developed. The most common change detection methods used are image differencing, principal component analysis (PCA), change vector analysis (CVA) and the post-classification change method (Lu et al., 2005).

Image differencing involves subtracting pixel by pixel images from two dates and threshold boundaries between change and stable pixels then are found for the difference image to produce the change map (Song, 2000). The advantage of this method lies in its simplicity of implementation and interpretation (Saxena, 2014). However, it is unable to provide a detailed change matrix (Bhatt, 2012). In PCA, the dominant modes of spatial, spectral and temporal variation of two four-channel multispectral images can be effectively summarized (Li and Yeh, 1998). It also offers an advantage in providing maximum visual separability of image features (Saxena, 2014) and therefore, PCA can improve the image classification accuracy. However, it is often difficult to identify the change areas without a thorough examination of the resultant image and field data or visual interpretation of the composite image (Lu et al., 2005). Another change technique is change vector analysis (CVA). An advantage of CVA is the ability to process any number of spectral bands to produce detailed change detection information (Lu et al., 2005). However, identifying the trajectory of the LULC changes is difficult and becomes the disadvantage of this method (Bhatt, 2012).

Using the post-classification change approach, the change area is recognized through direct comparison from two multi-temporal classified images that are separately extracted and labeled with correct attributes (Bhatt, 2012). This method is categorized as a classification based detection technique. The benefits of post classification comparison are not only that it can detect detailed “from-to” information, but also that it can overcome the difficulties linked with RS image analysis that is acquired from different sensors at different times of year (Coppin et al., 2004; Yuan et al., 2005). Moreover, the nature, rate and location of changes can be efficiently detected and it has been successfully used in urban areas. Disadvantages of the post classification comparison method include issues associated with the accuracy level of component classifications, sensors and data pre-processing methods. Therefore, individual classification should be as accurate

as possible (Coppin et al., 2004; Yuan et al., 2005) as a data error can produce a large number of erroneous indications of change.

3.6 Chapter Summary

This chapter reviews choices of RS Imagery for measuring LULC, LST and NDVI and the methodology to obtain LULC maps. Literature about related work shows that the combined use of remotely sensed imagery and GIS applications is a key tool in LULC and LST change detection and simultaneously extracting NDVI. The choice of RS data has to carefully consider the scope of study purpose. With the rapid development of RS techniques, many classification methods have been developed and are able to be grouped into the traditional pixel-based method and the object-based method, a choice that is primarily driven by the resolution of RS data. Moreover, along with the use of various remotely sensed data, evolution of RS technology also has accelerated the development of change detection techniques which are implemented through case studies. Different techniques have a balance between cons and pros and are useful to varying situations. This chapter also reviews methods for accuracy assessments most commonly used and therefore, recommended. In addition, the efficacy of various methods to be used is determined by the complex factors and objectives of each research. In accordance with the use of multi-temporal and multi-source RS data for tropical developing countries, the choice not only needs to consider possible optimum and best techniques but also attain the result aims with relatively low-cost analysis.

4 STUDY AREA AND DATA

To investigate LULC, LST, and NDVI using RS and GIS technology, information about the study area's characteristics is required. It is also important to achieve an interpretation result that is relevant to the actual changes that have occurred. Moreover, specific characteristics of the RS data used must be fully understood to employ image processing properly, since RS data is used for multiple purposes as well as assessing LULC, LST, and NDVI.

This chapter focuses on describing the characteristics of the study area and the data used in this study. The selection of the study area located in the southern part of Bali was not only due to the fact that this area has undergone the most significant change among islands in Indonesia, but also the area's availability of suitable RS imagery and ancillary data such as digital maps for compilation of reference data, as well as convenient access to the area for field checking. The study area is a famous destination for world-class tourism that plays a tremendous role in the Balinese and Indonesian economies.

Indonesia is an archipelagic country of about 17.000 islands with most of its population concentrated in coastal zones (Whitten et al., 1996). The most economically productive islands such as Bali, Java, and Sumatra are particularly vulnerable in the face of climate change (World Bank, 2009; Measey, 2010). Diverse human activities that directly affect LULC changes have been increasing in quantity and spatial distribution in Bali and have been expanding towards the coastal fringe area in the south part of the island. As a result, detrimental degradation of the environment over a long time has occurred in those areas in particular. This is caused by LULC conversions that often have not been based on the principles of sustainable development. Those notable changes are indicated by the disappearance of a large amount of essential natural landscapes (e.g., agricultural land, vegetation and mangrove forest), which are major potential

contributors to moderating the urban microclimate. The detrimental environmental functioning of the ecosystem that is triggered by the uncontrolled LULC change may very likely decrease tourist visits to Bali. Thus, many socioeconomic activities would gain benefits from a reduction in UHI effects based on this study outcome.

4.1 General Description of Study Area

The research focuses on the main southern coastal region of the island of Bali. Most of the urban development is located within a land area of approximately 272 km² (17 x 20 km). As a result of the uniqueness and beauty of the coastal culture and the area's environment, its tourism facilities have developed more rapidly than in other regions in Bali. The study area comprises the main capital city of Bali, Denpasar, and its surrounding suburban areas, known as the Sarbagita metropolitan area. The Sarbagita metropolitan area includes the city of Denpasar and the regencies of Badung, Gianyar and Tabanan (Figure 4.1). Geographically, the study area is on a relatively broad gently sloping surface with an elevation between approximately 0 and 100 m above sea level.

4.1.1 Socioeconomic condition

Bali is described as an important region in the Indonesian national development plan for the medium term (RPJMN) 2010-2014 (State Ministry of National Development Planning of Indonesia, 2013). The tourism industries, which consist of trade, hotels, and restaurants, are critical factors in the Gross Regional Domestic Product (GDRP) and contributed about 30% of the GDRP from 2010 to 2013. However, the study area is also still essentially dependent on the agricultural sector (about 20%), transport and communication (about 14%), and related services (about 14%). Other sectors such as mining, building, and finance contribute to less than 10% each. Table 4.1 shows the fluctuation of Bali's gross regional domestic product from 2010 to 2013 (Statistics Office of Bali Province,

2011). As a result of good economic conditions in Bali, migration of people from other islands and countries has increased, as has the population density.

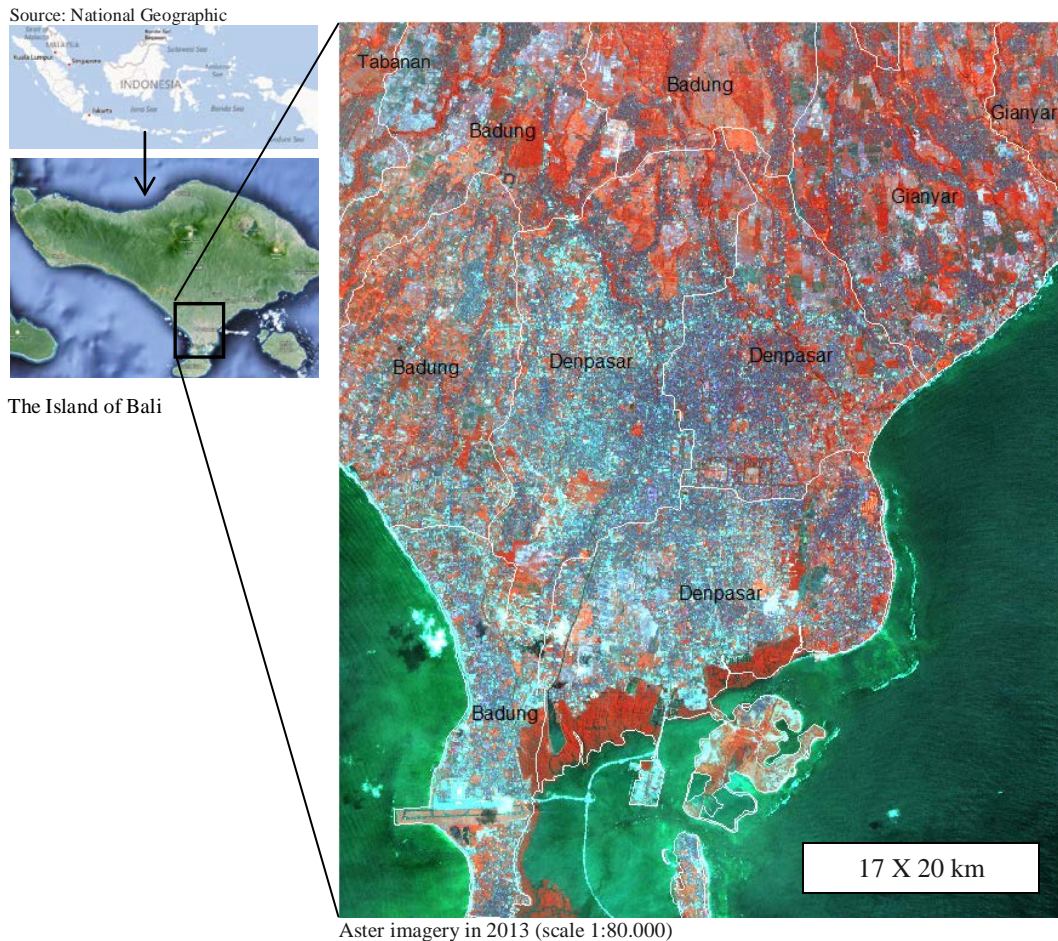


Figure 4.1 Location of the study area.

4.1.2 Climate and traditional growing season

The study area is located in the equatorial region with a typically tropical climate characterized by high humidity, abundant rainfall, and high temperatures. The area has a mean annual temperature of 33 °C, its humidity ranges between 70 and 90%, and average rainfall is more than 2,000 mm per year. Winds are moderate and predictable. There are two types of seasons in Indonesia. The dry season runs from May to September that is influenced by the Australian continental air masses

and the wet season runs from November to March that is influenced by the Pacific and Asian ocean air masses. Due to these different seasons, the natural water supply is not continuous throughout the year. It is therefore necessary to select and plan species of plants in green space planning that have more ability to retain and maintain the availability of groundwater. To prevent flooding in the rainy season, making ponds in parks that function as water reservoirs can be an alternative solution.

Table 4.1 Gross Regional Domestic Product of Bali (2010-2013) (Statistics Office of Bali, 2014)

Business sector	2010		2011		2012		2013*	
		%		%		%		%
Agriculture, livestock, forestry, fishery	12099	18.01	12737	20.78	14137	20.25	15903	16.82
Mining, excavation	471.2	0.70	545	0.89	660	0.95	758.21	0.80
Processing, industry	6152	9.16	6606	10.78	7471	10.70	8241.8	8.72
Electricity, gas, water	1263	1.88	1430	2.33	1704	2.44	1970.8	2.08
Building	3034	4.52	3440	5.61	4351	6.23	4862.7	5.14
Trade, hotel, and restaurant	20196	30.06	22702	37.04	25372	36.35	28260	29.89
Transport, communication	9683	14.41	10689	17.44	12299	17.62	13477	14.25
Finance, leasing	4619	6.87	5024	8.20	5663	8.11	6371.6	6.74
Services	9676	14.40	10857	17.71	12284	17.60	14712	15.56
Total	67194	100	61293	100	69805	100	94556	100

*provisional data

The transition months of April and October are characterized by changing winds and inconsistent weather. According to Setiawan (2012), temperature data recorded for the period 2004-2008 at Denpasar climatology stations shows that temperatures tend to decrease during the dry season, but tend to increase during the rainy season (Figure 4.2). The length of daylight hours between different seasons changes relatively little by about 48 minutes.

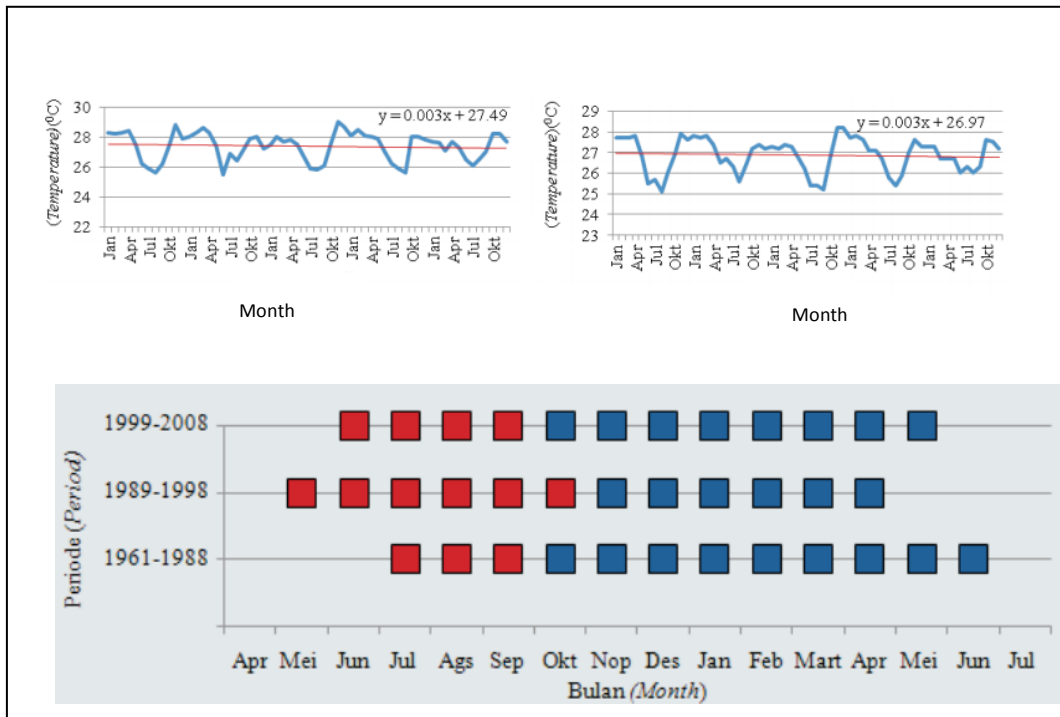


Figure 4.2 Pattern of monthly average temperature for the period of 2004-2008 and pattern of wet and rainy seasons during three periods in Bali (Setiawan, 2012).

These climate patterns interact with the relatively flat topographic conditions and allow crops to grow in the study area, where most of Bali's rice fields are located throughout the year. Since irrigated paddy fields' growing season needs a lot of water, the fields' productivity strongly depends on the availability of water. The allocation of river water for irrigation and land utilization in the farmlands is collectively controlled by local water communities called *Subak*. The reduction of river water and rainfall in the dry season is usually managed by planting horticulture plants that need less water. At this point, the paddy field is temporarily transformed into dry farmland for about three months. This change is also important to mitigate paddy diseases/pests and rehabilitate the soil structure. Another alternative management strategy to overcome water shortage during the dry season is planting paddy alternately between adjacent *subak* regions. Therefore, irrigation water is sufficient enough both in the dry and rainy seasons for entire *subak* areas. During the fallow period, farming work is usually focused

on maintaining vegetation or mixed gardens near the paddy fields. This system shows that local traditional responses in facing the local climatic situation has allowed the area of paddy fields to continue to be economically and physically productive throughout the year.

4.1.3 Urbanization in Bali

As in other developing countries, most people in Indonesia no longer live in villages. Indonesia's population living in urban areas grew steadily from the start of Indonesian independence in 1945 as a result of pressure on poverty in rural areas and continued to grow sharply in 1960s along with improved socioeconomic development. In the period 1980-1990, there was a sharp increase in the urban proportion of the population from 22% to 31%. The 2000 Indonesian population census showed that the urban population had reached more than 85 million people or about 42% of the total population. In 2020, the urban population is estimated to reach 132.5 million people or about 52% of total population (Indonesia Ministry of Environment, 1997).

Sarbagita metropolitan area in Bali has become one of the biggest metropolitan areas in Indonesia, which is experiencing tremendous urbanization that is predicted to continue until 2025 (Sutriadi and Haryo, 2009). The high level of urbanization in Bali is demonstrated by the capital city. Denpasar's 2010 population density reached 6400 persons/km² with 1270 prs/km² for other surrounding regions (Statistics Office of Bali, 2011). In addition, the area's population reached 1,747,151 in 2010 with an annual growth rate of 3.2% (Statistics Office of Bali, 2011), and became one of the largest population bases in Indonesia. Consequently, the need for housing and other facilities increases and leads to LULC changes.

Figure 4.3 shows the percentage of urbanization growth for Denpasar City in Bali province and other cities in Indonesia from 1971 to 2025. The level of

urbanization of Indonesia's five biggest cities including Denpasar (Bali), Jakarta, Yogyakarta, Tangerang (Banten), and Bandung (West Java) reached more than 70% from 2010 to 2015. Urbanized area means built-up areas including residential, commercial and service, transportation, communication and utilities, industrial and commercial, and mixed built-up area (Sutriadi and Haryo, 2009). This is due to the fact that these cities are more economically attractive than other Indonesian cities. In 2025, it is predicted that the urbanization level will reach over 80%, except Jakarta, which is approaching 100%, meaning that appearance of Jakarta has been completely categorized as urban (Saefuloh, 2011).

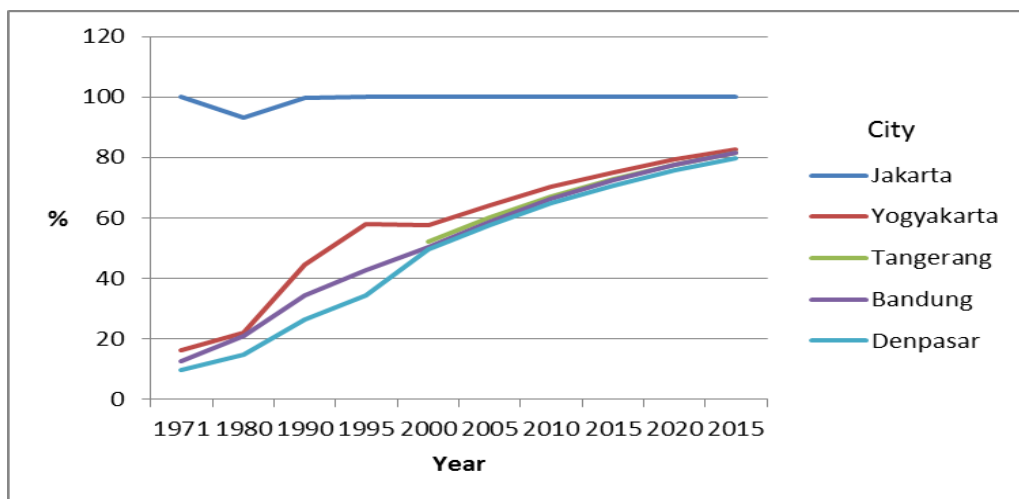


Figure 4.3 Urbanization trend in large Indonesian provinces (Sutriadi and Haryo, 2009).

4.1.4 Balinese traditional concept of conserving nature

Rapid LULC transformation in Bali has occurred due to urbanization. This transformation occurs not only in the downtown area of Denpasar, located in the middle of the study site, but has also expanded to the coastal areas of the Sarbagita metropolitan area. Traditionally, LULC in Bali is arranged around the principles of *Tri Hita Karana*. This is a concept indigenous to the Balinese community, which has been shown to be an ecologically sustainable system and has protected some of Bali's natural sacred green spaces. According to Putra

(2011), *Tri Hita Karana* is a local concept for attaining secular bliss through the harmonious relationship between humans and the environment (*palemahan*), between human beings (*pawongan*), and between human beings and God (*parhyangan*) into an integral oneness. However, because of recent population pressure, the structure and function of the traditional LULC patterns preserving natural and semi-natural areas have undergone fundamental changes in some areas. The amount of green agricultural space, water area, and forest has tended to be reduced by conversion to urban or related uses that have potentially contributed to the increase of an adverse thermal environment. Bali's indigenous cultural concept should be kept in use and integrated into the new concepts of urban spatial planning and management (Putra, 2011).

4.2 Remotely Sensed Data Preparation

The primary satellite data that were selected to measure LULC, LST, and NDVI and to compare the changing intensity were images from Landsat Thematic Mapper (TM) 5 and the Advanced Space-borne Thermal Emission and Reflection Radiometer (ASTER). Detailed information about the Landsat TM and ASTER data collected can be seen in Table 4.2. The choice of the dates (1995, 2003 and 2013) is determined by the purpose to examine the LULC changes in the past and current levels of LULC for the three different periods, given that urbanization in Indonesia shows a notable increase from 1995 (Soeroso, 2004), and the availability of remotely sensed data with relatively little cloud cover in the study area that only can be found on the date of 2003 and 2013. This is also supported by the availability of ancillary data in 1995 and 2003. Even though the percentage of cloud covers in images seems relatively high on those images, the study area had relatively little cloud cover.

Table 4.2 Satellite data used in this study

Image	Image label	Cloud cover (%)	Image date	Acquisition time	
				Greenwich mean time (GMT)	Local time
Landsat TM	LT51160661995034DKI00	20.42	3/2/1995	1:35:26	9:35:26
ASTER	ASTL1A0302240248130303180096	16	24/2/2003	2:48:13	10:48:13
ASTER	ASTL1A1304240247461304250055	50	24/4/2013	2:47:46	10:47:46

4.2.1 Landsat TM data

Landsat TM 5 data comes from a level 1 product generation system and was obtained free of cost through the United States Geological Survey (USGS) web interface (USGS.glovis.gov), and was generated by the National Land Archive Production System (NLAPS). The study site is located in path 115 and row 66. Landsat Level 1 images are geometrically corrected and use Standard Terrain Correction (Level 1T) that provides systematic geometric and radiometric accuracy by incorporating ground control points (GCPs) while employing a Digital Elevation Model (DEM) for topographic accuracy (USGS, 2000). The geodetic accuracy of the product depends on the accuracy of the GCPs and the resolution of the DEM used. Technical details of Landsat TM are provided at Table 4.3. Generally, a Landsat Level 1 image had the following (USGS, 2000):

- Map (north-up) image orientation and GeoTIFF output format.
- Cubic convolution resampling method.
As described in Chapter 2, cubic convolution re-sampling method creates totally new pixel values by calculating a distance-weighted average of a block of 16 pixels from the original image that surround the new output pixel location. As a result, the new appearance of image is less sharp.
- World geodetic system (WGS) 1984 datum and Universal Transverse Mercator (UTM) map projection.
- 30-meter (TM, ETM) and 60-meter (MSS) pixel size (reflective bands).
- File format is GeoTIFF.

4.2.2 ASTER data

ASTER is a collaborative project between Japan's Earth Remote Sensing Data Analysis Centre (ERSDAC); Japan's Ministry of Economy, Trade and Industry (METI); and NASA. The ASTER archive was available at the ASTER earth observing system data gateway (<http://gds.aster.ersdac.jspacesystems.or.jp>), which allows entering a number of search criteria. Data retrieved can be viewed and downloaded at level 1A, which combines the radiance at the sensor with the image's radiometric and geometric coefficients. It is provided in the HDF-EOS format, which some commercial image processing software such as ENVI and ER Mapper can read directly. The ASTER instrument consists of the visible-near infrared (three bands at 15 m/pixel), shortwave infrared (six bands at 30 m/pixel), and thermal infrared (five bands at 90 m/pixel) wavelength regions of the electromagnetic spectrum. The ASTER scene covers a 60 × 60 km area. The technical specification of the ASTER images used can be seen in Table 4.3.

Table 4.3 Characteristic of ASTER and Landsat TM imagery

Spectral subsystem	ASTER			LANDSAT TM			
	Band	Spectral Range (µm)	Spatial Resolution (m)	Spectral subsystem	Band	Spectral Range (µm)	Spatial Resolution (m)
Visible-near infrared (VNIR)	1	0.52-0.60	15	Visible Blue	1	0.45-0.52	30
	2	0.63-0.69		Visible Green	2	0.52-0.60	120*120
	3 N	0.78-0.86		Visible Red	3	0.63-0.69	
Shortwave-infrared (SWIR)	4	1.60-1.70	30	Near infrared	4	0.76-0.90	
	5	2.145-2.185		Shortwave IR-1	5	1.55-1.75	
	6	2.185-2.225		Thermal IR	6	10.40-12.50	
	7	2.235-2.285		Shortwave IR-1	7	2.08-2.35	30
	8	2.295-2.365					
	9	2.360-2.430					
Thermal infrared (TIR)	10	8.125-8.475	90				
	11	8.475-8.825					
	12	8.925-9.275					
	13	10.25-10.95					
	14	10.95-11.65					

The blue shaded area shows bands that selected for analysis of LULC, LST, and NDVI mapping.

Although several studies have shown that classification accuracy increases substantially with more bands, for the kind of classification used, a smaller

number of band is desirable and one way of doing this classification is to use the first three principle components of ASTER. In addition since April 2008 the visible and near infrared bands of the ASTER sensor (Bands 1, 2, and 3N) have been the only bands available for LULC classification since the ASTER SWIR bands of 4,5,6,7,8, and 9 were no longer useable due to saturation of values with noise and severe striping (ASTER Science Office, 2009). The ASTER bands of 1, 2, and 3N provide the highest spatial resolution and have proven useful for urban land cover classification (Zhu & Blumberg, 2002; Malekpour & Taleai, 2011; Cai et al., 2012). The most common band combination of spectral band 4, 5, and 3 of Landsat TM was used as this band combination of Landsat TM is often used for urbanized area, vegetation and agricultural areas (Gusso and Ducatti, 2012) which dominate in the study area in 1995 as the principal application of those bands is to distinguish soil and vegetation (Horning et al., 2010; U.S. Geological Survey, 2011).

4.2.3 Ancillary data

Ancillary data are used for various purposes such as geometric correction of RS data and delineating the boundaries of the region. In this study, a digital map of streets and rivers (Geospatial Information Agency of Indonesia, 2005) that contains a description of the ground surface was primarily used for geo-referencing satellite images. Some thematic layers of Bali's administrative boundaries in shapefile format also have been used to delineate the study area and to create the area of interest (AoI) and classification references.

Detailed LULC data from Udayana University for Bali from 2003 and 2008 were available and have been used for the accuracy assessment of image classification. These datasets are downloadable for the study area in shapefile format and provide comparable digital maps of Bali's LULC. Another secondary data source was a digital LULC Map of Bali from 1995/1997 produced by Indonesia Geospatial Information (Geospatial Information Agency of Indonesia, 1995).

These datasets are required as training data for the LULC classification. The scale of all output products was set to 1:50000, facilitating the detection of essential terrain features by means of satellite images and their representation.

Google Maps, Google Earth, and Quickbird imagery from 2005 for the Badung region obtained from the Department of Public Works of the Badung regency were also frequently used to check the classified data from RS images whenever confusion arose deciding the LULC type. Google Maps is a free web mapping service technology and a source of high-resolution satellite images covering all types of landscape (Das, 2007). A related product is Google Earth. It is a program that contains virtual globe, maps, and GIS that maps the earth by the superimposition of images gained from GIS 3D, global satellite imagery, and aerial photography (Das, 2007). The derived LULC data can easily be overlaid on Google Earth images in order to check and compare the classified images. The integration of LST maps with Google Earth was also used to facilitate low-cost techniques for detection of Micro Heat Islands (MUHI) in order to delimit the extent of UHI effects.

4.2.4 Field survey to obtain ground truth data and LULC types

A field survey was conducted to collect ground truth data in the study area, to define LULC types and classification assessments and to learn about the existing condition of LULC types. Data collection was conducted using a Global Positioning System (GPS) with 10m accuracy. Other necessary tools required included printed Google Earth maps and Quickbird images to locate features. LULC features and human activities from each sample study were also identified and described. In addition, important features were photographed using a field camera in order to supplement the produced maps. This field observation was also supported by literature to get long-term LULC information about the study area. The data utilized in this study were generally processed with ArcMap 10.1 and

ENVI 5.0. The statistics analysis was conducted with Microsoft Excel 2010 and IBM SPSS statistics 21.

4.3 Research Design Process

This study is a framework of RS image processing using Bali as a case study in order to plan urban green spaces that can mitigate UHI effects, as has been explained in Chapter 1. A general overview of the research process is shown in Figure 4.4 with detailed methodology for each analysis. The results and discussion will be described in each chapter. Proportions and conversions of LULC and LST from 1995, 2003, and 2013 and the relationship between biophysical factors are identified and analyzed using statistics after retrieving and validating maps of LULC, LST, and NDVI. The LULC data was then combined with normalized LST data to see the mean LST for each LULC classes for each year. In addition, an urban green space plan (block plan) is also developed and recommended based on the LST information.

4.4 Chapter Summary

The study area located in the southern part of Bali represents an urbanized area in the tropical tourism island of Indonesia. While the social, economic, and tourist activities of this study area are very sensitive to the environment, as they are located in the coastal areas, urbanization is constantly growing, triggering the alteration of LULC, and thus, potentially results in UHI effects and other detrimental environmental impacts. The choice of this study area was not only determined by those situations and benefits to the social, economic, and cultural activities and environment, but also the availability of suitable RS imagery and ancillary data as well as convenient access for field observation. A temporal series of RS images from Landsat TM and ASTER were selected, as those images offers fine spatial resolutions, relatively free cloud cover imagery, and have a relatively low cost of analysis.

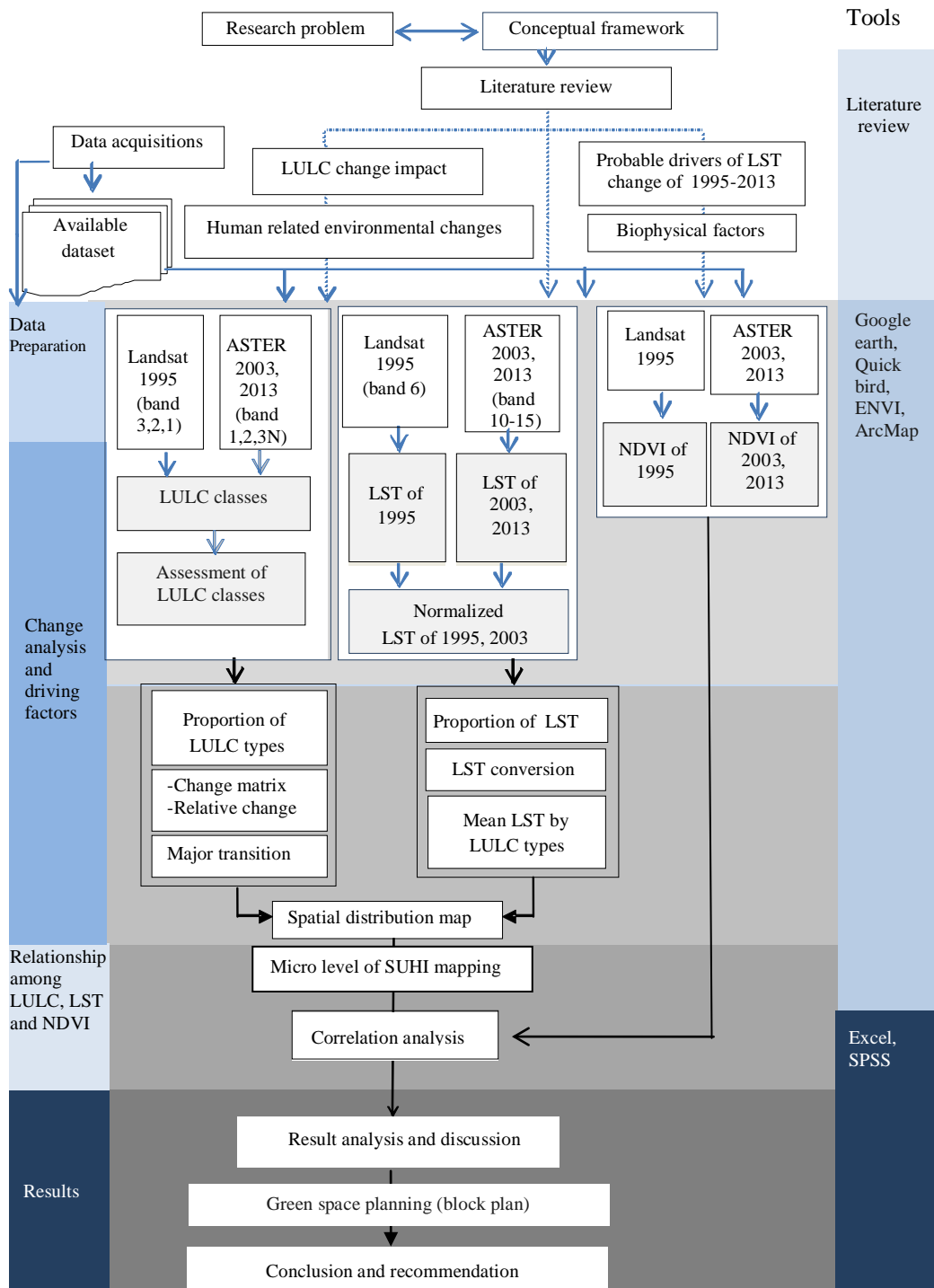


Figure 4.4 An overview of the research design

5 ANALYSIS OF LAND USE/COVER CHANGE IN SOUTHERN BALI

The LULC of southern Bali, as one of the most populous islands in Indonesia, is characterized by more built-up area for economic purposes (i.e. retail, industrial, commercial, transportation, recreation, and residential) compared to other areas in the island of Bali. The agricultural lands such as grasslands, paddy fields, dry fields, and forests that have balanced the urban ecosystem still exist sporadically. The necessity for land for many urban purposes has resulted in increased pressure on the environment, which led to the change in LULC and ensuing enormous costs to the environment. It is therefore, necessary to examine the changes in LULC, so that their effect on the terrestrial ecosystem can be discerned, and sustainable LULC planning is able to be formulated.

A range of RS sensed data has been used to map Bali's LULC previously (JICA, 2005; As-syakur, 2011); until recently, however, LULC classification was based on traditional pixel-based methods. This chapter describes LULC change analysis of southern Bali from 1995 to 2013 that uses OBIA with Landsat and ASTER data. This chosen method considers characteristics of the study area in a large and complex tropical urban-rural landscape and OBIA offers some advantages such as separability between most of the spectrally similar classes and thus, improves the accuracy of the final LULC classification (Shan and Hussain, 2010). In order to identify the changes of LULC in Bali, a post classification change approach was used. The results of this study are expected to provide valuable information for planners to devise sustainable LULC planning and management and to be used further for urban green space planning and policy.

5.1 Classification Process

5.1.1 Training data collection

Training data were classified using field validation, a reference LULC map of Bali from 1995/1997, and 2003 and high-resolution image interpretation. A total of 298 reference data for the 1995 map and 346 reference data for the 2003 map were used to assess the accuracy of LULC maps. A field survey was conducted to collect ground truth information to assess the accuracy of the 2013 LULC map. A set of 382 sample points was generated in order to get at least 5 points of each LULC class based on random sampling method in ArcGIS with a minimum allowed distance between points was 0.5 km. The positions of randomly selected points were physically visited in October 2013 and 2014, and locations were recorded using a GPS unit (Appendix V-4). Due to the difficulty of accessing some areas (e.g. mangrove, swamp areas, and vegetation), not all of these sites were able to be visited. Instead, the classes at those sites were manually interpreted. LULC and Expert knowledge obtained from a number of onsite activities combined with Google Earth and composite images of ASTER and Quickbird for the Badung region were used to identify the class at each point.

5.1.2 LULC classification system

Before classification, the classes were assigned and classification rules to describe each class were selected. The observed LULC information was used as the basis to determine the type and characteristics of LULC in the study area. The LULC classification scheme of Bali in 2003 (JICA, 2005) and the standard LULC classification for Indonesia (National Standardization Agency of Indonesia, 2010) were adapted to evaluate LULC changes for better acceptability and easy use. Other factors such as study purpose, spatial resolution, and spectral reflectance of images were also considered in designing the classification types. There are 11 primary classes can be identified in this study (Figure 5.1 and Figure 5.2). These

were: built up area, open space, vegetation, fish pond, mangroves, bush land, grass land, dry farm land, paddy field, swamp area, and water bodies (Table 5.1).

Table 5.1 The LULC classification schema (modification from Land Use Map of Bali JICA (2005) and National Standardization Agency of Indonesia (2010) for Bali.

LULC type			Description
Primari (Landsat and Aster)	Secondary	Tertiary (Aster)	
Urban	Built-up area	Very dense	Areas with built-up urban centers; approximately 80- 100% construction materials (e.g., asphalt, rooftops, concrete). House lots fewer than about 1 acre, frequent tree cover
		Dense	Areas with a mixture of constructed materials (50-80%) and vegetation; House lots about <3 acre – 1 acre
		Semi dense	Built-up areas with less than 50% constructed materials, large house lots (typically about >3 acre)
		Bright rooftop	Buildings with bright rooftops
Non urban	Vegetation	Vegetation	Plantations, mixed gardens, woodlots, greenways along rivers and streets and roads, deciduous vegetation, conifers
	Paddy field	Dry	Rice plant farms
		Harvested	
		Watered	
		Vegetative	
	Fish pond	Fish pond	Ponds
	Mangrove forest	Dense mangrove	Evergreen mangrove forests
		Non dense mangrove	
	Bush land	Bush land	Shrubs
	Grass land	Grass land	Golf courses, lawns, sod fields
	Open space	Open space	Exposed soil, landfill sites, areas of active excavation, open concrete areas, sand beaches
Dry farm land	Dry farm land	Crop fields, fallow lands, vegetable lands	
Swamp area	Swamp area	Swamp areas, low-lying areas	
Water bodies	Bodies of water	Rivers, reservoirs, freshwater, permanent open waters	

The classes of paddy field, built-up area, and mangrove forest were subdivided for 2003 and 2013 ASTER imagery analysis into subclasses to differentiate the vegetation level at the time of the image acquisition (tertiary LULC types). A more detailed classification scheme of LULC types was applied due to the different spectral reflectance of classes. Those tertiary classes were then

reclassified into the secondary LULC types, before all the main differences become only urban and non urban area in order to see the urban growth.

- a) A mangrove forest is characterized by natural trees located along the south beach. The classifications of mangrove forests in Bali consist of primary/natural forests and secondary/disturbed forests. Trees in mangrove forests vary in terms of species, such as *Rhizophora* spp, *Avicennia* spp. *Bruguiera* spp.; diameter distribution; and total area for each age class.
- b) A paddy field is a wetland planted with rice plants, describes both irrigated rice and unirrigated paddy fields, and is commonly found around alluvial plains or near the natural river. Operations start long before planting is done, depend its planting time, and are carried out using draught oxen and hand hoe.
- c) Bush land is characterized by the presence of woody shrubs that in some areas grow together with sparse grass. Bush land in the study area is generally a same former vegetation cover, paddy field, or other agricultural area, that has regrown.
- d) Grass land consists of permanent natural and planted grasses. Natural grass land is located at the international airport. Some areas also include land with scattered shrubs and trees and are used for livestock grazing and browsing. Artificial grass lands are in parks and on golf courses and are used for recreation and sport.
- e) Built-up areas are construction/building area including residential, commercial and services, industrial area and road both in rural and urban areas.
- f) Dry farm land is land hosting cultivated horticultural crops such as vegetables and flower beds, which are very intensively managed.
- g) Open space is mainly covered by bare soil and exposed rocks and has only a little or no vegetation cover.
- h) Vegetation is diverse, containing either natural or planted vegetation that has been altered by prolonged cultivation and human settlements. Vegetation cover consists of annual or perennial woody and succulent plants and usually existed adjacent to irrigated paddy fields, catchment areas for protection plantations, and road sides. Such areas include urban and peri-urban

plantations operated by the government, non-government bodies, and the local community. Such areas are composed of both monoculture types of industrial plants such as bamboo and mixed bushy and woody lots (mixed garden) with various functions such as fruit production (avocado, jackfruit, longan).

- i) Water bodies are areas covered by water (oceans, estuaries, and rivers).
- j) Swamp areas are areas of seasonal low-lying land that are frequently flooded and are dominated by woody plants. Such land is found close to the Airport.
- k) Fishponds are a freshwater ponds stocked with fish.

5.1.3 Pre-processing of satellite images

a) Geo-rectification processing

The ortho-rectification process was applied to correct non-systematic geometric errors or the different viewing angles typical of multi-temporal datasets and also to ensure that all images and secondary products overlay perfectly. Each scene was geo-referenced using the “image to map” technique, based on the digital map of Bali and only the ASTER images needed to be projected into UTM WGS 84 zone 50 S. Approximately 15-20 ground control points (GCPs) were chosen from each entire image. The nearest neighborhood algorithm was used during re-sampling as it has the advantages of preserving the original image’s nearest pixel values, which is useful for further image classification, and gave overall root mean square errors (RMS) of less than about 0.7 pixels (Appendix V-1 and V-2). To obtain better results of LULC changes from 2003 to 2013, small cloud patches in the 2013 ASTER image were removed. All three images were clipped to the study site boundaries via a clipping operation. Topographic correction was not performed, as most of areas in the study area are flat.

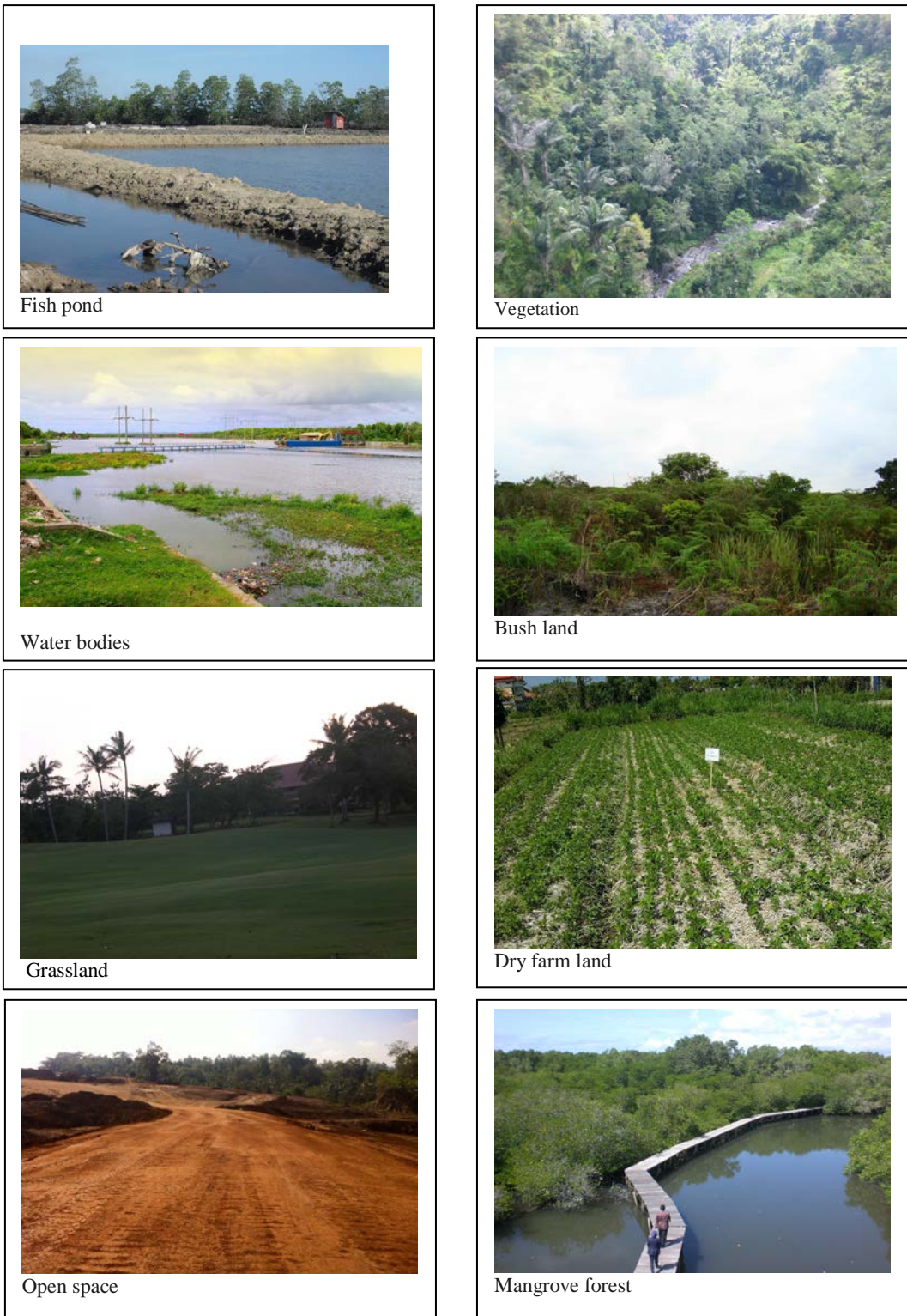


Figure 5.1 LULC types



Figure 5.2 LULC types

b) Atmospheric correction

When using remotely sensed data, geometric and radiometric accuracy are required for reliable change detection. To minimize the influence of noise and other errors caused by atmosphere, atmospheric correction using FLAASH in ENVI was applied, and digital numbers (DN) were converted into reflectance. FLAASH, ENVI's atmospheric correction algorithm based on MODTRAN4 code, was applied to the image data. The required sensor spectral response function file was provided by DigitalGlobe. Model adjustments for the other parameters were kept at their default values according to the FLAASH user's manual for multispectral imagery (ENVI, 2009). The FLAASH modules in ENVI software can be used not only for atmospheric correction but also to convert digital numbers (DN) into reflectance. Most of the atmospheric correction parameters used were from the header file of image data, and the specific parameter data is shown in Appendix V-3. After obtaining the required parameters, the true

surface reflectance of the whole image can be calculated pixel by pixel. Figure 5.3 shows the workflow for LULC classification and change analysis.

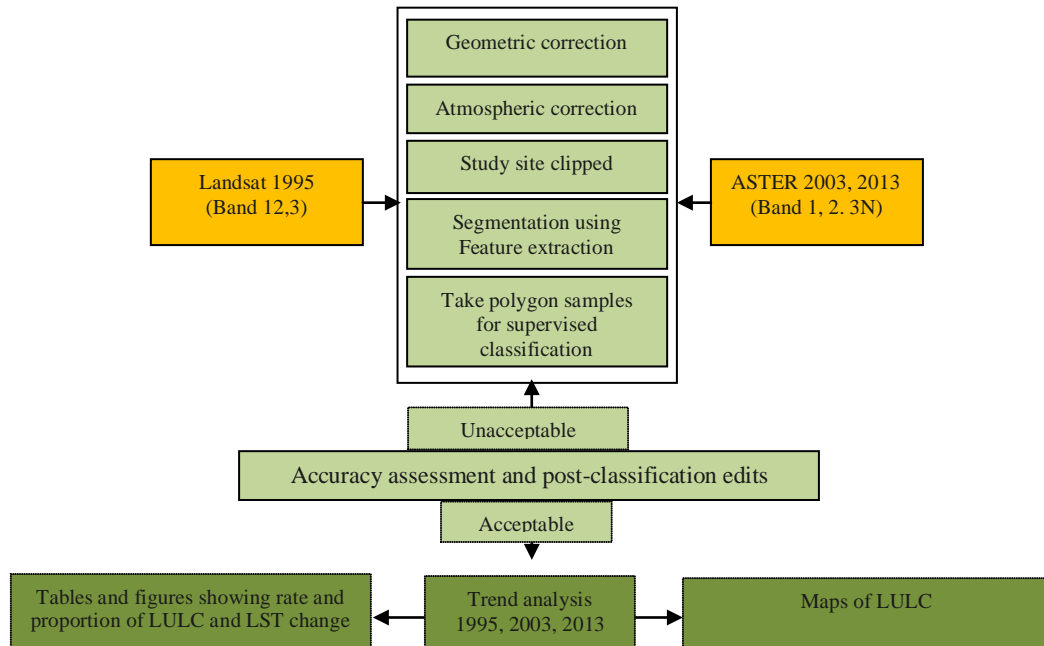


Figure 5.3 Workflow for LULC classification and change analysis

5.1.4 Object-based classification method

This study used the object-based classification approach for image classification. This OBIA method was chosen due to the relatively heterogenous LULC types in this study area, considering the spatial and spectral resolution of the imagery used, and for expectation of acceptable results. As discussed in Chapter 3, one of OBIA advantages is it offers an improvement in separability between most of the spectrally similar classes and thus, improves the accuracy of the final LULC classification (Shan and Hussain, 2010).

The appropriate scale at which to segment LULC types was decided based on the different spectral and spatial characteristics of different LULC types. The trial and error method was employed in the image segmentation process as there is no universally accepted rule for setting the scale of segmentation. Different scale levels ranging from 20 to 80 were tried to find the most appropriate scale. After that, segmentation results were manipulated interactively. The segmentation size was adjusted and thus enables to represent the minimum sized feature of objects or LULC types (e.g. paddy fields and built-up area) and to analyze whether objects and feature boundaries were already well matched. The merge level, a parameter for merging small segments based on homogeneity r , was then defined to group contiguous segments into larger objects. This is more practical and reliable in finding the appropriate scale for each LULC type. For this study, user-specified segmentation was finally conducted at a scale parameter of 50 (on a scale from 0 to 100) and a scale merge of 90 (on a scale from 0 to 100) as objects (e.g. paddy field and built-up area) were considered internally homogenous (Figure 5.4).

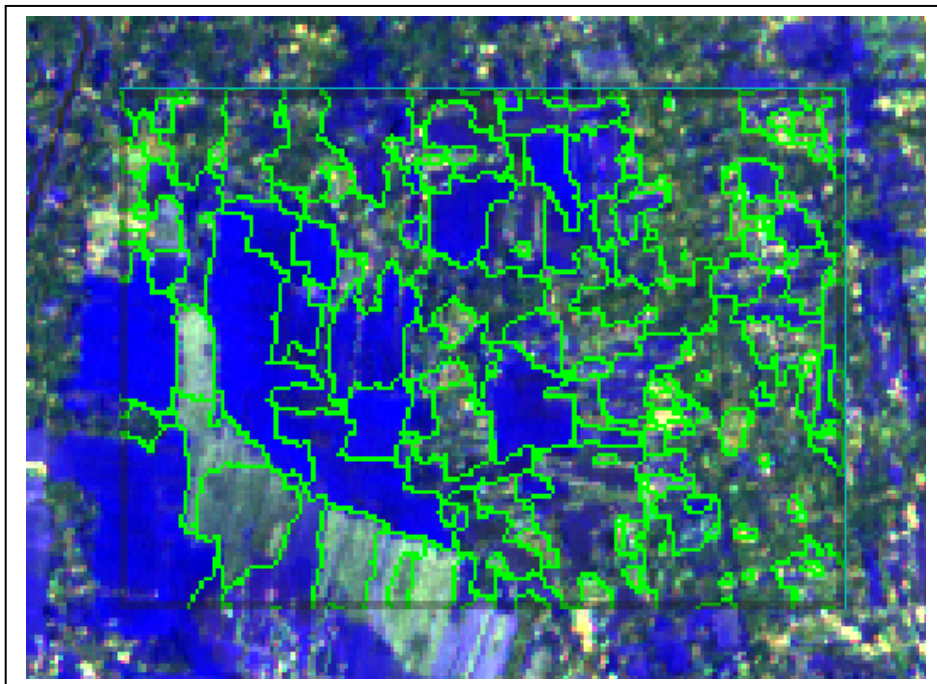


Figure 5.4 Sample of segmentation result (scale parameter of 50)

Evenly-distributed representative polygon samples of each LULC were selected and labeled based on previous segmented and merged objects using information from the field, a good knowledge of the study area, and ancillary data. Approximately the same number of representative samples was selected for each class throughout each image, although some classes of LULC (i.e. built-up, vegetation, paddy field) were more frequently present in the area than others. Feature Extraction offers three methods for supervised classification: K Nearest Neighbor (KNN), Support Vector Machine (SVM), or Principal Components Analysis (PCA). A supervised maximum likelihood classifier was chosen to classify each of the polygon objects in the image into LULC types which classifies segments based on their proximity to neighboring training regions. The K Nearest Neighbor classification method examines the Euclidean distance in n-dimensional space of the target to the elements in the training data. The k parameter is described by the number of object attributes or neighbours considered during classification. The K nearest distances was used as a majority vote to determine which class the target belongs to (ENVI, 2008). The K Nearest Neighbor method is much less sensitive to outliers and noise in the dataset and generally produces a more accurate classification result. In addition, it is more rigorous than the other methods, and it more accurately distinguishes between similar classes (ENVI, 2008). The same segmentation, merge and classification parameters were utilized for other composite dataset. At the end of the process the classified objects were exported to a thematic vector layer with classes of LULC.

During the classification process of the ASTER images, more detailed structures of LULC types (secondary LULC types) were able to be applied due to their different spectral reflectance. Those classes were very dense built-up area, dense built-up area, semi-dense built-up area, irrigated paddy field, watered paddy field, harvested paddy field, dry paddy field, dense mangrove, and semi-dense mangrove. Moreover, more detailed information about built-up areas is required in this study, as information about those LULC types is beneficial for the further

purpose of green space planning. All object types were finally reclassified into 11 classes of primary LULC type to see the LULC changes from 1995 to 2013. However, an enormous number of small objects was the result. The elimination and merger of those small polygons to reduce the number of small objects and make further LULC analysis easier was conducted using GIS tools.

A number of incidents of confusion arose in distinguishing between watered paddy fields and non-dense mangrove forest, vegetation and vegetative paddy field, beach sand, and open space. The confusion over vegetation cover and vegetative paddy field might be related to the process of segmentation. In some cases the low contrast boundaries between vegetative paddy fields and vegetation areas resulted in these regions being merged into a single polygon object although these two classes had sufficient spectral difference for fine classification. The confusion between watered paddy fields and non-dense mangrove forests and between beach sand and open space were not a result of segmentation, as generally these two classes were well delineated. Nevertheless, because the spectral radiances of the two categories were sometimes very similar, confusion occurred. This arose due to similar material factors; for example, water occurs in both watered paddy fields and non-dense mangrove forests. Minor adjustments or post classification processing were then employed to correct the misclassified classes. GIS tools such as area of interest, query builder, and field calculator were then used to recode the incorrect classes based on ground observation. The overall accuracy of LULC classification can be improved through the use of these techniques (Manandhar et al., 2009).

5.1.5 Classification accuracy assessment

To evaluate the accuracy of classified images, accuracy assessment was performed based on random sampling method. The LULC map of 1997 (Geospatial Information Agency of Indonesia, 1995) was used as a reference for the LULC map of 1995 while, LULC map of 2003 (JICA, 2005) was used as the

reference for the LULC map of 2003. For the LULC map of 2013, the reference classes were recorded based on Google image, collecting samples, and field reconnaissance. Error matrix tables were produced and the reference class values were compared with the classified data. Overall accuracy finally was then computed.

5.1.6 Post-classification comparison change detection

The approach to change detection was based on multi-date object based-post-classification comparison (map-to-map comparison). The determination of the transformation in quantity from a particular class to other LULC types and their corresponding areas over the period was facilitated and evaluated by cross-tabulation analysis. Using GIS union tools and geometry processing, three shapefiles of classified LULC maps were used as the input data and information on how classes had changed from one type to another can be calculated from the resulting attribute table. Finally, a two-way cross-matrix explaining the LULC changes was created and a thematic layer containing different combinations of “from-to” change in classes was produced. Changes during two intervals were obtained: 1995–2003 and 2003–2013.

5.2 Classification Result

5.2.1 Landsat image classification and accuracy assessment

Using the object-oriented approach, Landsat TM can produce a smooth classification of LULC types devoid of the mixed pixel effect. The overall accuracy was 84.9% with a Kappa Coefficient of 0.8136 (Table 5.2). User’s accuracy of individual classes ranged from 44.68% to 100%, and producer’s accuracy of individual classes ranged from 33.33% to 100%. The overall accuracy for some LULC categories (i.e. paddy field, grass land) was lower than the minimum level of interpretation accuracy, which according to Anderson (1976) should be at least 85%. However, according to Monserud and Leemans (1992), a

Kappa coefficient that ranges from 0.70 to 0.85 still indicates a good overall classification.

Table 5.2 Accuracy assessment of LULC map of 1995

No	LULC type	1995	
		Accuracy (%)	
		Prod. Acc.	User Acc.
1	Built-up area	98.63	87.80
2	Open space	100.00	90.91
3	Vegetation	80.77	44.68
4	Fish pond	100.00	100.00
5	Mangrove forest	100.00	51.52
6	Bush land	100.00	100.00
7	Grass land	33.33	50.00
8	Dry farm land	100.00	100.00
9	Paddy field	65.09	93.24
11	Swamp area	100.00	100.00
12	Water bodies	100.00	100.00
	Overall Accuracy (%)	84.9%	
	Kappa Coefficient	0.81	

5.2.2 ASTER image classification and accuracy assessment

The overall accuracies for LULC classes of ASTER images were established as 86.99% and 80.37%, and the Kappa coefficient was 0.86 and 0.79 for the 2003 and 2013 images, respectively (Table 5.3). User's accuracy of individual classes ranged from 62.50% to 100%, and producer's accuracy of individual classes ranged from 57.14% to 100%. However, for some classes there was a low accuracy below the "85%" cutoff level for an acceptable result.

Table 5.3 Results of first accuracy assessment for the LULC maps of Aster in 2003 and 2013

LULC type	2003 Classification		2013 Classification	
	Accuracy (%)		Accuracy (%)	
	Prod. Acc.	User Acc.	Prod. Acc.	User Acc.
Dense built-up area	100.00	90.38	77.50	65.96
Very dense built-up area	91.18	83.78	81.13	70.49
Semi dense built-up area	89.74	100.00	87.50	75.00
Bright rooftop built up area	83.72	97.30	63.33	82.61
Open space	100	75.00	90.91	76.92
Vegetation	83.33	62.50	73.17	93.75
Fish pond	100	100	100.00	100.00
Dense mangrove forest	90.91	95.24	100.00	92.00
Non dense mangrove forest	90.00	81.82	71.43	100.00
Bush land	57.14	88.89	78.95	100.00
Grass land	100.00	100.00	100.00	100.00
Dry farm land	54.55	75.00	70.00	77.78
Watered paddy field	77.78	77.42	77.78	95.45
Harvested paddy field	87.50	95.24	70	82.35
Vegetative paddy field	76.92	80.00	100.00	68.97
Dry paddy field	100.00	66.67	94.44	70.83
Beach sand	85.71	100.00	66.67	100.00
Swamp area	100	100.00	100.00	100.00
Water bodies	69.23	100.00	66.67	88.89
Overall Accuracy (%)	86.99 %		80.37 %	
Kappa Coefficient	0.8591		0.7874	

In order to identify the change in LULC over three different decades for the same LULC categories, the 2003 and 2013 ASTER maps needed to be reclassified. All the types of built-up areas (dense, very dense, semi-dense, bright roof top built-up area) were reclassified into “built-up area”. “Dense mangrove” and “Non dense mangroves” were combined into “Mangroves”. The various “Paddy field” types (vegetative, watered, harvested, and dry paddy field) were also combined into “Paddy field”.

5.2.3 General LULC condition and distribution

The spatial pattern of LULC change in 1995, 2003 and 2013 using OBIA yielded a visually pleasing classification (Figure 5.5 – 5.10). Built-up areas are located irregularly and commonly in a linear pattern along the road and covered most of downtown Denpasar and the Kuta sub-district, the location of the international

airport and tourist accommodation center. In the downtown areas, vegetation can mainly be seen on the riverbanks, in the roadsides, and parks. Mangrove forest can be seen along the south beach of the study area. Open space existed most extensively at the Ngurah Rai Airport, on the island of Serangan, and along the beach.

5.2.4 LULC changes

Figure 5.7- Figure 5.10 and Table 5.4 show there had been considerably changes in LULC configuration in the study area over the 18-year period. Generally, there were three major LULC type in the study area: built-up area, vegetation and paddy field. Table 5.8 shows a summary of the major LULC conversions, namely ‘from-to’ information as post-classification comparison reveals various changes in LULC types in the southern part of Bali. It is useful to clarify the informational value of a LULC magnitude and its spatial changes. The 1995-2003’s and 2003-2013’s transformation LULC classes can be seen in Table 5.6 and Table 5.7. Since the classifications are not 100% accurate, some errors occurs in the “from-to change” information. For example from built-up area to paddy, from built-up area to vegetation are rare in the field. The comparison map of change detection for understanding the spatial pattern of change can be seen in Figure 5.10 and Figure 5.11.

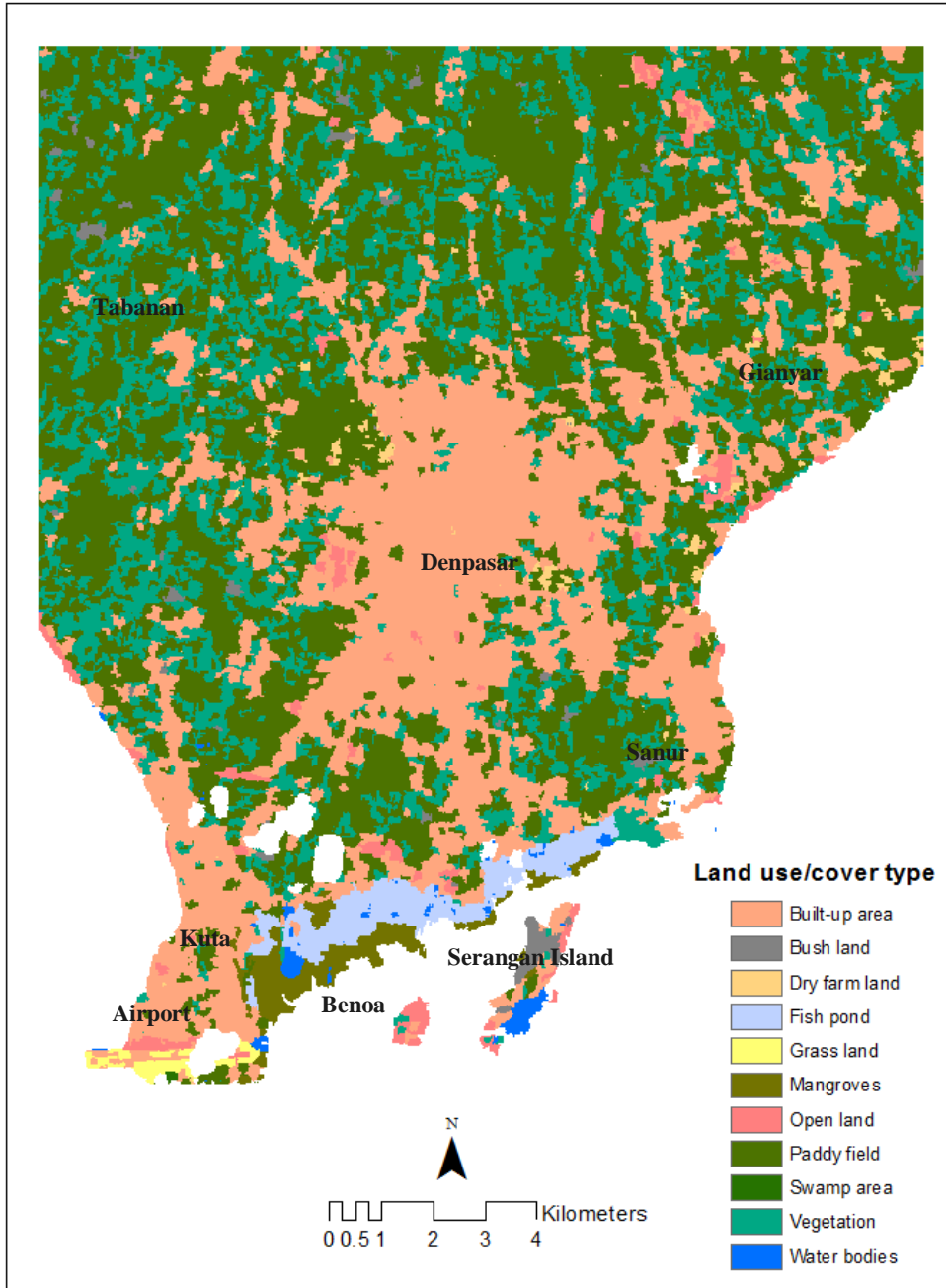


Figure 5.5 LULC of 1995

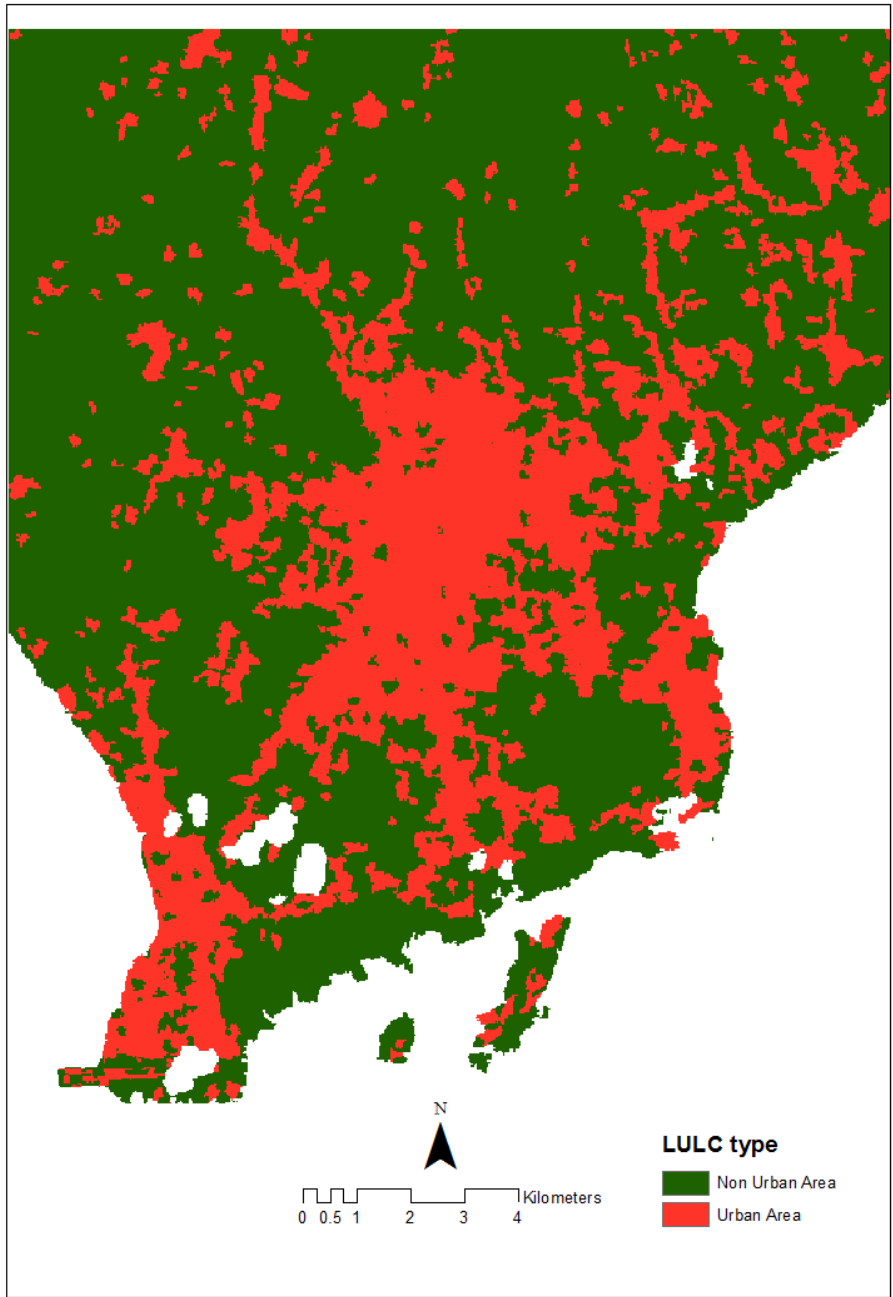


Figure 5.6 Urban and non urban area of 1995

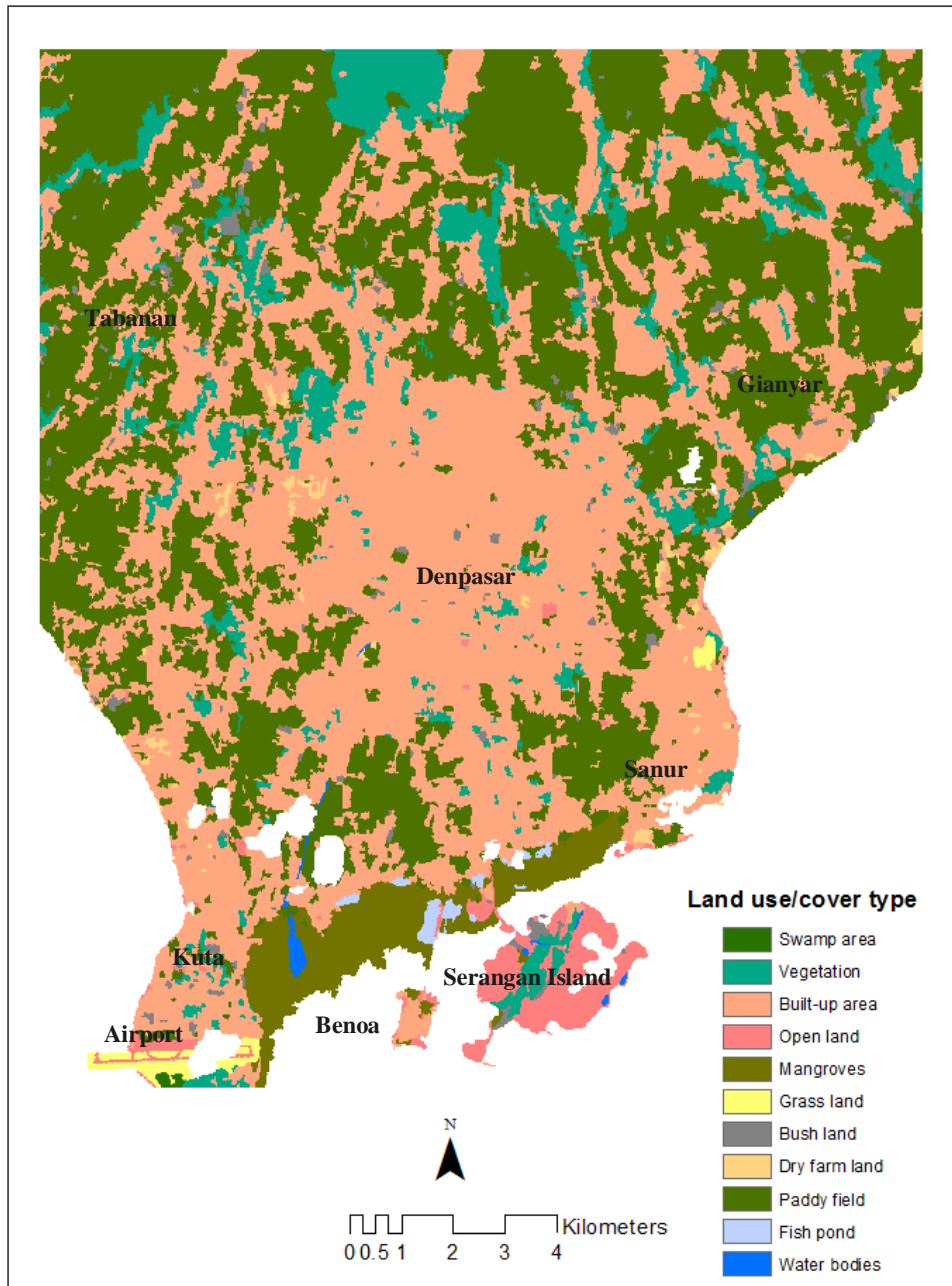


Figure 5.7 LULC of 2003

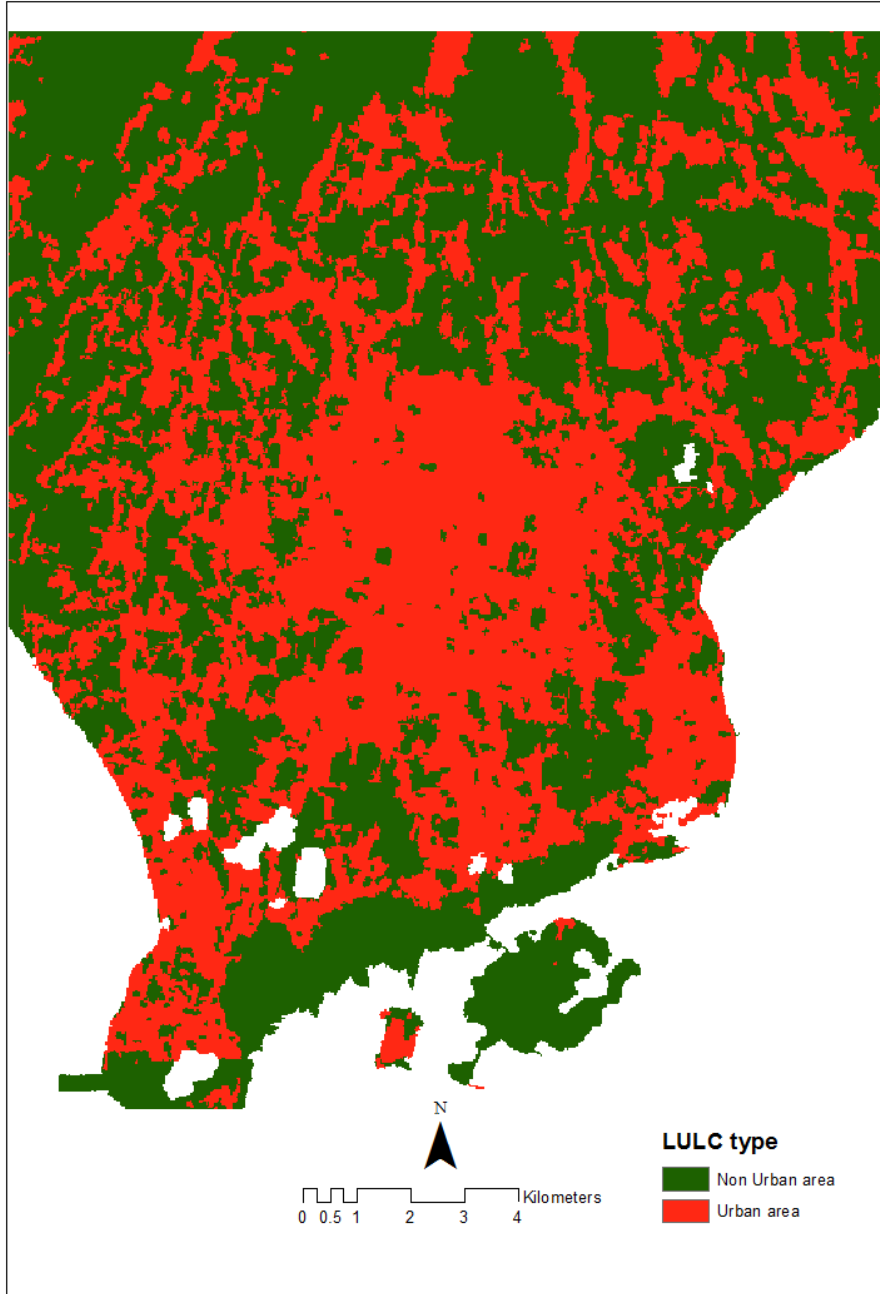


Figure 5.8 Urban and non urban area of 2003

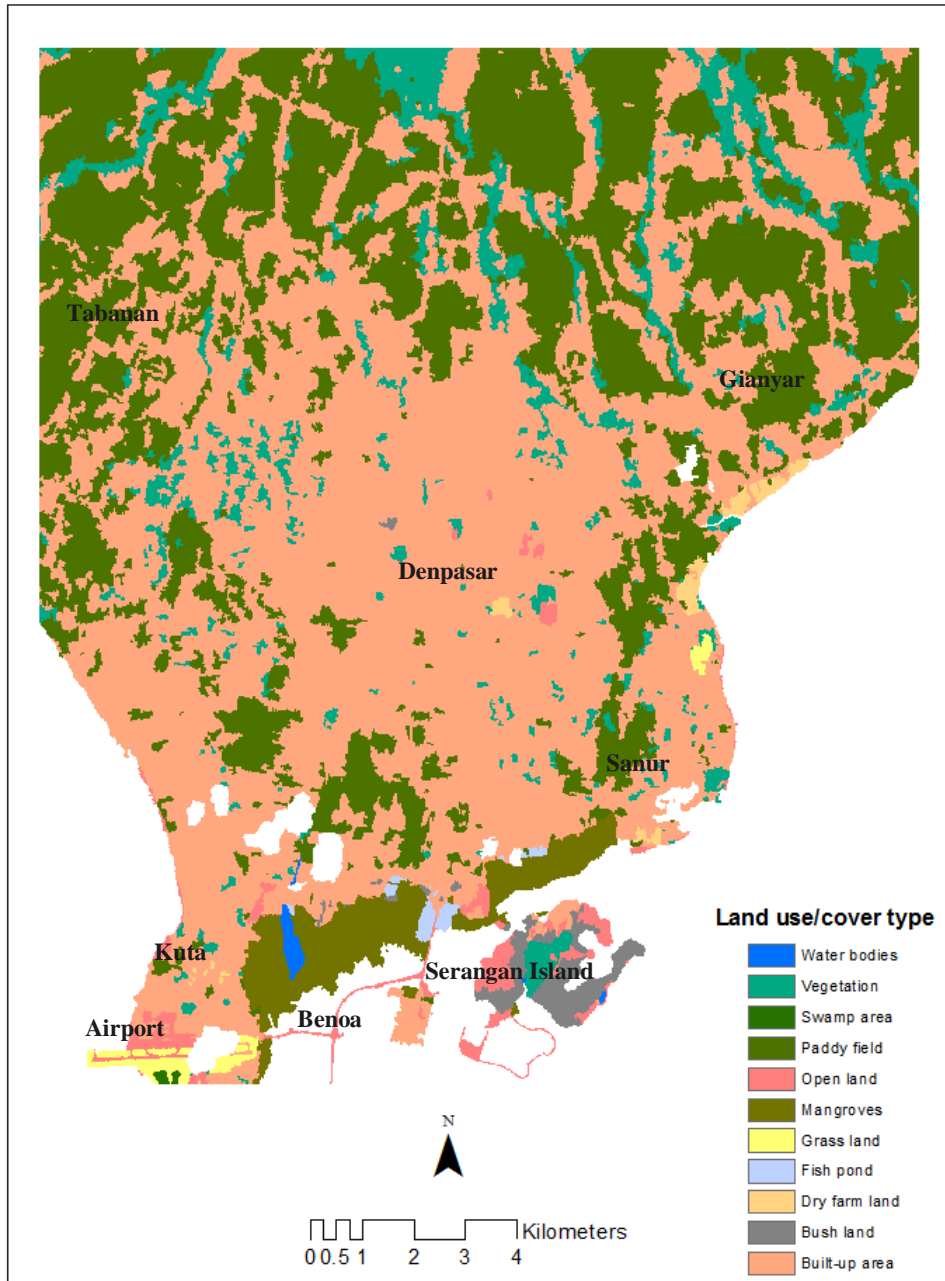


Figure 5.9 LULC of 2013

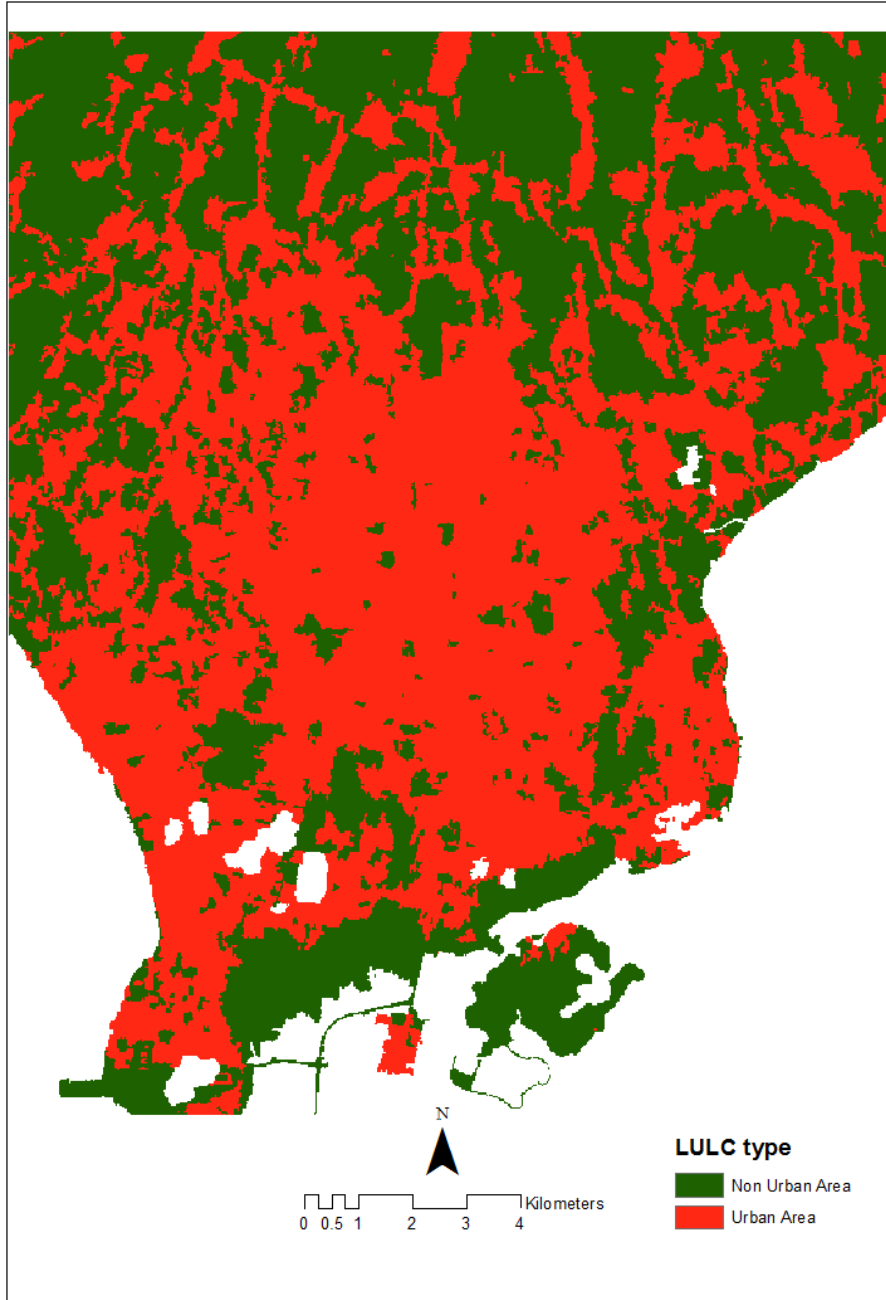


Figure 5.10 Urban and non urban area of 2013

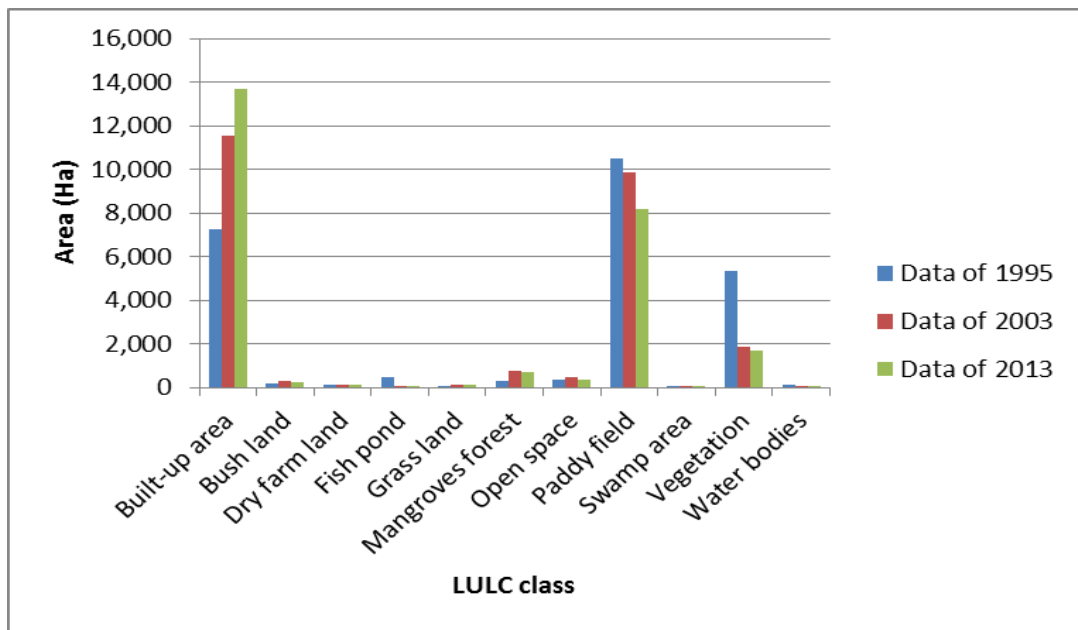


Figure 5.11 LULC distributions in Southern Bali

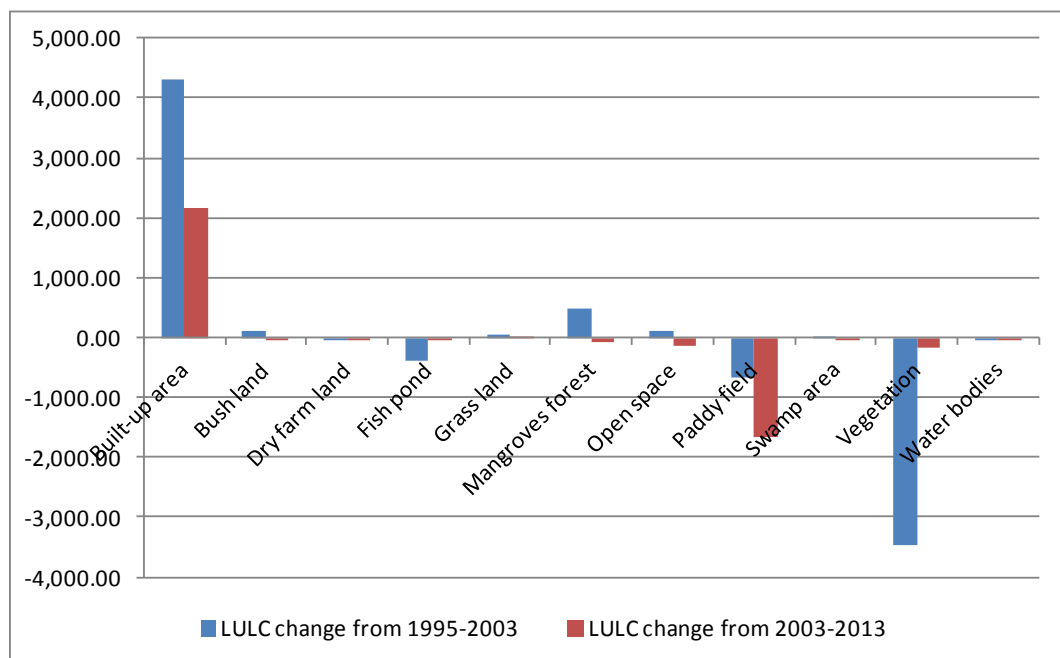


Figure 5.12 LULC changes of Southern Bali

Table 5.4 Area statistics of LULC change of Southern Bali

LULC class	Area (Ha)						Change of area (1995-2003)	Change of area (2003-2013)
	1995	%	2003	%	2013	%		
Built-up area	7,227	29.23	11,522	45.79	13,678	54.31	4,294	2,156
Bush land	189	0.76	284	1.13	239	0.95	95	-45
Dry farm land	145	0.59	122	0.49	108	0.43	-23	-14
Fish pond	445	1.80	64	0.26	55	0.22	-381	-9
Grass land	72	0.29	110	0.44	117	0.47	38	7
Mangroves forest	300	1.21	778	3.09	699	2.78	478	-79
Open space	376	1.52	486	1.93	344	1.37	110	-141
Paddy field	10,511	42.52	9,852	39.15	8,188	32.51	-659	-1,664
Swamp area	4	0.02	11	0.05	9	0.04	7	-2
Vegetation	5,350	21	1,889	7.51	1,704	6.77	-3,461	-185
Water bodies	100	0.41	42	0.17	40	0.16	-58	-1
Total area	24,723		25,164		25,185			

It can be seen from Table 5.4 that in 1995, paddy field was the dominant area (10,511 ha), followed by built-up areas (7,227 ha) and vegetation (5,350 ha). But, in 2013 built-up area became the dominant category (13,678 ha) followed by paddy field (8,188 ha), and vegetation (1,704 ha).

5.2.4.1 General increase

From 1995 to 2003, the area of mangrove forest designated for conservation clearly increased by 478 ha (Table 5.4) and this change has also influenced the total area difference among three different years. The rehabilitation project of mangrove forests has replaced most of the fish and salt production areas that existed in 1995. Figure 5.15 shows the areal increase and decrease of the three main LULC types over the observed period. A subtraction of increase and decrease of each class approximately was equal to the observed differences in Table 5.4 (in column of 'change of area').

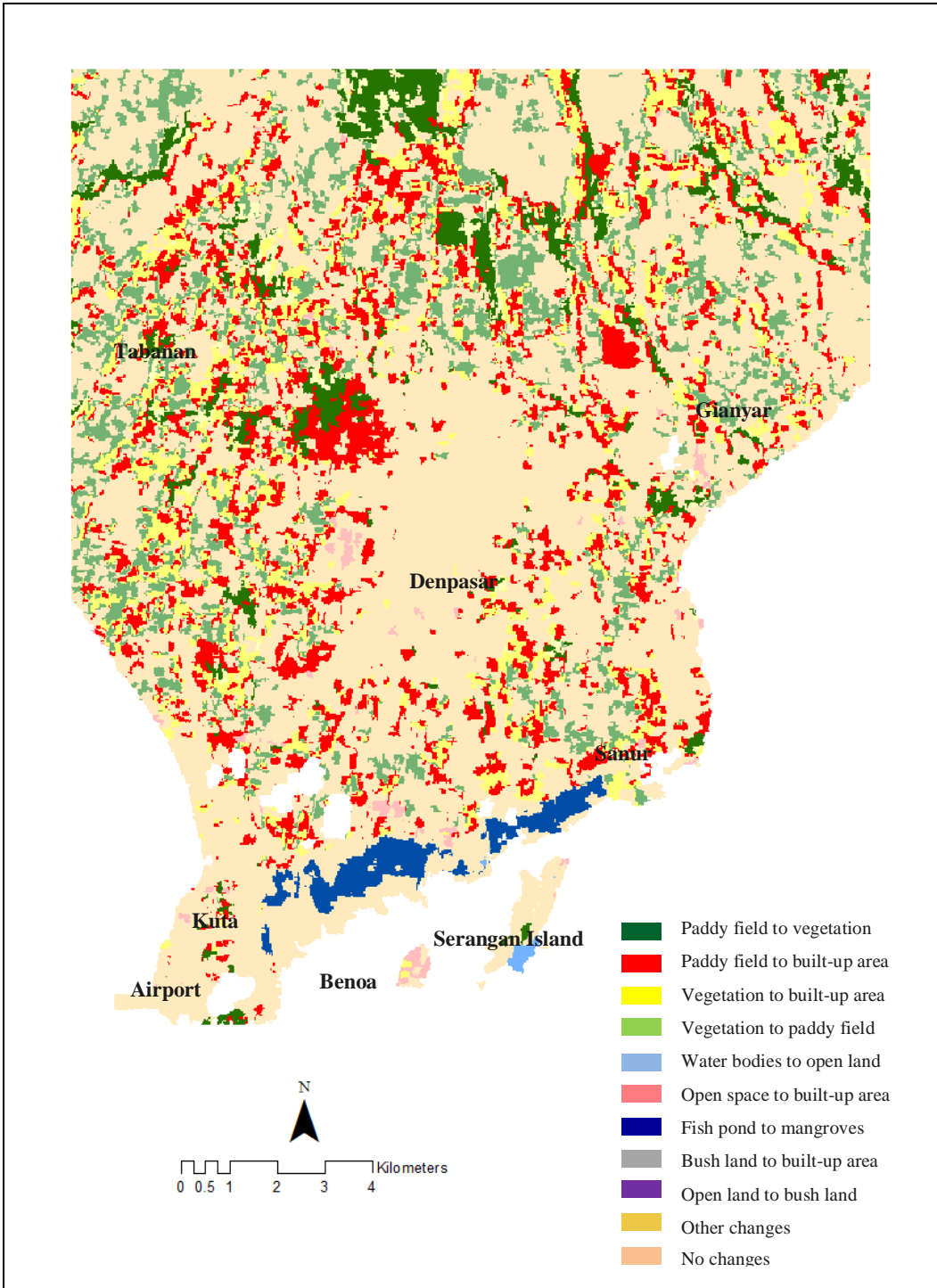


Figure 5.136 Major LULC conversions in Bali of 1995–2003

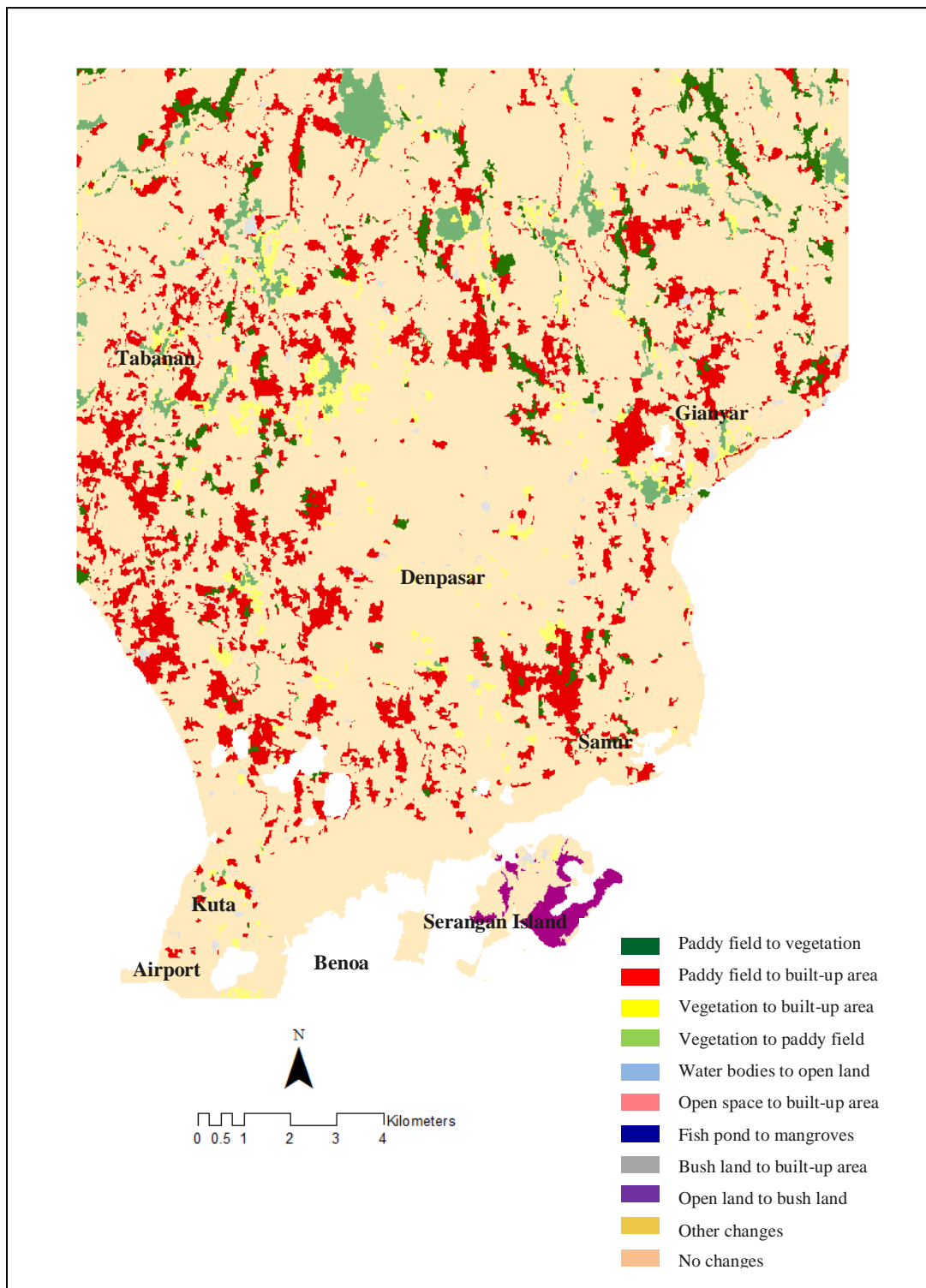


Figure 5.14 Major LULC conversions in Bali of 2003-2013

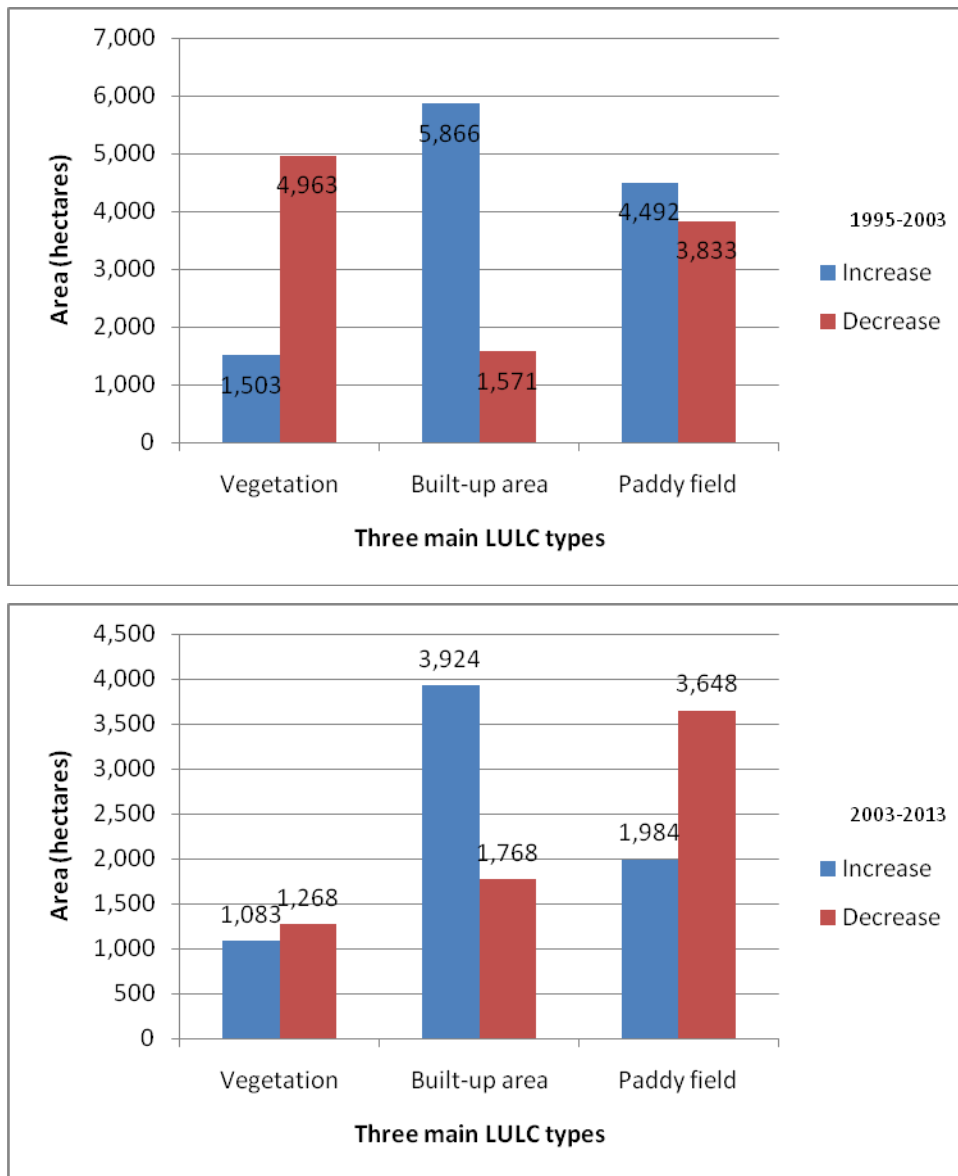


Figure 5.157 Areal increase and decrease of three main LULC types

The largest LULC increase from 1995 to 2003 was in the built-up area class (4,294 ha) (Table 5.4). The increase in built-up area was largely caused by the conversion of paddy field (3,081 ha), vegetation (2,408 ha), and open space (152.35 ha) (Table 5.5). The second largest increase in LULC was the mangrove forest class (478.67 ha) (Table 5.4), which gained area from the conversion of fish pond (346.89 ha) (Table 5.5). Between the period of 2003 and 2013, the increase in built-up area continued by 2,156 ha. The increase of built-up area was largely

made up of land change from paddy field (2,936 ha), vegetation (609.29 ha), and bush land (123.90 ha).

Table 5.5 Major LULC conversions from 1995 to 2013

“From class”	“To class”	1995-2003 (ha)	2003-2013 (ha)
Bush land	Built-up area	50.96	123.90
	Paddy field	66.90	95.12
	Vegetation	47.87	35.87
Dry farm land	Built-up area	63.50	68.39
Fish pond	Built-up area	23.89	21.05
	Mangrove forest	346.89	4.79
Mangrove forest	Built-up area	32.71	63.64
Open space	Built-up area	152.35	52.53
	Bush land	1.30	167.42
	Water bodies	27.25	56.31
Paddy field	Built-up area	3,081.37	2,936.10
	Bush land	138.05	0.16
	Dry farm land	62.10	60.06
	Vegetation	1,159.10	605.43
Vegetation	Built-up area	2,408.35	609.29
	Bush land	57.76	28.23
	Paddy field	2,441.72	595.22

5.2.4.2 General decrease

Between 1995 and 2003, a significant decrease in area was observed in vegetation and paddy fields. Vegetation cover decreased from 5,350 to 1,889 ha, and meanwhile paddy fields also decreased slightly, by around 6.3% (from 10,511 to 9,852 ha). The largest decrease in vegetation (about 3,460 ha) as it was converted to built-up area (2,408.35 ha), paddy field (2,441.72 ha) and bush land (57.76 ha). Paddy field experienced the second largest loss (659.03 ha) due to the conversion into built-up area (3,081.37 ha), vegetation (1,159.10 ha) and bush land (138.05 ha).

Between 2003 and 2013, the main LULC decreases were found in the paddy field, vegetation, and open space classes with 38.65% (1,664 ha), 4.30% (185 ha), and

3.28% (141 ha), respectively (Table 5.4 and Table 5.5). At the same time, the lost paddy field was mainly converted into built-up area (2,936.10 ha), vegetation (605.43 ha), and dry farm land (60.06 ha), while the decrease of vegetation was mainly converted into built-up area (609.29 ha), paddy field (595.22 ha), and bush land (28.23 ha). In contrast, built-up area shows a loss into paddy field (1,247 ha) and vegetation (406.75 ha) that were seldom in reality (Figure 5.14). This apparently unreal change of built-up areas into other LULC types was also occurred in the 1995-2003' transformation LULC, for example some built-up areas apparently changed into bush land (61.94 ha), dry farm land (27.73 ha), fish pond (2.20 ha), and water bodies (3.50 ha) (Figure 5.13).

5.3 Discussion

5.3.1 Seasonal difference impact on LULC changes

Between 2003 and 2013, the considerable conversion from paddy field to vegetation may be because of the abandonment of paddy fields due to water scarcity. The development of settlements often blocked irrigation systems. As result, instead of continuing paddy field activity, paddy fields were converted to mixed gardens (vegetation class). In addition, planting rotation activity might also have been applied in paddy fields, which may also influence the large change from paddy field to vegetation, and vice versa. When the land and crop's water content was lower and paddies had been harvested, several paddy fields were often in the transitional period (April). Paddy fields were then usually temporally replaced by mixed plantation varieties such as vegetable, cassava, corn, and banana. The purpose of diversified planting is to break the chain of pests and diseases, rejuvenate soil fertility, and increase farmer income. The farmers usually run this system for 3-6 months before the next paddy season. As a result, the change from paddy field to vegetation increased.

Table 5.6 The 1995-2003's transformation LULC classes

Area (Ha)	2003												
	1995	Built-up area	Bush land	Dry farm land	Fish pond	Grass land	Mangroves	Open land	Paddy field	Swamp area	Vegetation	Water bodies	Blank area (sea water)
Built-up area	5,656.65	61.94	27.73	2.20	20.73	35.03	53.96	1,092.97	1.07	254.26	3.50	17.63	7,227.68
Bush land	50.96	10.84	0.00	0.00	0.00	1.34	8.89	66.90	0.00	47.87	1.76	0.51	189.08
Dry farm land	63.50	1.98	3.70	0.00	1.65	0.00	0.36	65.70	0.00	8.82	0.00	0.01	145.72
Fish pond	23.89	0.59	0.00	38.84	0.00	346.89	16.30	8.27	0.00	0.03	10.43	0.01	445.25
Grass land	0.24	0.00	0.00	0.00	60.84	0.79	6.29	0.00	1.12	0.85	0.00	2.29	72.41
Mangroves	32.71	1.82	0.00	0.13	0.05	256.49	1.50	1.10	0.00	4.82	0.79	0.71	300.13
Open land	152.35	1.30	3.34	0.00	2.24	7.34	38.96	131.13	0.00	12.38	0.38	26.87	376.30
Paddy field	3,081.37	138.05	62.10	4.32	17.47	17.26	9.55	6,019.01	0.15	1,159.10	1.60	2.00	10,511.98
Swamp area	0.00	0.00	0.00	0.00	2.00	0.00	0.00	0.00	2.14	0.00	0.00	0.00	4.14
Vegetation	2,408.35	57.76	22.47	0.84	1.45	14.04	7.75	2,441.72	0.00	386.70	3.89	5.20	5,350.16
Water bodies	3.07	1.78	1.27	4.76	2.20	24.50	25.69	7.08	0.00	2.68	13.61	14.02	100.66
Blank area (sea water)	49.48	8.06	1.66	13.28	1.42	75.11	316.77	19.09	7.09	12.12	6.35	0.00	510.44
Grand Total	11,522.56	284.12	122.27	64.38	110.04	778.80	486.02	9,852.96	11.57	1,889.62	42.32	69.27	25,233.93

Table 5.7 The 2003-2013's transformation LULC classes

Area (Ha)		2013											
2003	Built-up area	Bush land	Dry farm land	Fish pond	Grass land	Mangroves	Open land	Paddy field	Swamp area	Vegetation	Water bodies	Blank area (sea water)	Grand Total
Built-up area	9,754.34	9.18	23.75	0.38	4.76	10.13	52.93	1,247.45	0.00	406.75	1.27	11.62	11,522.56
Bush land	123.90	12.07	1.91	0.00	0.00	1.64	12.37	95.12	0.00	35.87	0.00	1.24	284.12
Dry farm land	68.39	0.00	7.14	0.00	0.00	0.00	0.08	28.92	0.00	16.08	0.00	1.66	122.27
Fish pond	21.05	0.04	0.00	34.82	0.00	4.79	1.22	1.41	0.00	0.00	0.00	1.06	64.38
Grass land	4.06	0.00	0.00	0.00	98.87	0.25	4.31	0.00	0.28	1.18	0.00	1.09	110.04
Mangroves	63.64	13.38	0.00	15.51	0.06	648.87	9.81	5.11	0.00	0.27	9.07	13.07	778.80
Open land	52.53	167.42	0.18	1.72	4.05	7.53	175.21	4.40	0.00	16.66	0.53	55.78	486.02
Paddy field	2,936.10	0.16	60.06	2.62	0.00	4.05	18.39	6,204.19	0.00	605.43	2.57	19.39	9,852.96
Swamp area	0.00	0.00	0.00	0.00	2.64	0.00	0.00	0.00	8.93	0.00	0.00	0.00	11.57
Vegetation	609.29	28.23	14.38	0.00	6.15	1.55	10.63	595.22	0.04	621.36	0.28	2.49	1,889.62
Water bodies	5.26	3.65	0.05	0.10	0.00	0.64	0.55	2.76	0.00	0.63	26.75	1.94	42.32
Blank area (sea water)	40.22	4.90	0.69	0.11	1.42	19.71	59.39	3.71	0.00	0.36	0.00	0.00	130.51
Grand Total	13,678.78	239.03	108.15	55.25	117.97	699.15	344.90	8,188.29	9.25	1,704.58	40.48	109.34	25,295.17

5.3.2 Possible error sources of LULC classification and change detection

Considering that urban areas in developing countries are typically a chaotic mixture of rural and urban LULC and one purpose of this research is to explore LULC changes in Bali which are different from other areas in Indonesia, more detail LULC types were determined based on standard LULC classification for Indonesia and previous reference maps. One of limiting factors that contributes to the possible low accuracy in this classification process was small sample size for some small LULC types which were used in accuracy test. Several classes such as dry farm land, grass land, and fish pond had small reference points which less than 10 samples due to their small areas. The lower the sample size, the higher margin of error and lower confidence level. This means that the data becomes less reliable and thus should be revisited in the future to significantly improve the LULC result. Another possible cause of error in collecting of samples was due to the time of collecting reference data. Reference data for 2013 LULC map was collected from a field survey in October 2013, which was a different paddy field season from the acquired image from April 2013. Moreover, the difference in spatial resolution between classification and reference data may also influence the result. The ground truth data used for the year 1995 and 2003 collected from reference maps and Google images may also have adversely affected classification accuracy.

The high diversity and detailed LULC classification in a relatively large area may also influence separation between objects not too precise and contribute to the possible low accuracy under the 85% cutoff level. For example the features of paddy fields and vegetation, or other similar LULC types such as grass land, dry farmland, and bush land might have easy to be misclassified due to the closeness in location and spectral similarity. The low contrast feature boundaries and spectral similarity between mixed plantations on paddy fields and surrounding vegetation areas resulted in these regions being merged into single polygon

objects. Therefore, this error was caused by segmentation problems. Image objects may have been generated by either over-segmentation or under segmentation. Although it is possible to classify all pixels in an over-segmented image object to their true class, they often do not represent the properties of real objects so that they are not very useful. In contrast, some objects may have been generated at large scale or under segmented image object suffer from mixed classes within the objects and thus, the possible classification accuracy that can be achieved is always less than 100%. Thus, examining a segmentation object scale is very important and recommended. The application of OBIA in a smaller study area with higher spatial resolution image than ASTER and Landsat may also increase the accuracy.

As a result of these misclassifications, some errors in change detection occurred that was carried out using map-to-map comparison approach. For example built-up area that apparently changed into vegetation and paddy field. These changes were actually rare in the field. It was mainly located in peri-urban areas where semi dense built-up areas were mostly located. This rare change phenomenon is also may cause by misclassifications of the images due to under or over segmentation of the image. Similar spectral signatures of semi dense built-up surfaces (typically composed by both impervious and vegetative surfaces), paddy field and vegetation caused wrong delineated objects. The high scale level used may have caused the objects boundaries between segments was not be properly delineated and thus, the absence of an object occurred in some places. Moreover, many small segments that cannot be improved using a proper scale level of merge may also occur and influenced these misclassification results. Considering some of the errors which were found in the classification and in order to more clearly see the urban growth, the classification was aggregated into two the primary LULC , urban (built-up) and non-urban areas.

5.3.3 LULC change trend and impacts on environment

The change detection map locates areas of LULC change. Due to urban expansion, a mixture of rural and urban LULC types has become a major feature in the study area. New built-up areas were observed, particularly in the suburban areas. Urban expansion that extends further eastward and northeastward mainly occurred since the new road along the east coastal area connecting Gianyar to Denpasar was built in 2003. Generally, the growth of property developments, hotels, and roads has been the primary cause of LULC change in the study area, while mangrove forest and fishing industries were apparently the predominant drivers of the LULC changes in coastal areas.

Looking at LULC maps from 1995 to 2003, the rapid urbanization process was detected mainly at this period as urban areas (classified as built-up areas) expanded. This is indicated by the expansion of built-up areas by 4,294.89 ha over the 8-year period as a result of uncontrolled development in all directions. This means that for each year, urban areas increased by 536 ha. The increase of built-up types in this study area was much greater when compared to other tropical cities in Southeast Asia during a similar period such as Penang in Malaysia, with an urban expansion rate of only 102 ha/year from 1989 to 2002 (Tan et al., 2010). Bekasi, another city in Indonesia located close to the main capital city of Jakarta, shows a rate of urban expansion of 267 ha/year from 2003 to 2010.

Built-up areas were converted mostly from productive paddy fields and vegetation cover. This agrees with the previous study from As-syakur et al. (2011). Paddy fields are often located in a relatively flat area and thus, they have been good for accessibility of settlements. Moreover, paddy field land also indicates a high groundwater capacity for household water resource, making paddy fields ideal sites for settlement. The decrease in paddy field land may result in urban environmental problems, particularly flooding in the study areas. It has been noted that bad flooding occurred in south Bali in 2009 (Balipost, 2009). According to

Mizutani (2002), the shape and construction of paddy fields gives them an effective ability to restrain water and filter sediment before those materials are released downstream. A deliberate strategy should be made by the local government to sort out the massive agriculture and paddy field changes as this will lead to problem with food security and deep water shortage and imbalance urban ecosystem.

During the period 1995-2003, the total area increased by 2,444 ha due to land reclamation. In the late 1990s, Bali's local government promoted a plan to make Bali a world tourism destination that attracted many investors. At that time the island of Serangan was reclaimed for resort and tourism development and it was connected to the mainland of Bali by a bridge. The land reclamation mined sand and coral from the ocean floor in order to build a foundation for a new section of the island as a tourist enclave (Nakad, 2008). However, in 1997-1998 this reclamation was halted due to the Indonesian financial crisis, and until recent years, construction on the island was abandoned and had come to a standstill. This land reclamation may have resulted in detrimental environmental impacts such as habitat fragmentation and substantial loss of scarce natural resources. Other distinct environmental problems were massive flooding in the south region of Denpasar in 2009, sand beach erosion, loss of diversity (e.g. fish, turtle), and social economic problems (Nakad 2008; Sudiarta, 2012). The LULC maps clearly show the spatial distribution of the exposed sand as a new open space and depict the transformation of seawater bodies to open landfills on the Island of Serangan.

5.3.4 Driving Forces

The available literature suggests that urban development in Bali strongly depended on economic growth, and it developed relatively more quickly since the tourism boom in the late 1980s. The rapid economic development has attracted people to migrate to downtown Denpasar and the surrounding tourist destination areas in south Bali. The rate of population growth in Bali was relatively high at

1.40% per year (Statistics of Bali Province, 2011), as people have come not only from rural areas of Bali, but also from other islands in Indonesia and other countries. This population growth rate was similar to that of the capital city of Jakarta from 2000 to 2010 (Statistics of Bali Province, 2011). The increase of the population rate has triggered the growth of built-up area in order to meet settlement demand in the study area. Coastal areas in the Kuta and Sanur regions have become the most notable places where the main tourism facilities have been built. However, the economic growth of south Bali declined dramatically due to terrorist bomb blasts in 2003 and 2005. This is seen in the change in built-up areas that increased by a lower percentage from 2003 to 2013 (8.52%). This shows as suggested by Wu et al. (2008), that the population and economic growth of a territory obviously influences the changes in LULC.

Although urbanization in the study area is strongly influenced by economic growth and demographic change, the nature of urban expansion is also influenced by transportation and land value factors. Coastal land and road accessibility have played a pivotal role in Bali's built-up area expansion. Land speculation had a marked influence on the development of peripheral areas, as the more scarce available land was, the more expensive land became, as was confirmed during fieldwork. In response to escalating land prices and growing demand for housing, vegetation cover and paddy fields in suburban areas were rapidly transformed into built-up areas by individual households, the public sector, and private developers. Those sectors were all responsible for land developments in Bali. There is also indication that the redefinition of the Denpasar metropolitan area plan in 2008 that included the adjacent cities of Badung, Tabanan, and Gianyar (SARBAGITA) and led to the development of transportation also played a pivotal role in shaping rapid urban expansion. This is visible from the uncontrolled expansion of urbanization southwestward and eastward in response to this development.

Between the period of 2003 and 2013, there has been a reduction in the spatial changes of built-up area and vegetation compared to the period between 1995 and

2003 and there is a possibility of continual reduction over the next few years in the study area. This may suggest that the city has become less attractive for people to migrate into the area because of unaffordable land price. As a result, built-up area will likely expand further into rural areas outside the study area leading to peri-urbanization, urban sprawl and fragmentation.

The remaining urban paddy fields owned by local people were strongly influenced by the local government's conservation rule, which has restrained the massive change rate of those lands. In addition, preservation of these fields was also obviously influenced by local wisdom and the belief of local people in *subak*, the Balinese water irrigation community system. Many people still understand that paddy fields are difficult to transform directly into other LULC types, as this would disturb the surrounding paddy fields that use the same water irrigation system. However, rapid conversion of urban paddy fields to other non-farming uses still continues due to economic factors. Poor coordination among government agencies leads to the reduction of observed paddy fields. For example, several urban paddy fields in conservation areas had been illegally converted to built-up areas (residential) without any approval from the relevant authorities and without strict law sanctions. This condition illustrates the lack of effective coordination among involved agencies in Bali's LULC development and planning.

5.4 Chapter summary

Information about the patterns of LULC change, its driving factors and the impacts on the environment is important for effective urban management. This chapter has demonstrated the usefulness of RS and GIS approaches to retrieve LULC maps and estimate LULC changes using relatively low-cost remotely sensed imageries in this large and complex tropical urban-rural landscape. OBIA has been a valuable tool for producing LULC map information and the change detection comparison method is suitable for change detection purposes. However,

the OBIA approach requires a very good accuracy level in both classifications because the accuracy of the change map is the accumulation of the accuracies of the individual classifications. Some classification errors were caused by high diversity LULC types, the small number of samples for some LULC types, segmentation errors, time difference of collecting reference data, and difference in spatial resolution between classification and reference data. Using ASTER and Landsat imagery, 11 LULC classes were determined in the study site, which can be identified with good overall accuracy for classified images from 1995, 2003, and 2013 that were 85%, 87%, and 80% accurate and had kappa coefficients of 0.81, 0.85 and 0.78, respectively. Change detection showed that the southern part of Bali has experienced rapid urban expansion over the 18-year period, with the majority of built-up areas primarily acquired by converting paddy field particularly between 2003 and 2013 and vegetation areas along peripheral zones particularly between 1995 and 2003. These LULC changes were governed by population growth, rapid economic growth from agriculture to tourism sector, and road development, and were accelerated by rising land value. In addition, inconsistent and ineffective government regulation and poor coordination among involved agencies in enforcing planning strategies contributed to the fast LULC changes. In the other hand, the Balinese local wisdom helped to restrain the fast change during these periods.

6 IMPACT OF LAND USE AND LAND COVER CHANGE ON LAND SURFACE TEMPERATURE

Urban climate change at both the local and regional levels is currently of interest due to the increased alteration of vegetation and soil cover to impervious surfaces, particularly in urban areas. One profound impact of this alteration is a change in the energy balance of urban surfaces, which increases land surface temperatures (LSTs). The increase of LSTs leads to the formation of an Urban Heat Island (UHI), in which urban areas tend to have higher air and surface temperatures compared to temperatures in the rural surrounding areas.

A UHI is also an example of degradation in the urban environment that is caused by LULC change. Thus, the measurement and availability of LST information is very crucial in supporting urban management as the expanse of human pressure to the environment continues. Moreover, the impact of these changes on the LST varies from one place to another because UHI effects and distribution depend on the characteristics of human activities and local conditions.

This chapter focuses in understanding the UHI phenomenon, identifies driving factors of UHI effects by examining LST and NDVI in Bali, and discusses the change patterns in LST and NDVI during the 18-year period from 1995 to 2013. Moreover, as measurement of LST driven by LULC changes allows identification of the influence of human-related urban changes on LST, analysis of the quantitative relationship of LST by LULC types over the study area, as well as the influence of LULC and NDVI spatial patterns on LST was also carried out.

6.1 Method of NDVI and Land Surface Temperature Retrieval

6.1.1 Retrieving NDVI

The scaled NDVI of each year was required in this analysis. This is because NDVI values are subject to error due to seasonal variation. A scaled NDVI, therefore, was computed with the following formula (Lo and Quattrochi 2003; Dewan and Corner, 2014):

$$\text{NDVI}^* = \frac{\text{NDVI} - \text{NDVI}_{\min}}{\text{NDVI}_{\max} - \text{NDVI}_{\min}} \quad (6.1)$$

Where:

- NDVI* = Scaled NDVI value
- NDVI min = Minimum NDVI value
- NDVI max = Maximum NDVI value

6.1.2 Preparation of the land surface emissivity and the normalized difference vegetation index

Numerous factors need to be quantified to extract LST from satellite thermal data as LST is controlled by the surface energy balance, atmospheric conditions, surface thermal properties, and subsurface mediums (Becker and Li, 1990). Land surface emissivity (ϵ) is one of the factors required to calculate LST when using the Planck's relation. Emissivity is the ratio of the radiant energy emitted from the real world body to that released by a black body at a similar temperature (Jensen, 2000). Land surface emissivity (LSE) varies for different materials depending on their ability to absorb heat energy. It can be obtained using the normalized difference vegetation index thresholds method (NDVI^{THM}). Sobrino et al. (2004) consider three different cases:

- a) Fully bare ground
- b) Fully vegetated land
- c) Combination of bare soil and vegetation

Although the NDVI threshold method does not appear to be the best LSE estimation method for urban areas because several studies performed on inter comparison of NDVI threshold and validation against other LSE algorithms methods showed the lowest RMSE with the use of in situ data from the urban surfaces (Oltra- Carrio et al., 2012), it is the most appropriate option for Landsat TM data and to estimate urban LST patterns as a thermal band or a nighttime image is not required (Sobrino et al., 2004; Walawender et al., Bokwa, 2014). The process used to retrieve LST in this study is shown in Figure 6.1.

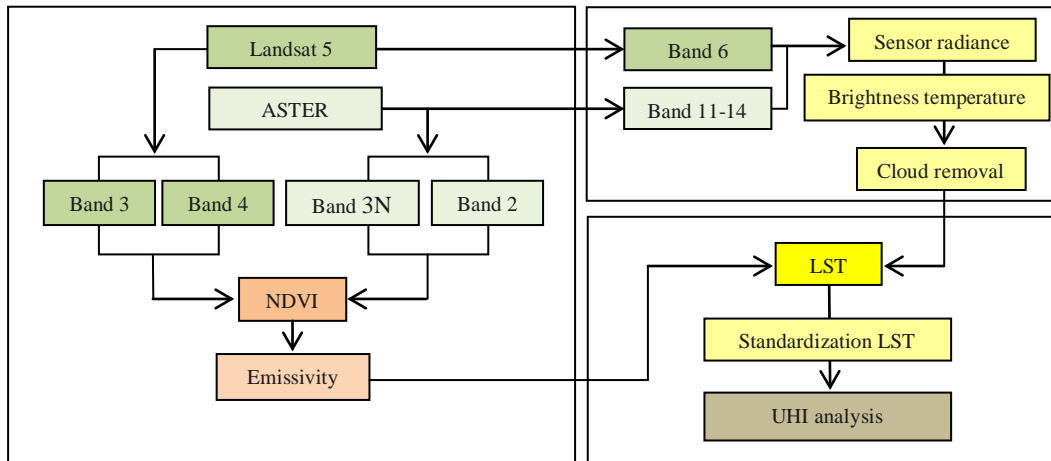


Figure 6.1 LST and NDVI retrieval.

In order to apply this methodology, the values of soil and vegetation emissivity are required. In this work, the emissivity value of 0.99 is used for vegetated surface and the emissivity value of 0.97 is for soil surface. The applicability of the values to global conditions and urban areas on the earth is assumed (Sobrino et al., 2004; Sobrino et al., 2012). In the case that a pixel is composed of a combination of bare soil and vegetation and if the surface is also flat, the basic emissivity equation is expressed as formula 6.2 (Sobrino et al., 2004; Sobrino et al., 2012; Widyasamratri et al., 2013).

$$\varepsilon = 0.004 PV + 0.986 \quad (6.2)$$

The proportion of vegetation (PV) is calculated using the following formula (Carlson and Ripley, 1997; Sobrino et al., 2004):

$$PV = \left[\frac{NDVI - NDVI_{min}}{NDVI_{max} - NDVI_{min}} \right]^2 \quad (6.3)$$

NDVI was computed using the following formula (Rouse et al., 1974):

$$NDVI = (NIR - R)/(NIR + R) \quad (6.4)$$

For Landsat TM: $NDVI = (Band\ 4 - Band\ 3)/(Band\ 4 + Band\ 3)$,

For Aster: $NDVI = (Band\ 3N - Band\ 2)/(Band\ 3N + Band\ 2)$

6.1.3 Retrieving LST from Landsat 5 TM

The Landsat 5 TM thermal infrared data that was acquired on 3/2/1995 has a wavelength range of 10.40 to 12.50 μm and a resolution of 120 m. This image was corrected and resampled to 30 x 30 m pixels (USGS, 2014). There are three types of methods which have been developed to retrieve LST from at-sensor and auxiliary data: single-channel method, split-window technique, and multi-angle method. Because the last two methods require at least two channels, the single-channel method is the only method that can be applied to the Landsat platform, with one thermal channel (Sobrino ., 2004). Traditionally, the main disadvantage of single-channel method is that some atmospheric parameters need to be considered, usually by a complicated procedure of radiosounding. In this study, LST were derived from the corrected TM TIR band (11.45 –12.50 m) by using the method described in Chander and Markham (2003), which does not require atmospheric parameters and is used widely in urban areas (Xiao et al., 2007). The extraction of the LST was carried out in the following phases:

- a) The digital number (DN) of the Landsat TM thermal infrared band was converted into spectral radiance using the gain and bias values specific to the individual scene. To extract the brightness temperatures and remove the intrinsic errors of the sensors, radiometric calibration was carried out,

which transformed the DN values data into a physically meaningful radiometric scale by averages of the equation 6.5 (Markham and Barker, 1987; Chander et al., 2009;):

$$L\lambda = \frac{(LMAX\lambda - LMIN\lambda)}{(Qcalmax - Qcalmin)} (Qcal - Qcalmin) + LMIN\lambda \quad (6.5)$$

or

$$L\lambda = Grescale \times Qcal + Brescale$$

$$Grescale = \frac{(LMAX\lambda - LMIN\lambda)}{(Qcalmax - Qcalmin)}$$

$$Brescale = LMIN\lambda - \frac{(LMAX\lambda - LMIN\lambda)}{(Qcalmax - Qcalmin)} Qcalmin$$

Where:

$L\lambda$ = Spectral radiance at the sensor's aperture [$W/(m^2 \text{ sr } \mu m)$]

$Qcal$ = Quantized calibrated pixel value [DN]

$Qcalmin$ = Minimum quantized calibrated pixel value corresponding to $LMIN\lambda$ [DN]

$Qcalmax$ = Maximum quantized calibrated pixel value corresponding to $LMAX\lambda$ [DN]

$LMIN\lambda$ = Spectral at-sensor radiance that is scaled to $Qcalmin$ [$W/(m^2 \text{ sr } \mu m)$] = 1.2378

$LMAX\lambda$ = Spectral at-sensor radiance that is scaled to $Qcalmax$ [$W/(m^2 \text{ sr } \mu m)$] = 15.3032

$Grescale$ = Band-specific rescaling gain factor [$(W/(m^2 \text{ sr } \mu m))/DN$]

$Brescale$ = Band-specific rescaling bias factor [$W/(m^2 \text{ sr } \mu m)$]

b) Conversion from Radiance to Brightness Temperature

The retrieved spectral radiance values were converted to a brightness temperature value by applying the inverse of Planck's function. This brightness temperature value is the effective at-satellite temperatures with a unity emissivity assumption (NASA, 2011):

$$TB = \frac{K2}{\ln[(K1/L\lambda + 1)]} \quad (6.6)$$

Where:

TB = Effective at-satellite temperature in Kelvin (K)

$K1$ = Calibration constant 1 in watts/(meter squared*ster* μm)

$K2$ = Calibration constant 2 in Kelvin.

For Landsat TM,

$K2$ = 1260.56 K

$K1$ = 607.76 $\text{Wm}^{-2}\text{sr}^{-1}\mu\text{m}^{-1}$

$L\lambda$ = Spectral radiance in $\text{Wm}^{-2}\text{sr}^{-1}\mu\text{m}^{-1}$

The three LST images derived were then converted to the most common unit – degrees Celsius – by subtracting the three LST dataset with absolute zero (approximately – 273.15 °C) (Xu and Chen, 2004) using “band math”. The temperature value obtained is not the actual LST, but the at-sensor brightness temperature. The at-satellite brightness temperature can be used to reflect the distribution of the LST as long as the water vapor content of the atmosphere is assumed constant and uniform for a relatively small region. This assumes then that the influence of the atmosphere on radiance temperature would be negligible (Chen et al., 2006; Du et al., 2014).

- c) Considering the nature of LULC, adjustment for spectral emissivity was necessary. Thus, the emissivity corrected LSTs were then computed using equation 6.7 (Artis and Carnahan, 1982):

$$LST = \frac{TB}{1 + (\lambda \times TB/\rho)\ln(\epsilon)} \quad (6.7)$$

Where:

λ = Wavelength of emitted radiance (the peak response and the average of the limiting wavelengths ($\lambda = 11.5 \mu\text{m}$) (Markham and Barker, 1987)

ρ = $h c / \sigma$ ($1.438 \times 10^2 \text{ mK}$)

h = Planck's constant ($6.26 \times 10^{-34} \text{ J s}$)

c = the velocity of light ($2.998 \times 10^8 \text{ s}^{-1}$)

σ = Stefan–Boltzmann's constant ($1.38 \times 10^{-23} \text{ J K}^{-1}$)

ε = Surface emissivity.

6.1.4 Retrieving LST from Aster

In this study, LSTs were retrieved from the 5 TIR bands of ASTER (Table 5.1) with the ground resolution of 90 m. According to Hulley et al. (2012), more bands in the TIR region used could lead to better LST estimation. As with the processes to retrieve LST from Landsat, a two-step process using equations 5.4 – 5.5 were also applied (ASTER Users Handbook, 2007):

- a) Conversion of DN to spectral radiance.

Conversion of the DN to spectral radiance ASTER for the 5 ASTER bands using formula 5.4 can also be translated into:

$$L\lambda = (\text{DN}_j - 1) \times \text{UCC}_j \quad (6.8)$$

Where:

$L\lambda$ = ASTER spectral radiance at the sensor's aperture measured in a wavelength j

J = ASTER band number

DN_j = Unitless DN values for an individual band j

UCC_j = Unit Conversion Coefficient ($\text{W m}^{-2}\text{sr}^{-1} \mu\text{m}^{-1}$)

The unit conversion coefficient of each band (bands 10-15) can be seen in Table 6.1.

Table 6.1 Unit conversion coefficients and calibration constants of ASTER thermal bands

Bands	Bandpass (μm)	Effective Wavelength (μm)	UCC ($\text{W m}^{-2} \text{sr}^{-1} \mu\text{m}^{-1}$)	K_1 ($\text{W m}^{-2} \mu\text{m}^{-1}$)	K_2 (K)
10	8.125-8.475	8.291	0.006882	3040.136402	1735.337945
11	8.475-8.825	8.634	0.006780	2482.375199	1666.398761
12	8.925-9.275	9.075	0.006590	1935.060183	1585.420044
13	10.25-10.95	10.657	0.005693	866.468575	1350.069147
14	10.95-11.65	11.318	0.005225	641.326517	1271.221673

b) Conversion of the spectral radiance into at-sensor brightness temperature.

The conversion of the spectral radiance into at-sensor brightness temperature (TB) was carried out using equation 6.6. This equation needs K_1 and K_2 which are coefficients governed by the effective wavelength of a satellite sensor. For example, effective wavelength of the ASTER band 10, $\lambda=8.291 \mu\text{m} = 8.291 \times 10^{-6} \text{m}$, thus the equation should be as below (Banerjee et al., 2014):

$$\begin{aligned}
 K_1 &= C_1/\lambda^5 \\
 &= 1.19104356 \times 10^{-16} \text{ W m}^2 / (8.291 \times 10^{-6} \text{ m})^5 \\
 &= 3040136402 \text{ W m}^{-2} \mu\text{m}^{-1} \\
 &= 3040.136402 \text{ W m}^{-2} \mu\text{m}^{-1} \\
 K_2 &= C_2/\lambda \\
 &= 1.43876869 \times 10^{-2} \text{ m K} / (8.291 \times 10^{-6} \text{ m})^5 \\
 &= 1735.337945 \text{ K}
 \end{aligned}$$

The value of other bands are given in Table 6.1.

The two processes above can also be estimated using ENVI software since the proper calibration coefficients to transform the integer DN into floating-point radiance values are available and can be applied automatically (The Yale Center of Earth Observation, 2014). Therefore, the two-step processes that apply basic atmospheric correction and conversion of the emissivity bands to a brightness temperature map (in degrees Kelvin) in the ENVI package were applied in this study.

- c) For determining the LST from Aster images, equation 6.6 was also used. As with retrieving the LST for Landsat, the emissivity for Aster was also computed using formula 6.1 and formula 6.7.

6.1.5 Cloud removal

The gross technique of checking the cloud area, which was successfully carried out by Saunders and Kriebel (1988) using the brightness LST value, was employed. Contaminated pixels tend to be seen as localized lower values of LST. Such pixels need to first be identified, and in this case they were less than 19 °C. Those cloud pixel values were excluded using “set null” tools in the ArcMap package.

6.1.6 Standardization of LST

It was not appropriate to directly compare and assess LST variability between LST images with multiple time periods since the LST value among the images might still represent different year and season parameters. Therefore, to bring all of the variables into proportion with one another, the data had to be standardized. The standardized LST was required to accommodate the temporal consistency and spatial comprehensiveness of the dataset comparison (Salama et al., 2012). According to Walawender (2013), the role of the proposed standardization of LST is to enable:

- Objective evaluation of the LST pattern derived from images acquired in different atmospheric conditions and in different vegetative periods
- Restriction of more general LST features
- Comparative analysis of LST spatial variability in relationship to various LULC types

Technically, the standardization using the Z-score (standard score) of the LST raster data reflects how many standard deviations of the LST data decrease from

the mean value over the whole data (Walawender et al., 2014). The Z-score standardized method measures the distance of the individual LST data points from the mean LST in terms of the standard deviation by subtracting the overall mean LST value from each individual LST pixel value in each of the gridded LST datasets and dividing it by the sample's standard deviation. This method accords to the following formula 6.9 (Salama et al., 2012; Eden, 2012):

$$LST' = \frac{LST - LST\mu}{LST\sigma} \quad (6.9)$$

Where:

LST' = Standardized LST in °C.

LST = Individual LST pixel value (of 1995 or 2013)

$LST\mu$ = Mean of the LST image (of 1995 = 20.90 °C or 2013 = 25.12 °C)

$LST\sigma$ = Standard deviation of the LST image (of 1995 = 0.96 or 2013 = 3.11).

LST' is negative if the raw score is below the mean and is positive if above the mean. However, while many researchers (i.e., Walawender et al., 2014) continue by using the Z-score standardization value in the LST analysis, the normalized LST of 2003 and 2013 was back computed to degrees Celsius in this case. In order to maximize the greater range of data sets of the UHI impact on the study site, the 2003 data sets was used as a base image to standardize the 1995 and 2013 data sets, using the following equation 6.10:

$$LST_j = (LST'_j \times LST\sigma_i) + LST\mu_i \quad (6.10)$$

Where:

LST_j = Individual LST pixel value (of LST map in 1995 and 2013)

LST'_j = Standardized LST (of 1995 or 2013) in °C

$LST\mu_i$ = Mean of the LST image (of 2003 = 25.99 °C)

$LST\sigma_i$ = Standard deviation of the LST image (of 2003 = 2.89)

This type of back computation is more commonly used with Min-max standardization. However, Min-max normalization is highly sensitive to outliers

in the data as the Min-max method scales the temperature between the highest and the lowest of the LST values (Dewan and Corner, 2014; Amiri et al., 2009; Carlson and Arthur, 2000). Standardizing the Z-score is the preferred method because this method produces meaningful information about each set of data, preserves range (maximum and minimum), and reflects the dispersion of the datasets (Etszkorn, 2012).

The distribution of observation data after the post-standardization of the LST value for each LULC type can also be examined using the box plot method. A box plot is a graphic summary of the distribution of samples that describe the shape of the data distribution, measure the central tendency, and measure the dispersion (diversity) of the observational data. The sample size of the LST for each LULC type that is less than 10 was excluded in the box plot analysis. The box plots of 1995, 2003, and 2013 that correspond to the minimum, low quartile ($q3$), median ($q2$), upper quartile ($q1$), and the maximum values were created. The important information in the box plots here can examine the shape properties and the spread the tendency of the original data sets by LULC types after the standardization and the differences over difference years which cannot be achieved using mean and standard deviation.

6.1.7 The LST pattern using transect analysis

In addition to the descriptive analysis of the LST maps, the LST pattern could also be visually evaluated using a transect graph for each image to examine the magnitude pattern. A transect in the west-to-east and the north-to-south direction was evaluated based on the variety of LULC maps whose production is discussed in Chapter 4. The LST was displayed on the vertical axis with the LULC type and on the horizontal axis with the distance.

6.1.8 Analysis of relationship between LST and LULC and NDVI

In order to measure the quantitative relationship between LST and the biophysical factors that were LULC and NDVI, two approaches were applied. In the first approach, analysis with regard to all LULC types over the study area was conducted to reveal the impact of LULC changes on LST. The vector data of LULC maps in 1995, 2003 and 2013 were super-imposed onto each of the LST layers in 1995, 2003, and 2013 using intersect tools in GIS to determine the statistical features of LST among the LULC types. Basic zonal statistics of LST across the LULC types were calculated and a series of descriptive statistics produced summarizing basic findings for the study area. The LST of different LULC types in 1995, 2003 and 2013 were then compared to examine the thermal environment change.

In the second approach, the degree of association between LST and NDVI was assessed by conducting a correlation analysis between both the normalized LST values and scaled NDVI by LULC type on pixel-by-pixel basis (Weng, 2001). The use of NDVI and PV in LST correction in highly urbanized areas and eventual comparison of LST and NDVI by correlation analysis were used in some studies such as Xiao et al., (2008) in China, Liu & Zhang (2011) in Hong Kong, Zhou & Wang (2011) in China, and Aduah et al., (2012) in Ghana. Moreover, Pearson's correlation coefficients were also measured between those two variables to see the direction and strength of a linear relationship between LST and NDVI by LULC types. The same sample data set of NDVI and LST was required for correlation analysis. In this case, swamp area was excluded as low sample and a two tailed test for statistical significance (significant at 0.01) was used.

Pearson correlation coefficient is referred to as the r-value that ranges from -1 to +1. The closer to the value of 1, the stronger the linear relationship between LST and NDVI and the closer to the value of 0, the weaker the linear relationship

between LST and NDVI. The positive r-value means the higher score on LST is associated with a higher score on the NDVI and vice versa. The negative r-value means the higher scores on LST are associated with lower score NDVI and vice versa, while not significant means there is no predictable relationship between those two variables. Moreover, there are two decision rules that are used for assessing if the Pearson correlation test is significant (for $\alpha = 0.05$). Those are:

- P value < 0.05 means the test is significant or there is a significant relationship between LST and NDVI
- P value > 0.05 means the test is not significant or there is not a significant relationship between LST and NDVI

6.2 Results

6.2.1 Spatial pattern of NDVI

Figure 6.2 – Figure 6.4 show the distribution of scaled NDVI of the three different years with scale bars were -0.5-0.3, 0.4-0.6, and 0.7-1. The maximum and minimum NDVI value vary from -0.4 to 1 in 1995, -0.3 to 0.9 in 2003 and -0.2 to 0.9 in 2013. According to Rouse (1974) the NDVI value is in the range of -1 to +1. Negative values represent inactive vegetation as well as vegetation with lower density and health such as water bodies, buildings, roads, and open area. In contrast, highly vegetated areas have correspondingly positive or higher NDVI values, which were found here in paddy field and mangrove forest. This is because the green vegetation is more sensitive to R band than to NIR band in terms of absorption and thus, the reflectance of NIR band is larger than R band that influence the higher NDVI value (Rouse, 1974).

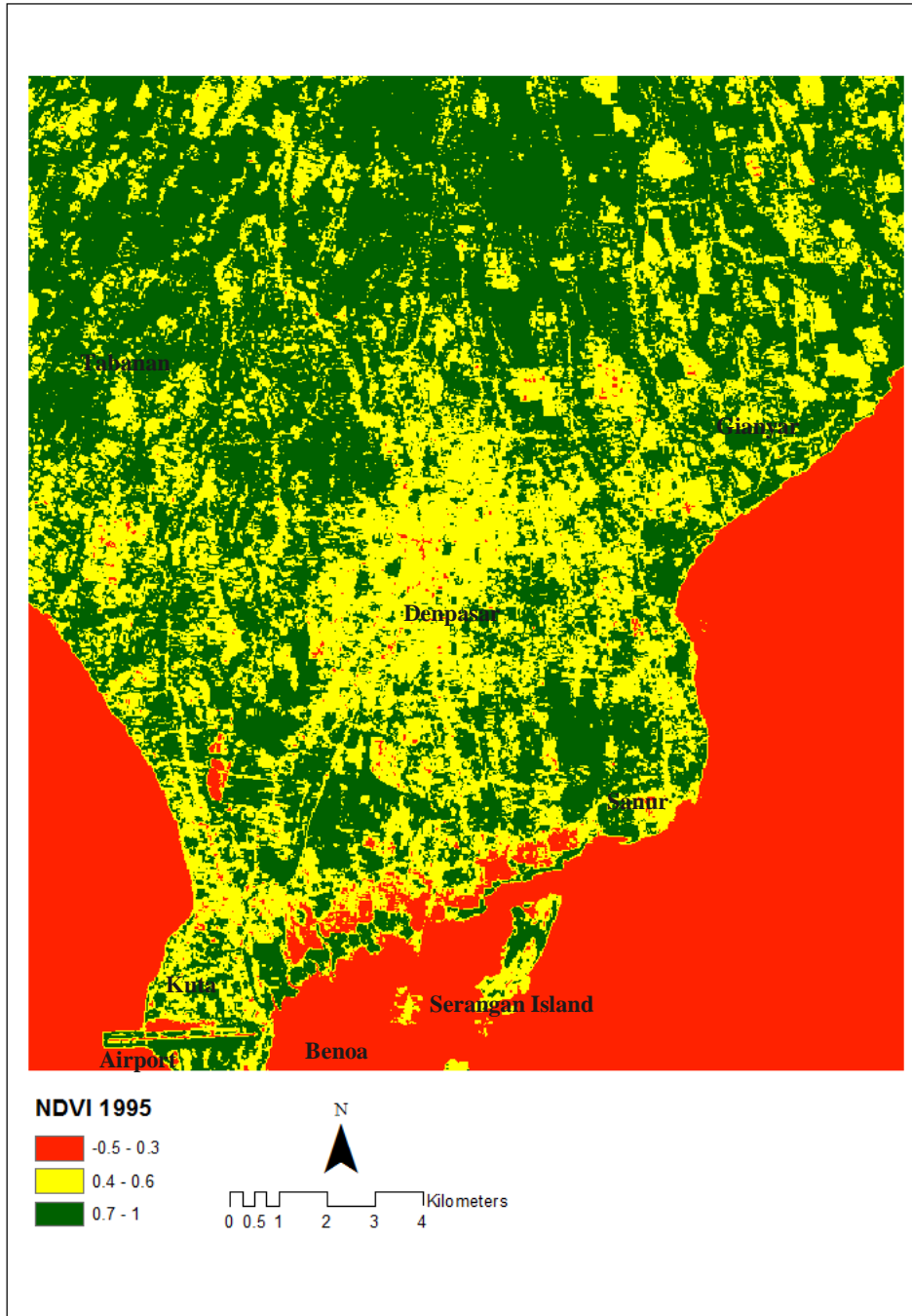


Figure 6.2 Scaled NDVI of 1995

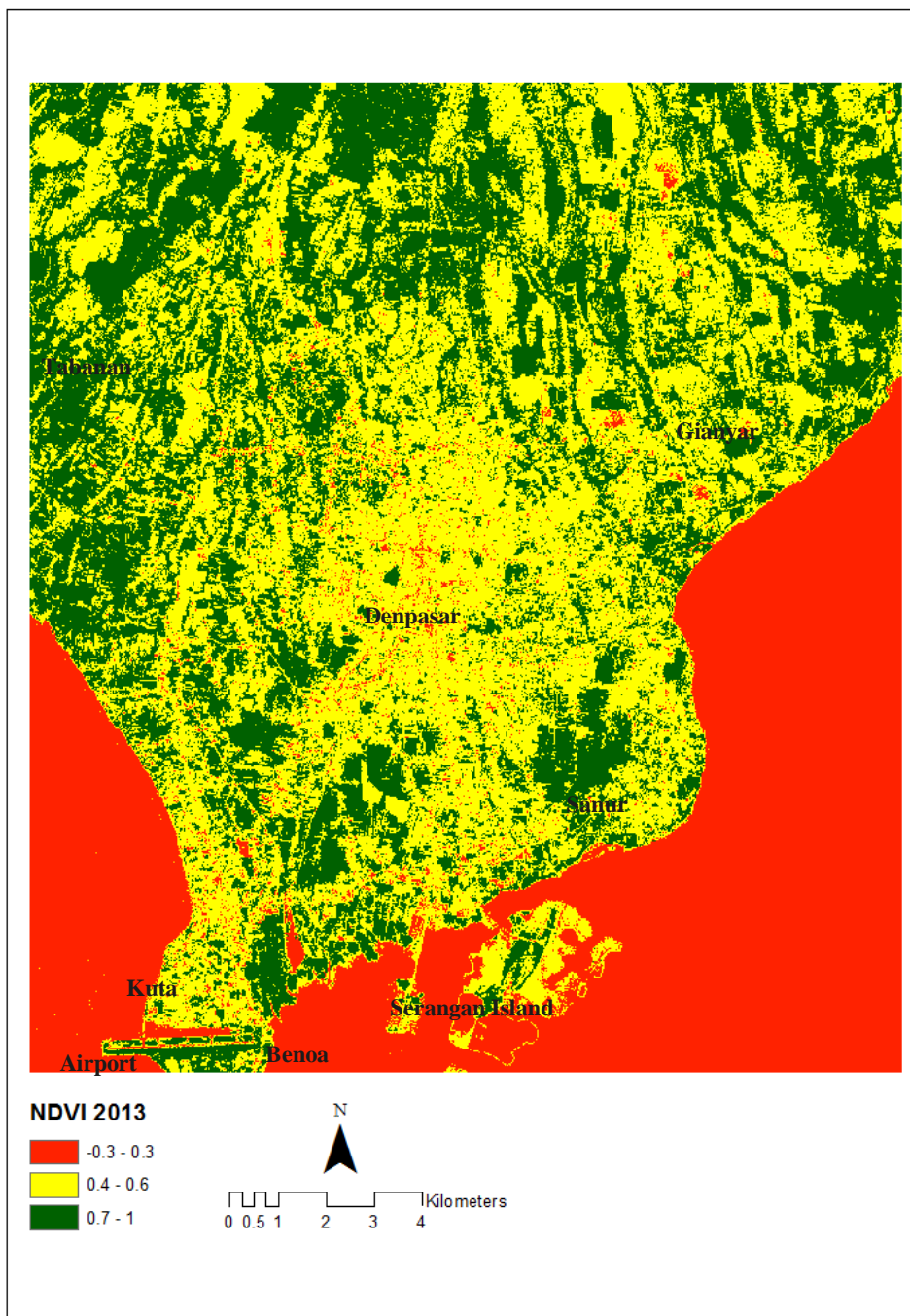


Figure 6.3 Scaled NDVI of 2003

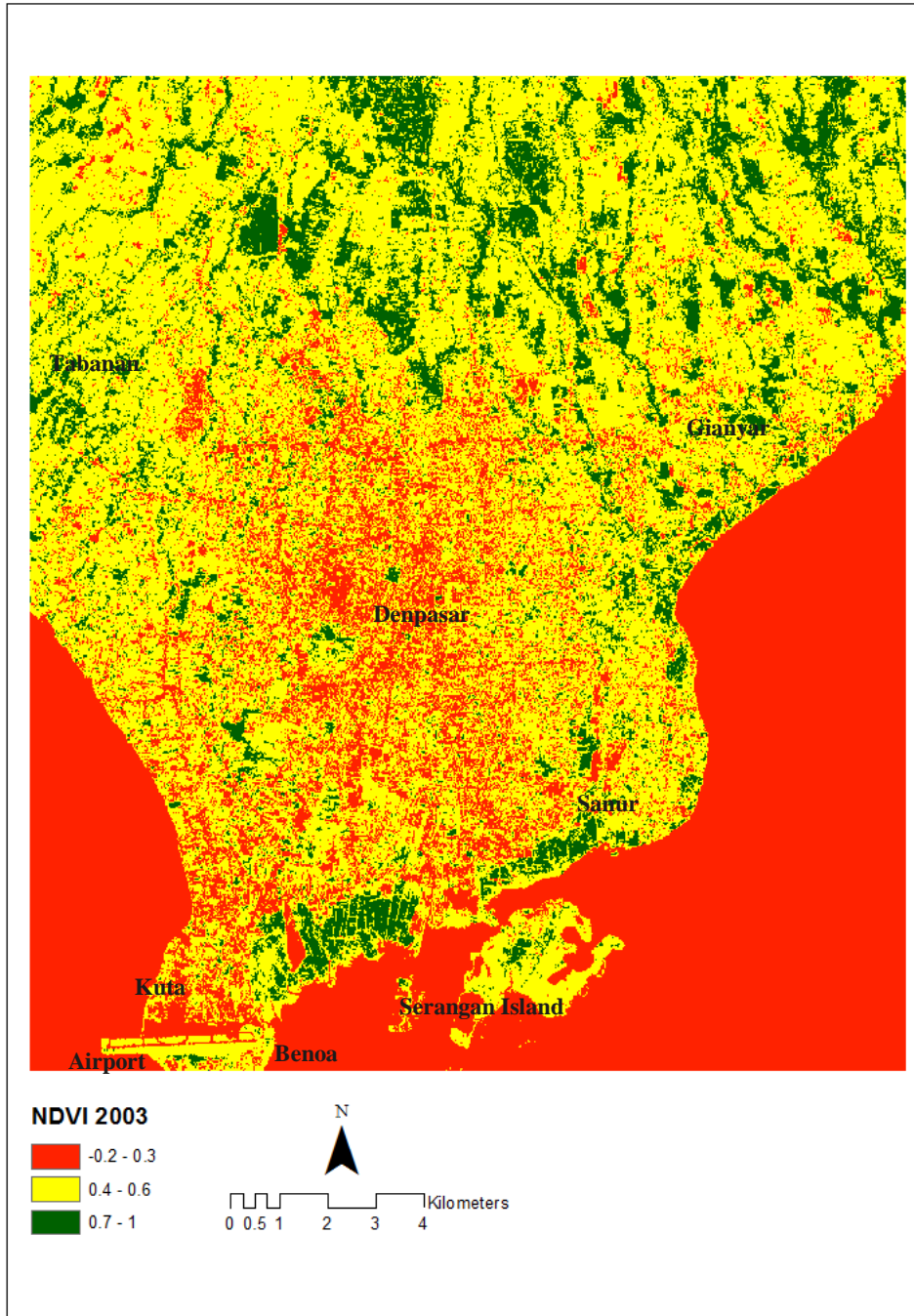


Figure 6.4 Scaled NDVI of 2013

6.2.2 Standardization of the LST

The means of the LST pre Z-score standardizations for the years of 1995, 2003, and 2013 were 20.90 °C, 25.99 °C, and 25.12 °C, respectively (Table 6.2). After the images of 1995 and 2013 were standardized, the dataset had the average value of 0 and the standard deviation value of 1. Since the dataset was then computed to degrees Celsius using the 2003 image as the standard, all of the standardized images then had the same mean value as the 2003 image, about 25.99 °C.

Even though the post-standardization of the LST value looked like it had undergone a substantial change in the mean and standard deviation values, the shape properties of the original dataset were actually retained. For the 1995 map, which was along the expanded temperature range, the mean temperature sharply increased from 20.76 °C to 25.82 °C, and the standard deviation increased from 0.96 to 2.89. The normalization effect for the mean temperature of 2013 was less than that for the 1995 image, which decreased by 1.07 °C. The standard deviation decreased from 3.10 to 2.76.

Table 6.2 Comparison of the LST image means for pre- and post-standardization in 1995, 2003, and 2013

Statistics	Land surface temperature				
	Standardized 3/2/1995	3/2/1995	24/2/2003	Standardized 24/4/2013	24/4/2013
Minimum	23.28	20	19.02	20.31	19.01
Maximum	38.33	25	36.39	33.12	32.79
Mean	25.98	20.90	25.99	25.99	25.12
Standard deviation	2.89	0.96	2.89	2.89	3.11

6.2.3 Spatial pattern of LST changes

A comparison of the visual and thermal bands for the images showed that the cloud and haze pixels had values less than 19 °C for both the 1995 and 2003 images and 23 °C for the 2013 image. The cloud-covered areas were masked out, which resulted in the area becoming null as shown by the white color. Figure 6.5

- 6.7 show the results of the LST extraction from 1995, 2003, and 2013, while Appendix V-1 – V-3 show the spatial distribution of the increasing LST. Increasing LST maps were produced by subtracting the standardized LST map, for example, by subtracting the LST map of 2013 from that of 2003.

There is no standard for the LST scale that describes features of “hotspots,” or so called UHI effects, which indicates relatively higher LST values for the surrounding areas. UHI effects are commonly described on the basis of their relative thermal intensity in the surrounding area (Mitchell, 2011). Some UHI studies in the cities of Indonesia, such as that in Tangerang city, described hotspot areas when the average LST values were above 30°C (Wibowo, 2013). In Bandung city, the average hotspot features were scaled at over 27.5 °C (Ramdani and Setiani, 2014). The average higher LST in Bandung was generally found to be lower than those of other cities since the city is located at a relatively higher elevation. Consequently, the average LST value of the UHI hotspot features in the study area was determined to be over 29 °C, based on the analysis of the three images.

Generally, UHI hotspots that were distributed in the study area can be easily identified in areas where buildings, roads, parking areas, and other non-vegetation surface types were dominant (Figure 6.5- Figure 6.7). Scattered hotspot features can be seen at Ngurah Rai International Airport, Kuta, Sanur, Benoa, the island of Serangan, Tabanan city, Gianyar city, and along coastal areas and traffic intersections. In addition, the new bypass road over the sea connecting Benoa to another Peninsula in southern Bali, which was constructed in 2013 shows an increasing LST value. In contrast, the considerably lower temperatures, which were less than 26 °C, were consistently found in the mangrove forest and paddy field areas as a result of their evapotranspiration process. Locations and distributions of the UHI hot-spots tended to expand wider from 1995 to 2013, and there was a tendency for the UHI effects to influence not only the coastal areas but also northward rural areas.

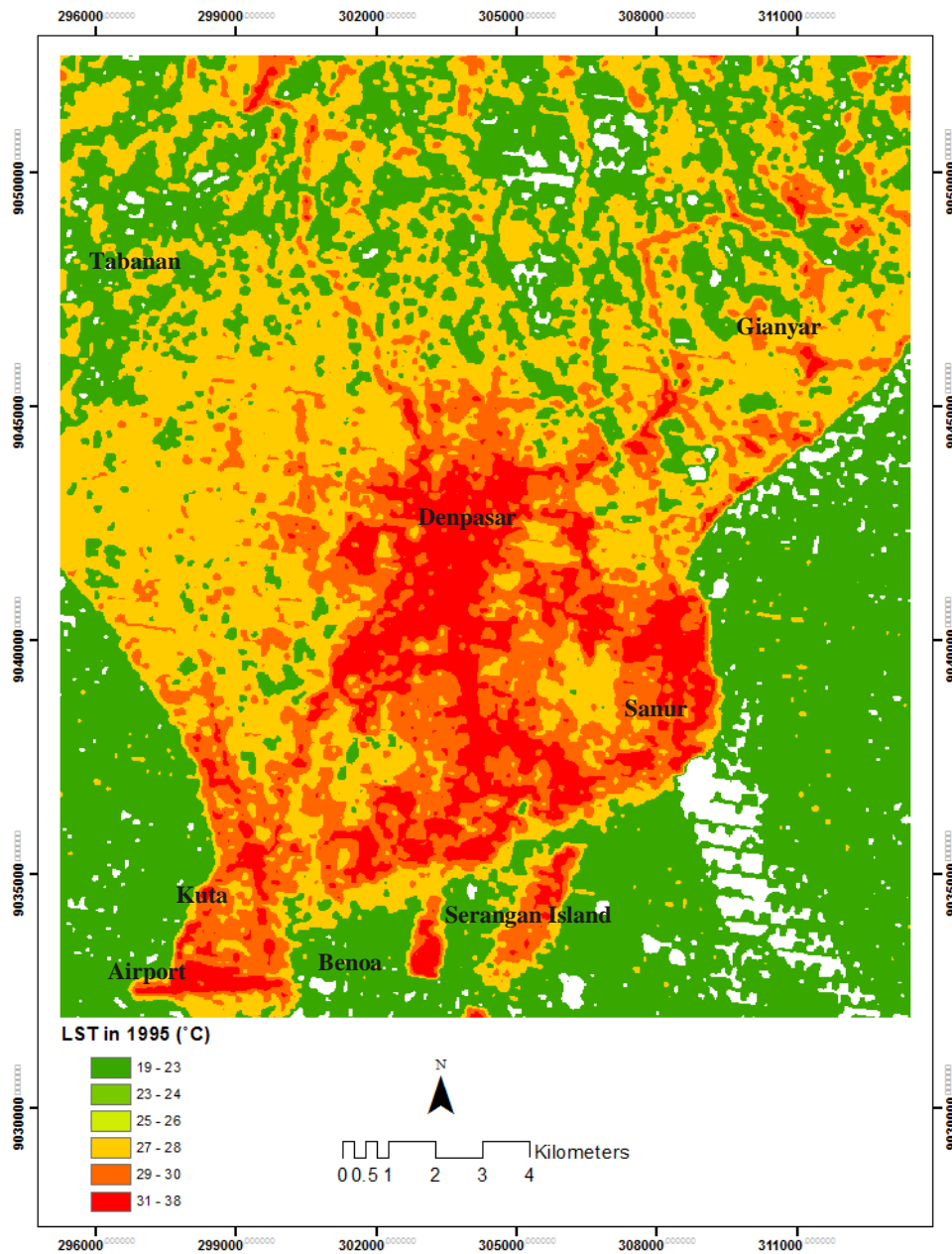


Figure 6.5 Spatial distribution of normalized LST in 1995

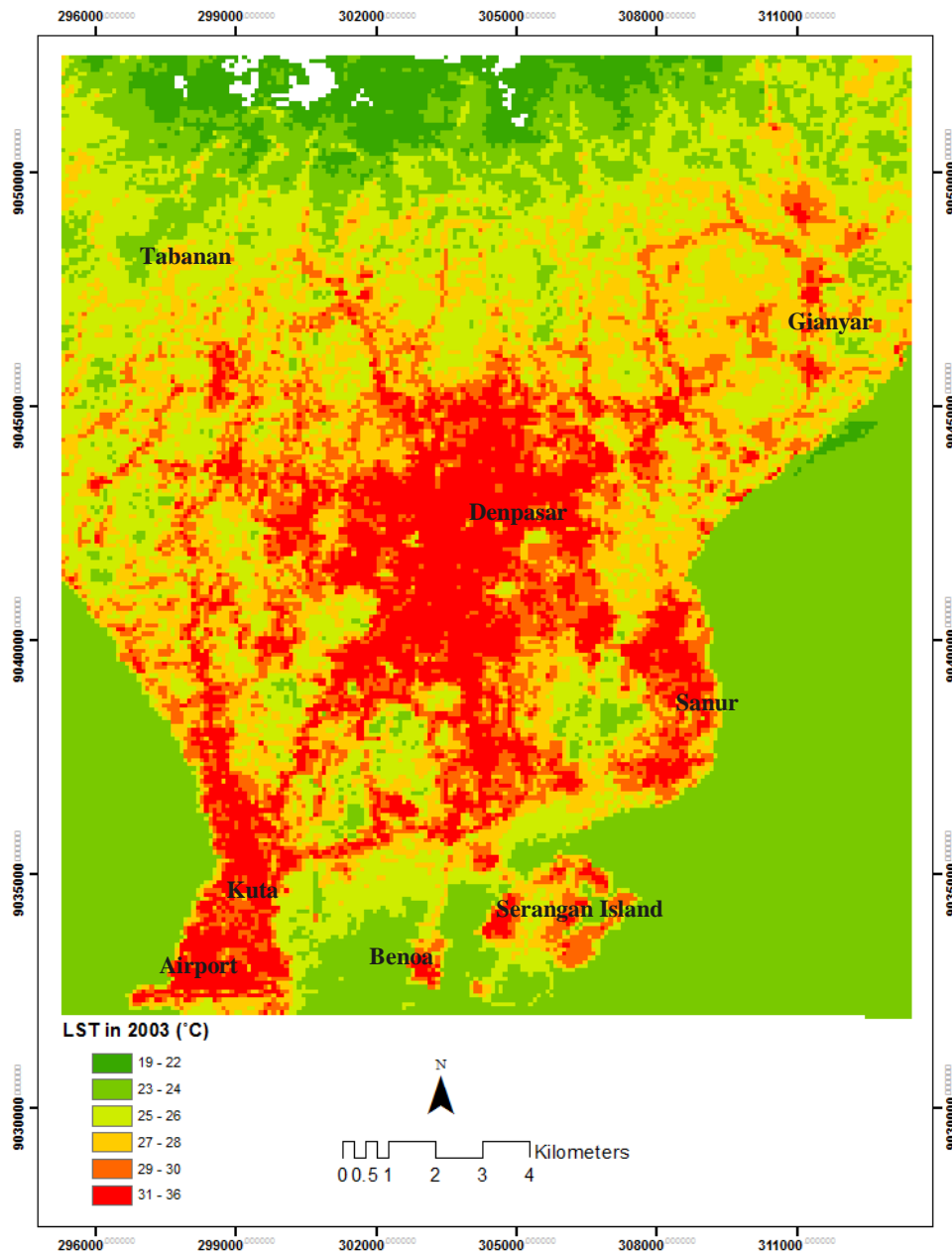
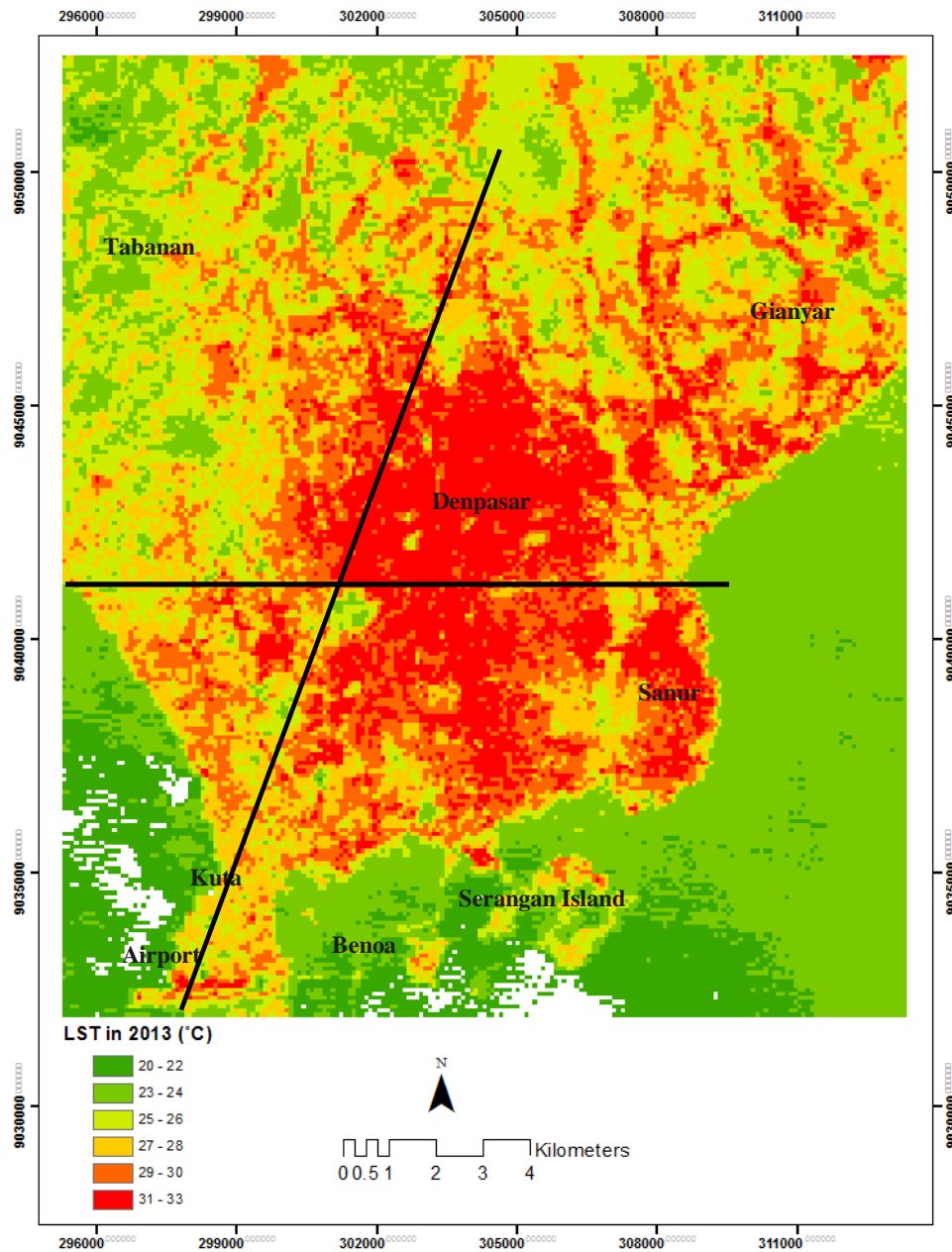


Figure 6.6 Spatial distribution of normalized LST in 2003



————— : a transect sample

Figure 6.7 Spatial distribution of normalized LST in 2013

6.2.3.1 The LST area

To support spatial distribution data of the increasing LST areas, the LST areas from 1995 to 2013 with more detail fluctuation of the LST areas (ha) were also quantified. From Figure 6.8 it can be seen that in 1995, the areas with an LST of 26 °C were the dominant areas of about 6000 ha. Similarly, in 2003, areas with an LST of 25 °C and 26 °C were persistently still the dominant LST areas of about 4000 ha, whereas in 2013, areas with the higher LST of 29 °C became the major LST areas of 6500 ha. This finding indicates that areas with a higher LST were more dominant in 2013 compared to previous years.

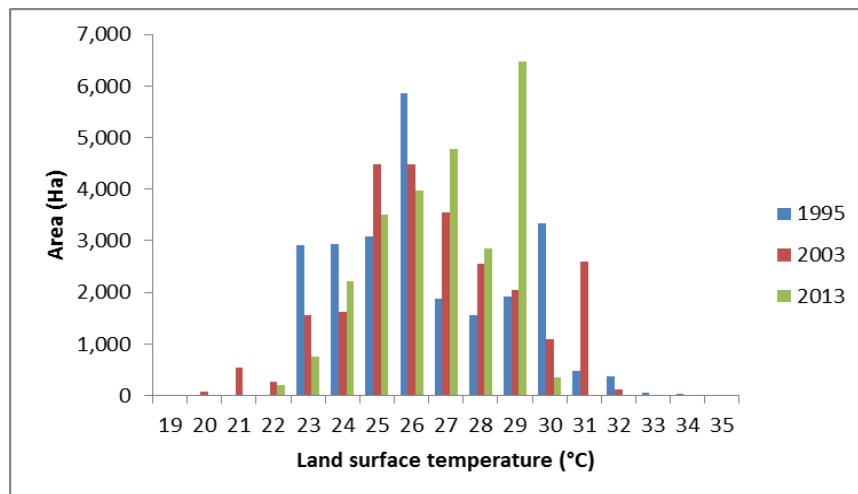


Figure 6.8 Statistics of LST area (ha) in 1995, 2003, and 2013

The fluctuations of the LST areas between 1995 and 2013, between 2003 and 2013 and between 1995 and 2013 are shown in Figure 6.9. Generally, between 1995 and 2013 and between 2003 and 2013, the increasing LST areas of 29 °C by 4000 ha were the major changes, although the LST areas of 30 °C and 31 °C decreased. In contrast, the relatively lower number of LST areas of below 26 °C persistently decreased along 1995-2013, as would be expected.

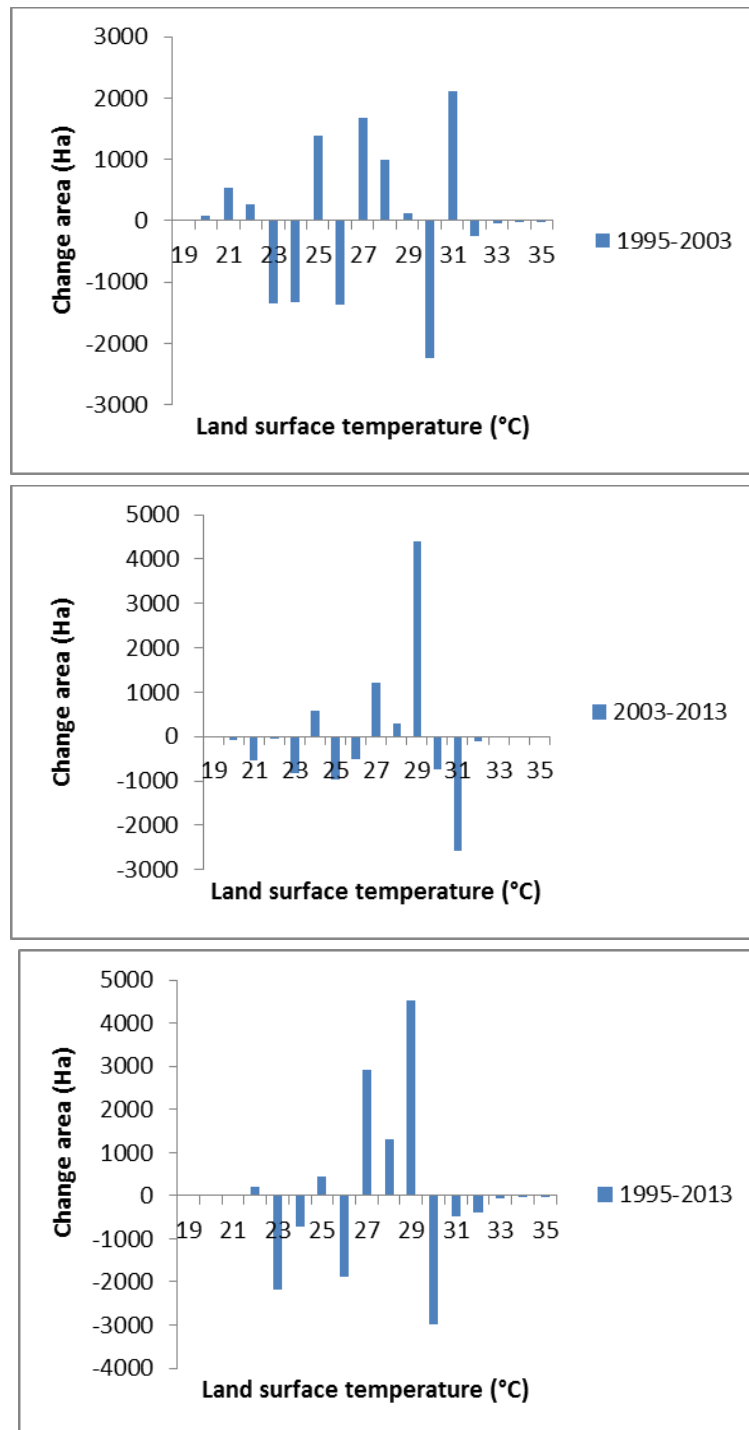


Figure 6.9 The changes in the number of LST areas (ha) from 1995 to 2013

6.2.3.2 LST graphs

The detailed local thermal pattern of UHI effects for the three different images can be seen from the transect graphs of the LSTs (Figure 6.10 – Figure 6.11). The transect location can be seen in Figure 6.7. The transect graphs of the LSTs (West-to-East) show that the LST increased from the sub-urban areas towards the inner city areas, and the lower LST was particularly dominant in the paddy fields and vegetations. The increasing LST at the urban fringes is shown by a relatively steep gradient that gradually inclined as the LULC shifted to a built-up area type at the downtown with more intensive impervious surfaces. The stable increasing temperature gradient remained high until reaching the highest temperature point at the center of the city; then it went down. In contrast, there were still some declining temperature gradients found at the downtown areas as results of the cooling effects of the LULC types such as vegetation and water bodies. The cooler temperature gradient afterward was found close to the sea basin vegetation, and it extended to the sea water.

The similar pattern also can found in the transect graphs of the LSTs (South-to-North) among three different years. However, the higher LST was not only found in the downtown of Denpasar but also in the airport area and surrounding (Kuta). Paddy field areas located between those two locations shows notable lower LST and distinctly can be recognized in the LST graph pattern (Figure 5.11). The higher thermal uniformity of built-up areas in the downtown area indicates a reduction in urban thermal quality, which needs mitigation. In order to prevent formation of more UHIs in regional areas, it is important to keep separating the hotspots from the business center of Denpasar city by conserving paddy fields, vegetation, and other LULC types proven to have low LSTs.

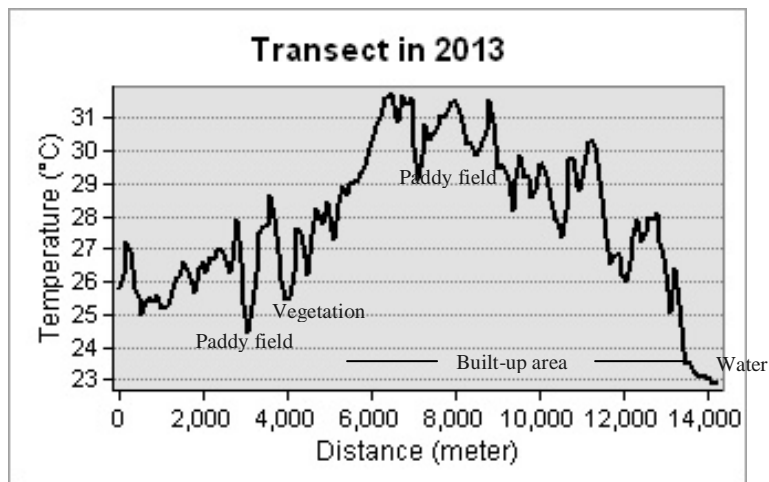
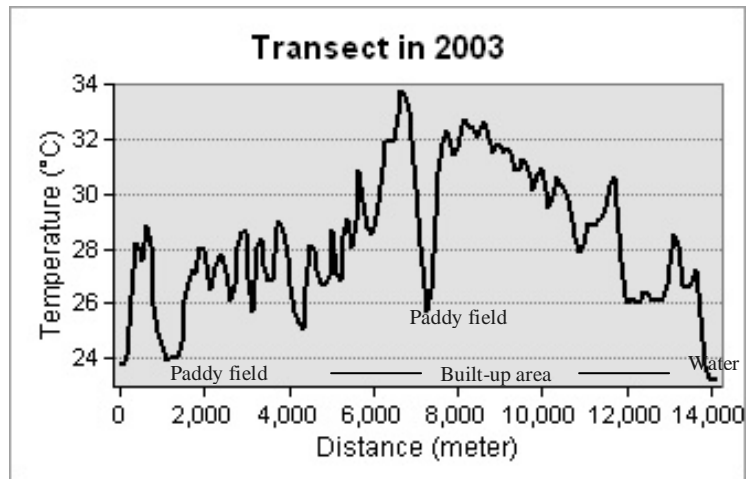
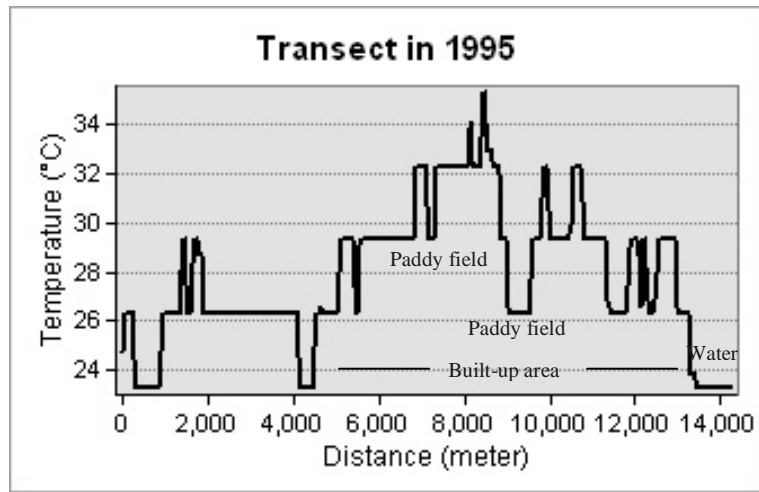


Figure 6.10 Transect graphs transect graphs of the LSTs (West-to-East)

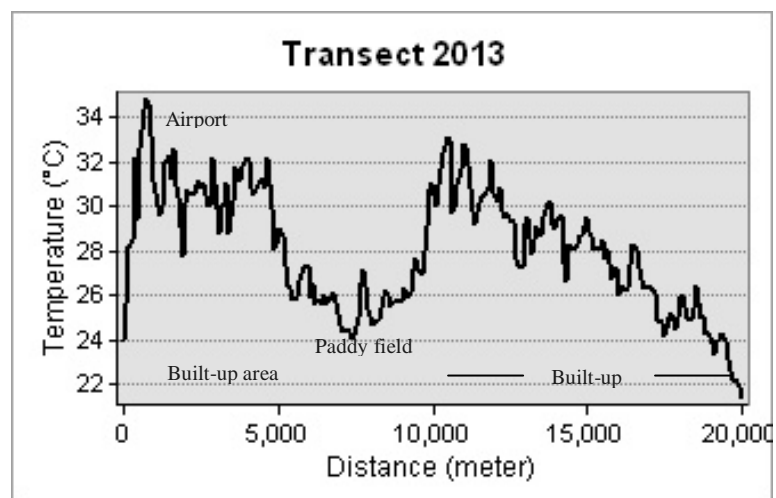
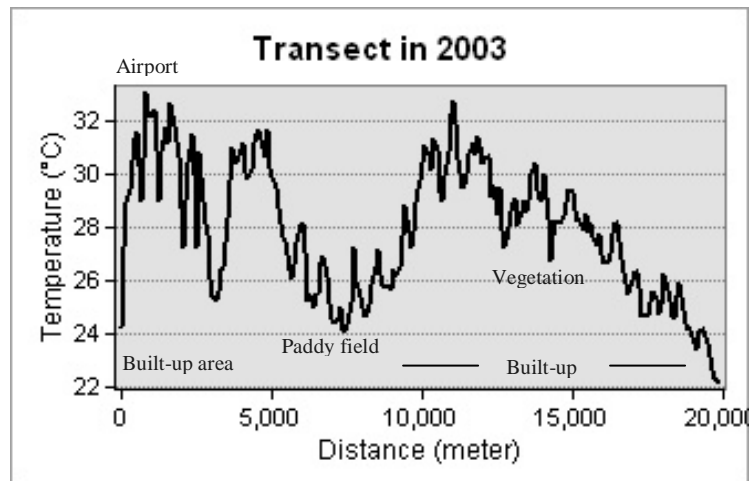
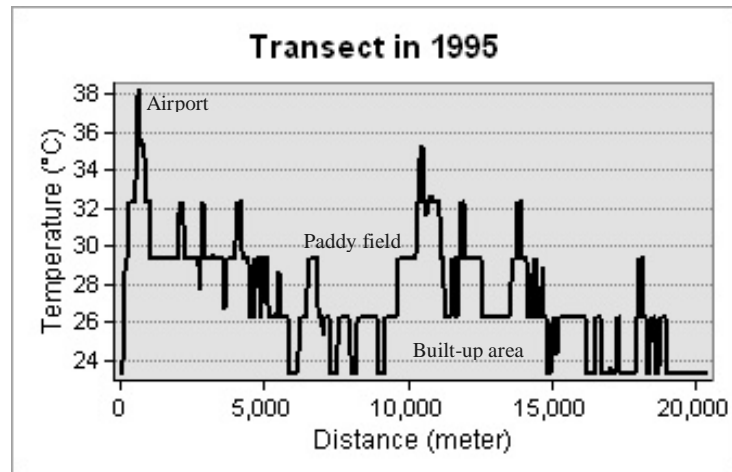


Figure 6.11 Transect graphs transect graphs of the LSTs (South-to-North)

6.2.4 The LST of different LULC types

The statistics of standardized LST of different LULC types are shown in Table 6.3 and Figure 6.12. Inspection shows that the mean LST among the 11 LULC categories varied from 1993 to 2013. The lowest mean of temperature was observed in paddy field (25.69°C), followed by mangrove (26.01°C), and vegetation (26.04°C). The highest LST in 2003 and 2013 was in built-up areas. In 1995, fish pond (29.79 °C) exhibited the highest average LST followed by built up area (29.24 °C), and open land (28.82 °C). Mostly the high mean temperature of the fish pond located close to the mangrove due to various functions of ponds. According to the field work, it reveals ponds were not only used for fishery, but also for preparation of mangrove forest recovery and salt production. Therefore, pond surfaces were not only fully covered by the water, but also by sand and salt. It can be indicated from the highest SD value of fish pond in 1995 by 2.22. The higher LST of built-up areas and open land were not surprising as a result of its relatively low thermal inertia (Carnahan and Larson, 1990).

Table 6.3 Statistical features of standardized LST by LULC type

LULC type	1995		2003		2013		Mean 1995, 2003, 2013 (°C)
	Mean (°C)	SD (±)	Mean (°C)	SD (±)	Mean °C	SD (±)	
Built-up area	29.24	2.71	28.65	2.49	28.51	1.85	29
Paddy field	25.69	2.15	25.20	1.87	26.42	1.76	26
Open space	28.82	3.87	28.73	2.36	25.77	2.55	28
Fish pond	29.79	2.22	26.84	1.39	24.88	1.88	27
Water bodies	27.66	2.29	25.84	1.99	24.42	1.61	26
Mangroves	26.01	1.97	25.93	1.34	23.72	1.47	25
Swamp area	26.29	0.00	25.48	0.44	24.26	0.99	25
Vegetation	26.04	2.06	25.53	2.42	26.36	1.86	26
Bush land	26.93	2.60	26.87	2.12	24.63	2.08	26
Grass land	28.61	2.87	29.19	2.41	26.63	2.01	28
Dry farm land	27.05	1.85	28.02	1.51	26.99	1.55	27

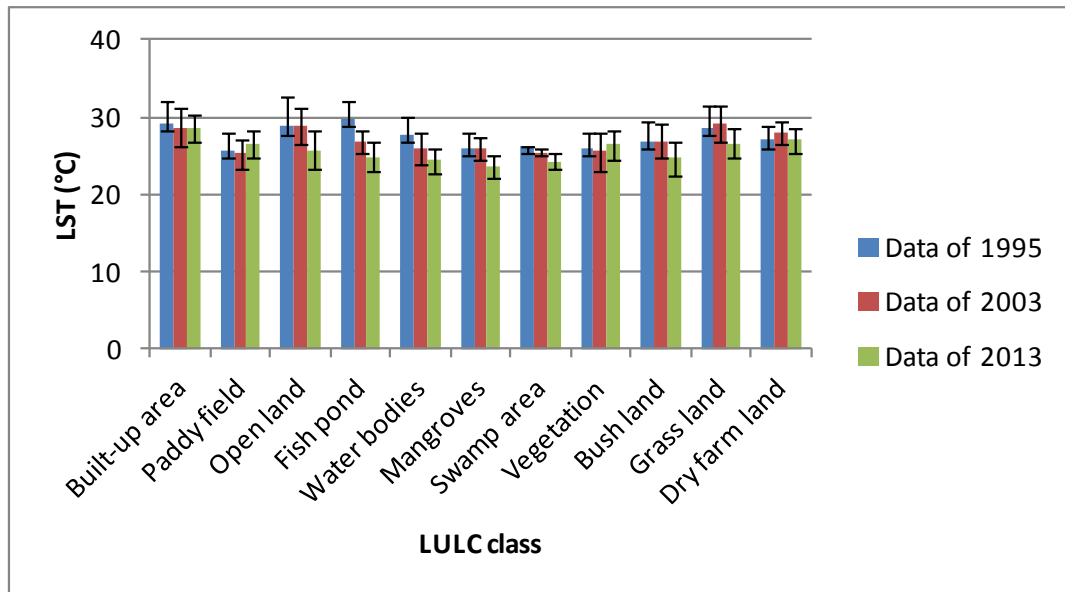


Figure 6.12 The LST by LULC type

The largest standard deviation of LST of built-up areas occurred in 1995 (2.71 °C) meaning that these surfaces experienced a wide variation in LST because of varying surface materials. In contrast, the smallest standard deviation of LST in built-up area was in 2013 (1.85 °C) owing to their greater homogeneity by that time. Distinctive changes of standard deviation were also found in other main LULC types (paddy field and vegetation). Their relatively lesser change of standard deviation indicates that these LULC types experienced homogeneity of surface characteristics.

Along with the transformation of fish pond areas into mangrove forest in 2003, composition of the highest mean LST class in 2003 was also slightly changed into grass land (29.19 °C), open land (28.73 °C), and built up area (28.65 °C). Paddy field, swamp area, and vegetation as the part of greenery areas had the lowest mean LST value of 25.20 °C, 25.48 °C, and 25.53 °C, respectively. The grass land in 2003 was located next to the apron of the international airport which is fully covered large concrete surface that may influences the LST value of the grass. Moreover, the condition of the grass land was possibly not fully covered by

the grass that can be seen from their relatively high SD value (2.41). In 2013, the highest of average LST was in built-up area (28.51°C), followed by dry farm land (26.99 °C), and grass land (26.63 °C). Similar with the case study in 1995 and 2003, mangroves, swamp areas, and water bodies in 2003 are consistently linked to the relatively lowest LST level of 23.72 °C, 24.26 °C and 24.42°C, respectively. Mangroves, swamp areas, and water bodies in 2013 are also consistently linked to the relatively lowest LST level of 23.72 °C, 24.26 °C, and 24.42 °C, respectively. Those areas have proven as a substantial role in reducing the effect of thermal radiation as a result of their high thermal inertia.

Figure 6.13 shows box plots for 1995, 2003, and 2013, which correspond to the minimum, low quartile (q_3), median (q_2), upper quartile (q_1), and maximum values and the interquartile range ($q_3 - q_1$), which covers the central 50% of the data. Swamp area, grassland, and open land were excluded due to low sample sizes. The symmetric data is indicated by the middle median value position and the whiskers that show the highest and lowest value of data sets have the same length. Among the three dominant LULC types in the study area (built-up area, vegetation and paddy field) from 1995 to 2013 that generally show a symmetric data distribution, a notable difference is shown by the LST data distribution of built-up area and paddy field in 1995. The LST data of built-up area in 1995 has a median of about 27 °C. The data distribution was not symmetric as is shown by the median not being located in the middle of the box plots and the whiskers that show the highest and lowest value of data sets do not have the same length. LST data of built-up area in 1995 was skewed upwards. The part of the box to the below of the median (representing the lower LST) was shorter than the part to the above of the median (representing the higher LST). That means the lower LST of the built up areas were closer together than the higher LST of the built up areas or most of observed built-up area data concentrated on the lower LST. In contrast, LST data of paddy field in 1995 was skewed downwards that means most of paddy field data concentrated on the higher LST.

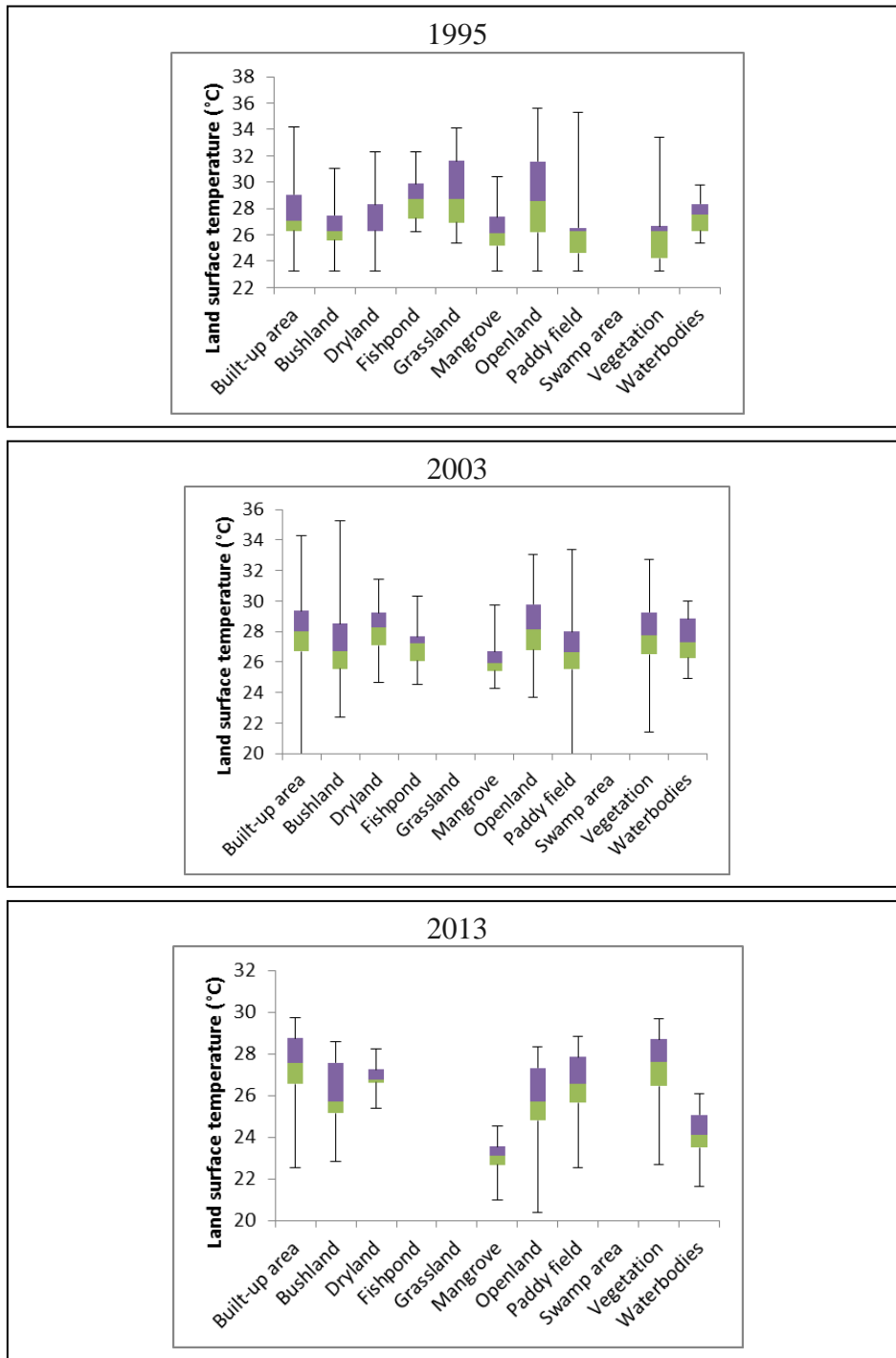


Figure 6.13 Box plots of the standardized LST of each LULC type

Although the LST data distribution of built-up area in 2003 and 2013 were symmetric with median of about 28 °C, the range of LST data in 2003 was larger

than that in 2013. From these box plots it can be seen that although the mean of built-up area was higher in 1995, the range of data in 2003 and 2013 was larger than the data in 1995 or the LST of built-up area more varied. These box plots have proven as a good measure of spread in likely skewed distributions which cannot be examined using mean and standard deviation.

6.2.5 The correlation between LST and NDVI by LULC

As can be seen in Table 6.4 average NDVI and LST values associated with different LULC types were significantly different and only built-up area, paddy field and vegetation show persistently negative significant relationship between LST and NDVI over three different years. It was indicated by their P values being less than 0.05. This means the higher LST of built-up areas is related to the lower NDVI values of built-up areas. In contrast, the lower LST of paddy field and vegetation was influenced by the higher NDVI values of those LULC types.

The result of not persistently significant relationship from other LULC types here may be because the size of sample used was not large enough to be significant or less sample statistics deviates from the population parameters. However, the strongest negative relationship between NDVI and LST factors by LULC types was found for bush land type in 1995 ($r = -0.55$). This means the lower LST value of bush land has a relationship with the higher NDVI value of bush land. Another stronger negative relationships between LST and NDVI was also occurred on paddy field category in 1995 ($r = 0.46$) and vegetation ($r = 0.46$) in 2003. The built-up area was also negatively correlated and the strongest correlation was found in 1995 ($r = 0.34$). The relatively weak and moderate relationship of the linear relationship compared with other studies may be attributed to the widespread heterogeneous LULC type in the study area. For example, built-up areas are actually composed not only of buildings but also attached vegetations between the building spaces. Moreover, vegetation type was composed not only by evergreen wooden trees, but also mixed with annual and

deciduous species with various leaf conditions. Those factors might have influenced the strength of the linear relationship between LST and NDVI by LULC types.

Table 6.4 Pearson's correlation coefficients between LST and NDVI by LULC types (significant at 0.05)

Land use/cover type	1995		2003		2013	
	r	P value	r	P value	r	P value
Built-up area	-0.34	0.00	-0.18	0.00	-0.11	0.01
Paddy field	-0.46	0.00	-0.18	0.00	-0.12	0.00
Open space	-0.01	0.97	-0.04	0.77	0.25	0.10
Fish pond	-0.53	0.00	0.32	0.34	0.64	0.09
Water bodies	-0.07	0.27	-0.38	0.22	0.39	0.61
Mangroves	-0.18	0.20	-0.25	0.90	0.15	0.36
Vegetation	-0.24	0.00	-0.46	0.00	-0.22	0.00
Bush land	-0.55	0.00	-0.26	0.00	0.07	0.83
Grass land	0.39	0.27	-0.74	0.06	0.23	0.58
Dry farm land	-0.16	0.03	-0.20	0.23	-0.14	0.69

Shaded blue areas indicates the mean LST and NDVI values associated with the LULC type were significantly different

6.3 Discussion

6.3.1 Impact of LULC change on LST

As in other research, in the southern part of Bali, Indonesia, the daytime mean LST varies with various LULC types among three different years. Generally, based on the mean LST value by LULC types from 1995 to 2003, the impact level of LULC types on LSTs can be divided into:

- a) The high impact (over 29 °C) in built-up areas.

The high impact of built-up areas on LST is indicated by their consistent higher LST values among LULC types from 1995 to 2013. This is not surprising that built-up areas associated with building or impervious surfaces have been correlated to the higher LST as impervious materials typically have a high solar radiation absorption as well as a high thermal

capacity and conductivity for releasing heat stored during the day and night. Moreover, the high LST of built-up areas is related to the lower density and health of vegetation as indicated by their low NDVI values.

- b) The moderate impact (27-28 °C) was open space, grass land, paddy field, fish pond, water bodies, vegetation, bush land and dry farm land. Those LULC types are typically composed of mixed water, vegetation and soil which have lower thermal conductivity compared to impervious surfaces. Those LULC types play a significant role in reducing the amount of thermal radiation as a result of its high thermal inertia (Xiao et al. 2008).
- c) The low impact (25-26 °C) was swamp area and mangroves that can help to reduce LST and the high radiant temperature of the built-up area.

These impact levels of LULC types on LST have an implication for the further LULC management in the study area to reduce the LST value. The mitigation and adaptation effort should be more focused on LULC types such as built-up areas, open space and grass land through green space planning or using lighter-coloured materials for reflective surfaces effects. Built-up area plays an important role in forming UHI centers and composed 50% of the study area in 2013 while open land and grass land shows the higher LST value although their LST varied from 1995 to 2013.

6.3.2 The increasing LST and driving factors

Figure 6.15- Figure 6.17 show area where LST has increased from 1995 to 2013. Most of the increasing LST from that period occurred at the northern sub-urban or in the rural areas, while the downtown areas of Denpasar and Tabanan as well as the southern coastal areas such as Kuta, Bena harbour, and the island of Serangan shows a relative lower increasing LST areas from 1995 to 2013. This phenomenon indicates an impact from the LULC changes in sub-urban and rural areas and a consequence of urban expansion. The continuing urbanization that

was indicated by increasing built-up areas in sub-urban and rural areas results in relatively high LST.

In contrast to the UHIs in 2013, coastal areas in Kuta, Bena harbour, and the island of Serangan had more UHI effects in 1995 and 2003 (Figure 6.14). This possible difference of UHI pattern is confirmed by IPCC (2007), which states that UHI effects are often localized and are dependent on local climate factors such as cloudiness and windiness, and these effects in turn depend on proximity to the sea and season. However, the seasonal changes that influence in day length and Sun angle of incidence have been excluded by standardization process in this analysis. Moreover according to Pidwirny (2013), locations near the equator have only small variations in solar input annually, so that they did not influence the difference of this UHI pattern.

As there was no cloud cover on those areas, the variation of this UHI effect is possibly caused by wind that taking away heat energy on the surfaces. Cold surface currents that occur at the ocean's surface that are driven by the winds may influence the lower LST of coastal locations. Cold surface ocean currents originate in polar and temperate latitudes that are driven by atmospheric circulation generally flow towards the equator (Pidwirny, 2013) and in this case may moderate LST over Kuta, Bena harbour, and the island of Serangan. The wind speed and direction that flowed from the west (Indian Ocean) were suggested the influencing drivers as these areas were located in the western part of the study area and were close to and between Indian Oceans. It is confirmed by another coastal area in the eastern part of the study area (Sanur) that was not directly influenced by Indian Ocean did not show fewer UHI effects either; these UHI effects were even more extensive in 2013 (Figure 6.14). However, it is necessary to further examine the impact level of the wind on UHI effects for these coastal urbanized areas.

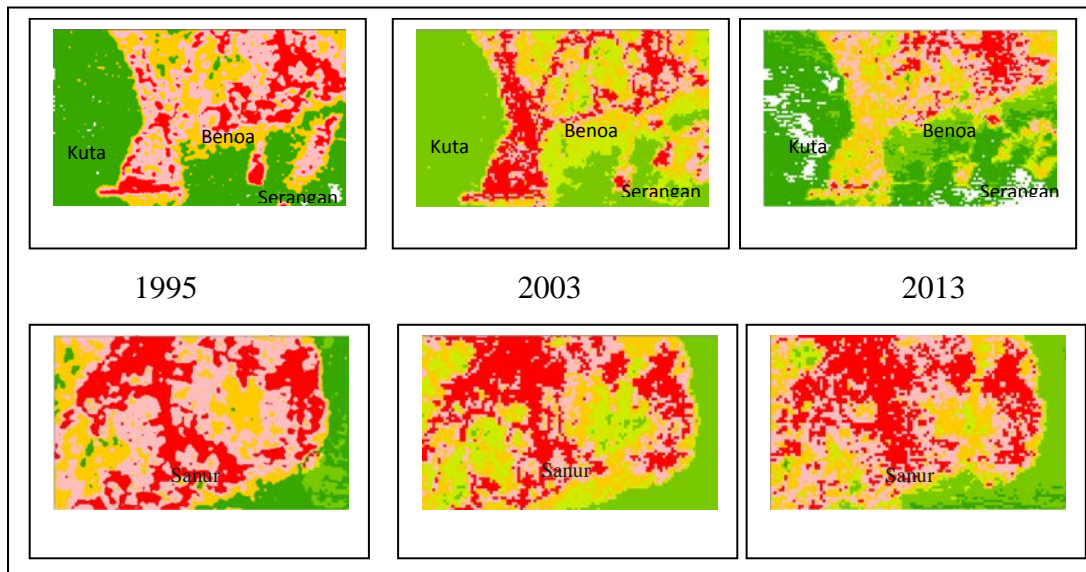


Figure 6.14 The different change of UHI pattern at Kuta and Sanur in 1995, 2003 and 2013

In contrast to the coastal areas, UHI effects in the downtown area of Denpasar from period of 2003-2013 were more widespread. Wind may also influence the LST in the downtown area as according to Erellet al. (2011) in the tropics, a wind velocity of 1–1.5 m/s can create cooling effect which is equal to a 2 °C drop in temperature. However, the influence of wind factor in LSTs in the downtown areas may not be as strong as in coastal areas. Another possible factor of this difference in UHI pattern is the impact of LST standardization that may have slightly changed the data distribution. The factor of increasing impervious surfaces in built-up areas suggesting this as one of main drivers for these increasing UHIs, has been confirmed by the lower NDVI value. The impact of increasing built-up areas (impervious surfaces) on UHI effects needs further detailed study and will be presented in Chapter 7. Consequently, management strategies to reduce these UHI effects need to be different between these locations.

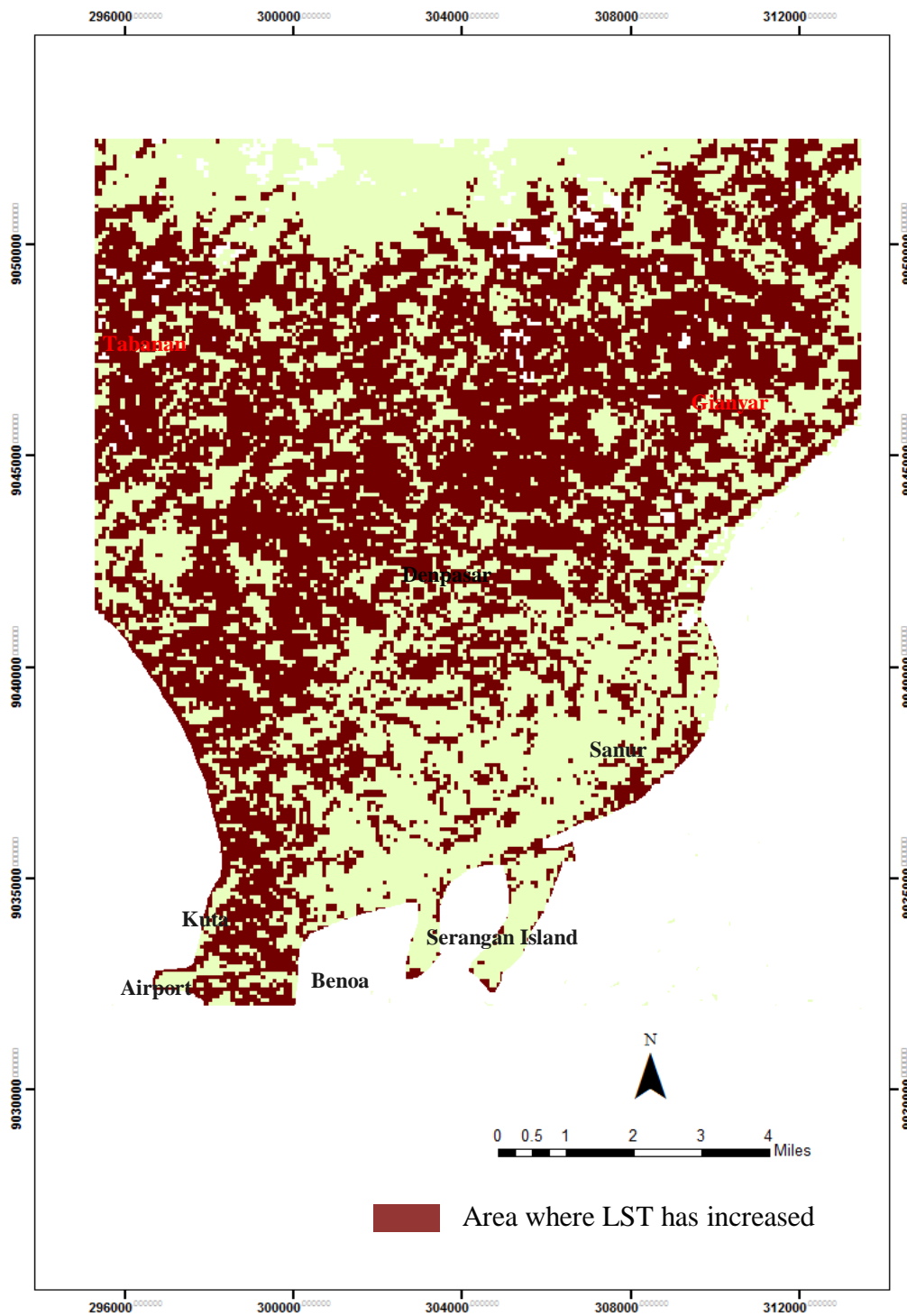


Figure 6.15 Spatial distributions of the increasing LST from 1995 to 2003

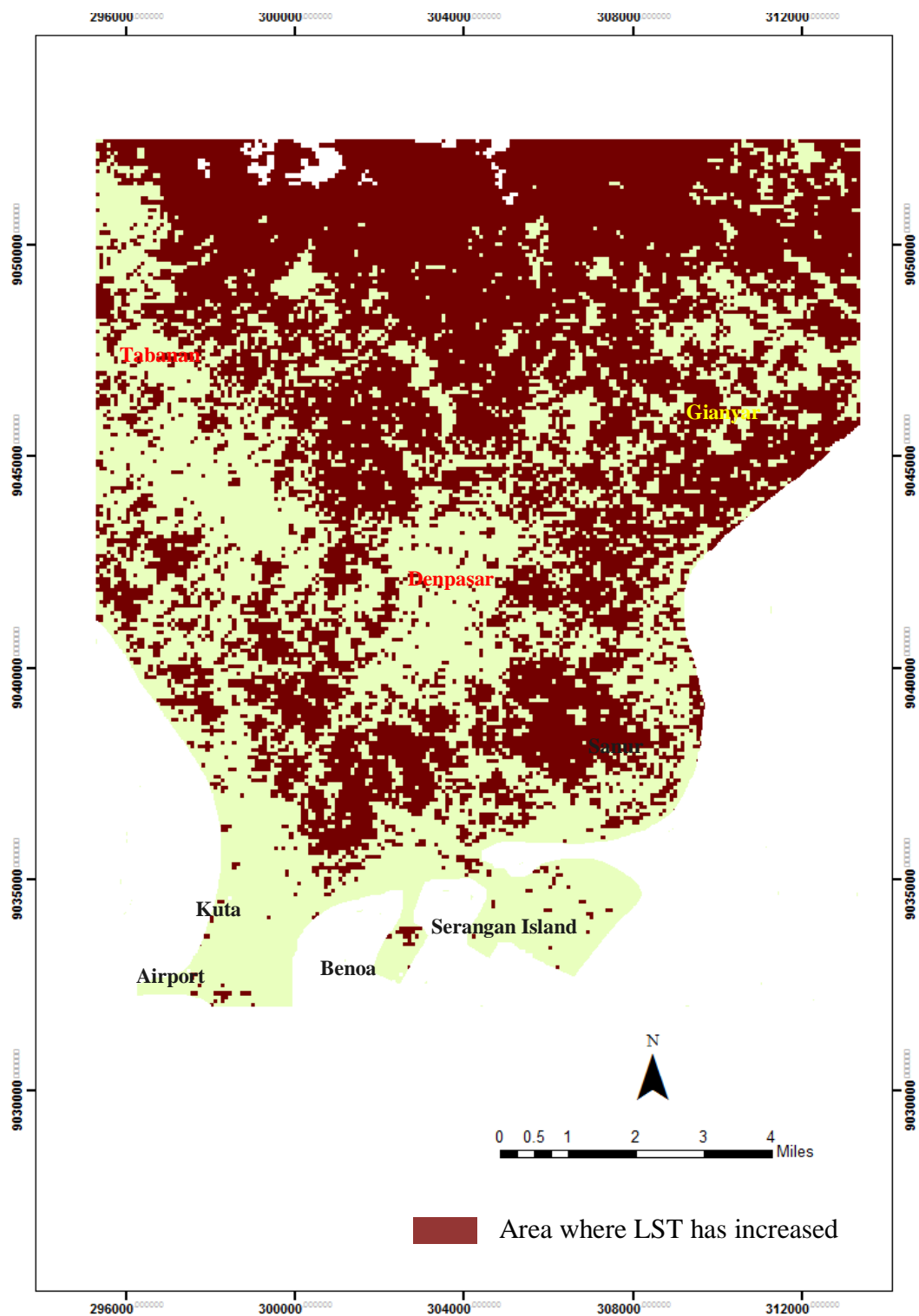


Figure 6.16 Spatial distributions of the increasing LST from 2003 to 2013

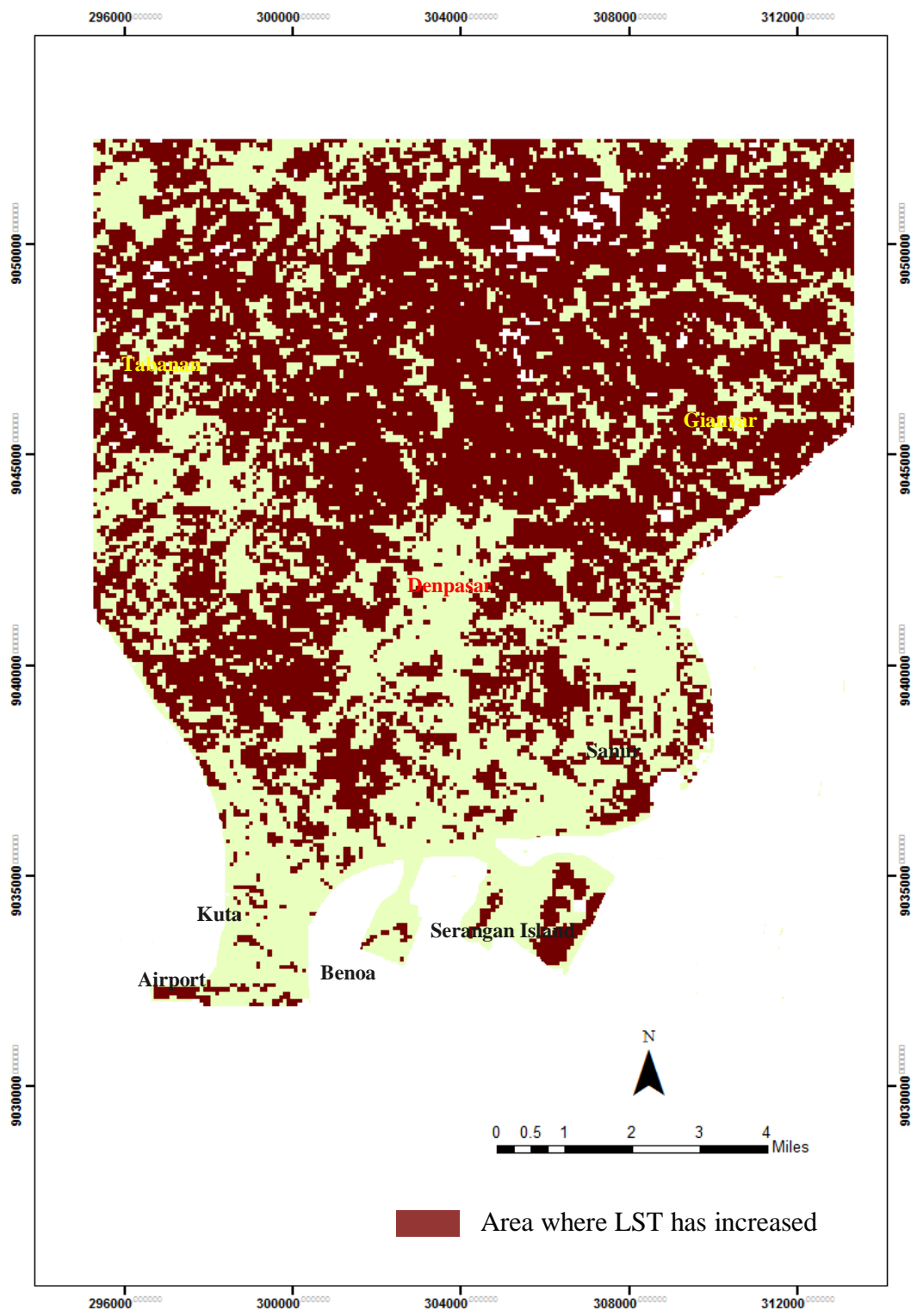


Figure 6.17 Spatial distributions of the increasing LST from 1995 to 2013

6.4 Chapter summary

The usefulness of the GIS and remotely sensed thermal data for mapping LST distributions using Landsat and ASTER has been demonstrated in this chapter. To extract the LST map, the DN of thermal infrared bands was transformed into spectral radiance and an effective at-sensor brightness temperature, and an emissivity value was thus obtained. The LSTs were not able to be directly compared due to the different seasons and times of the year of the acquired images. Therefore, a standardization of those LST data, to accommodate the accuracy of the comparison between different years and seasons, was conducted. Besides the lack of an entirely cloud-free cover image for this study, the standardization of the retrieved LST map using LST data directly recorded from real object properties or in-situ observation was also missing in this study. Thus, improvements by refining LST retrieval with in situ measurement of LST are needed for future research.

The LST derived from thermal data has provided temporally synchronous LSTs from 1995 to 2013, and, generally, the derived LST images show that UHI effects increased from 1995 to in 2013. The use of GIS is not only able to measure the spatio-temporal pattern of the LST but also to detect the spatial pattern of the UHI effects by transect graphs. The transect graph represents the lower temperature gradient of paddy fields and vegetation cover in rural areas. The temperature gradient gradually climbs as those LULC transform to built-up areas in downtown Denpasar, which is composed of more impervious surfaces. The impact level of LULC types on LSTs can be divided into: the high impact LULC (over 29 °C) was built-up areas, the moderate impact LULC (27 °C - 28 °C) was open land, grass land, paddy field, fish pond, water bodies, vegetation, bush land and dry farm land, as well as the low impact LULC (25 °C - 26 °C) was swamp area and mangroves.

The relationship between LST and LULC was revealed through determining the impact of LULC changes on LST and the change of LST area (ha). Wind as well as standardization result are of considerable importance in the different appearances of UHI effects between eastern coastal areas and downtown of Denpasar in April 2013 and, in turn, influence the strategies needed to reduce the UHI effects. The mitigation and adaptation effort through green space planning should be more focused on built-up areas as it plays an important role of forming UHI centers and has covered most of the study area in 2013. According to this above result, LST, NDVI and built-up areas types can be considered to be three basic parameters to contribute to further evaluation of green space zoning with RS and GIS. The significant negative correlation between LST and NDVI by vegetation, paddy field and built-up area category shows the higher LST has a relationship with the lower value of NDVI and vice versa. This analysis provides applicability of relatively low cost, fine-moderate spatial resolution satellite imagery, then to examine the impact of LULC change on the urban environment in Bali.

7 GREEN SPACE PLANNING AND MANAGEMENT TO MITIGATE UHI IN BUILT-UP AREAS

In the study area, there has been a tremendous reduction in the area of vegetation. Built-up areas linked to impervious surfaces (such as roads, buildings, and parking lots) now cover these previous vegetation areas, which has resulted in the capture of more incoming solar radiation during the day and subsequent re-radiation of it at night. As a result, UHI occurs, when the atmospheric temperature and LST are hotter than their rural surroundings. Therefore, the mitigation and adaptation effort through green space planning should be more focused on LULC types of built-up areas as it plays an important role in forming UHI centers and covered most of the study area by 2013.

To anticipate UHI effects, several mitigation and adaptation strategies can be employed, such as using lighter-coloured materials for reflective surfaces effects. However, a more practical method of mitigating UHI effects is carried out by strategic planting of vegetation or developing green spaces in urban areas. This strategy has a relatively low cost, which is why it may serve as an affordable solution for developing countries. Moreover, it optimizes the advantages of the tropical climate, which allows evergreen broad-leaf trees to grow throughout the entire year.

As built-up areas play an important role in forming UHI centers and composed 50% of the study area in 2013, this chapter analyses LST patterns, specifically in the built-up areas at micro scale level (MUHI) to investigate mitigating the UHI effects through developing urban green space and revealing the influential factors. Detection of MUHI is conducted to directly see the UHI hotspots that show higher LST than surrounding areas. A priority zone for green space planning in the built-up area category was also suggested by numerical classification and thus, the green space management strategy in each zone can then be developed.

7.1 Method of analysis

7.1.1 Analysis the impact of LULC on LST in urban area types

The local scale pattern discussed in Chapter 5 was fragmented into a series of samples that consist of smaller hot islands and cooler islands at the micro-scale level (up to 1 km) taken from three types of urban areas and statistically measured. Three types of built-up areas that have been extracted from the previous analysis of the LULC map in Chapter 4 were used to identify the change of LULC by using polygons of MUHI samples focusing on the built-up areas and their surroundings. For this purpose, the size of a MUHI sample was defined to 1 km² resolution based on the UHI urban boundary layer (UBL) at micro scale that occurs up to 1 km or more (Voogt, 2004), as explained in Chapter 2. This size of sample area also has been applied by Mitchell (2011) with a different technique for taking MUHI samples.

The number of sample areas taken in each urban area type varied from seven to ten. Both the number and distribution of samples were determined based on the persistent built-up area throughout the three years and the UHI “hot spots” tendency on LST maps. A 1 km² polygon sample included other adjacent different LULC types such as vegetation, paddy field, mangroves, and so on. To detect the features that consist of smaller thermal “hot and cool spots”, the LST map and Quickbird imagery were used.

7.1.2 Data and analysis of green space zone

The raster maps of built-up areas, LST and NDVI in 2013 were further used as the factors to determine the priority zone for developing green space using a suitability analysis method. By using Weighted Overlay and Spatial Analyst tools in GIS, the priority zone for urban green spaces was determined. A reclassification process was conducted on each raster map to define their priority level for developing the green spaces. The value of reclassification was defined by

the significance level to develop green spaces based on the raster map value (Table 7.1). For instance, a very dense urban area was considered 3; a dense urban area was considered 2, and so on. Surveys of experts' opinions are usually used for this sort of analysis to determine the weight value of factors used, but these were not conducted in this study. It is therefore assumed that these factors have an equally important role in determining the priority zone for urban green space and thus, have the same weighted score value. From this suitability analysis, the final value of 1 given the lowest priority urban areas for a green space, but the value of 3 was the highest priority for a green space in urban areas (Figure 7.1). Therefore, based on the resulting priority zone for green spaces, the management for such green spaces in each priority zone could then be suggested. The boundary of the district was combined to measure the priority distribution of each district in the study area since the role of agencies and government cannot be ignored in the development of green spaces to adapt with UHI effects.

Table 7.1 Criteria of scoring and weighting for each factor

No	Factor	Value		
		Weight	score	
1	Urban area	Semi dense	0.33	1
		Dense area		2
		Very dense		3
2	LST	19.02-25.02	0.33	1
		25.03-28.56		2
		28.57-36.39		3
3	NDVI	0.665-1.043	0.33	1
		0.434-0.663		2
		0.034-0.434		3

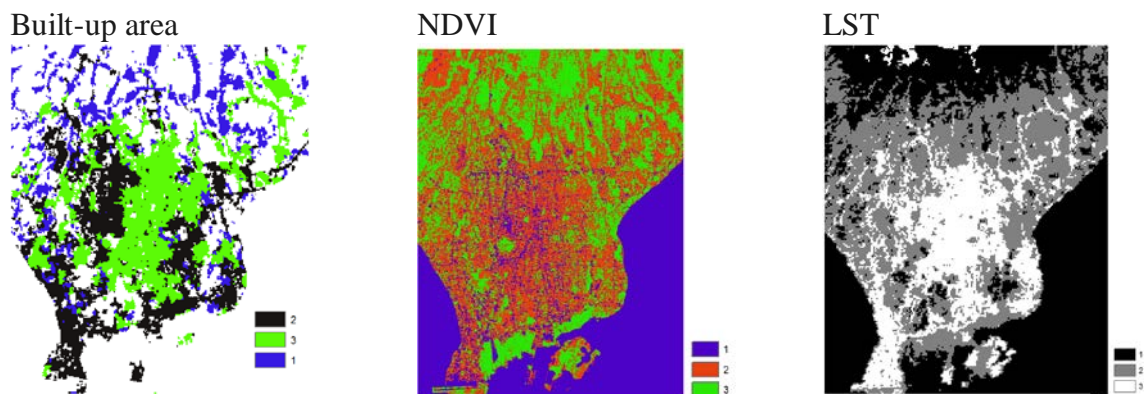



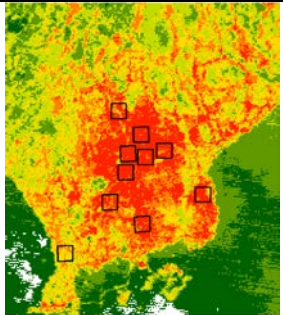

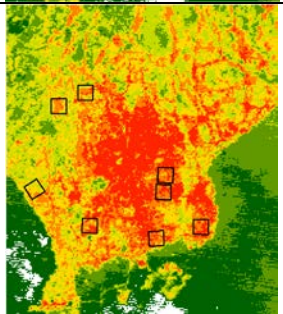

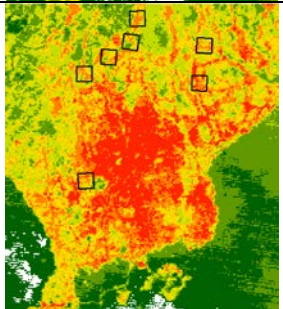
Figure 7.1 Reclassification of raster map of built-up area type, NDVI and LST

7.2 Results

7.2.1 Sample distribution

MUHI samples were taken in three types of urban area (Table 7.2). The urban area types were divided based on the proportion and density level of the built-up area category in a sample. The first urban area type was a very dense urban area. A sample polygon of very dense urban area was composed by approximately 80-100% of very dense built-up areas and less than 20% of other LULC such as vegetation, paddy field, and open land. The second type was a dense urban area. A sample polygon of dense urban area is composed by 50 - 80% of dense built-up area. The last urban area type was a semi-dense urban area where in a sample area was composed of less than 50% of semi-dense built-up area. These samples were commonly distributed in traditional Balinese residential compounds with dense vegetation between the vacant building spaces.

Table 7.2 Polygon samples of built-up areas types

Urban area type	General description	Google Earth image (data SIO, NOAA, U.S. Navy, NGA, GEBCO, Landsat image)	Location of polygon samples
Very dense urban area	A sample area is composed of 80-100% of very dense built-up areas		
Dense urban area	A sample area is composed of 50-100% of dense built-up areas		
Semi dense urban area	A sample area is composed of less than 50% of semi dense built-up area		

7.2.2 The LST fluctuation by diversity of LULC types in built-up area types

Analysis of LST change by diversity of LULC types within urban area samples was conducted and the results can be seen in Table 7.3 (which shows the LST fluctuation of each LULC class in each year; data does not include a comparison of values across years). It can be seen in Table 7.3 that all LULC types in very dense urban areas had higher temperature than other urban area types. The LST of all LULC types gradually decreased to the dense and semi-dense built-up areas. The difference of LST in very dense urban areas were 3 °C – 5 °C higher than in the semi-dense urban areas depending on the year. For example, in 2003, LST in

very dense urban areas was 31.22 °C and in semi-dense urban areas, it was 26 °C; meanwhile in 2013, the LST in the very dense urban area type was 30.20 °C and in semi-dense urban area type was 27.91 °C.

The higher LST in very dense urban areas not only occurred in built-up area types, but also on paddy fields and vegetation areas. The density of built-up areas appears to have strongly influenced the UHI effect as suggested by Oke (1982); many complex factors are involved in the UHI phenomena and the most influential factors are the distribution of a mosaic of complex surface covers and urban morphology, such as geometry and density of building materials, which combine to create microclimate systems and a limitless array of energy balance.

7.2.3 The change of LST by urban area types

Among urban area types, very dense urban areas had the highest average LST of 29.02 °C, 29.34 °C, and 28.92 °C in 1995, 2003 and 2013, respectively (Figure 7.2). A very dense urban area causes anthropogenic heat, which when released from surfaces is trapped in the city, which increases the overall heat. In addition, surface heat on the ground, such as on roads and pavements cannot be effectively released out of the urban region because there is a small sky view from the ground and physical objects such as buildings absorb most of the emitted heat from the ground, keeping the heat trapped within the city (Sailor & Fan, 2002). In contrast, semi-dense urban areas had the lowest average LST of 26.01, 25.62, and 26.84 °C in 1995, 2003, and 2013, respectively. The highest LST being in the very dense urban areas gives an indication that the green space development must be firstly focused on these areas.

Table 7.3 Change of LST by the LULC types in urban area types

LULC type	LST (°C)		
	1995	2003	2013
<u>Very dense urban area</u>			
Paddy field	29.42	28.38	28.67
Built-up	30.98	31.22	30.20
Vegetation	28.53	29.14	28.49
Open land	29.30	-	29.70
Dry farm land	26.89	29.74	-
Bushland	-	29.36	-
Grassland	-	28.19	27.56
Average	29.02	29.34	28.92
<u>Dense urban area</u>			
Paddy field	27.67	27.37	27.48
Built-up	29.64	28.77	28.69
Vegetation	27.67	27.68	28.88
Open land	28.15	29.17	28.52
Dry farm land	28.41	29.60	-
Bushland	28.10	28.31	28.70
Fishpond	29.67	28.31	-
Mangroves	-	-	-
Waterbodies	28.67	-	-
Average	28.50	28.46	28.45
<u>Semi dense urban area</u>			
Paddy field	24.78	25.62	26.27
Built-up	26.64	26.00	27.91
Vegetation	25.64	24.55	26.35
Dry farm land	26.29	-	-
Open land	26.20	-	-
Bushland	26.51	26.30	-
Average	26.01	25.62	26.84

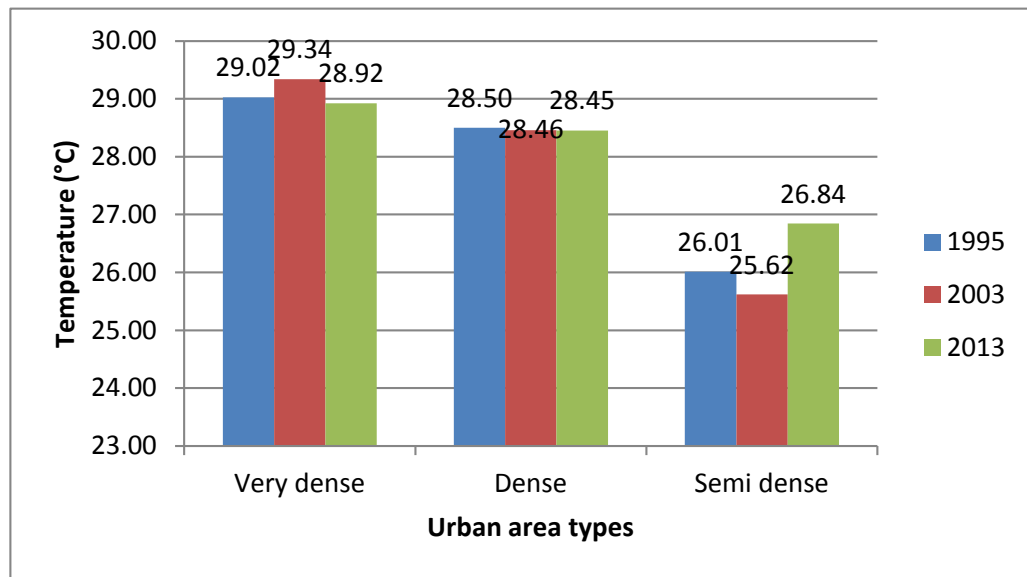


Figure 7.2 LST changes of urban area types

Although it generally appears that the LST of urban areas has changed slightly within the last two decades, there was an contradictory variation of urban temperature changes. From 1995 to 2003, the mean LST of very dense urban areas increased from 29.02 °C to 29.34 °C. In contrast, it dropped by about 1°C to 28.92 °C and is the lowest LST value among other very dense urban areas from 2003 to 2013. This decrease of LST was not consistent with the LST dynamics in other urban area types. In dense urban area, the LST slightly decreased from 1995 to 2013. In contrast, The LST in semi dense urban area sharply increased from 1995 to 2013. The possible reason of this fluctuation in LST might still be associated with the different seasons, which, thus, influences human behavior and activities, such as air conditioner use, that it is hard definitely separate from those associated with LULC change.

This result is confirmed by the result of a t-test paired with two means of LSTs (Table 7.4). Most of the paired data shows there was no significant difference of LST changes. The exception occurs on paired LST data of very dense built-up areas that reduced from 2003 to 2013, and that of the semi dense urban areas from 2003 to 2013 and from 1995 to 2013. For which the P values were lower than the

significance level (0.05). This means the null hypothesis is rejected and comparison of their average LSTs shows there were statistically significant differences between them.

Table 7.4 Statistical result of t-test paired two means of LST (significant at 0.05)

Built-up type	Paired Mean	T-stats	T critical stats	P value
Very dense	2003-2013	2.42	1.86	0.02
	1995-2013	1.71	1.86	0.06
	1995-2003	0.26	1.85	0.4
Dense	2003-2013	0.83	1.94	0.22
	1995-2013	0.96	1.94	0.19
	1995-2003	0.6	1.94	0.29
Semi dense	2003-2013	2.55	2.02	0.03
	1995-2013	8.70	2.02	0.00
	1995-2003	0.28	2.02	0.39

The blue shaded areas indicated the period with a significant difference of LST change

7.2.4 Analysis of green space planning

The purpose of green space planning is to mitigate UHI effects in the study area by determining green space allocation based on measurement result of NDVI, LST, and built-up area types. The spatial analysis of green space planning using Weighted Overlay and Spatial Analyst tools in GIS produced a block plan that shows spatial allocation of green space priority. The local social-cultural factor was not used in this planning but will be integrated descriptively in the proposed green space management.

There were three priority zones of green spaces resulting from the spatial analysis as a block plan (Figure 7.3). The allocation of a block plan and total area in each district in the study area can be seen in Table 7.5:

a) High priority zone for green space:

The total area for this zone was found to be 3400 ha that covered 43.21% of built-up areas and mostly covered very dense urban areas. This zone is characterized by higher LSTs and low green space areas.

b) Low priority zone for green space:

The total area for this zone was 4434 ha (56.44%) and it is the largest zone that mostly covered dense urban areas. This zone had a moderate number of green spaces and moderate LSTs.

c) Not a priority zone for green space:

This zone had a good green space area and low LST with the total area for this zone being 0.27 km² (27 ha) and covering 0.34% of urban areas.

From Table 7.5 and Figure 7.3 the allocation of the high and low priority of green spaces can be seen, spread across eleven districts including: Kediri; Abiansemal; Sukawati; Ubud; Mengwi; Denpasar Barat; Denpasar Timur; Kuta Utara; Kuta; Denpasar Selatan; and Blahbatuh. The district with a high priority zone for green space development was mostly located in Denpasar city with the total area of about 5-6 km², while the district of Kuta and Kuta Utara as a centre of tourism area in Bali had a total area of 1.23 and 372 ha, respectively. In contrast, Sukawati, located far from Denpasar and Kuta, also had a relatively large high-priority zone of 5 km². The proposed parks' locations in the high priority zone of green space can be seen in Figure 7.4. These locations were allocated based on the priority green space zone and the possible available areas in 2013 that is covered by LULC types of paddy fields, vegetation areas, and open land.

Table 7.5 Priority zone of urban green space based on district areas

No	Green space zone	Name of district	Area (Ha)	%
1	Not a priority zone	Mengwi	3	0.04
		Sukawati	1	0.01
		Denpasar Barat	5	0.07
		Kuta Utara	4	0.05
		Denpasar Selatan	8	0.11
		Kuta	2	0.03
2	Low priority zone	Kediri	5	0.07
		Mengwi	162	2.13
		Abiansemal	76	1.00
		Sukawati	290	3.81
		Ubud	1	0.01
		Blahbatuh	17	0.22
		Denpasar Barat	1200	15.76
		Denpasar Timur	504	6.62
		Kuta Utara	533	7.00
		Denpasar Selatan	971	12.76
		Kuta	546	7.17
3	High-priority zone	Kediri	25	0.33
		Abiansemal	117	1.54
		Sukawati	500	6.57
		Ubud	2	0.03
		Mengwi	199	2.61
		Denpasar Barat	677	8.89
		Denpasar Timur	666	8.75
		Kuta Utara	372	4.89
		Kuta	123	1.62
		Denpasar Selatan	583	7.66
		Blahbatuh	19	0.25
Total area			7611	

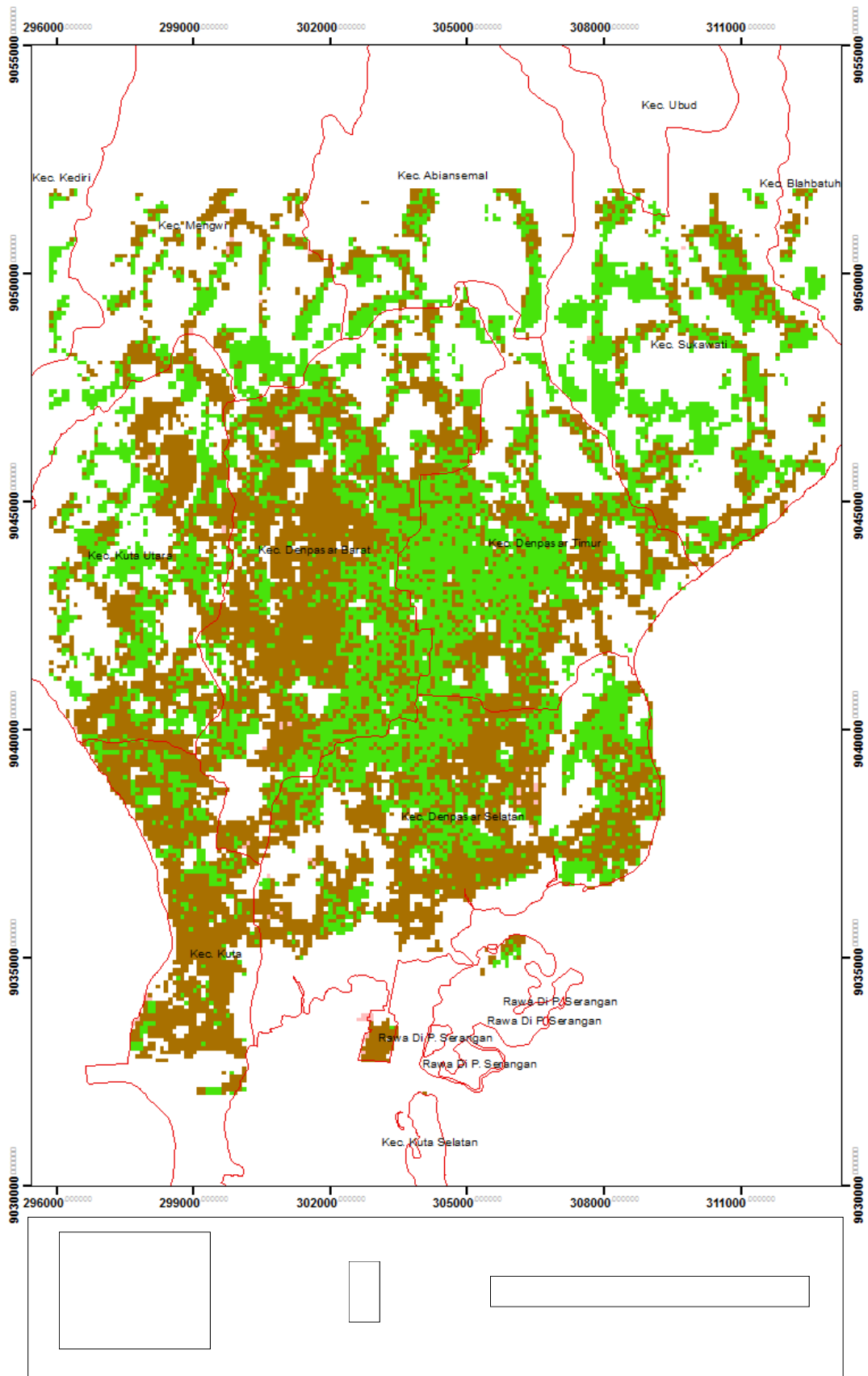
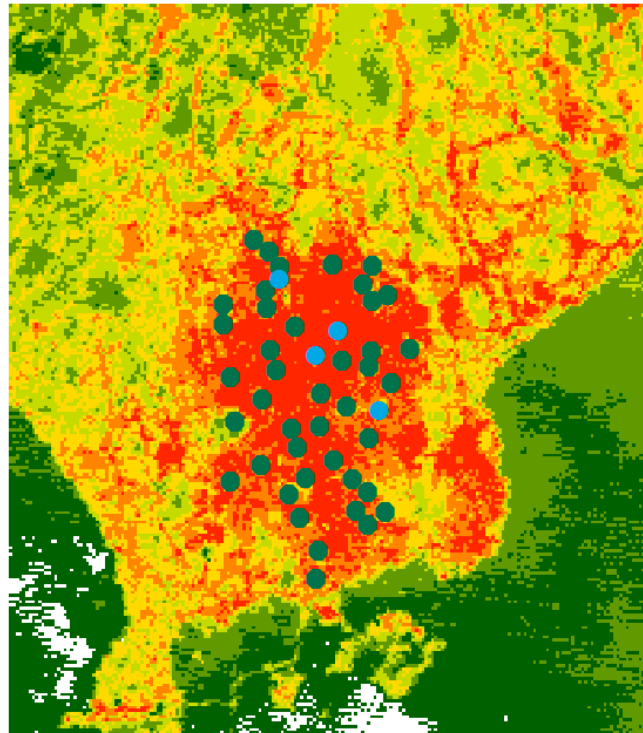


Figure 7.3 Block plan of green space in urban areas



- : Old parks
- : Location of proposed new parks

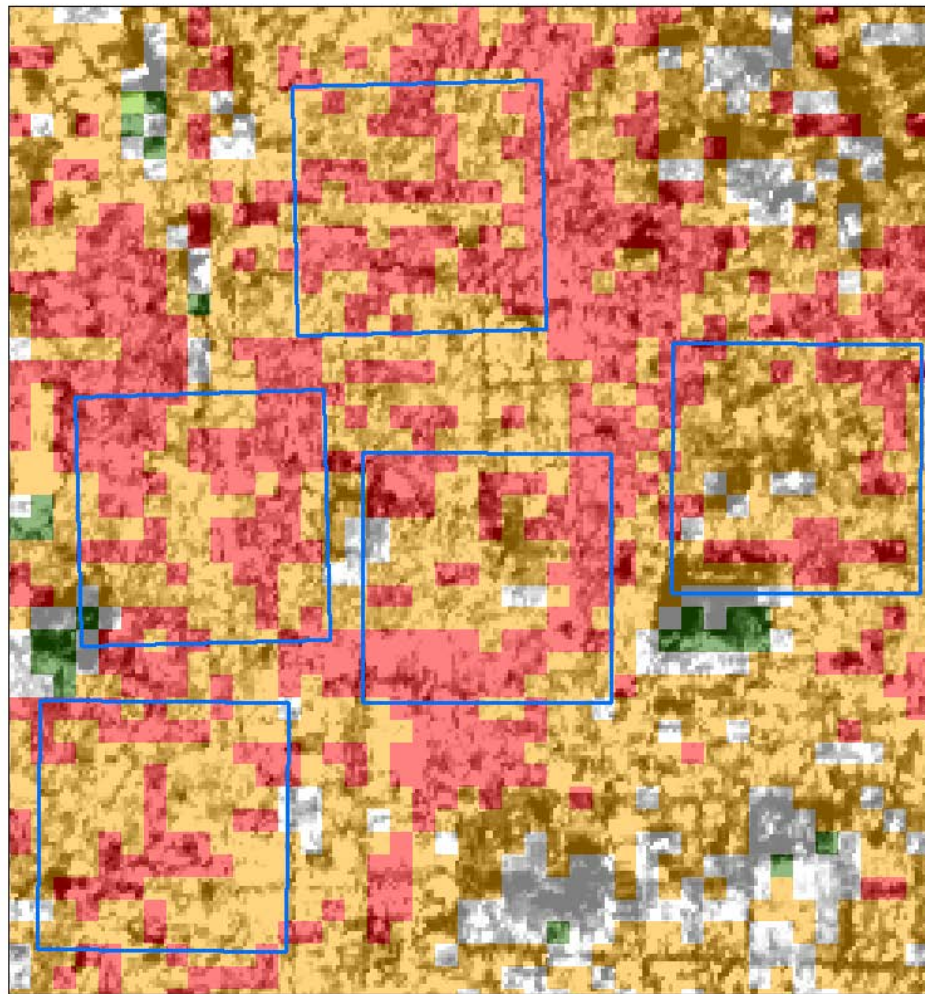
Figure 7.4 Suggested locations for new urban parks in high-priority zone

7.2.5 MUHI detection in urban area types

To support a tree planting plan in green space zones, examination of higher LST to determine the detailed location of the planting plan using GIS is described below:

a) Very dense urban areas

Figure 7.5 shows a typical thermal pattern in very dense urban areas. The thermal pattern of “hot spots” defined for this study’s aim was areas with temperatures over 29 °C. Most LST in very dense urban areas was within the temperature range of 29.1 °C – 33 °C. Rooftops with low albedo definitely show the highest level of surface temperature (over 31.1 °C) in the sample region and the coldest areas (below 29 °C) was greatly contributed to by paddy fields and vegetation features in parks, road sides, cemeteries, and temples.



Legend

- Very dense urban area
- 20.3 - 22 °C
- 22.1 - 25 °C
- 25.1 - 27 °C
- 27.1 - 29 °C
- 29.1 - 31 °C
- 31.1 - 33 °C

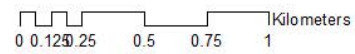


Figure 7.5 Cooling thermal spots provided by features of parks, lawns, vacant land, paddy fields, and cemeteries, illustrated by white and green shaded areas in very dense urban areas.

b) Dense urban areas

Most LSTs in dense urban areas were in the temperature range of 29.1 °C – 31 °C. Natural to semi-natural LULC types (i.e., vegetation, paddy field, mangrove forest) provided cool thermal spots to the surrounding built-up areas. Some sample spots of densely urban areas were close to irrigated paddy fields and water bodies that predominantly exhibited LST of 29.1 °C – 31 °C. In contrast, the other dense urban areas located close to irrigated paddy fields, parks, and vegetation shows the lower LST zone (25.1 °C – 27 °C). This difference in cooling effect to the adjacent densely built-up areas would be influenced by environmental factors such as the size of the densely built-up areas, configuration of vegetation in dense urban areas, and the nature of the elements of densely built-up areas (i.e., roof building, trees, and road). The hot and cold thermal spots also can be seen in the existing park of Niti Mandala located in a densely urban area sample (Figure 7.6). The big trees of parks and settlements provided cooling benefits and the presence of asphalt parking lots close to the park had higher LST (over 31 °C) that needs to be reduced.

c) Semi dense urban areas

Figure 7.7 shows that most LST in the semi-dense urban areas was within the temperature zone 27.1 °C–29 °C. The lower temperature of semi dense urban areas was influenced by the paddy fields and vegetation area, which in the temperature range of 25.01 °C – 27 °C. Moreover, the semi dense built-up area was sparse and planted with more vegetation than other built-up area types.

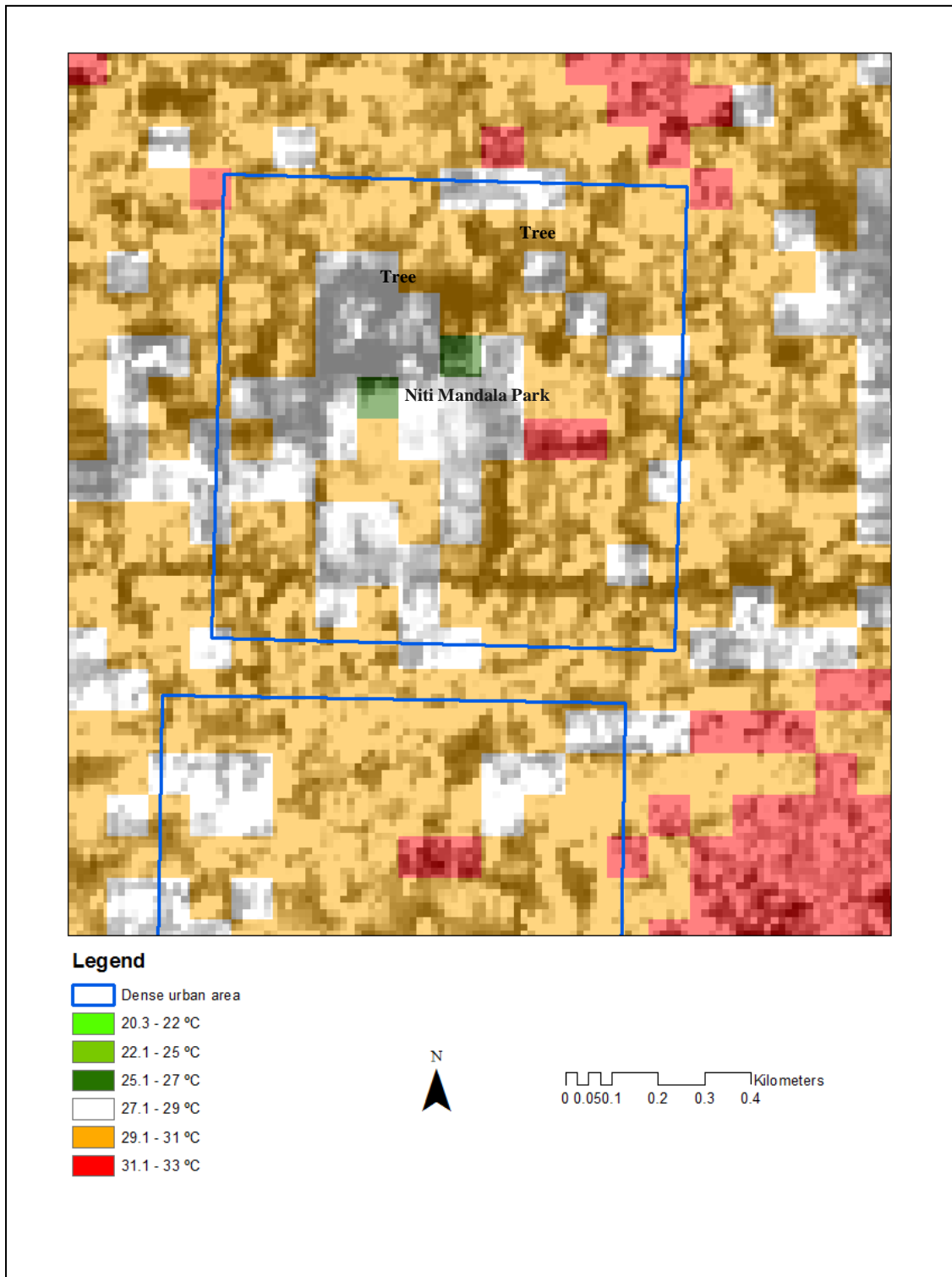


Figure 7.6 Typical thermal sample in densely urban areas (Niti Mandala Park)

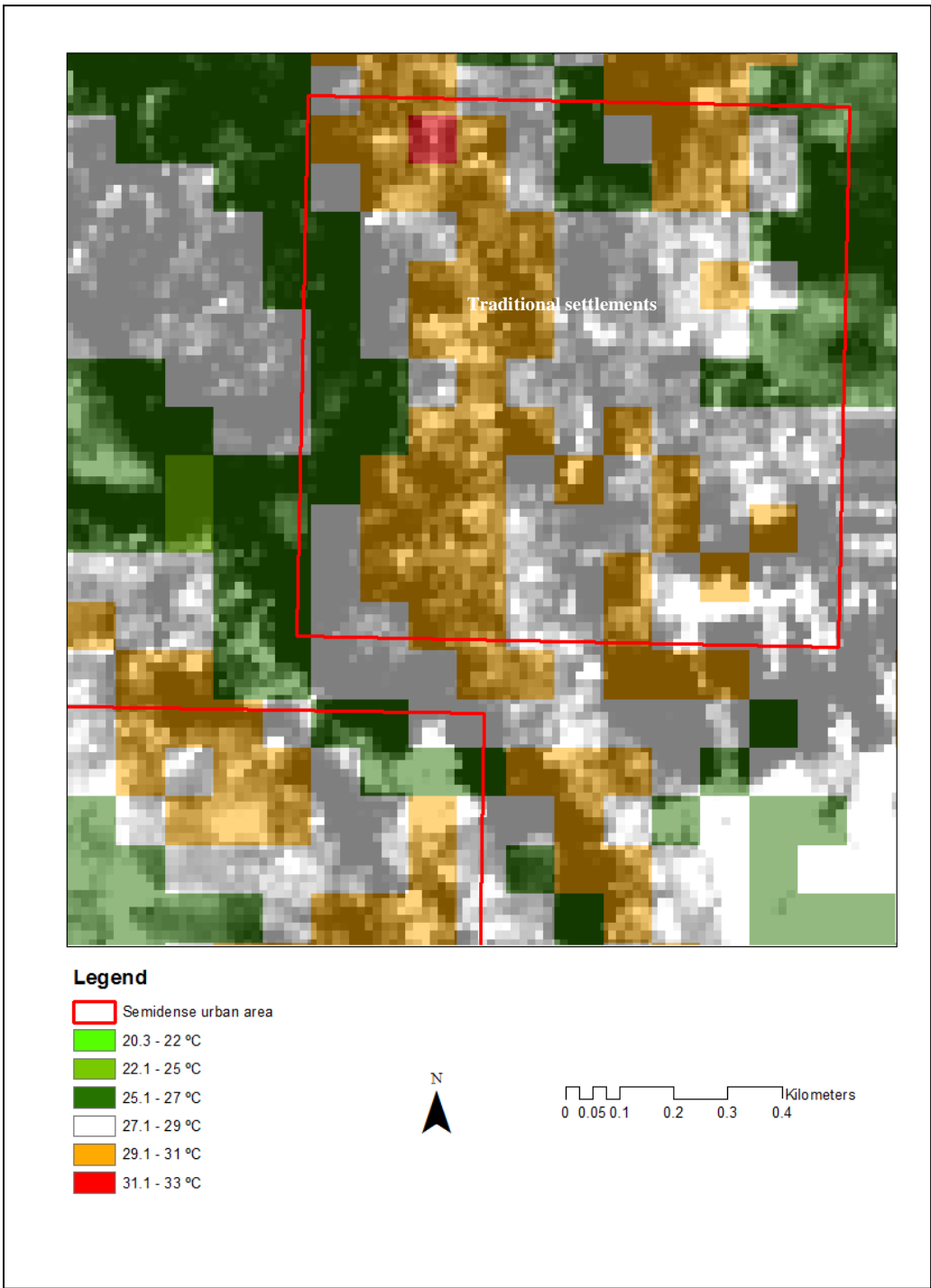


Figure 7.7 Typical thermal sample in semi-dense urban areas

7.3 Discussion

7.3.1 Factors that influence LST changes among built-up areas

This discussion is only focused on influencing factors of LST changes in the change period that shows significant difference in the LST value based on the t-statistics test that were very dense of 2003-2013, semi dense of 2003-2013, and semi-dense of 1995-2013 (Table 7.5). The possible factor that influences this variation of LST changes is factors of time of day, seasonality, and LULC condition (Zhou and Wang; 2011). The three images used in this study were captured at around the same local time at around 9-10 AM, thereby theoretically excluding the influence of the time-of-day factor. In addition, the seasonal factor that can influence LST difference also has been excluded by standardization in this analysis. Thus, this variation of UHI is assumed to be caused only by the LULC condition that is triggered by anthropogenic factors. The increasing temperature as well as the dense building density and geometry influence limited wind circulation that further impact human comfort and trigger the use of air cooling. As a result, the artificial heat sources and also air pollution influence the LST change. The more air conditioners are used, the more heat released, and vice versa, which eventually leads to the variation of UHI hot spot features. Therefore, the possible reason of this significant declined LST might be associated with the different seasons influencing human behavior and activities.

There are two types of season in this study area. The dry season runs from May to September and wet seasons runs from November to March. Different from other images that captured on a rainy day of February, the LST of 2013 was in April, which is the transitional season (from the rainy to dry season). The secondary data of monthly average air temperature for 2004-2008 period also shows the monthly temperature of April from the year of 2004 to 2008 tended to be lower than those of February (Setiawan, 2012). The pattern of wet and rainy season can be seen in Figure 4.2 (Chapter 4). This possible assumption was also confirmed by

comparing the estimated LST to the secondary data of ground-based air temperature at Ngurah Rai weather station located at 8°75'53"S and 115°17'02"E that shows the air temperature pattern in February 2003 was also higher than in April 2013. In addition, in accordance with the recorded air temperature pattern, the air temperature on 24 February 2003 was 32°C and the air temperature on 24 April 2013 was 28°C, while the measured LST on 24 February 2003 was 35.23°C and the measured LST on 24 April 2013 was 31.09°C (Chapter 6). Therefore, the temperature in 2013 was much lower compared to the temperature in 2003 and has influenced the lower use of air conditioner.

In contrast, semi urban areas from 1995 to 2013 and 2003 to 2013 shows that massive changes of paddy fields to semi dense built-up area had a significant impact on sharp LST increase. Also a significant increase in impervious surfaces is another possible reason of this increase in LST. Different from other types, most semi-dense urban areas were particularly distributed at suburban areas that were adjacent to large paddy field areas. The acquired image date of April 2013 was typically in the end part of the growing paddy season. On this condition, those areas might be dominantly influenced by the majority bare land and pre-emergent state of crops' growth. Developed paddy fields in pre-emergent state of crops' growth tend to have similar spectral and radiant characteristics as open soil, which may have an exceptionally strong impact on overall LST. This is confirmed by the LST of paddy fields, which increased from 1995 to 2013 (Table 7.4). However, the impact of growing activities in paddy fields on LST needs to be investigated by further research. Images with more obviously different seasons and more detailed investigation on LST change by LULC type condition in the built-up area type is required. This result also indicates the limitation of UHI nature as UHI is not a stable pattern. There are also many possible external factors, such as wind, which is hard to take into account in these built-up areas and might also influence the state of UHIs.

7.3.2 Concept of green space planning

The development of green spaces was regulated by Indonesian government regulation No. 5/1988 and 2007, which requires that the minimum extensive green space is set to be 30% of the total area, and regulation No. 63/2002, which requires that the minimum urban state forest area is at least 10% of the total city area. However, from the field survey, it can be seen that only one new public park was developed during the 18 years. This is a contrasting condition as the urban population and development of built-up areas increased tremendously from 1995 to 2013. The number of public parks was too low, although parks have distinctly proven to lower LST pockets among built-up areas.

The basic concept of green space planning is to develop green spaces in the study area in order to mitigate UHI effects as well as to provide urban public facilities. Therefore, a better local thermal environment and livable city can be achieved. The number of green spaces needs to be highly developed in the high priority zone (Figure 7.4). The alternative action could be by developing lots of parks in the available vacant land (Figure 7.5) and by planting a large number of trees along the road sides, river banks, residential and office yards, and other potential areas. Increasing the number of trees in new parks due to their multiple benefits would be more of a plausible solution as it requires relatively low technology and is cost-effective.

Planting trees located in parks, cemeteries, vacant land, and recreation facilities, particularly in very dense built-up areas, can offer cooling effect pockets, as trees reduce LST directly through the evapotranspiration process. Trees reduce local thermal surfaces by absorption and reducing overall heat, through refracting sunlight and shading pavements, as well as affecting wind flow (Dwyer et al., 1992; Parker, 1983). Larger tree areas would be more effective, as they provide a greater canopy and shade cover. Therefore, developing new parks can provide larger areas for tree planting that is urgently required and would be a first-priority action. There is no doubt that the presence of green spaces can moderate the UHI

effect (Yuan & Bauer, 2007), ensure energy flow (Yeh & Huang, 2006) along with providing cleaner air and water (Davies et al., 2008).

In order to maximize benefits of green spaces, the development of green spaces should be approached from the micro-level areas. Community parks should be provided by neighbourhoods or from villages to districts. The current problem of the unavailability of government land, which has served as a barrier to having a large amount of public parks, could be overcome by purchasing of private land. If this plan can be implemented, this can affect the local surface energy balance and potentially lower LST in very dense urban areas. Increasing urban green spaces through developing new parks, planting trees, and applying green vertical walls and roofs would lower the energy demand and reduce costs for businesses, institutions, and residential structures. This is also in accordance with actions of the EPA (2009), which has promoted a mitigation strategy based on increasing urban green spaces (urban forestry), cooling the roofs of structures, and cooling pavements.

To have more significant impact on controlling the temperature, planting trees and other vegetation requires a planting design and proper management. The increase of vegetation should be focused on surrounding houses and residential areas, roads, and commercial buildings in urban areas. In addition, a specific emphasis should also be applied for green rooftops and green vertical walls on the side of buildings. Placing trees in front of windows and on the sunniest sides of a house will maximize energy savings and would be effective due to the blocking of the morning and afternoon sun. In the tropics, trees should be placed along the southern exposures of structures (Bowler et al., 2010). Figure 7.8 shows applied UHI mitigation in built-up areas in the study area.



Figure 7.8 A cooling pavement in a very dense urban area

To build new parks that can mitigate UHI effects, the hot climate with high humidity in the study areas should be considered in the park design and planning. Some basic green space concepts are suggested are to reduce LST and minimize humidity and modify wind direction, to provide maximum shade in the afternoon, to maximise the use of vegetation as a radiation absorbent surface that has shade-giving properties. As mentioned by Asimakopoulos et al. (2001), shading from trees can significantly decrease the energy required for cooling, decrease the rate of heat convection inside buildings due to shaded surfaces that have a lower temperature, and decrease the radiation exchange of the wall with the sky.

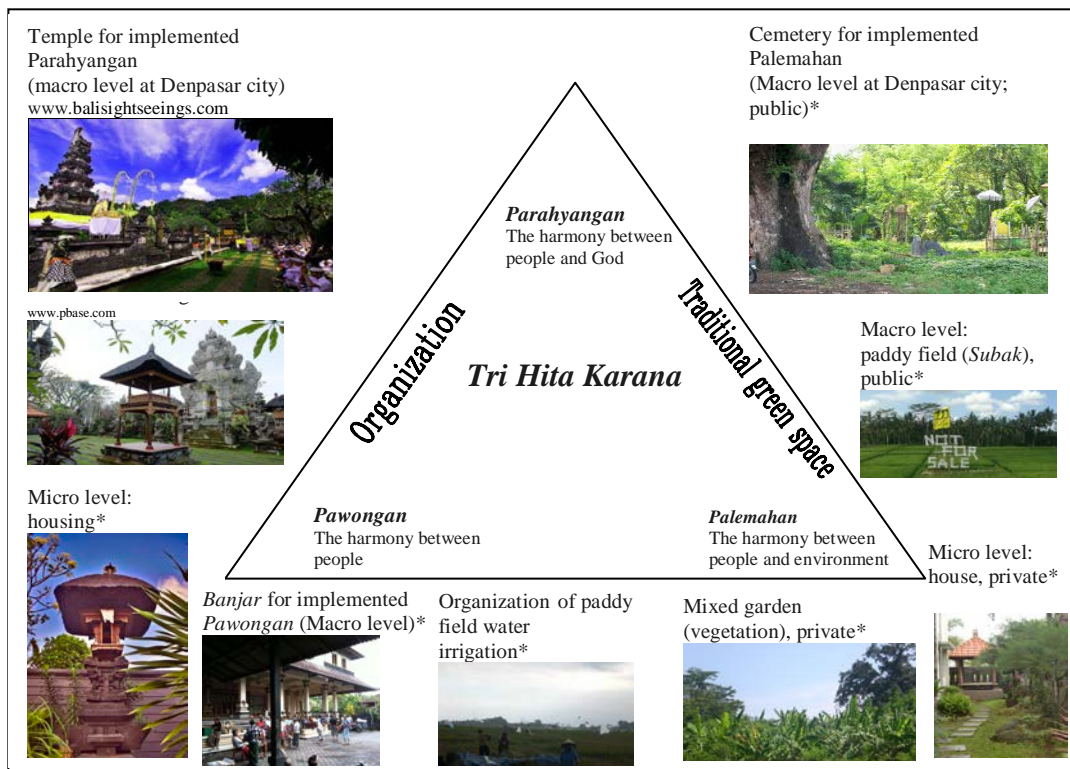
Adapting the green space basic concept in park element designs can be done by considering the points below (Shahmohamadi et al., 2011):

- Wind is increased through the use of hard and soft landscape materials to create air pressure differences and air movement.
- Minimize paved areas and orient active areas to the southeast to protect from afternoon sun.
- Sun-exposed surfaces use light colour materials.
- Shaded pathways use canopy trees for airflow and parking lots shall be covered by trees or pergolas.

7.3.3 Adaptation of local cultural concepts in green space management

Besides defining green space planning and management based on raster maps of built-up area types, LST and NDVI, the indigenous planning concept of green space, called *Tri Hita Karana* that exists in the study area also needs to be adopted. This will empower UHI mitigation efforts because this indigenous planning concept of green space conserves urban paddy fields and protects some natural sacred green spaces in Bali such as traditional sacred places, cemetery, and temples. Space arrangement in Bali was traditionally based on an indigenous life concept of the Balinese community called *Tri Hita Karana (THK)* as discussed in Chapter 4. The concept of *Tri Hita Karana* was applied in human space arrangement from the micro level (household level) to macro level (urban) and the application is shown in Figure 7.9. A field study in a very dense, built-up area of Denpasar shows the application of THK concept in individual houses can still be found either on the features of *Parhyangan* and *Pawongan* and most residents still have a good understanding of the concepts of *Tri Hita Karana*.

However, in recent years with population pressure, the traditional structure and function of the LULC pattern has had a fundamental change. The implementation of the *Palemahan* concept, which would have a small, open space in the house for the trees and garden, can hardly be applied today (Akuntomo and Suratman, 2013). Narrow houses and economic conditions were the dominant driving factors that influenced the transformation in the application of the THK concept in the space arrangement (Paturusi & Diartika, 2010). Therefore, the trees and garden are often absent which leads to the increase of UHI effects. This situation becomes worse if the house was inhabited by immigrants as they tend to ignore the THK concept. Moreover, there was no rule from the local government regulation that strongly tied all citizens to apply the THK concept. Therefore, in the future the THK concepts that once applied to individual housing might eventually disappear.



*Pictures were taken during field survey

Figure 7.9 The applied THK concept of green space

Because of the green space zones they provide, all paddy fields located in the high priority zone have to be preserved and must not be transformed into other LULC types. The quality of existing green space areas that has strong relationship with the THK concept should also be increased. As basic local wisdom of Bali, THK needs to be more consistently implemented and more empowered to develop sustainable urban green spaces. The embedded local, indigenous concepts would also give added value for the identity of Bali's urban green spaces that cannot be found in other areas. The analysis of the relationship between the THK concept and the modern green space typology in Indonesia would give the result seen in Figure 7.10. From the relationship between THK with the typology of green open space development in Indonesia, the THK concept would still be relevant to be implemented in the modern conditions and the most possible space for developing tree plantation is on the public space of temple and cemetery. For example there

were 35 villages that have existed in Denpasar and each of them has three temples and at least one cemetery. The green space that existed with them will never be converted into another LULC type. Therefore, those areas need to be optimally developed as urban green spaces. This is the most enabling suggestion to overcome the limited availability for public areas in the study site.

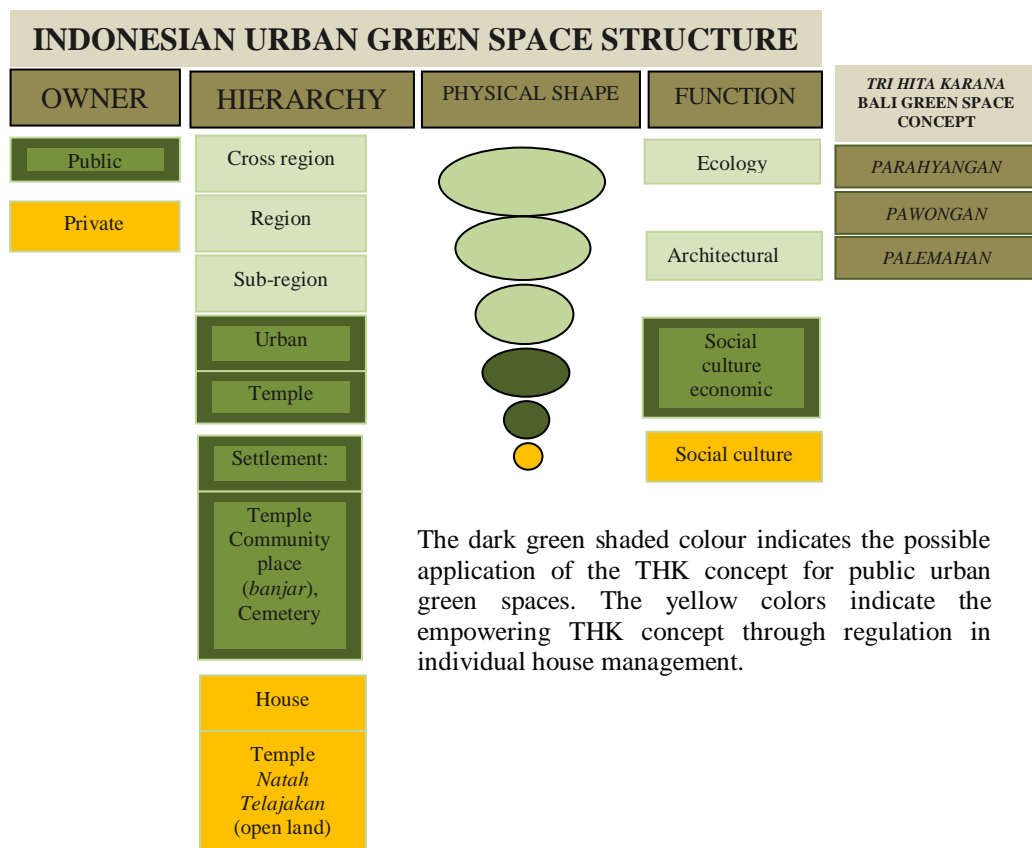


Figure 7.10 The relationship between applied THK concept and Indonesia green space structure (Adapted from Space Plan Bureau of Indonesia, 2006; Paturusi and Diartika, 2010)

7.4 Chapter summary

This chapter employed LST information of three different urban area types for the purpose of green space planning. The average LST increased from the semi-dense urban areas to the very dense urban areas. The higher mean LST in very dense urban areas indicates that the density of urban area strongly influenced the UHI effect. It also gives an indication that the green space development should be

firstly focused on this urban area type. The impact of LULC change on increasing LST change shows it was significant in semi-dense urban areas. The change of LST in very dense urban areas was also influenced by anthropogenic activities. Based on a weighted overlay of raster maps of LST, NDVI and urban area types, three zones of green space planning and management were identified. Those were the high-priority zone, low-priority zone, and not a priority zone. The amount of green spaces and tree planting plan must be highly increased in the high-priority zone as green spaces can give a distinct cooling spot in very-dense and densely urban areas. Despite zoning, adaptation of the local cultural factor, *Tri Hita Karana*, which cannot be seen physically, is also considered in green space management. The concept needs to be more empowered and applied particularly at the public level through evergreen tree plantation. At the private level, application of green space should be supported by government rules that strongly prepare citizens to anticipate more migrants in the future. Although paddy field LST in very dense urban areas was higher than LST in other urban area types, the paddy field in the adjacent built-up areas had provided cold thermal spots in this urban area types. More attention should be paid to conserving these paddy fields in urban areas, particularly those were located in high priority zones of green spaces. Additional recreation value and plant diversification that has been running well to conserve paddy fields in some city areas should be intensively improved. The limited availability of vacant areas and the private status of paddy fields that accelerate the changing of paddy field into other things should be overcome by buying those private lands by the local government.

8 CONCLUSION AND FUTURE DIRECTION

When examining the impact of LULC on LST and urban green space planning, land managers and policy makers need detailed map information as a baseline management tool. However, making LULC and LST maps with labour-intensive surveys becomes less practical and increases costs. RS and GIS technology offer a way to derive necessary information in a spatiotemporal LULC and LST. The study presented in this thesis demonstrates four types of analysis that can be retrieved:

- a) Historical multispectral remotely sensed images can be analysed to reconstruct the spatial rates and patterns and rates of change of LULC from 1995 to 2013;
- b) Historical multispectral remotely sensed images can be analysed to reconstruct the spatial patterns and rates of change of LST from 1995 to 2013;
- c) The relationship between LULC changes and LST and NDVI can be determines; and,
- d) Mitigation and adaptation of UHI effects through allocation of green spaces is proposed.

A summary of these studies is described with recommendations for future study.

8.1 Spatial and temporal LULC rates and patterns

Chapter 5 examined LULC change rates and patterns between 1995 and 2013 over a 240 km² study area using a temporal series of multispectral RS images. This chapter also demonstrated the usefulness of object-based image analysis in deriving LULC classification. This type of information is important for updating spatial data for urban management, determining past and current levels of LULC, as well as the change rate for LULC monitoring. The spatial and temporal LULC change was then studied, and revealed that:

- a) The OBIA approach requires a very good accuracy level in both classifications because the accuracy of the change map is the product of

the accuracies of the individual classifications. Some classification errors are caused by high diversity LULC types, segmentation and merge errors, time difference of collecting reference data, and difference in spatial resolution between classification and reference data.

- b) There are 12 main LULC classes that can be identified using ASTER and Landsat images, with an overall accuracy of 85%, 87 and 80% for maps of 1995, 2003 and 2013, respectively. Both images types were useful in determining various LULC types in heterogeneous areas, but suffered in the detection of the detail of built-up areas and paddy fields (i.e., harvesting, watering, and vegetative stage) in 1995 due to the lower spatial resolution of the Landsat data.
- c) The study site experienced fast urban growth that expanded into vegetation and agricultural areas on the fringes. LULC maps show that in the two periods urban expansion occurred in all directions and was distributed unevenly in all directions. The city associated with the built-up area category expanded an average of 360 ha/year over 8 years (1995-2003), with an average of 400 ha/year over 10 years (2003-2013). The highest rate of vegetation and paddy field transformation into built-up areas occurred particularly during the period of 1995-2003. The decrease in paddy field land may result in urban environmental problems, particularly floods, food security issues, deep water shortages, and imbalance of the urban ecosystem.
- d) LULC changes were governed by a combination of demographic changes, economic growth, land value, and road development. Inconsistent and ineffective government regulation and little coordination among involved agencies accelerated the changes in LULC. On the other hand, the Balinese local wisdom helped to restrain the changes during the same periods.

8.1.1 Recommendations

- a) The imagery and classification techniques in this study did not always accurately detect paddy fields, vegetation and built-up areas. In order to develop a more accurate and detailed heterogeneous urban structure classification, it is recommended that the classification process should be revisited and more reference samples be collected to significantly improve the classification result. Moreover, the object-based classification technique used in this study may be transferred to higher spatial resolution imagery with smaller grid cells (less than 15 m² of spatial resolution).
- b) The technique used to determine the main driving force variables of LULC changes, particularly in fringe areas, needs to be more intensively explored as it is useful for predicting future LULC. This information is also important to the development of strategies and practices for urban planning and management.
- c) A deliberate strategy should be crafted by the local government to sort out the massive vegetation and paddy field changes. Remaining paddy field areas should receive designation as timeless paddy fields. Financial subsidies money and land tax concessions could be alternative solutions.

8.2 Spatial and temporal LST rates and patterns

Chapter 6 examined LST retrieval using ASTER and Landsat thermal data of 1995-2013. A pattern of UHI effect was related to LULC patterns and changes. This analysis has the following results:

- a) Thermal data of both Landsat TM and ASTER is a useful component in LST monitoring. A standardization process is necessary to exclude seasonal factors and to maintain the temporal consistency for data set comparison. Retrieved LST was in accordance with the observed annual air temperature pattern from secondary data and temperature data from Ngurah Rai climate station. This result makes a contribution by being the

first spatial and temporal study of LST patterns in the fastest growing area of Bali using RS and GIS technology.

- b) The magnitude and spatial patterns of UHI in Bali can be revealed by visually identifying the derived LST images that tended to be more widespread in 2013. The thermal pattern of “hot spots” classified for the aim of this study was areas with temperatures over 29°C. Those areas were linked with built-up area structures that were characterized by building roofs and asphalt parking lots. Thermal patterns of “cool spots” consisted of paddy fields and vegetation, which created a lower temperature. The local patterns from transect graph show the lower LST in paddy fields and vegetation areas, and the LST gradient gradually climbed in the downtown area of Denpasar. This is also an effective technique for locating local scale of thermal features of UHI effects by LULC types.
- c) The RS and GIS processing techniques used, which depict a combination of satellite thermal data of Landsat TM and ASTER sensor and high resolution aerial photograph of Google, are well suited for detecting thermal patterns from micro scale of three different density types of built-up areas for the UHI mitigation effort. Images from all three dates, 1995, 2003, and 2013, on built-up area types displayed broadly similar patterns with distinct micro UHI effects.

8.2.1 Recommendations

Aside from the limited availability of cloud-free satellite data, although the synoptic coverage, accuracy, and spatial resolution of ASTER and Landsat can reduce requirements for in-situ measurements of temperature, corrected real object properties and in-situ observation data of LST that are lacking in this study are still required for more comprehensive validation of retrieved LST data.

8.3 The relationship between LULC change on LST and NDVI

Chapter 6 also studied how LULC classes were related with LST changes and quantified the relationship between LST and the biophysical parameters (LULC and NDVI). The analysis of the relationship between the LST, LULC and NDVI would provide the basis for the mitigation of UHI effects, offering better living conditions to the city. The study revealed that:

- a) The impact level of LULC types on LSTs can be divided into: high impact LULC (over 29 °C) in built-up areas, moderate impact LULC (27-28 °C) in open land, grass land, paddy fields, fish ponds, water bodies, vegetation, bush land and dry farm land, as well as the low impact LULC (25-26 °C) of swamp area and mangroves.
- b) LULC changes had an impact on LST changes from 1995 to 2003, particularly in the urban fringe areas. The changes in LST in coastal areas were more influenced by the cold sea currents caused by wind factors, while LCT change in the downtown areas were caused by anthropogenic activities such as air conditioning and transportation pollution.
- c) Statistical analysis using Pearson's correlation coefficient indicates built-up, paddy field and vegetation types persistently demonstrated a negative significant relationship between LST and NDVI across all three years. This significant negative correlation shows the higher LST is related to lower value of NDVI and vice versa. The weakness of the relationship might be due to the heterogeneous condition of LULC types.

8.3.1 Recommendations

All further urban research depends on the quality of classification results, which are possible misinterpreted and influence the weakness value of the relationship between LULC change on LST and NDVI. Therefore, the accuracy of the LULC classification should be improved for further study.

8.4 Mitigating the UHI effect through green space planning

As built-up areas play an important role in the formation of UHI centers and comprised 50% of the study area in 2013, Chapter 7 analyses the LST pattern specifically in the urban area types at the micro scale level (MUHI) in order to mitigate the UHI effects through the development of urban green space. Detection of MUHI was conducted to directly see the UHI hotspots that showed higher LST than surrounding areas. A priority zone for green space planning in the urban area category was also suggested by numerical classification, and thus the green space management plan for each zone may be developed. The study revealed that:

- a) The density of built-up areas influenced the UHI phenomena. The LST of all LULC types in the very dense urban areas was consistently higher than temperature in dense and semi dense urban areas. The warmer mean LST in very dense urban area types indicates green space development should be firstly focused on these areas.
- b) LULC changes in very dense and dense urban areas did not have a significant impact on LST changes from 1995 to 2013, with the exception of the rise of LST in very dense urban areas from 2003 to 2013, which may have been influenced by anthropogenic activities. Yet, the significant increase of LST in semi dense urban areas may have been caused by LULC changes.
- c) Weighted overlay of raster maps of LST, NDVI and urban area types resulted in three zones of green space planning and management. Those were the high priority green space, low priority green space and not a priority green space. The amount of green space and the tree planting plan must be increased in priority zones, as green space can offer a distinct cooling spot in very-dense and dense urban areas.
- d) Adaptation of the local cultural concept, *Tri Hita Karana*, is also considered in green space planning and management. The concept needs to be more empowered and applied, particularly at the public space level, through evergreen tree planting. On the private level, the application of

green space should be supported by government rules in anticipation of continued future migration.

8.4.1 Recommendations

- a) The study results also indicate the limitations of UHI, as UHI is not a stable pattern. Investigation of the impact of anthropogenic factors (i.e., paddy field stage, use of air conditioner) and wind that possibly influences LST values is recommended for future research.
- b) Although LST of paddy fields in very dense urban areas was much higher than LST in other built up types, the paddy fields adjacent to the built-up areas offered the reduction impact on the edge of built-up areas. Therefore, more attention should be paid to conserving urban paddy fields, particularly in the green space zones of high priority. Additional recreation value and plant diversification that have worked well to conserve paddy fields in some city areas should be intensively improved. The limited availability of vacant areas and the private status of paddy fields frequently converted to other uses should be addressed by the local government's purchase of private lands.
- c) Further research into urban green space structures (species, composition, function) that have effectively reduced the LST in the study site should be conducted in order to develop comprehensive green space planning and management. This can be followed by classification of urban green space structures and impervious material structures, and thus more detailed investigation of LST changes by more detail built-up area structures is required.

REFERENCES

- Abrams, M. (2000). The Advanced Spaceborne Thermal Emission and Reflection Radiometer (ASTER): Data products for the high spatial resolution imager on NASA's Terra platform. *International Journal of Remote Sensing*, 21(5), 847-859.
- Abrams, M. & Hook, S. (2002). Aster users handbook, Version 1. Pasadena: Jet Propulsion Laboratory. Accessed 23 July 2012 from http://www.gis.usu.edu/~doug/RS5750/resources/ASTER_User_Handbook.pdf
- Aduah, M. S., Mantey, S., Tagoe, N.D., & TRegoe, N. D. (2012). Mapping land surface temperature and land cover to detect urban heat island effect: A case study of Tarkwa, South West Ghana. *Research Journal of Environmental and Earth Sciences*, 4(1), 68-75.
- Aguiar, A.C. (2012). Urban Heat Islands: differentiating between the benefits and drawbacks of using native or exotic vegetation in mitigating climate. Thesis collections of University of Wollongong. Research online.
- Ahmad, S. & Hashim N. M. (2007). Effects of soil moisture on urban heat island occurrences: case of Selangor, Malaysia. *Humanity & Social Sciences Journal*, 2(22):132-138.
- Amiri, R., Weng, Q., Alimohammadi, A., & Alavipanah, S. K. (2009). Spatial-temporal dynamics of land surface temperature in relation to fractional vegetation cover and land use/cover in the Tabriz urban area, Iran. *Remote Sensing of Environment*, 113(12), 2606-2617.
- Anderson J.R., Hardy E.E., Roach J.T., & Witmer R.E. (1976). A land use and land cover classification system for use with remote sensor data, *US Geological Survey Professional Paper* 964, 28 pp.
- Aniello, C., Morgan K, Busbey A., & Newland L. (1995). Mapping micro urban heat islands using Landsat TM and a GIS. *Comparative Geoscience*, 21; 965-969.
- Argaud L, Ferry, T., Le, Q.H., Marfisi, A., Ciorba, D., Achache, P., Ducluzeau, R., Robert, D. (2007). Short and long term outcomes of heatstroke following the 2003 heat wave in Lyon, France. *Internal medicine*, 167(20), 2177-83.
- Arizona Board of Regents. (2007). Urban climate-climate study and UHI via the internet way back machine change: forcings, feedbacks, and the climate benefits of forests. *Science*. 320, 1444-1449.

- Artis, D.A. & Carnahan, W.H. (1982). Survey of emissivity variability in thermography of urban areas. *Remote Sensing of Environment*, 12(4), 313-329.
- As-syakur (2011). Land use cover change in Bali. *Ecotrophic*, 6 (1).
- Aster Science Office. (2009). ASTER SWIR Data Status Report. Accessed 18th July 2012 from http://www.science.aster.ersdac.jspacesystems.or.jp/t/en/about_aster/swir_en.pdf.
- Baatz, M., Hoffmann, C. & Willhauck, G. (2008). Progressing from object-based to object-oriented image analysis. In Blaschke, T., Lang, S., Hay, G.J. (Eds.), *Object based image analysis*: Springer, Heidelberg, Berlin, New York, pp. 29–42
- Baja, S., Mustafa, M. & Arief, S. (2011). Spatial Dynamics of land use/land cover in South Sulawesi Indonesia. Paper presented in Asia Geospatial forum 17-19 October 2011, Jakarta.
- Balipost. (2009). Floods hit Denpasar. Accessed 18th March 2014 from <http://issuu.com/epaper-kmb/docs/bp12012009>.
- Banerjee K., Panda, S., Jain, M.K., Jeyaseelan, A.T., & Sharma R. K. (2014). Comparison of Aster Thermal Bands and feature Identification Using Advance Spectroscopic Techniques. *International Journal of Innovation and Scientific Research*, 7 (1), 2351-8014.
- Benz U.C., Hofmann P., Willhauck G., Lingenfelder I., Heynen M. (2004). Multi-resolution, object-oriented fuzzy analysis of remote sensing data for GIS-ready information. *ISPRS J. Photogramm. Remote Sens*, 58(3–4), 239–258.
- Bin Md Hashim, Bin Ahmad, A. & Binti Abdullah, M. (2007). Mapping urban heat island phenomenon: remote sensing approach. Accessed 8 March 2012 from http://dspace.unimap.edu.my/dspace/bitstream/123456789/13743/1/02500_Mapping%20Urban.pdf
- Bin Jamaludin, J.A. (2010). Relationship between urban surface temperature and land uses application of remote sensing and GIS in Johor Bahru. Report of researches and academic activities in IDEC, Hiroshima University. (October 1, 2010 – March 31, 2010). Japan. Accessed 12 September 2012.

- Bornstein and Lin. (2000). Urban heat island and summertime convective thunderstorms in Atlanta: three case studies. *Atmospheric Environment*, 34(3), 507-516.
- Bretz. S., Akbari, Hashem & Rosenfeld, A. (1998). Practical issues for using solar-reflective materials to mitigate urban heat islands. *Atmospheric environment*, 32 (1).
- Buyantuyev, A. & Wu, J. (2009). Urban heat island and landscape heterogeneity: linking spatiotemporal variations in surface temperatures to land-cover and socioeconomic patterns. *Landscape Ecology*, 25(1): 17-33.
- Cai G., Mingyi Du., Yong Xue. (2012). Monitoring of urban heat island effect in Beijing combining ASTER and TM data. *International Journal of Remote sensing*, 32(5), 1213-1232.
- Canada Centre for Mapping and Earth observation. (2015). Accessed 5 July 2015 from [https://www.natureindex.com/institutionoutputs/Canada/Canada%20Centre%20for%20Mapping%20and%20Earth%20Observation%20\(CCMEO\)](https://www.natureindex.com/institutionoutputs/Canada/Canada%20Centre%20for%20Mapping%20and%20Earth%20Observation%20(CCMEO))
- Carlson, T.N. and Arthur, S.T., 2000, The Impact of Land Use-Land Cover Changes Due to Urbanization on Surface Microclimate and Hydrology: A Satellite Perspective. *Global and Planetary Change*, 25, 49-65.
- Carlson, T. N., & Ripley, D. A. (1997). On the relation between NDVI, fractional vegetation cover, and leaf area index. *Remote Sensing of Environment*, 62(3), 241-252. doi: [http://dx.doi.org/10.1016/S0034-4257\(97\)00104-1](http://dx.doi.org/10.1016/S0034-4257(97)00104-1).
- Carnahan, W. H., & Larson, R. C. (1990). An analysis of an urban heat sink. *Remote Sensing of Environment*, 33(1), 65-71.
- Chandler, G., Markham, B. L., & Helder, D. L. (2009). Summary of current radiometric calibration coefficients for Landsat MSS, TM, ETM+, and EO-1 ALI sensors. *Remote Sensing of Environment*, 113(5), 893-903.
- Chen, G., Notaro, M., Liu, Z. Y. (2013). Simulated local and remote bioMaD, *et al. Chin Sci Bull*, 17 (58) No.17 2081 physical effects of afforestation over Southeast United States in boreal summer. *J Clim*, 25: 4511–4522.
- Chen, S., Zeng, S., & Xie, C. (2000). Remote sensing and GIS for urban growth analysis in China. *Photogrammetric Engineering and Remote Sensing*, 66(5), 593-598.

- Chen X.L., Zhao H.M., Li P.X., & Yin Z.Y. (2006). Remote sensing image-based analysis of the relationship between urban heat island and land use/cover changes. *Remote sensing of environment*, 104, 133-146.
- Chen, Z. (2008). Satellite image processing methods for land use and land cover mapping and change detection and applications to landslide studies in the three gorges area, China (Order No. NR39255). Available from ProQuest Dissertations & Theses Full Text; ProQuest Dissertations & Theses Global. (304382097). Retrieved from <http://search.proquest.com.dbgw.lis.curtin.edu.au/docview/304382097?accountid=10382>
- Chen, Z. M., Babiker, I. S., Chen, Z. X, Komaki, K., Mohamed, M. A. A., & Kato, K. (2004). Estimation of interannual variation in productivity of global vegetation using NDVI data. *International Journal of Remote Sensing*, 25(16), 3139–3150.
- Cheng, Y., Nie, J., Li, G., Zhang, C. & Wang, W. (2008). Study on land use and land cover change with the integration of RS, GIS and GPS technologies-the case of Baotou City in the ecotone of agriculture-animal husbandry, China. *Geoscience and Remote Sensing Symposium Presented in IGARSS 2008 International IEEE*, pp. IV.
- Chrysoulakis, N., Abrams, M., Feidas, H., & Arai, K. (2010). Comparison of atmospheric correction methods using ASTER data for the area of Crete, Greece. *International Journal of Remote Sensing*, 31(24), 6347-6385. doi: 10.1080/01431160903413697
- Chudnovsky, A., Ben Dor, E., & Saaroni, H. (2004). Diurnal thermal behavior of selected urban objects using remote sensing measurements. *Energy and Buildings* 36(11), 1063–1074.
- Collier, C.G. (2006). The impact of urban areas on weather. *Q. J. R. Meteorol. Soc.* 132, 1–25.
- Colombi, A., Pepe, M, Rampini, A & De Michele, C. (2007). Estimation of daily mean air temperature from MODIS LST in Alpine areas. In Bochenek, Z. (ed.). *New Developments and Challenges in Remote Sensing*, Millpress, Rotterdam, ISBN 978-90-5966-053-3
- Congalton, R. G. 1991. A review of assessing the accuracy of classifications of remotely sensed data. *Remote Sensing of Environment*. 37: 35-46.
- Congalton, R, G. 2007. Thematic and positional accuracy assessment of digital remotely sensed data In: McRoberts, R. E.; Reams, Gregory A.; Van Deusen, P. C.; McWilliams, W. H.,(eds). *Proceedings of the seventh*

annual forest inventory and analysis symposium; October 3-6, 2005; Portland, ME. Gen. Tech. Rep. WO-77. Washington, DC: U.S. Department of Agriculture, Forest Service: 149-154.

- Coppin, P., Jonckheere, I., Nackaerts, K., Muys, B., & Lambin, E. (2004). Review Article Digital change detection methods in ecosystem monitoring: a review. *International Journal of Remote Sensing*, 25(9), 1565-1596. doi: 10.1080/0143116031000101675.
- Coutts, A., Beringer, J & Tapper, N. (2010). Changing urban climate and CO2 emissions: implications for the development of policies for sustainable cities. *Urban Policy and Research*, 28(1), 27-47. doi: 10.1080/08111140903437716.
- Dell'Acqua, F., Gamba, P. & Lisini, G., (2003). Improvements to urban area characterization using multitemporal and multiangle SAR images. *IEEE Transactions on Geoscience and Remote Sensing*, 41(9), 1996-2004.
- Deo, R.C. (2011). Links between native forest and climate in Australia. *Weather*, 66:64-9.
- Dewan, A., & Corner, R. (2014). Impact of Land Use and Land Cover Changes on Urban Land Surface Temperature. In Dewan, A & Corner, R. (Eds.), *Dhaka Megacity: Geospatial perspectives on urbanization, environment and health*: Springer. Netherlands, 219-238.
- Dewan, A., & Yamaguchi, Y. (2009). Using remote sensing and GIS to detect and monitor land use and land cover change in Dhaka Metropolitan of Bangladesh during 1960-2005, *Environmental Monitoring and Assessment*, 150, 237-249. <http://dx.doi.org/10.1007/s10661-008-0226-5>.
- Ear-Slater, I. (2002). *The handbook of clinical trials and other research*. Radcliffe Medical press. UK.
- Eden U. (2012). Drought assessment by evapotranspiration mapping in Twente, The Netherland, *Thesis of Faculty of Geo-Information Science and earth Observation* The University of Twente.
- Effendy, S. (2007). Relationship between green open space and and *Urban Heat island in Jabotabek*. Thesis of Forestry Bogor Agricultural Faculty, Bogor.
- Erell, E., Pearlmutter, D., Williamson, T.T.J., (2011). *Urban microclimate: designing the spaces between buildings*. Routledge.

- Etszkorn, B. (2012). Data normalization and standardization. Accessed 6 July 2015 from <http://www.benetz Korn.com/wp-content/uploads/2011/11/Data-Normalization-and-Standardization.pdf>
- Feizizadeh, B., Blaschke, T., Nazmfar, H., Akbari, E., & KoHbanani, H.R. (2013). Monitoring land surface temperature relationship to land use/land cover from satellite imagery in Maraqeh County, Iran. *Journal of Environmental Planning and Management*, 56(9), 1290-1315.
- Ferreira, M.J., Oliveira, A.P. & Soares, J., (2010). Anthropogenic heat in the city of São Paulo, Brazil. *Theoretical and Applied Climatology* 104(1-2), 43–56.
- Franklin, S. E., & Wulder, M. A. (2002). Remote sensing methods in medium spatial resolution satellite data land cover classification of large areas. *Progress in Physical Geography*, 26(2), 173–205.
- ENVI. (2008). ENVI feature extraction module user's guide. Spectral sciences and ITT visual information solutions.
- ENVI. (2009). Atmospheric correction module: QUAC and FLAASH user's guide. Spectral sciences and ITT visual information solutions.
- Galletti, C., & Myint, S. (2014). Land-Use Mapping in a Mixed Urban-Agricultural Arid Landscape Using Object-Based Image Analysis: A Case Study from Maricopa, Arizona. *Remote Sensing*, 6(7), 6089-6110.
- García-Cueto O.R., Jáuregui E., Toudert D., Tejeda A. (2007) Detection of the urban heat island in Mexicali, B.C., Mexico and its relationship with land use. *Atmósfera* (20):111–132.
- Giri, C.P. (2012). Brief overview of remote sensing of land cover. In Weng, Q. ed. Remote sensing of land use and land cover principles and applications. Taylor Francis series in RS applications.
- Global daily weather statistic. (2015). Accessed 2 February 2015 from http://geodata.us/weather/show_full.php?usaf=972300&uban=99999&m=4&c=Indonesia&y=2003"http://geodata.us/weather/show_full.php?usaf=972300&uban=99999&m=4&c=Indonesia&y=2003
- Godfrey, C. M., D. J. Stensrud, and L. M. Leslie, 2007: A new latent heat flux parameterization for land surface models. Preprints, *21st Conf. on Hydrology*, San Antonio, TX, Amer. Meteor. Soc., CD-ROM, 6A.3.

- Golden, J. S., & Kaloush, K. E. (2006). Mesoscale and microscale evaluation of surface pavement impacts on the urban heat island effects. *International Journal of Pavement Engineering*, 7(1).
- Google map (2013). Bali map. Accessed 1st August 2013 from <https://maps.google.com.au/>
- Graham, S. 1999. Clouds and radiation. Earth observatory. NASA. Accessed 27th September 2015 from <http://earthobservatory.nasa.gov/Features/Clouds/>
- Gupta, R.P. (2013). Remote sensing Geology. Berlin Springer, Berlin Heidelberg New York, 655 pp.
- Gusso, A.; Ducati, J.R. (2012). Algorithm for Soybean Classification Using Medium Resolution Satellite Images. *Remote Sens.*, 4, 3127-3142.
- Hadjimitsis, D. G. & Clayton, C. R. I. (2008). The use of an improved atmospheric correction algorithm for removing atmospheric effects from remotely sensed images using an atmosphere–surface simulation and meteorological data. *Met. Apps*, 15: 381–387. doi: 10.1002/met.80
- Hamada, S & Ohta, T. (2010). Seasonal variations in the cooling effect of urban green areas on surrounding urban areas. *Urban For Urban Green* 9(1):15–24
- Harman, I. N. & Belcher, S. E. (2006). The surface energy balance and boundary layer over urban street canyons. *Meteorol. Soc*, 132: 2749-2768.
- Hermann, G. Generalized Geometric Error Correction in Coordinate Measurement. Intelligent Engineering Systems and Computational Cybernetics. J. A. Tenreiro Machado, Béla Pátkai, Imre J. Rudas 267-276. Springer Netherlands
- Herold, M., Goldstein, N. C. & Clarke, K. C. (2003). The spatiotemporal form of urban growth: measurement, analysis and modeling. *Remote Sensing of Environment*, 86(3), 286-302.
- Hollinger, D. Y., Ollinger, S. V., Richardson, A. D., Meyers, T. P., Dail, D. B. (2010). Albedo estimates for land surface models and support for a new paradigm based on foliage nitrogen concentration. *Glob. Change Biol.*, 16, 696–710.
- Horning, N., Robinson J.A., Sterling, E.J., Turner, W., Spector S. (2010). Remote sensing for ecology and conservation a handbook of techniques. Oxford University Press. New York. 467p.

- Huang, G., Zhou, W. & Cadenasso, M. L. (2011). Is everyone hot in the city? Spatial pattern of land surface temperatures, land cover and neighborhood socioeconomic characteristics in Baltimore, MD. *Journal of Environmental Management*, 92 (7): 1753-1759.
- Hulley, G. C., C. G. Hughes & S. J. Hook. (2012), Quantifying uncertainties in land surface temperature and emissivity retrievals from ASTER and MODIS thermal infrared data. *J. Geophys. Res.*, 117, D23113, doi:10.1029/2012JD018506.
- Igusky, K. & Jackson, R., (2008). Quantifying albedo and surface temperature over different land covers: implication for carbon offsets. Thesis at Duke University.
- Indonesia Department of Work. (2006). Green space as an essential component of urban planning. Jakarta: Indonesian Department of Work.
- Indonesia Ministry of Environment. (1997). Indonesia Country Profile National Implementation of Agenda 21. Accessed 24th April 2015 from <http://www.un.org/esa/earthsummit/indon-cp.htm>
- Manakos, I., Manevski, K., Kalaitzidis, C. & Edler D. (2011). Comparison between FLAASH and ATCOR atmospheric correction modules on the basis of worldview-2 imagery and in situ spectro radiometric measurements, in: 7th EARSeL Workshop on Imaging Spectroscopy, Edinburgh. Accessed 17th July 2015 from http://www.earsel2011.com/content/download/Proceedings/S12_4_Manakos_paper.pdf
- IPCC. (2003). Good practice guidance for land use, land change and forestry. Special Report of the Intergovernmental Panel on Climate Change. In Penman, J., Gytarsky, M. (Russia), Hiraishi, T, Krug, T, & Kruger, D (Eds.). Japan: Institute for Global Environmental Strategies (IGES).
- IPCC. (2007). Changes in atmospheric constituents and in radiative forcing (Chapter 2). Special Report of the Intergovernmental Panel on Climate Change.
- Irwan, Z. D. (2005). Environmental Challenges and Urban forest landscape (*Tantangan Lingkungan dan Lanskap Hutan kota*). Bumi Aksara. Jakarta.
- Jasinski, M. F. (1990). Sensitivity of the Normalized Difference Vegetation index to subpixel canopy cover, soil albedo, and pixel scale. *Remote Sensing of Environment* 32, 169–187

- Jensen J. R. (2000). *Remote Sensing of the Environment: An Earth Resource Perspective*. 2nd Ed. Upper Saddle River, NJ: Prentice-Hall, Inc., p. 544.
- Jensen, J. R. (2004). Digital change detection, introductory digital image processing: A remote sensing perspective, pp. 467–494. New Jersey'Prentice-Hall.
- JICA. (2005). *The comprehensive study on water resources development and management in Bali Province, The Republic of Indonesia*, Japan International Cooperation Agency-Directorate General of Water Resources Ministry of Public Works.
- Jim, C.Y. & Chen S. S. (2003). Comprehensive greenspace planning based on landscape ecology principles in compact Nanjing city, China. *Landscape and Urban Planning* 99, 1–22.
- Junfeng, L., Zhibao, D. Guangyin, H., Changzhen, Y., Zhenhai, W., & Xiang, S., (2011). Land use and land cover change and its driving forces in the source region of the Yangtze River during 1990–2005. *Water Resource and Environmental Protection (ISWREP)*. pp. 2571.
- Kalkhan, M.A., Reich, R. M., & Czaplewski, R. L. (1997). Variance estimates and confidence intervals for the Kappa measure of classification accuracy. *Canadian Journal of Remote Sensing* 23, 210–216.
- Kalinoswki A. and Oliver S. (2004). Aster mineral index processing manual. Remote sensing applications geoscience Australia. Accessed on 21st July 2014 from http://www.ga.gov.au/webtemp/image_cache/GA7833.pdf
- Kayadibi, O. (2011). *Evaluation of imaging spectroscopy and atmospheric correction of multispectral images (Aster and Landsat 7 ETM+)*. Paper presented at the 5th International Conference of the Recent Advances in Space Technologies (RAST) on 9-11 June 2011.
- Kazimierz, K. and Krzysztof F. (1999). Temporal and spatial characteristics of the urban heat island of Łódź, Poland. *Atmospheric Environment*, 33(24):3885-3895.
- Kessler, A. & Jaeger, L. (1999). Long-term Changes in Net Radiation and its Components above a Pine Forest and a Grass Surface in Germany. *International Journal of Climatology*, 19, 211-226.

- Kikegawa et al. (2003). Development of a numerical simulation system toward comprehensive assessments of urban warming countermeasures including their impacts upon the urban buildings, *Applied Energy*, 76, 449-446.
- Kim, J. H. and Jackson, R. B. (2012). A global analysis of groundwater recharge for vegetation, climate, and soils. *Vadose Zone Journal*. 11, DOI: 10.2136/vzj2011.0021RA
- Kim, J. P. (2007). Land use planning and the urban heat island effect. PhD dissertation at Ohio University.
- Koutsias, N., & Karteris, M. (2003). Classification analyses of vegetation for delineating forest fire fuel complexes in a Mediterranean test site using satellite remote sensing and GIS. *International Journal of Remote Sensing*, 24(15), 3093-3104. doi: 10.1080/0143116021000021152
- Krause, C. W., Lockard, B., Newcomb, T. J., Kibler, D., Lohani, V. and Orth, D. J. (2004), Predicting influences of urban development on thermal habitat in a warm water stream. *Journal of the American Water Resources Association*, 40: 1645–1658. doi: 10.1111/j.1752-1688.2004.tb01612.x
- Kumar U. (2006). Comparative evaluation of the algorithms for land cover mapping using hyperspectral data. Thesis at ITC. Netherland.
- Lambin E.F., H.J., Geist., E. Lepers. (2003). Dynamics of land use and land cover change in tropical regions. *Annu. Rev. Environ. Resour.* 28: 205-241.
- Li, J., Song, C., Cao, L., Zhu, F., Meng, X., Wu, J. (2011). Impacts of landscape structure on surface urban heat island: a case study of Shanghai, China. *Remote Sensing of Environment* 115: 3249-3263.
- Li X., Zhou W., Ouyang Z., Zheng H. (2012). Spatial pattern of greenspace affects land surface temperature: evidence from the heavily urbanized Beijing metropolitan area, China. *Landscape ecology* 27(6): 887-898
- Li X., Zhou W., Ouyang Z. (2013). Relationship between land surface temperature and spatial pattern of greenspace: What are the effects of spatial resolution? *Journal of Landscape and Urban Planning* 114:1-8
- Li, X., & Yeh, A. G. O. (1998). Principal component analysis of stacked multi-temporal images for the monitoring of rapid urban expansion in the Pearl River Delta. *International Journal of Remote Sensing*, 19(8), 1501-1518. doi: 10.1080/014311698215315

- Li, Y. & Zhao, X. (2012). An empirical study of the impact of human activity on long-term temperature change in China: A perspective from energy consumption. *Journal of Geophysical Research* 117.
- Lillesand, T., Ralph, W.K. & Chipman, J. (2008). Remote Sensing and Image Interpretation (ed. 6). John Wiley & Sons, Inc.
- Liu, C., Frazier, P. & Kumar L. (2007). Comparative assessment of the measures of thematic classification accuracy. *Remote Sensing of Environment* (107) 606–616. doi: 10.1016/j.rse.2006.10.010.
- Liu, H. & Weng, Q. (2008). Seasonal variations in the relationship between landscape pattern and land surface temperature in Indianapolis, USA. *Environmental Monitoring and Assessment* 144(1-3): 199-219.
- Liu, L. & Zhang, Y. (2011). Urban heat island analysis using the Landsat TM data and ASTER data: A case study in Hong Kong. *Remote Sens.*3:1534-1552; doi:10.3390/rs3071535.
- Lo, C. P., Quattrochi, D. A. & Luvall J. C. (1997). Application of high-resolution thermal infrared remote sensing and GIS to assess the urban heat island effect. *Int. J. Remote Sens.* 18:287–304.
- Lo, C. P., & Quattrochi, D. A. (2003). Land-use and land-cover change, urban heat island phenomenon, and health implications: a remote sensing approach. *Photogrammetric Engineering & Remote Sensing* 69 (9): 1053-1063. Mendely.
- Long, H., Tang, G., Li, X. & Heilig, G. K. (2007). Socio-economic driving forces of land use change in Kunshan, the Yangtze River Delta economic area of China. *Journal of Environmental Management*, (83), 351–364.
- Loveland, T.R. & DeFries, R. (2004). Observing and Monitoring Land Use and Land Cover Change, In DeFries, R., Asner, G., & Houghton, R., (eds.), *Ecosystems and Land Use Change*, Geophysical Monograph Series, Volume 153, American Geophysical Union, Washington, DC, 231-246.
- Lu, D & Weng, Q. (2005). Urban classification using full spectral information of Landsat ETM+ imagery in Marion County, Indiana. *Photogrammetric Engineering and Remote Sensing* 71:1275–1284.
- Lubis, J. P. G. & Nakagoshi, N. (2011). Land use and land cover change detection using remote sensing and geographic information system in Bodri Watershed, central Java, Indonesia. *Journal of International Development and Cooperation*, 18 (1), 139-151.

- Ma D. Liu, Z.Y., Lu S. H., Michael, N., Rong, X. Y., Cheng G. S. & Wang, F.Y. 2013. Short-term climatic impacts of afforestation in the East Asian monsoon region. *Chinese Science Bulletin Atmospheric Science* 58 (17): 2073-2081.
- Mahavir D. (2000). High (spatial) resolution vs. low resolution images: a planner's view point. *International Archives of Photogrammetry and Remote Sensing*, 33 (7).
- Maimaitiyiming M., Ghulam A., Tiyip T., Pla F., Carmona P.L., Halik. M., & Caetano M. (2014). Effects of green space spatial pattern on land surface temperature: Implications for sustainable urban planning and climate change adaptation. *Journal of Photogrammetry and Remote Sensing*, (89): 59–66.
- Malekpour, P & Taleai, M. 2011. Modeling of relationship between land use/cover and land surface temperature using ASTER datasets. *Journal of Environmental Studies*, 37 (58): 29-42.
- Mallick J and Rahman A. (2012). Impact of population density on the surface temperature and micro climate of Delhi. *Current science*, 102(12):1708-1713.
- Mallinis G, Koutsias N, Tsakiri-Strati M, Karteris M. (2008). Object-based classification using Quickbird imagery for delineating forest vegetation polygons in a Mediterranean test site. *ISPRS Journal of Photogrammetry and Remote Sensing*, (63):237–250.
- Manakos I., Manevski K. & Kalaitzidis, Edler D. (2011). Comparison between FLAASH and ATCOR atmospheric correction modules on the basis of worldview-2 imagery and in situ spectroradiometric measurements. Accessed 22nd April 2015 from http://www.earsel2011.com/content/download/Proceedings/S12_4_Manakos_paper.pdf
- Manandhar R., Odeh I.O.A. & Ancev T. (2009). Improving the Accuracy of Land Use and Land Cover Classification of Landsat Data Using Post-Classification Enhancement. *Remote Sens.*, 1,330-344; doi:10.3390/rs1030330
- Marc, V. & Robinson, M. (2007). The long-term water balance (1972–2004) of upland forestry and grassland at Plynlimon, mid-Wales. *Hydrol. Earth Syst. Sci.*, 11, 44–60.

- Markham, B. L. & Barker, J. L. (1987). Radiometric properties of U.S. processed landsat MSS data. *Remote Sensing of Environment*, 22(1), 39-71. doi: [http://dx.doi.org/10.1016/0034-4257\(87\)90027-7](http://dx.doi.org/10.1016/0034-4257(87)90027-7)
- Matthews, T., Lo, A.Y. & Byrne, J.A. (2015). Reconceptualizing green infrastructure for climate change adaptation: Barriers to adoption and drivers for uptake by spatial planners. *Landscape and urban planning* (138), 155-163.
- McGee, T. G. (1991). The emergence desakota regions in Asia: expanding a hypothesis. In Ginsburg, N., B. Koppel, and T. G. McGee (eds.), *The extended metropolis: settlement transition in Asia*, Honolulu: University of Hawai Press, pp. 3-25.
- McInerney, D. & Kempeneers, P. (2014). *Open source geospatial tools: application in Earth observation*. Springer.
- Measey M. (2010). Indonesia: a vulnerable country in the face of climate change. *Global Majority E-journal 1* (1), 31-45.
- Meehl, G.A., et al. (2007). Global Climate Projections. Report of the Intergovernmental Panel on Climate Change. In Solomon, S., D. Qin, M. Manning, Z. Chen, M. Marquis, K.B. Averyt, M. Tignor and H.L. Miller (eds.), *Climate Change (2007): The Physical Science Basis*, Cambridge, United Kingdom and New York, NY, USA, pp. 747–846.
- M'ikiugu, M.M., Kinoshita, I., Tashiro, Y. (2012). Urban Green Space Analysis and Identification of its Potential Expansion Areas. *Procedia - Social and Behavioral Sciences*, 35, 449-458.
- Millard, K.; Richardson, M. (2015). On the Importance of Training Data Sample Selection in Random Forest Image Classification: A Case Study in Peatland Ecosystem Mapping. *Remote Sens.*, 7, 8489-8515.
- Mimura, N. (2008). The rapidly changing environment of the Asia and Pacific region and its implications for sustainability of the coastal zones in Asia Pasific coast and their management in states of environment. N. Mimura (ed), Springer, Netherlands. 345-358.
- Mitchell B.C. (2011). Urbanization and land surface temperature in Pinellas County, Florida. Graduate thesis and dissertations. University of South florida. Accessed 7th August 2014 from <http://scholarcommons.usf.edu/etd/3250>.

- Mizutani, M. (2002). Multi-functional roles of paddy field irrigation in the Asia monsoon region. Paper presented in World Water Council 3rd World Water Forum, Shiga, Japan.
- Monserud, R. A. & Leemans, R. (1992). Comparing Global Vegetation Maps with the Kappa Statistic." *Ecological Modelling*, 62 (4): 275-293.
- Moore, C.J. (1976). A comparative study of radiation balance above forest and grassland. *Quarterly Journal of the Royal Meteorological Society*, 102, pp. 889-899.
- Moran, E.F. (2010). Land Cover classification in a complex urban rural landscape with quickbird imagery. *Photogramm Eng Remote Sensing* 76(10), 1159–1168.
- Murai, S. (1998). GIS work book (technical course). Japan Association of Surveyors (JAS). Japan.
- Murakami, A. A., M. Zain, K. Takeuchi, A. Tsukenawa, and S. Yokota. (2005). Trends in urbanization and patterns of land use in the Asian mega cities Jakarta, Bangkok, and Metro Manila. *Landscape and Urban Planning* 70(3-4): 251-259.
- Nagayama, T., Okatani, T., Numata Y., Yamada, Y. (2012). Development of land cover data for urban heat island monitoring and simulation by combination of ASTER data and framework geographic dataset. Paper presented in 5th ASTER workshop. Accessed 26th January 2013 from http://www1.gsi.go.jp/geowww/EODAS/hi_data/060609ASTM-WS.pdf
- Nakad, J. (2008). The cost of progress: failed development and community response on Pulau Serangan. School for international training Bali-Indonesia arts and culture program. Accessed 5th July 2013 from http://digitalcollections.sit.edu/cgi/viewcontent.cgi?article=1704&context=isp_collection.
- NASA. (2011). Landsat 7 science data user's handbook. Accessed 2nd February 2012 from http://landsathandbook.gsfc.nasa.gov/pdfs/Landsat7_Handbook.pdf.
- NASA. (2015). A Landsat timeline. Accessed 2nd November 2015 from <http://landsat.gsfc.nasa.gov/?p=3166>
- National Agenda 21. (1997). Agenda 21 Indonesia-a national strategy for sustainable development. Retrieved on 10 October 2011 from <http://www.un.org/esa/agenda21/natlinfo/countr/indonesia/social.htm>.

- National Geographic. (2013). Indonesia map. Accessed 1th April 2013 from <http://travel.nationalgeographic.com.au/travel/countries/indonesia-map/>.
- National Standardization Agency of Indonesia. (2010). Land use cover classification. Accessed 17th June 2015 from <http://www.bakosurtanal.go.id/assets/download/sni/SNI/15.%20SNI%207645-2010%20Klasifikasi%20penutup%20lahan.pdf>.
- Nichols C.T. (2012). Land Use/Land Cover classification methods to overcome pixel confusion and the effects of tree shadows in very high resolution multispectral imagery. Thesis. Northwest Missouri State University.
- Odindi J, Mhangara P, Kakembo V. (2012). Remote sensing land-cover change in Port Elizabeth during South Africa's democratic transition. *S Afr J Sci.* 108(5/6). <http://dx.doi.org/10.4102/sajs.v108i5/6.886>.
- Oke, T. R. (1981). Canyon geometry and the nocturnal heat island: Comparison of scale and field observations *J. Climatol.*, 1, 237–254.
- Oke, T. R. (1982). The energetic basis of the urban heat island. *Q. J. R. Meteorol.Soc.*, 108, 1–24.
- Oke, T. R. (1988). Boundary layer climates, 2nd edn. London:Routledge. 435pp.
- Oke, T.R. (1988). Street design and urban canopy layer climate. Energy and buildings, 11(1-3), 103-113.
- Ultra-Carrio, R, Sobrino, J. A., Franch, B., and Nerry, F. (2012). Land surface emissivity retrieval from airborne sensor over urban areas. *Remote Sens. Environ.* 123, 298–305.
- Omran, E. S. E. (2012). Detection of Land-Use and Surface Temperature Change at Different Resolutions. *Journal of Geographic Information System*, 4 (3), 15. doi: 10.4236/jgis.2012.43024.
- Owen, T. W., Carlson, T. N., & Gillies, R. R. (1998). An assessment of satellite remotely-sensed land cover parameters in quantitatively describing the climatic effect of urbanization. *International Journal of Remote Sensing*, 19, 1663–1681.
- Pan S, Li, G, Yang, Q, Ouyang, Z, Lockaby, G, & Tian, H. (2013). Monitoring Land-Use and Land-Cover Change in the Eastern Gulf Coastal Plain 3 using Multitemporal Landsat imagery. *J Geophys Remote Sensing*, 2:108. doi:10.4172/2169-0049.1000108

- Parker, D.S. & Barkaszi, S.F., (1997). Roof solar reflectance and cooling energy use: field research results from Florida. *Energy and Buildings*, 25(2), pp.105–115.
- Paturusi S.A. & Diartika I W. (2010). Menuju Kota Hijau, melalui kearifan lokal (memberdayakan potensi terpendam Tri Kahayangan di Denpasar sebagai Hijauan Kota yang abadi). *Local wisdom*, 2 (1) 38-44.
- Peng, S.S., Piao S., Zeng, Z., Ciais, P., Zhou, L., Li, L.Z.X., Myneni, R.B., Yin, Y. & Zeng, H. (2014). Afforestation in China cools local land surface temperature. *PNAS* 111(8), 2915-2919.
- Perumal, K & Bhaskaran, R. (2010). Supervised classification performance of multispectral images. *Journal of computing*, 2, 124-129.
- Petit, C. C., & Lambin, E. F. (2002). Impact of data integration technique on historical land-use/land-cover change: Comparing historical maps with remote sensing data in the Belgian Ardennes. *Landscape Ecology*, 17(2), 117-132.
- Pidwirny, M. (2013). Factors influencing surface air temperature. The encyclopedia of Earth. Accessed 5th September 2015 from <http://www.eoearth.org/view/article/162614/>.
- Putra, G. K. D. (2011). Implementation of green tourism and green culture based on Tri Hita Karana philosophy in promoting Bali clean and green program. Accessed 21th July 2013 from <http://www.kgdharmaputra.blogspot.com.au/>.
- Pons, X., Pesquer, L., Cristobal, J., & Guerrero, O. G. (2014). Automatic and improved radiometric correction of Landsat imagery using reference values from MODIS surface reflectance images. *International Journal of Applied Earth Observation and Geoinformation*, 33, 243–254.
- Portier, C.J., Thigpen Tart, K., Carter, S.R., Dilworth, C.H, et al. (2010) A Human Health Perspective On Climate Change: A Report Outlining the Research Needs on the Human Health Effects of Climate Change. Research Triangle Park, NC: Environmental Health Perspectives/National Institute of Environmental Health Sciences. doi:10.1289/ehp.1002272.
- Powell, S.L., Pflugmacher, D., Kirschbaum, A.A.; Kim, Y., Cohen, W.B. (2007). Moderate resolution remote sensing alternatives: a review of Landsat-like sensors and their applications. *Journal of Applied Remote Sensing*, 1, 1-6.
- Quattrochi, D. A., J. C. Luvall, D. L. Rickman, M. G. Estes, C. A. Laymon, B. F. Howell. (2000). A decision support information system for urban

landscape management using thermal infrared data. *Photogrammetric Engineering and Remote Sensing*, 66 (10), 1195-1207.

Quinn, J.W. (2001). Band Combination. Accessed 25th July 2012 from <http://web.www.pdx.edu/emch/ipl/bandcombination.html>.

Ramdani, F., & Setiani, P. (2014). Spatio-temporal analysis of urban temperature in Bandung City, Indonesia. *Urban Ecosystems*, 17(2), 473-487. doi: 10.1007/s11252-013-0332-1.

Reis, S. (2008). Analyzing Land Use/Land Cover Changes Using Remote Sensing and GIS in Rize, North-East Turkey. *Sensors*, 8(10), 6188.

Richards, J.A. (2012). Remote sensing digital image analysis. Springer science and business media. 494p.

Riggan, N. D. & Weih, R. C. (2009). A comparison of pixel-based versus object-based land use/land cover classification methodologies. Cambridge University Press.

Rizwan, A. M., Dennis, L. Y. C. & Liu, C. (2008). A review on the generation, determination and mitigation of Urban Heat Island. *Journal of Environmental Sciences*, 20(1), 120-128. doi: [http://dx.doi.org/10.1016/S1001-0742\(08\)60019-4](http://dx.doi.org/10.1016/S1001-0742(08)60019-4).

Rocchini, D. (2007). Effects of spatial and spectral resolution in estimating ecosystem α -diversity by satellite imagery. *Remote Sensing of Environment*, 111(4), 423-434. doi: <http://dx.doi.org/10.1016/j.rse.2007.03.018>.

Rogan, Z.M., Martin, D., Ratick, S., Cuba, N. & DeLaue V. (2013). The impact of tree cover loss on land surface temperature: a case study of central Massachusetts using Landsat Thematic Mapper thermal data. *Applied Geography* 45, 49-57.

Rost, J., H. Mayer. (2006). Comparative Analysis of Albedo and Surface Energy Balance of a Grassland Site and an Adjacent Scots Pine Forest. *Climate Research*, 30, 227-237.

Roth M., Oke T. R. & Emery W. J. (1989). Satellite-derived urban heat islands from three coastal cities and the utilization of such data in urban climatology. *International Journal of Remote Sensing*, 10 (11).

Roth, M. (2013). Urban heat islands. In Fernando, H.J.S. (Ed), *Handbook of Environmental Fluid Dynamics, Volume Two*. CRC Press/Taylor & Francis Group, LLC.

- Rouse, J.W., Haas, R.H., Scheel, J.A., and Deering, D.W. (1974) Monitoring Vegetation Systems in the Great Plains with ERTS. Proceedings, 3rd Earth Resource Technology Satellite (ERTS) Symposium, vol. 1, p. 48-62).
- Roush, B.T. (2012). Quantifying urbanization in Grand Traverse County, MI. Honour thesis paper. Western Michigan University.
- Rozenstein, O., & Karnieli, A. (2011). Comparison of methods for land-use classification incorporating remote sensing and GIS inputs. *Applied Geography*, 31(2), 533-544. doi: <http://dx.doi.org/10.1016/j.apgeog.2010.11.006>
- Saefuloh A.A. (2011). Urbanisasi, kesempatan kerja, dan kebijakan ekonomi terpadu. In Susiana, S. (eds), *Tenaga Kerja Indonesia antara kesempatan kerja, kualitas dan perlindungan* (pp. 1-31). Jakarta: Pusat Pengkajian Pengolahan Data dan Informasi Sekretariat Jenderal Dewan Perwakilan Rakyat Republik Indonesia.
- Sailor, D.J., & Fan, H. Modelling the diurnal variability of effective albedo for cities. *Atmospheric Environment*, 36 (4).
- Salah, S.A.H. (2011). Impact of urban expansion on surface temperature in Baghdad, Iraq using remote sensing and GIS techniques. *Canadian Journal on Environmental, Construction and Civil Engineering*, 2 (8).
- Salama, M. S., Van der Velde, R., Zhong, L., Ma, Y., Ofwono, M., & Su, Z. (2012). Decadal variations of land surface temperature anomalies observed over the Tibetan Plateau by the Special Sensor Microwave Imager (SSM/I) from 1987 to 2008. *Climatic Change*, 114(3-4), 769-781. doi: 10.1007/s10584-012-0427-3.
- Saunders R. W. & R. T. Kriebel. (1988). An improved method for detecting clear sky and cloudy radiances from AVHRR data. *Int. J. Remote Sensing*, 9(1), 123-150.
- Shan and Hussain. Object-based data integration and classification for high-resolution coastal mapping, In Wang Y (ed), *Remote Sensing of Coastal Environment*, Taylor and Francis. New York, , 209-234.
- Selcuk, R., Nisanci, R., Uzun, B., Yalcin, A., Inan, H., & Yomralioglu, T., 2003. Monitoring land-use changes by GIS and remote sensing techniques: case study of Trabzon. Accessed 22 July 2013 from http://www.fig.net/pub/morocco/proceedings/TS18/TS18_6_reis_el_al.pdf 5.

- Setiawan, O. (2012). Rainfall and Temperature Variability Analysis in Bali (Indonesian version). *Jurnal analisis kebijakan kehutanan*, 9 (1), 66-79. Indonesia: Pusat Penelitian dan Pengembangan Perubahan Iklim dan Kebijakan Badan Penelitian dan Pengembangan Kehutanan. Accessed 23rd June 2013 from <http://www.forda-mof.org/index.php/content/download/info/1498>.
- Serra, P., Pons, X., Saurí, D. (2008). Land-cover and land-use change in a Mediterranean landscape: A spatial analysis of driving forces integrating biophysical and human factors. *Applied Geography*, 28(3), 189- 209.
- Shahmohamadi, P., Che-Ani, A. I., Maulud, K. N. A., Tawil, N.M., & Abdullah, N. A. G. (2011). The Impact of Anthropogenic Heat on Formation of Urban Heat Island and Energy Consumption Balance. *Urban Studies Research*, 2011. doi:10.1155/2011/497524
- Shan, J and Hussain, E. (2010). Object-based data integration and classification for high-resolution coastal mapping. In Weng, Y (Ed), *Remote Sensing of Coastal Environment*. Taylor and Francis Group.
- Smith, G. & Morton, D. (2008). Segmentation: The Achilles' heel of object-based image analysis? In G. . Hay, T. Blaschke, & D. Marceau, eds. *IGEOBIA 2008 – Pixels, Objects, Intelligence. GEOgraphic Object Based Image Analysis for the 21st Century*. University of Calgary, Calgary, Alberta, Canada ISPRS WG IV/4 Landscape Modeling and Visualization.
- Snyder, R. L., Melo-Abreu, J. P. & Matulich, S. (2005). Mechanism energy transfer (Chapter 3). In FAO, *Frost Protection: fundamentals, practice and economics volume 2*. Rome: FAO Environment and Natural Resources Service Series.
- Sobrino, J. A., Jiménez-Muñoz, J. C., & Paolini, L. (2004). Land surface temperature retrieval from LANDSAT TM 5. *Remote Sensing of Environment*, 90(4), 434-440. doi: <http://dx.doi.org/10.1016/j.rse.2004.02.003>.
- Sobrino, J. A., Oltra-Carrió, R., Jiménez-Muñoz, J. C., Julien, Y., Sòria, G., Franch, B., & Mattar, C. (2012). Emissivity mapping over urban areas using a classification-based approach: Application to the Dual-use European Security IR Experiment (DESIREX). *International Journal of Applied Earth Observation and Geoinformation*, 18(0), 141-147. doi: <http://dx.doi.org/10.1016/j.jag.2012.01.022>.
- Soeroso, S. (2004). Mengarusutamakan pembangunan berwawasan kependudukan di Indonesia (Indonesia version). Jakarta:EGC.

- Solecki W.D, Rosenzweig C., Parshall L., Pope G., Clark M., Cox J, Wiencke M., (2005). Mitigation of the heat island effect in urban New Jersey, *Global Environmental Change Part B: Environmental Hazards*, 6(1), 39-49.
- Solomon, S., Qin, D., Manning, M., Chen, Z., Marquis, M., Averyt, K. B., Tignor, M.& Miller, H. L. (2007). *Climate Change: The Physical Science Basis* (pp. 996). Cambridge, United Kingdom: Cambridge University Press.
- Srivanit, M., Hokao, K. & Phonekeo V. (2012). Assessing the Impact of Urbanization on Urban Thermal Environment: A Case Study of Bangkok Metropolitan. *International Journal of applied Science and Technology*, 2(7), 243-256.
- State ministry of national development planning of Indonesia. (2013). Evaluasi paruh waktu RPJMN 2010-2014. Accessed 8th March 2015 from http://www.bappenas.go.id/files/1613/7890/3140/Buku-Evaluasi-Paruh-Waktu-RPJMN_Bappenas.pdf
- Statistics of Bali Province. (2011). Area, number household, and total population by regency/municipality in Bali in 2010. Accessed 22nd January 2012 from <http://bali.bps.go.id/>.
- Stefanov, W.L. and Netzband, M. (2005). Assessment of ASTER land cover and MODIS NDVI data at multiple scales for ecological characterization of an arid urban center. *Remote Sensing of Environment*, 99(1–2), 31-43.
- Stefanov, W.L., Prashad, L., Eisinger, C., Brazel, A., and Harlan, S. (2004). Investigations of human modification of landscape and climate in the Phoenix Arizona metropolitan area using MASTER data. *The International Archives of the Photogrammetry, Remote Sensing, and Spatial Information Sciences*, 35(7), 1339-1347.
- Stehman, S. V. (1997). Selecting and interpreting measures of thematic classification accuracy. *Remote Sensing of Environment*, 62:77–89.
- Stoney, W.E. 2006. *ASPRS guide to land imaging satellites*. http://www.asprs.org/a/news/satellites/ASPRS_DATABASE_021208.pdf. (accessed 15 January 2015).
- Streutker, D. R. (2003). Satellite-measured growth of the urban heat island of Houston, Texas. *Remote Sensing of Environment*, 85: 282–289.
- Sudhakar S & Kameshwara R.SVC. . land use and land cover analysis. In Roy, P.S., Dwivedi R.S and Vijayan D. (eds.), *Remote Sensing Applications* (pp.21-48). National Remote Sensing Centre Indian Space Research

Organization. Accessed 13th November 2015 from http://www.nrsc.gov.in/Learning_Centre_EBook.html.

Sudiarta, I K. (2012). Sustainable tourism development: Case study in Denpasar Municipality, Bali, Indonesia. *Tropical coasts*, 17 (2), 46-56

Sun D. & Pinker R. T. (2003). Estimation of land surface temperature from a Geostationary Operational Environmental Satellite (GOES-8). *J. Geophys. Res.*, 108: pp. 4326-4241.

Sundara Kumar, K., Udayabhaskar, P. & Padmakumari K. (2012). Estimation of land surface temperature to study urban heat island effect using Landsat ETM+ image. *International Journal of Engineering, Science and Technology*, 4(2), 807-814.

Sutriadi R., & Haryo, W. (2009). Identification of metropolitan development in Indonesia (Indonesia version). Accessed 12th April 2013 from http://www.sappk.itb.ac.id/ppk/index.php?option=com_content&task=view&lang=en&id=259

Swann, A. L., Fung, I. Y., Levis, S., Bonan, G. B. & Doney, S. C. (2010). Changes in Arctic vegetation amplify high-latitude warming through the greenhouse effect. *Proc. Natl. Acad. Sci. U. S. A.*, 107, 1295–1300.

Syrios, K., & Hunt, G. R. (2008). Passive air exchanges between building and urban canyon via openings in a single façade. *International Journal of Heat and Fluid Flow*, 29: pp. 364–373.

Tan, K., Lim, H., MatJafri, M., & Abdulla, K. (2010). Landsat data to evaluate urban expansion and determine land use/land cover changes in Penang Island, Malaysia. *Environmental Earth Science*, 60, 1509-1521.

Taubenbock, H., Esch, T., Felbier, A., Roth, A. & Dech, S. (2011). Pattern-based accuracy assessment of an urban footprint classification using TerraSAR-X Data. *IEEE Geoscience and Remote Sensing Letters*, 8(2), 278-282. doi: 10.1109/lgrs.2010.2069083

Taylor, C, Lambin, E.F, Stephenne, N, Harding, R, Essery, R. (2002). The influence of land-use change on climate in the Sahel. *J. Clim.*, 15(24), 3615–29

The Yale Center of Earth Observation. (2014). Aster Images. Accessed 22nd January 2014 from <http://www.yale.edu/ceo/Documentation/ASTER.pdf>

Tian, Q & Xiangjun, M. (1998). Advances in study on vegetation indices. *Advance in Earth Sciences*, 13(4), 327–333.

- Tibbetts, J. (2002). Coastal cities: *Living on the edge*, 110, pp. A674-A681.
- Tursilowati, L. (2005). Urban Heat Island Due to Land use and Land Cover change in Bandung dan Bogor (Indonesia). *Jurnal Sains Dirgantara*, 3, pp. 43-64.
- Tursilowati, L., Sri Sumantyo, J.T., Kuze, H., Adiningsih, E. S. (2012). The integrated WRF/Urban modeling system and its application to monitoring urban heat island in Jakarta-Indonesia. *Journal of Urban and Environmental Engineering*, 1(6), 1-9.
- US EPA (Environmental Protection Agency). (2009). *Heat Island Effect*. Accessed 9th June 2013 from <http://www.epa.gov/hiri>.
- United Nations. (2007). World urbanization prospects: the 2007 revision Data tables and highlights. New York.
- U.S. Geological Survey. (2000). National land archive production system (NLAPS) systematic format description document. Accessed 25th September 2015, from http://landsat.usgs.gov/documents/NLAPS_II.pdf
- U.S. Geological Survey. (2011). Landsat a global land imaging mission. USGS. Accessed 8th July 2015 from <https://pubs.usgs.gov/fs/2012/3072/fs2012-3072.pdf>
- U.S. Geological Survey. (2013). Product guide: Landsat climate data record (CDR). Surface reflectance Department of the Interior U.S. Geological Survey. Accessed 14 July 2016 from http://landsat.usgs.gov/documents/cdr_sr_product_guide.pdf
- Valle-Díaz, O., Blanco-García, A., Bonfil, C., Paz, H., & Lindig-Cisneros, R. (2009). Altitudinal range shift detected through seedling survival of *Ceiba aesculifolia* in an area under the influence of an urban heat island. *Forest Ecology and Management*, 258(7), 1511-1515.
- Verburg, P. H., Van De Steeg, J., Veldkamp, A. & Willemsen, L. (2009). From land cover change to land function dynamics: a major challenge to improve land characterization. *Journal of environmental management*, 90 9(3), pp. 1327-1335.
- Voogt, J. A., & Oke, T. R. (1997). Complete urban surface temperatures. *Journal of Applied Meteorology*, 36: 1117-1132.
- Voogt, J. A., & Oke, T. R. (2003). Thermal remote sensing of urban climates. *Remote Sensing of Environment*, 86(3), 370-384. Sciencedirect.

- Voogt, J. A. (2004). Urban heat islands: hotter cities. Accessed 18th March 2012, from <http://www.actionbioscience.org/environment/voogt.html#primer>.
- Wan, Z., and Dozier, J. (1996). A generalized split-window algorithm for retrieving land-surface temperature from space. *IEEE Transactions on Geoscience and Remote Sensing*, 34(2), 892–905.
- Wang, L., Sousa, W. P, Gong, P., and Biging, G. S. (2004). Comparison of IKONOS and QuickBird images for mapping mangrove species on the Caribbean coast of panama. *Remote Sensing of Environment* , 91:432–440.
- Walawender, J., Szymanowski, M., Hajto, M., & Bokwa, A. (2014). Land Surface Temperature Patterns in the Urban Agglomeration of Krakow (Poland) Derived from Landsat-7/ETM+ Data. *Pure and Applied Geophysics*, 171(6), 913-940. doi: 10.1007/s00024-013-0685-7
- Weih, R., & Riggan, N. (2010). Object-based Classification vs. Pixel-based Classification: Comparative Importance of Multi-resolution Imagery. The International Archives of the Photogrammetry, Remote Sensing and Spatial Information Sciences, Vol. XXXVIII-4/C7. Accessed 23rd July 2014 from <http://www.isprs.org>
- Wen, Y. (2011). Data application of multi-temporal and multi-source data for land cover change detection in Guam, USA. *Geoinformatics, 19th International Conference on IEEE*, , pp. 1.
- Weng Q, (2001), A remote sensing-GIS evaluation of urban expansion and its impact of surface temperature in Zhujiang Delta, China, *Int J Remote Sens*, 22(10), 1999-2014.
- Weng Q. (2003). Fractal analysis of satellite-detected urban heat island effect. *Photogrammetric Eng. Remote Sens* 69, 555–566.
- Weng, Q., Lu, D. & Liang, B. (2006). Urban surface biophysical descriptors and land surface temperature variations. *Photogrammetric Engineering & Remote Sensing*, 72 (11), 1275–1286
- Weng, Q. (2009). Thermal infrared remote sensing for urban climate and environmental studies: methods, applications, and trends. *ISPRS Journal of Photogrammetry and Remote Sensing*, 64 (4), 335-344.
- Weng, Q, Lu, D, Schubring, J (2003) Estimation of land surface temperature–vegetation abundance relationship for urban heat island studies. *Remote Sens Environ*, 89(4), 467–48.

- Weng, Y. C. (2007). Spatiotemporal changes of landscape pattern in response to urbanization. *Landscape and Urban Planning*, 81(4): 341-353
- Whiteside, T., & Ahmad, W. (2005). A comparison of object-oriented classification methods for mapping land cover in Northern Australia. Proceedings of SSC 2005 Spatial intelligence innovation and praxis, The national biennial Conference of the Spatial Sciences Institute, September 2005. Melbourne: Spatial Sciences Institute.
- Whitten, T., Soeriaatmadja R. E, & Afiff S. (1996). The ecology of Java and Bali. Singapore: Periplus edition.
- Wibowo A. (2013). Spatial-temporal analysis of urban heat island in Tangerang City. *Indonesian Journal of Geography*, 45 (2).
- World Bank. (2009). *Indonesia Rising: Mainstreaming Climate Change for Sustainability* (Jakarta, Indonesia: World Bank Office Jakarta). Accessed 20 August 2012 from <http://go.worldbank.org/JIGX6UTVJ0>.
- Wu, K.-y., Ye, X.-y., Qi, Z.-f., & Zhang, H. (2013). Impacts of land use/land cover change and socioeconomic development on regional ecosystem services: The case of fast-growing Hangzhou metropolitan area, China. *Cities*, 31(0), 276-284. doi: <http://dx.doi.org/10.1016/j.cities.2012.08.003>
- Wu, X., Shen Z., R. Liu R. & Ding X. (2008). "Land Use/Cover Dynamics in Response to Changes in Environmental and Socio-Political Forces in the Upper Reaches of the Yangtze River, China". *Sensors*, 8., 8104-8122.
- Xian G., & Crane M. (2006). An analysis of urban thermal characteristics and associated land cover in Tampa Bay and Las Vegas using Landsat satellite data. *Remote Sensing of Environment*, 104 (2), 147-156.
- Xiao, H. & Weng, Q. (2007). The impact of land use and land cover changes on land surface temperature in a karst area of China. [Research Support, Non-U.S. Gov't Research Support, U.S. Gov't, Non-P.H.S.]. *J Environ Manage*, 85(1), 245-257. doi: 10.1016/j.jenvman.2006.07.016
- Xiao, J. Y., Shen, Y. J., Ge, J. F., Tateishi, R., Tang, C. Y. & Liang, Y. Q. (2006). Evaluating urban expansion and land use change in Shijiazhuang, China, by using GIS and remote sensing. *Landscape and Urban Planning*, 75, 69-80.
- Xiao, R.; Weng Q., Ouyang Z., Schienke E.W. & Zhang Z. (2008). Land surface temperature variation and major factors in Beijing China. *Photogrammetric engineering and RS* 74(4), 451-461.

- Xu, H. & Chen, B.Q., 2004, Remote sensing of the urban heat island and its changes in Xiamen city of SE China, *J environ Sci*, 16(2): 276-281.
- Yin, J., Yin, Z., Zhong, H., Xu, S., Hu, X., Wang, J., & Wu, J. (2011). Monitoring urban expansion and land use/land cover changes of Shanghai metropolitan area during the transitional economy (1979-2009) in China. [Research Support, Non-U.S. Gov't]. *Environ Monit Assess*, 177(1-4), 609-621.
- Young, A. (1999). Is there Really Spare Land? A Critique of Estimates of Available Cultivable Land in Developing Countries. *Environment, Development and Sustainability*, 1(1), 3-18.
- Yu, Q., Yue, D., Wang, J., Zhang, Q., Li, Y., Yu, Y., . . . Li, N. (2016). The optimization of urban ecological infrastructure network based on the changes of county landscape patterns: a typical case study of ecological fragile zone located at Deng Kou (Inner Mongolia). *Journal of Cleaner Production*. doi: <http://dx.doi.org/10.1016/j.jclepro>.
- Yuan, F. & Bauer, M. E. (2007). Comparison of impervious surface area and normalized difference vegetation index as indicators of surface urban heat island effects in Landsat imagery. *Remote Sensing of Environment* 106(3), 375-386.
- Yuan, F., Sawaya, K. E., Loeffelholz, B. C. & Bauer, M. E. (2005). Land cover classification and change analysis of the twin cities (Minnesota) metropolitan Area by multitemporal Landsat remote sensing. *Remote Sensing of Environment*, 98(2-3), 317-328.
- Yuen, B. & Kong L. (2009). Climate change and urban planning in Southeast Asia. *S.A.P.I.E.N.S.* 2(3). Accessed 23 February 2011 from sapiens.revues.org/pdf/881
- Yüksel, A., Akay, A. & Gundogan, R. (2008). Using ASTER Imagery in Land Use/covers Classification of Eastern Mediterranean Landscapes According to CORINE Land Cover Project. *Sensors*, 8(2), 1237-1251.
- Zhang, J. & Wang, Y. (2008). Study of the Relationships between the Spatial Extent of Surface Urban Heat Islands and Urban Characteristic Factors Based on Landsat ETM+ Data. *Sensors*, 8(11), 7453-7468.
- Zhou, W., Ji, S., Chen, T.-H., Hou, Y. & Zhang, K. (2014). The 2011 heat wave in Greater Houston: Effects of land use on temperature. *Environmental Research*, 135, 81-87.

Zhou, W, Troy, A, Grove, J.M. (2008). Object-based land cover classification and change analysis in the Baltimore metropolitan area using multi-temporal high resolution remote sensing data. *Sensors*, 8:1613–1636.

Zhou, X., & Wang, Y.-C. (2011). Dynamics of Land Surface Temperature in Response to Land-Use/Cover Change. *Geographical Research*, 49(1), 23-36.

Zhu, G & Blumberg, D. G. (2002). Classification using ASTER and SVM algorithms: the case study of Beer Sheva, Israel. *Remote Sensing of Environment*, 80, pp 233-240

Zoran, M. & Anderson, E. (2006). The use of multi-temporal and multispectral satellite data for change detection analysis of the Romanian Black Sea coastal zone. *Journal of optoelectronics and advanced materials*, 8(1), pp. 252

“Every reasonable effort has been made to acknowledge the owners of copyright material. I would be pleased to hear from any copyright owner who has been omitted or incorrectly acknowledged”

APPENDICES

Appendix V-1 GCPs of Geometric correction Landsat

X source	Y source	X Map	Y map
296769.7	-967341	296756.4	-967415
292375.1	-952913	292320.5	-952973
311163.9	-952561	311131	-952641
300670.4	-949089	300614.8	-949156
298451.5	-956925	298412.9	-956995
296589.3	-950181	296531.5	-950246
299729	-964546	299712.5	-964619
298772.4	-950097	298716.5	-950163
307567.7	-953026	307530.5	-953102
303548	-951938	303503.3	-952010
311298.6	-948999	311255.6	-949077
298092.2	-960178	298061.8	-960249
305607	-962656	305591.8	-962736
299177.2	-955148	299135.3	-955217
305894.9	-959086	305871.1	-959164
304489.1	-961661	304470.2	-961739
300874.5	-956677	300838.6	-956749
295821.4	-955066	295775.4	-955132
290709.9	-948600	290641.3	-948657
305658.2	-956372	305627.3	-956448

Total Rms error 0.69274

Appendix V-2 GCPs of Geometric correction for ASTER

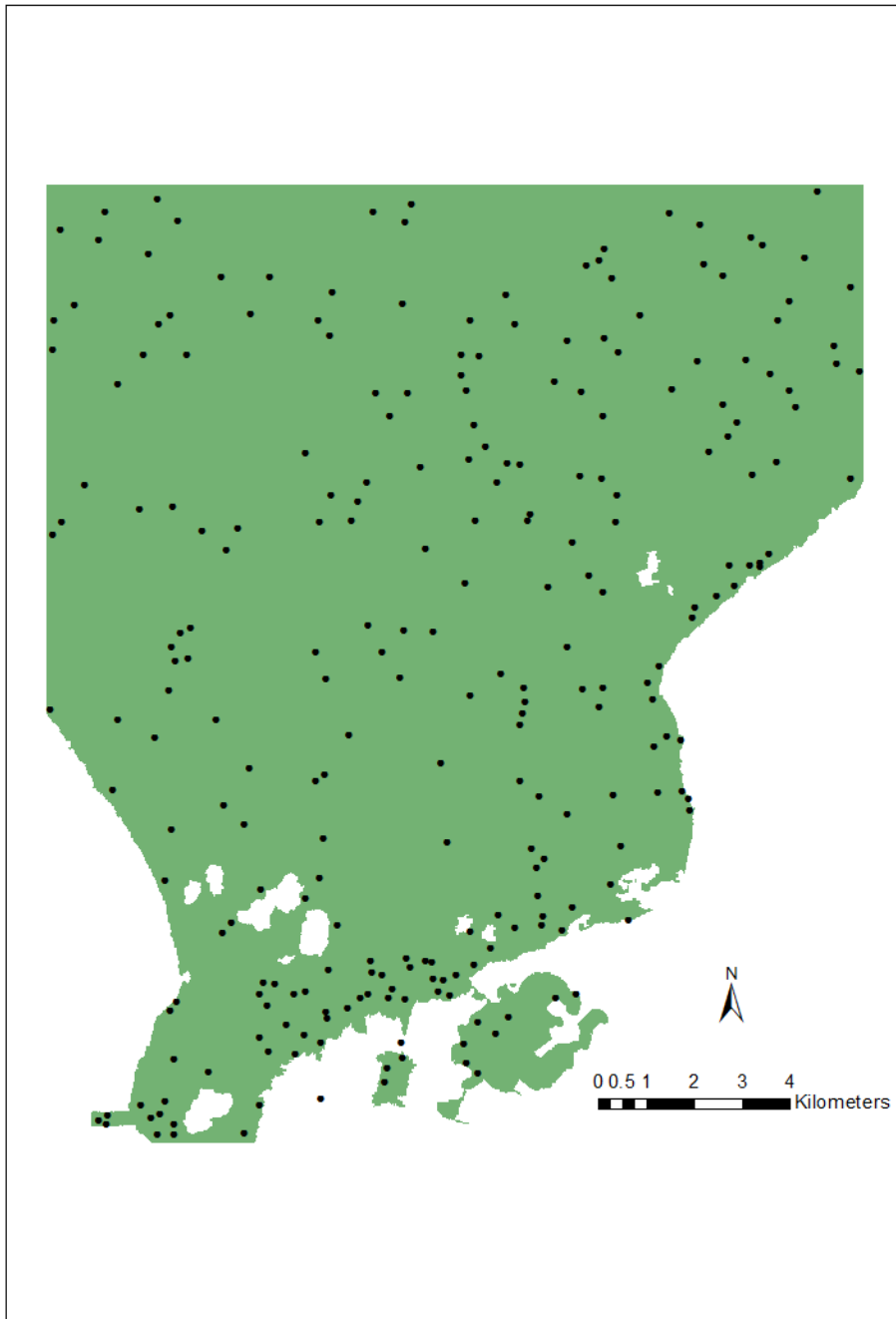
	Base X	Base Y	Warp X	Warp Y	Predict X	Predict Y	Error X	Error Y	RMS
#1+	104.25	1348.00	103.50	1351.75	103.5183	1351.3067	0.0183	-0.4433	0.4437
#2+	856.75	559.50	855.00	560.75	855.1426	560.6871	0.1426	-0.0629	0.1558
#3+	112.50	92.75	112.50	91.75	112.4256	91.3995	-0.0744	-0.3505	0.3583
#4+	729.50	1174.25	727.50	1177.50	727.8420	1176.9817	0.3420	-0.5183	0.6209
#5+	1090.25	321.25	1088.00	322.00	1088.3313	322.1735	0.3313	0.1735	0.3739
#6+	291.00	515.25	290.75	515.50	290.3908	515.6724	-0.3592	0.1724	0.3984
#7+	782.50	1019.00	780.75	1020.75	780.8225	1021.3259	0.0725	0.5759	0.5804
#8+	425.25	854.25	424.00	855.50	424.2436	855.9176	0.2436	0.4176	0.4834
#9+	20.75	749.50	19.75	750.25	20.4804	750.5135	0.7304	0.2635	0.7764
#10+	686.50	777.25	685.50	779.50	685.0891	778.8634	-0.4109	-0.6366	0.7577
#11+	424.25	512.25	423.50	513.00	423.4115	512.8165	-0.0885	-0.1835	0.2038
#12+	800.00	146.75	799.00	147.00	798.6673	146.7918	-0.3327	-0.2082	0.3925
#13+	422.75	1307.25	422.00	1310.00	421.5274	1310.3748	-0.4726	0.3748	0.6032
#14+	213.75	1004.50	213.25	1006.50	213.0209	1006.5700	-0.2291	0.0700	0.2396
#15+	429.25	133.25	428.50	132.25	428.5868	132.6057	0.0868	0.3557	0.3661

Total RMS Error: 0.485257

Appendix V-3 Input parameters of FLAASH atmospheric correction

Atmospheric Model	Aerosol	Sensor	Altitude (km)	Pixel size	Atmospheric Model	Aerosol	Center Latitude (°)	Center Longitude (°)	Aerosol retrieval	Visibility (km)
24/4/2013	2:47:46	ASTER	0.5	15	tropical	urban	-8.701946	115.299273	none	100
24/2/2003	2:48:13	ASTER	0.5	15	tropical	urban	-8.708575	115.345918	none	100
3/2/1995	1:35:26	Landsat TM	0.5	30	tropical	urban			none	100

Appendix V-4 Random ground truth locations of 2013



Appendix V-5 Error matrix of the LULC in 1995

LULC type	Reference data											Grand Total	Users' accuracy (%)	Error of commission (%)
	BUA	BL	DFL	FP	GL	M	OS	PF	SA	V	WB			
BUA	72	0	0	0	2	0	0	8	0	0	0	82	87.8	12.2
BL	0	11	0	0	0	0	0	0	0	0	0	11	100.0	0.0
DFL	0	0	9	0	0	0	0	0	0	0	0	9	100.0	0.0
FP	0	0	0	17	0	0	0	0	0	0	0	17	100.0	0.0
GL	1	0	0	0	1	0	0	0	0	0	0	2	50.0	50.0
M	0	0	0	0	0	17	0	0	0	0	0	17	51.5	48.5
OS	0	0	0	0	0	0	30	3	0	0	0	33	90.9	9.1
PF	0	0	0	0	0	0	0	69	0	5	0	74	93.2	6.8
SA	0	0	0	0	0	0	0	0	0	0	0	2	100.0	0.0
V	0	0	0	0	0	0	0	26	0	21	0	47	44.7	55.3
WB	0	0	0	0	0	0	0	0	0	0	4	4	100.0	0.0
Grand Total	73	11	9	17	3	17	30	106	2	26	4	298		
Producers' accuracy (%)	98.6	100.0	100.0	100.0	33.3	100.0	100.0	65.1	100.0	80.8	100.0		Overall accuracy: 84.9 %	
Error of omission (%)	1.4	0.0	0.0	0.0	66.7	0.0	0.0	34.9	0.0	19.2	0.0			

BUA : Built-up area BL : Bush land
 DFL : Dry farm land FP : Fish pond
 FP : Paddy field M : Mangrove
 OS : Open space SA : Swamp area
 V : Vegetation WB : Water bodies
 GL : Grass land

Appendix V-6 Error matrix of the LULC in 2003

LULC type	Reference data																		Total	Users' accuracy (%)	Error of commission (%)
	BS	VDB	DB	SDB	BRB	BL	DFL	DPF	FP	HPF	MA	MB	OS	SA	V	VPF	WB	WPF			
BS	6	0	0	0	0	0	0	0	0	0	0	0	0	0	0	0	0	0	6	100.00	0.00
VDB	0	47	2	0	2	1	0	0	0	0	0	0	0	0	0	0	0	0	52	90.38	9.62
DB	0	0	31	4	0	0	0	0	0	0	0	0	0	0	0	0	2	0	37	83.78	16.22
SDB	0	0	0	35	0	0	0	0	0	0	0	0	0	0	0	0	0	0	35	100.00	0.00
BRB	1	0	0	0	36	0	0	0	0	0	0	0	0	0	0	0	0	0	37	97.30	2.70
BL	0	0	0	0	0	8	1	0	0	0	0	0	0	0	0	0	0	0	9	88.89	11.11
DFL	0	0	0	0	0	0	6	0	0	0	0	0	0	0	2	0	0	0	8	75.00	25.00
DPF	0	0	0	0	1	0	0	6	0	0	0	0	0	0	0	1	0	1	9	66.67	33.33
FP	0	0	0	0	0	0	0	0	4	0	0	0	0	0	0	0	0	0	4	100.00	0.00
HPF	0	0	0	0	0	0	0	0	0	14	0	0	0	0	0	0	0	0	14	95.24	4.76
MA	0	0	0	0	0	0	0	0	0	0	20	1	0	0	0	0	0	0	21	95.24	4.76
MB	0	0	0	0	0	0	0	0	0	0	2	9	0	0	0	0	0	0	11	81.82	18.18
OS	0	0	0	0	2	1	0	0	0	0	0	0	9	0	0	0	0	0	12	75.00	25.00
SA	0	0	0	0	0	0	0	0	0	0	0	0	0	2	0	0	0	0	2	100.00	0.00
V	0	0	0	0	1	4	2	0	0	0	0	0	0	0	15	2	0	0	24	62.50	37.50
VPF	0	0	0	0	0	0	2	0	0	2	0	0	0	0	1	20	0	0	25	80.00	20.00
WB	0	0	0	0	0	0	0	0	0	0	0	0	0	0	0	0	9	0	9	100.00	0.00
WPF	0	0	1	0	1	0	0	0	0	0	0	0	0	0	3	2	24	0	31	77.42	22.58
Total	7	47	34	39	43	14	11	6	4	16	22	10	9	2	18	26	13	25	346		
Producers' accuracy (%)	85.7	100	91.2	89.7	83.7	57.1	54.6	100	100	87.5	90.9	90	100	100	83.3	76.9	69.2	96		Overall accuracy: 86.99%	
Error of omission (%)	14.3	0.00	8.8	10.3	16.3	42.9	45.5	0.0	0.00	12.5	9.10	10	0.0	0.0	16.7	23.1	30.8	4			

- | | | |
|------------------------------------|--------------------------------|----------------|
| BS : Beach sand | VDB : Very dense built up area | GL : Grassland |
| DB : Dense built up area | SDB : Semi dense built up area | |
| BRB : Bright rooftop built up area | BL : Bush land | |
| DFL : Dry farm land | FP : Fish pond | |
| HPF : Harvested paddy field | DFP : Dry paddy field | |
| WPF : Watered paddy field | VPF : Vegetative paddy field | |
| MA : Dense mangrove | MB : Non dense mangrove | |
| OS : Open space | SA : Swamp area | |
| V : Vegetation | WB : Water bodies | |

Appendix V-7 Error matrix of the LULC in 2013

LULC type	Reference data																			Total	Users' accuracy (%)	Error of commission (%)
	BS	VBD	DB	SDB	BRB	BL	DFL	DPF	FP	HPF	MA	MB	GL	OS	SA	V	VPF	WB	WPF			
BS	8	0	0	0	0	0	0	0	0	0	0	0	0	0	0	0	0	0	0	8	100.0	0.0
VBD	1	31	5	0	8	0	1	0	0	0	0	0	0	0	0	1	0	0	0	47	66.0	34.0
DB	1	6	43	3	1	0	0	0	0	0	0	0	0	0	4	0	3	0	0	61	70.5	29.5
SDB	0	1	5	21	0	0	0	0	0	0	0	0	0	0	1	0	0	0	0	28	75.0	25.0
BRB	0	2	0	0	19	0	0	0	0	0	0	0	0	1	0	1	0	0	0	23	82.6	17.4
BL	0	0	0	0	0	15	0	0	0	0	0	0	0	0	0	0	0	0	0	15	100.0	0.0
DFL	0	0	0	0	0	0	7	0	0	0	0	0	0	0	2	0	0	0	0	9	77.8	22.2
DPF	0	0	0	0	0	1	0	17	0	6	0	0	0	0	0	0	0	0	0	24	70.8	29.2
FP	0	0	0	0	0	0	0	0	4	0	0	0	0	0	0	0	0	0	0	4	100.0	0.0
HPF	0	0	0	0	0	0	0	0	0	14	0	0	0	0	0	0	0	0	3	17	82.4	17.6
MA	0	0	0	0	0	0	0	0	0	0	23	2	0	0	0	0	0	0	0	25	92.0	8.0
MB	0	0	0	0	0	0	0	0	0	0	0	5	0	0	0	0	0	0	0	5	100.0	0.0
GL	0	0	0	0	0	0	0	0	0	0	0	0	8	0	0	0	0	0	0	8	100.0	0.0
OS	1	0	0	0	0	2	0	0	0	0	0	0	0	10	0	0	0	0	0	13	76.9	23.1
SA	0	0	0	0	0	0	0	0	0	0	0	0	0	0	3	0	0	0	0	3	100.0	0.0
V	0	0	0	0	1	1	0	0	0	0	0	0	0	0	0	30	0	0	0	32	93.8	6.3
VPF	0	0	0	0	1	0	2	0	0	0	0	0	0	0	0	2	20	1	3	29	69.0	31.0
WB	1	0	0	0	0	0	0	0	0	0	0	0	0	0	0	0	0	8	0	9	88.9	11.1
WPF	0	0	0	0	0	0	0	1	0	0	0	0	0	0	0	0	0	0	21	22	95.5	4.5
Total	12	40	53	24	30	19	10	18	4	20	23	7	8	11	3	41	20	12	27	382		
Producers' accuracy (%)	66.7	77.5	81.1	87.5	63.3	78.9	70.0	94.4	100.0	70.0	100.0	71.4	100.0	90.9	100.0	73.2	100.0	66.7	77.8		Overall accuracy: 80.37 %	
Error of omission (%)	33.3	22.5	18.9	12.5	36.7	21.1	30.0	5.6	0.0	30.0	0.0	28.6	0.0	9.1	0.0	26.8	0.0	33.3	22.2			

- BS : Beach sand
- DB : Dense built up area
- BRB : Bright rooftop built up area
- DFL : Dry farm land
- HPF : Harvested paddy field
- WPF : Watered paddy field
- MA : Dense mangrove
- OS : Open space
- V : Vegetation
- VDB : Very dense built up area
- SDB : Semi dense built up area
- BL : Bush land
- FP : Fish pond
- DFP : Dry paddy field
- VPF : Vegetative paddy field
- MB : Non dense mangrove
- SA : Swamp area
- WB : Waterbodies
- GL : Grassland